Dispersion of aqueous effluent from Hunterston power stations

Reference: ENE – 0328A/R1

Issue: 2.1

To: [redacted]
EDF Energy Nuclear Generation Ltd
Barnett Way
Barnwood
Gloucester
GL4 3RS

From: [redacted]

Eden
Nuclear and Environment

ISSUE DATE
20/04/2023

Eden Nuclear and Environment Ltd
Unit 1 Mereside, Greenbank Road, Eden Business Park, Penrith, Cumbria CA11 9FB

Tel: [redacted]
Email: [redacted]
Web: www.eden-ne.co.uk

This page has been intentionally left blank.

Document Issue Record	
Document Title:	**Dispersion of aqueous effluent from Hunterston power stations**
Project:	**EDF effluent dispersion**
Reference:	**ENE – 0328A/R1**
Project Manager:	[redacted]

Document Status

Issue	Description	Author(s)	Reviewer(s)	Approver	Date
1	Issued for client comment	[redacted]	[redacted]	[redacted]	20/02/2023
2	Revised following client comments	[redacted]	[redacted]	[redacted]	20/03/2023
2.1	Clerical corrections	[redacted]	[redacted]	[redacted]	20/04/2023

Document Restrictions and Accessibility

Any previous versions must be destroyed or marked superseded.

Distribution

Issue	Copies	Name	Organisation
2.1	1	Hunterston B Document Control, [redacted] and [redacted]	EDF Energy Nuclear Generation Ltd
2.1	1	Project file	Eden NE

This page has been intentionally left blank.

Executive Summary

Abstract

EDF Nuclear Generation Ltd are considering the arrangements they will use for discharge of radioactive effluent from Hunterston B power station during its decommissioning. This report discusses the dilution and dispersion in the environment for five different discharge scenarios. It is an input into EDF's decision making process.

We have modelled the effect of discharge location, discharge timing (relative to the tide) and discharge flow rate on the compartment-scale dilution and dispersion of discharges of radioactive liquid effluent from Hunterston power stations to the Firth of Clyde. When discharging near the shore, as in the current arrangements, the model calculates radionuclide activity concentrations in the immediate vicinity of the outfall to be one to two orders of magnitude greater than when discharging in the deeper channel. Otherwise, the discharge timing (relative to the tide) and flow rate have very little influence on dilution and dispersion in the Firth of Clyde. The model results agree well with monitoring of local H-3 concentrations after discharges.

Summary

We have created a compartment model of the Firth of Clyde and used this to model the dilution and dispersion of discharges from Hunterston nuclear power stations (see figure below). This model calculates average radionuclide concentrations in seawater and sediment in several regions of the Firth of Clyde. It is capable of modelling individual tidal cycles and discharges. We have compared the results of the model to real-world observations and to models run in the standard PC-CREAM 08 software. We have used the model to investigate the effect of discharge location, timing and flow rate on dilution and dispersion.

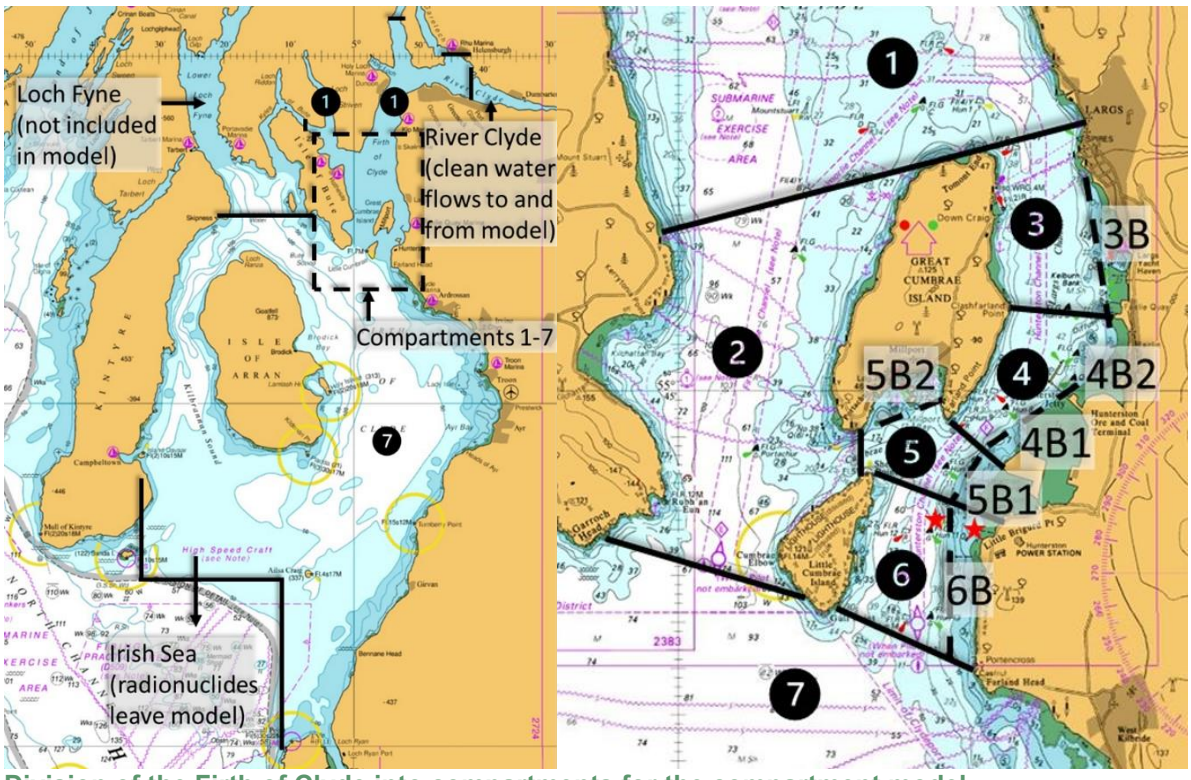

Division of the Firth of Clyde into compartments for the compartment model.

Five discharge scenarios were considered: the current system and four alternative arrangements. Four of the scenarios consider unit activity discharges (that is, Bq l^{-1} or Bq kg^{-1} per GBq y^{-1}). These can be scaled to permitted, forecast or actual discharges by multiplying the concentration by the annual discharge (in GBq). The other scenario considers both stations discharging at their permit limits.

The behaviour of radionuclides is very similar for all the discharge scenarios considered in all compartments except in the immediate vicinity of the current outfall. There are also some differences in the short-term behaviour of radionuclides (over a single tidal or discharge cycle), but these have no effect on the long-term build-up or average radionuclide concentrations.

Discharge at the present outfall location results in localised higher activity concentrations there (by one to two orders of magnitude, depending on radionuclide), compared to discharging to the deeper channel – see figure below. This is due to the smaller initial dilution volume and lower flow at this location. Concentrations elsewhere in the model are not affected. The significance of these higher concentrations near the outfall will depend on the amount of activity discharged and the dose that could result. These are not considered in this report.

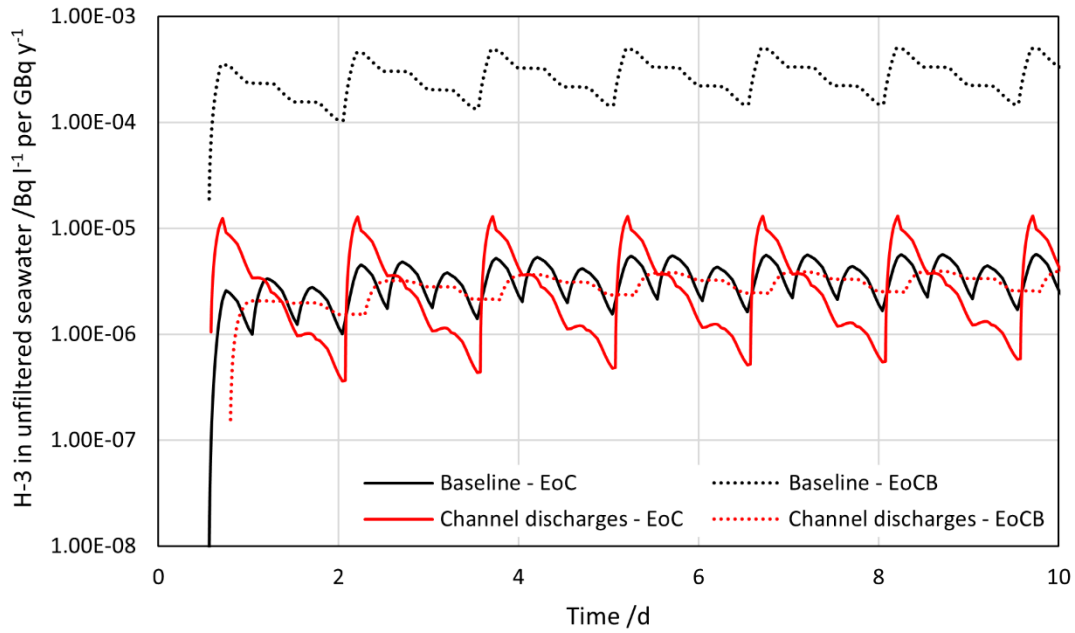

Comparison of H-3 concentration in seawater near the outfall (dotted, "EoCB") and in the channel (solid, "EoC") when discharging at the current outfall (black) and in the deeper channel (red). (Compartment abbreviations are defined in Table 4 in the body of the report.)

Directly discharged radionuclide concentrations in seawater rapidly build up to physicochemical equilibrium (see upper figure on next page). The equilibrium concentration depends on partitioning between the seawater and sediment phases, with more sorbing radionuclides having slightly lower seawater concentrations.

The behaviour of the concentrations of directly discharged radionuclides in sediment depends on the physicochemical and radiological properties of the nuclides. Short-lived and less-sorbing radionuclide (e.g. H-3) concentrations in sediment rapidly reach equilibrium, while long-lived and more-sorbing radionuclide (e.g. Pu-239) increase linearly through the modelled time period. Other radionuclides (e.g. Co-60, which is short lived and more sorbing) display intermediate behaviour, approaching equilibrium in sediment over intermediate timescales (five to ten years for Co-60 – see lower figure on next page).

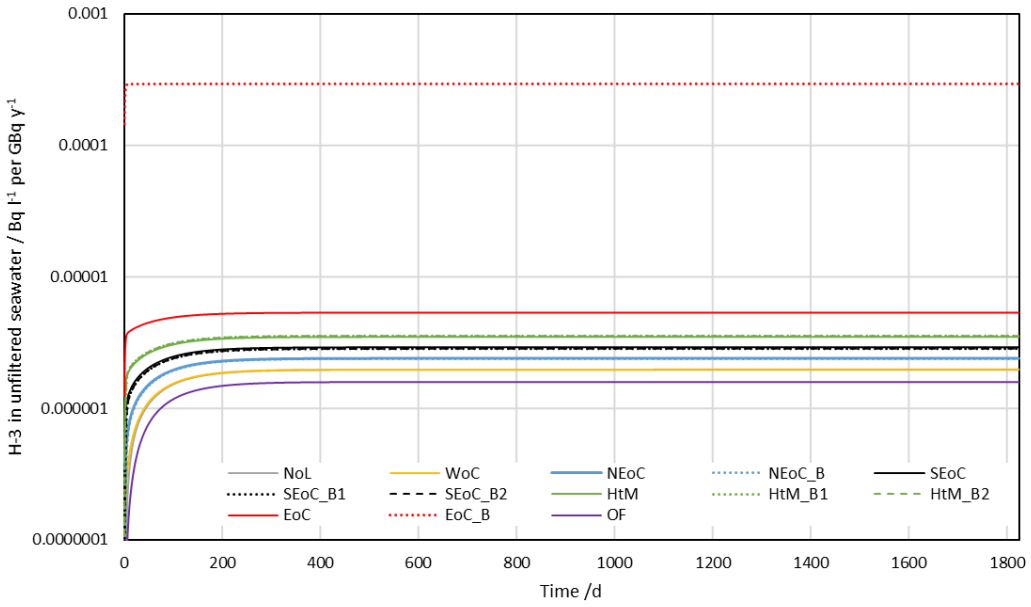

Discharge cycle moving average of H-3 concentration in unfiltered seawater in each region of the Firth of Clyde for five years (current discharge scenario). All compartments have reached equilibrium within 200 days. (Compartment abbreviations are defined in Table 4 in the body of the report.)

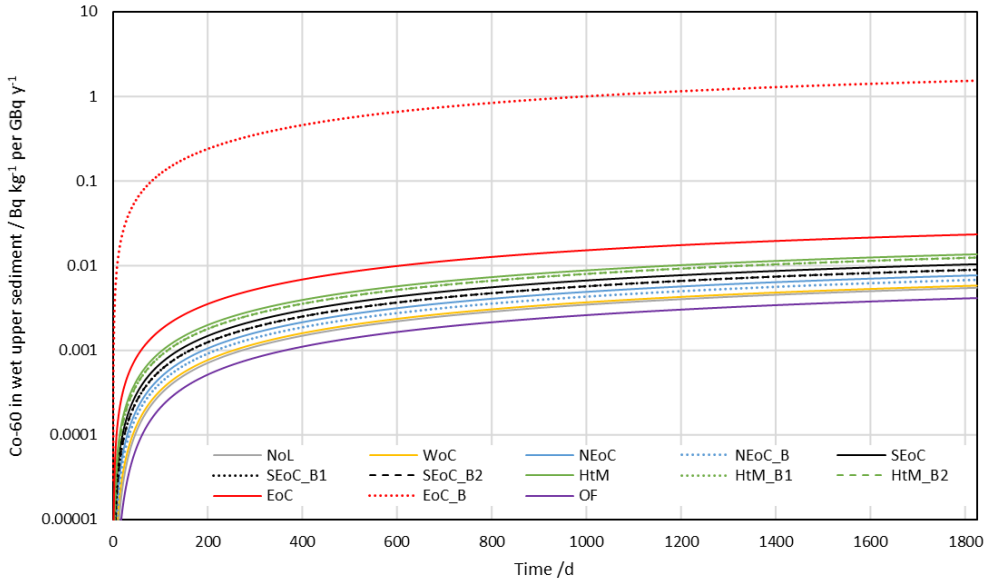

Co-60 concentration in wet top sediment in each region of the Firth of Clyde for five years (current discharge scenario). All compartments approach, but do not reach, equilibrium over this time. (Compartment abbreviations are defined in Table 4 in the body of the report.)

Concentrations of ingrown radionuclides depend on both their own physicochemical and radiological properties and their parent's properties. For example, U-235 ingrows from Pu-239. As Pu-239 builds up in sediment, the rate of ingrowth of U-235 increases. U-235 is less sorbing than Pu-239 and much of the U-235 is released back to seawater. Therefore, U-235 concentrations in seawater continually increase (super-linearly) throughout the model duration (see figure on next page). There is an initial rapid rise in concentration as the Pu-239 concentration in seawater builds up to equilibrium, followed by a slower long-term rise due to Pu-239 build-up in sediment and the partition of ingrown U-235 to seawater.

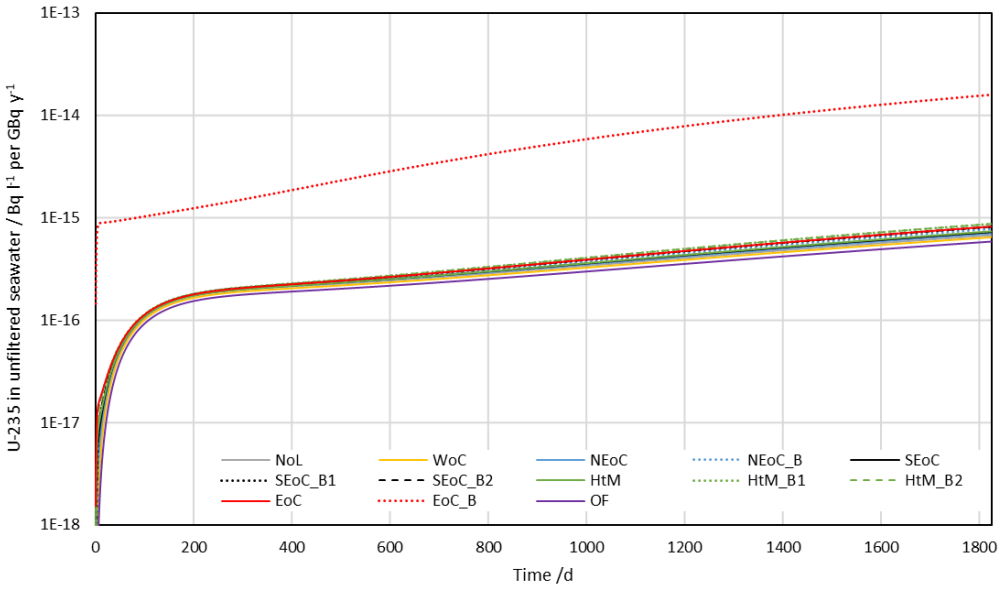

Discharge cycle moving average of U-235 concentration in unfiltered seawater in each region of the Firth of Clyde for five years (current discharge scenario). No compartments reach equilibrium over five years. (Compartment abbreviations are defined in Table 4 in the body of the report.)

Discharges to the current location at lower flow rates or during a different tidal cycle gave similar results to the baseline (current) arrangements. Only discharge to the channel gave different results, and that was only for the compartment where the discharge occurs. These results, together with a dose assessment based on them, will be used by EDF to optimise their new discharge arrangements and apply for the required permit variation.

We compared the results of our compartment model to a model run in PC-CREAM 08 (see figure on page 9). This used the default parameters provided in PC-CREAM 08 for the Hunterston site. Results from our compartment model were several orders of magnitude higher in the bank compartment but around a factor of two lower in the channel compartment than the results from the PC-CREAM 08 model. This is because the bank compartment we modelled is much smaller than the PC-CREAM 08 local compartment, leading to less initial dilution, but the ratio of exchange rate to compartment size in the channel compartment and the exchange rate from the Firth to the Irish Sea (based on Admiralty tidal data) were much greater than for PC-CREAM 08.

This reflects the fact that the channel is not well represented by the “sheltered coastal” parameters used in PC-CREAM 08. However, the rapid mixing and closely clustered concentrations in the Firth of Clyde support the use of the larger, well-mixed local compartment in PC-CREAM 08. Our model also shows a similar pattern of behaviour between different radionuclides as the PC-CREAM 08 model (allowing for the use of an updated distribution coefficient for cobalt).

The agreement between the PC-CREAM 08 model and our model builds confidence in the applicability of the annually and spatially averaged PC-CREAM 08 model to Hunterston (and, therefore, their use to assess the long-term build-up of discharges) and helps verify our model. It shows that the modelled short-term effects such as tidal-cycles and discharge scheduling do not influence the long-term build-up of radionuclides (except in the immediate vicinity of the outfall, the East of Little Cumbrae Bank compartment), but that the use of site-specific hydrography does.

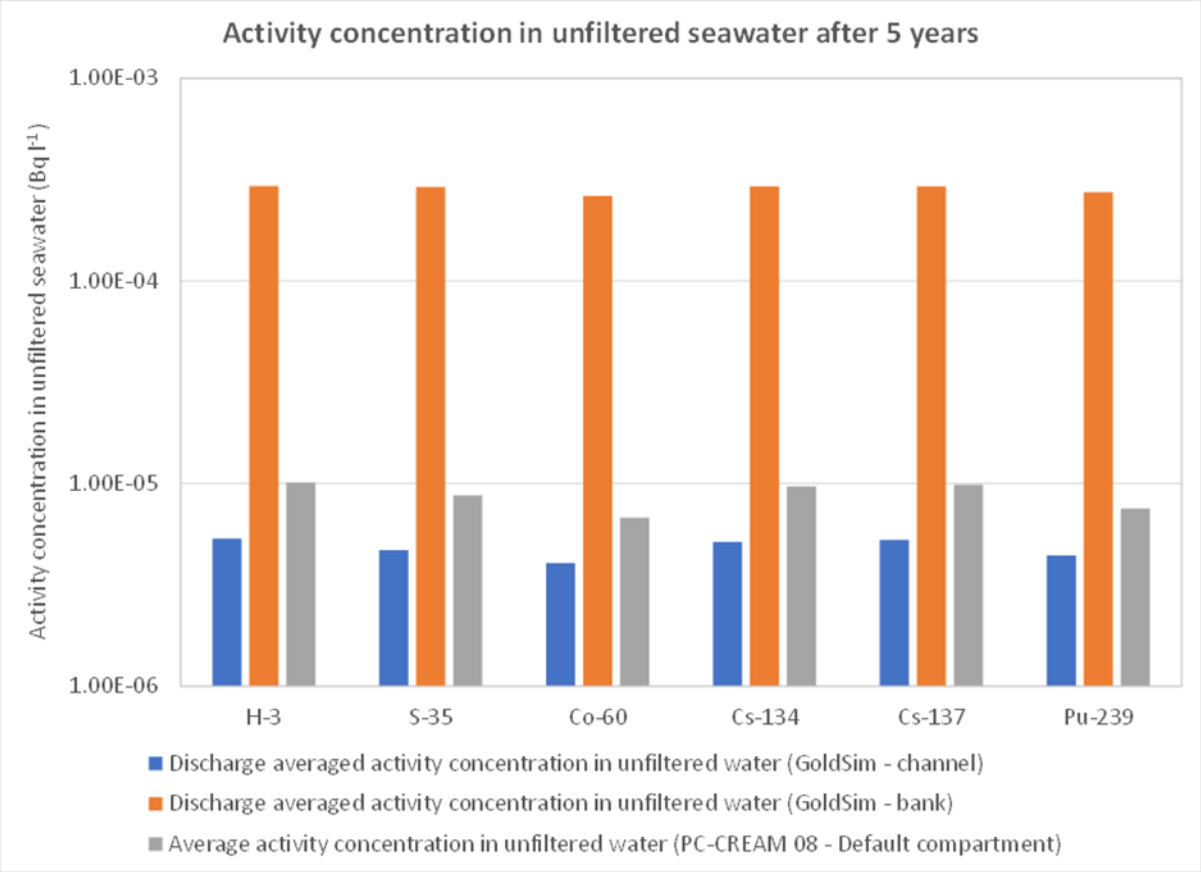

Comparison of activity concentrations in unfiltered seawater after 5 years per unit discharge (1 GBq y^{-1}), calculated in GoldSim and PC-CREAM 08.

Our model can reproduce the results of environmental monitoring of H-3 concentrations following discharges through the current discharge arrangements. The average H-3 concentration measured on the beach near the power stations after discharges is 180 Bq l^{-1}. A model run simulating such discharges calculates unfiltered seawater H-3 concentrations of 118 Bq l^{-1}. This is within a factor of two, which is good agreement for this type of model.

The measured H-3 concentrations have a significant range, from 1183 Bq l^{-1} to 4 Bq l^{-1}, depending on the location of the measurement and the discharge event in question. Much of this variation is likely to be due to the wind speed and direction during the discharge driving unusual marine mixing scenarios. The model does not attempt to simulate varying weather, instead assuming average conditions, nor does it calculate results for areas as localised as the sampling campaign, modelling at the compartment scale only. Therefore we do not expect it to reproduce the extremes of the range, only the average.

We attempted to compare the model to activity concentrations in sediment collected by EDF as part of their district sampling campaign and activity concentrations in sediment and seawater reported in RIFE-27. However, these concentrations are dominated by activity from Sellafield discharges that has migrated northward. Therefore, they are not suitable for comparison with the model results, which consider only discharges from the Hunterston power stations.

This page has been intentionally left blank.

Contents

1 Introduction 19
1.1 Site context 20
1.2 Modelling approaches 21

2 Scenarios 23
2.2 New discharge pipeline 24

3 PC-CREAM 08 model 27
3.1 Model and parameters for Hunterston site 27
3.2 Updated PC-CREAM 08 default parameters 28
3.3 Customised PC-CREAM 08 local compartment 29

4 GoldSim model 31
4.1 Radionuclide transport (including decay and ingrowth) 33
4.2 Flows 35
4.3 Channel compartments 38
4.4 Bank compartments 41
4.5 Discharges 41
4.6 Input data 43
4.6.1 Compartment properties 43
4.6.1.1 Channel water compartments 43
4.6.1.2 Bank water compartments 43
4.6.1.3 Sediment compartments 44
4.6.2 Flows 44
4.6.2.1 Flows between channel compartments 44
4.6.2.2 Flows between channel and bank compartments 45
4.6.2.3 Flows between sediment compartments 45
4.6.2.4 Flows from discharge pipe 45
4.6.3 Source term 46
4.6.4 Radionuclide properties and decay chains 47
4.6.5 Other model data 50
4.6.6 Simulation parameters 51
4.7 Outputs 51
4.8 Using the model 53

5 Results 55
5.1 Scenario 1: baseline 56
5.1.1 Exemplar mobile radionuclide – H-3 56
5.1.2 Exemplar less-mobile radionuclide – Co-60 59
5.1.3 Exemplar daughter radionuclide – U-235 62
5.1.4 Radionuclide concentrations after five years 66
5.2 Scenario 2: alternative discharge scenario to the bank – as baseline, but with low water flow rate through pipe 68
5.2.1 Exemplar mobile radionuclide – H-3 68
5.2.2 Exemplar less-mobile radionuclide – Co-60 70

5.2.3 Exemplar daughter radionuclide – U-235 71
5.2.4 Radionuclide concentrations after five years 73
5.3 Scenario 3: alternative discharge scenario to the bank, with discharges at permit limits 76
5.3.1 Both Hunterston A and Hunterston B discharging at permit limits 76
5.3.2 Hunterston A discharging at permit limits 76
5.3.3 Hunterston B discharging at permit limits 76
5.4 Scenario 4: discharge to the bank during flood tides 85
5.4.1 Exemplar mobile radionuclide – H-3 85
5.4.2 Exemplar less-mobile radionuclide – Co-60 88
5.4.3 Exemplar daughter radionuclide – U-235 90
5.4.4 Radionuclide concentrations after five years 91
5.5 Scenario 5: discharge to the channel with low water flow rate through pipe 94
5.5.1 Exemplar mobile radionuclide – H-3 94
5.5.2 Exemplar less-mobile radionuclide – Co-60 97
5.5.3 Exemplar daughter radionuclide – U-235 99
5.5.4 Radionuclide concentrations after five years 101
5.6 Sensitivity analysis – direct discharge to channel during flood tide 103
5.7 PC-CREAM 08 model results 105

6 Discussion 109
6.1 Interpreting radionuclide concentrations in compartment models 109
6.2 Summary of GoldSim results 110
6.3 Comparison of GoldSim model with PC-CREAM 08 111
6.3.1 Comparison 111
6.4 Confidence building and validation 114
6.4.1 Empirical input data 114
6.4.2 Confidence in underlying models 114
6.4.3 Hunterston site monitoring data 115
6.4.3.1 39” outfall H-3 monitoring 115
6.4.3.2 District sampling – sediment 118
6.4.3.3 *Radioactivity in food and the environment* reports 120
6.4.3.4 Thermal plume monitoring 121

7 Conclusions 123

8 References 125

Appendix A – Additional figures 129
A.1 Tidal flow from the North Channel to the outer Firth of Clyde 129
A.2 Water balance in channel compartments that have flows to bank compartments 130
A.3 Effect of discretisation on interpretation of results 131

Appendix B – Discharge pipe properties 133
B.1 Calculation of discharge start and end times 133
B.2 Other exemplar pipe configurations 134

Appendix C – Further detail on model and derivation of input data 137

C.1 Channel compartment flows 137
C.2 Bank compartment flows 140
C.3 Channel compartment geometry 140
C.4 Bank compartment geometry 143
C.5 Discharge scheduling and conservatism 143
C.6 Calculation of alternative environmental media concentrations 145

Appendix D – Results sampling 147

Appendix E – List of Terms and Acronyms 149

Table of Figures

Figure 1 – Location of Hunterston power stations in Scotland (blue pin). Reproduced from reference [9]. 20
Figure 2 – Hunterston power stations (A and B stations labelled in red) in their immediate surroundings. The cooling water outfall (the current discharge location) is labelled with a red x. Seabed depths are in m at low tide. Adapted from reference [10]. 20
Figure 3 – Decay chains used in PC-CREAM 08 (half-lives in black from PC-CREAM 08 manual [14]; half-lives in red not given in the manual and assumed to be the same as those from reference [31]) 28
Figure 4 – Model in the context of the Firth of Clyde and North Channel (base map reproduced from reference [10]) 31
Figure 5 – Detail of compartments used in the GoldSim model. The boundaries of compartments 1 and 7 extend beyond this map, as shown in Figure 4. Discharges are made to either compartment 6 or 6B (each marked with a red star). (Base map reproduced from reference [10].) 32
Figure 6 – Example of a channel compartment in GoldSim (Hunterston to Millport). The turquoise cells each represent either the water column or a sediment layer. The turquoise arrows between the cells represent radionclude transfer between the water and sediment layers, governed by the terms λ_1 to λ_5 (see equations (25) to (31)). The blue arrows represent advective transport of water and suspended sediment to adjacent compartments (see Subsection 4.2). The yellow containers each represent an adjacent bank compartment, and the turquoise arrows to these containers represent advective transport of water and suspended sediment (see Subsection 4.2). Conceptual model reproduced from reference [14]. 39
Figure 7 – Example of a bank compartment in GoldSim (Hunterston to Millport bank 1). The turquoise cells each represent the water column and the sediment. The turquoise arrows between the cells represent radionclude transfer between the water and sediment layers, governed by the terms λ_1 and λ_2 (see equations (25) and (27)). The blue arrow represents advective transport of water and suspended sediment to the adjacent channel compartment (see Subsection 4.2). Conceptual model adapted from reference [14]. 41
Figure 8 - Decay chains modelled (all branching ratios 1 unless otherwise stated) (decay chains, half-lives and branching ratios updated [27] from reference [31]) 48
Figure 9 – Screenshot of the model interface, or dashboard, in GoldSim Player 54
Figure 10 – Activity concentration of H-3 in unfiltered seawater for baseline scenario (per unit annual discharge) (semi-log plot) 56
Figure 11 – H-3 concentration in unfiltered seawater for East of Little Cumbrae and East of Little Cumbrae Bank compartments and tidal-cycle moving average of H-3 concentrations (semi-log plot) 58

Figure 12 – Tidal-cycle moving average of H-3 concentration in unfiltered seawater for five years (semi-log plot) 59
Figure 13 – H-3 concentration in wet top sediment for five years (semi-log plot) 59
Figure 14 – Activity concentration of Co-60 in unfiltered seawater for baseline scenario (unit annual discharge) (semi-log plot) 60
Figure 15 – Discharge-cycle moving average of Co-60 concentration in unfiltered seawater for five years (semi-log plot) 61
Figure 16 – Co-60 concentration in wet top sediment for five years (semi-log plot) 61
Figure 17 – Co-60 concentration in wet top sediment for five years (linear scale, EoC_B compartment has a different y-axis scale to the other compartments) 62
Figure 18 – Activity concentration of U-235 in unfiltered seawater for baseline scenario (unit annual discharge Pu-239) (semi-log plot) 63
Figure 19 – Discharge-cycle moving average of U-235 concentration in unfiltered seawater for five years (semi-log plot) 63
Figure 20 – Discharge-cycle moving average of U-235 concentration in unfiltered seawater for five years (linear plot) 64
Figure 21 – Build-up of Pu-239 in sediment (the build-up happens in all compartments, but only the East of Little Cumbrae Bank compartment is visible on the scale of this figure) 64
Figure 22 – U-235 concentration in wet top sediment for five years (semi-log plot) 65
Figure 23 – U-235 concentration in wet top sediment for five years (linear scale, EoC_B compartment has a different y-axis scale to the other compartments) 65
Figure 24 – Activity concentration of H-3 in unfiltered seawater for alternative discharge scenario to the bank (per unit annual discharge) (semi-log plot) 68
Figure 25 – Tidal-cycle moving average of H-3 concentration in unfiltered seawater for five years for alternative discharge scenario to the bank (per unit annual discharge) (semi-log plot) 69
Figure 26 – H-3 concentration in wet top sediment for five years for alternative discharge scenario to the bank (per unit annual discharge) (semi-log plot) 69
Figure 27 – Activity concentration of Co-60 in unfiltered seawater for alternative discharge scenario to the bank (per unit annual discharge) (semi-log plot) 70
Figure 28 – Discharge-cycle moving average of Co 60 concentration in unfiltered seawater for alternative discharge scenario to the bank for five years (semi-log plot) 71
Figure 29 – Co-60 concentration in wet top sediment for five years for alternative discharge scenario to the bank (per unit annual discharge) (semi-log plot) 71
Figure 30 – Activity concentration of U-235 in unfiltered seawater for alternative discharge scenario to the bank (per unit annual discharge Pu-239) (semi-log plot) 72
Figure 31 – Discharge-cycle moving average of U-235 concentration in unfiltered seawater for alternative discharge scenario to the bank for five years (semi-log plot) 72
Figure 32 – U-235 concentration in wet top sediment for five years for alternative discharge scenario to the bank (per unit annual discharge) (semi-log plot) 73
Figure 33 – Activity concentration of H-3 in unfiltered seawater for discharge to the bank during flood tides (per unit annual discharge) (semi-log plot) 85
Figure 34 – Comparison of H-3 concentration in East of Little Cumbrae compartment (solid) and adjacent bank compartment (dotted) for discharge during ebb (black – see Subsection 5.2.1) and flood (red) tides 86
Figure 35 – Tidal-cycle moving average of H-3 concentration in unfiltered seawater for five years for discharge to the bank during flood tides (per unit annual discharge) (semi-log plot) 87

Figure 36 – H-3 concentration in wet top sediment for five years for discharge to the bank during flood tides (per unit annual discharge) (semi-log plot)..... 87
Figure 37 – Activity concentration of Co-60 in unfiltered seawater for discharge to the bank during flood tides (per unit annual discharge) (semi-log plot)..... 88
Figure 38 – Tidal-cycle moving average of Co-60 concentration in unfiltered seawater for five years for discharge to the bank during flood tides (per unit annual discharge) (semi-log plot) 89
Figure 39 – Co-60 concentration in wet top sediment for five years for discharge to the bank during flood tides (per unit annual discharge) (semi-log plot)..... 89
Figure 40 – Activity concentration of U-235 in unfiltered seawater for discharge to the bank during flood tides (per unit annual discharge Pu-239) (semi-log plot) 90
Figure 41 – Tidal-cycle moving average of U-235 concentration in unfiltered seawater for five years for discharge to the bank during flood tides (per unit annual discharge Pu-239) (semi-log plot)..... 90
Figure 42 – U-235 concentration in wet top sediment for five years for discharge to the bank during flood tides (per unit annual discharge) (semi-log plot)..... 91
Figure 43 – Activity concentration of H-3 in unfiltered seawater for channel discharges scenario (per unit annual discharge) (semi-log plot) 94
Figure 44 – Comparison of H-3 concentration in East of Little Cumbrae compartment (solid) and adjacent bank compartment (dotted) for bank (black) and channel (red) discharges..... 95
Figure 45 – Tidal-cycle moving average of H-3 concentration in unfiltered seawater for five years for discharge to the channel (per unit annual discharge) (semi-log plot) 96
Figure 46 – H-3 concentration in wet top sediment for five years for discharge to the channel (per unit annual discharge) (semi-log plot)..... 96
Figure 47 – Activity concentration of Co-60 in unfiltered seawater for channel discharges scenario (per unit annual discharge) (semi-log plot) 97
Figure 48 – Tidal-cycle moving average of Co-60 concentration in unfiltered seawater for five years for discharge to the channel (per unit annual discharge) (semi-log plot) 98
Figure 49 – Co-60 concentration in wet top sediment for five years for discharge to the channel (per unit annual discharge) (semi-log plot) 98
Figure 50 – Activity concentration of U-235 in unfiltered seawater for discharge to the channel (per unit annual discharge Pu-239) (semi-log plot)..... 99
Figure 51 – Discharge-cycle moving average of U-235 concentration in unfiltered seawater for discharge to the channel for five years (semi-log plot)..... 100
Figure 52 – U-235 concentration in wet top sediment for five years for discharge to the channel (per unit annual discharge Pu-239) (semi-log plot)..... 100
Figure 53 – Activity concentration of H-3 in unfiltered seawater for discharge to the channel during flood tides (per unit annual discharge) (semi-log plot)..... 103
Figure 54 - Tidal-cycle moving average of H-3 concentration in unfiltered seawater for five years for discharge to the channel during flood tides (per unit annual discharge) (semi-log plot) 104
Figure 55 – Activity concentrations in unfiltered seawater per unit annual discharge (1 GB q y^{-1}) calculated by PC-CREAM 08 for the default Hunterston local compartment (semi-log plot). 105
Figure 56 – Activity concentration in dry sediment per unit annual discharge (1 GBq y^{-1}) calculated by PC-CREAM 08 for the default Hunterston local compartment (semi-log plot). 106

Figure 57 – Comparison of activity concentrations in unfiltered seawater after 5 years per unit discharge (1 GBq y^{-1}), calculated in GoldSim (East of Little Cumbrae and East of Little Cumbrae Bank compartments) and PC-CREAM 08 (log scale)..... 112
Figure 58 – Comparison of activity concentrations in unfiltered seawater after 5 years per unit discharge (1 GBq y^{-1}), calculated in GoldSim (East of Little Cumbrae compartment) and PC-CREAM 08 (linear scale) 112
Figure 59 – Comparison of activity concentrations in dry sediment after 5 years, calculated in GoldSim (East of Little Cumbrae channel compartment) and PC-CREAM 08..... 114
Figure 60 – Aerial photograph showing location of cooling water outfall and 39" outfall (base photograph from reference [39]) 115
Figure 61 – Measured H-3 concentrations (blue points) on the beach to the north and south of the 39" outfall following discharges through the cooling water outfall (maroon bars). Interpolations have been removed where they misleadingly imply a gradual build-up to the discharge peak. Adapted from reference [38]..... 116
Figure 62 – Hunterston district sampling locations for sediment and seaweed (red circles), shown with GoldSim model compartments (red lines). Adapted from reference [41]. 118
Figure 63 – Excerpt from tidal stream atlas showing tidal flow through the North Channel and from the North Channel into the outer Firth as the tide comes in (4 h 20 min before high water at Greenock). Flow speed is in units of 10^{-1} knots (1 knot = 0.5144 m s^{-1} [32]). Flow rates for spring and neap tides are separated by a comma (neap,spring). Reproduced from reference [28]. 129
Figure 64 – Water balance calculations showing the variation in volume in channel compartments due to flow to bank compartments. (The GoldSim model treats all channel compartments as having a constant volume and does not use these results.) 130
Figure 65 – Schematic of a hypothetical plume (blue) from a source (red x), showing how it would be represented in both low- and high-discretisation compartment models. Darker shading represents a higher concentration (not to scale). 131
Figure 66 – Locations for which admiralty tidal stream data are available. Base map reproduced from reference [10]. 137
Figure 67 – Map showing grid used to define the Outer Firth compartment. The numbers in each grid square are depths in m, taken from reference [10]. 141
Figure 68 – Maps showing grids used to define compartments in the Firth of Clyde. The numbers in each grid square are depths in m, taken from reference [10]..... 142
Figure 69 – Timelines showing how the number of discharges per calendar year can vary depending on the juxtaposition between the discharge schedule and the calendar year. 144
Figure 70 – Comparison of the moving average of H-3 concentration over a discharge cycle for the high-resolution (every timestep; that is, every 0.1 h) and low resolution (every ten timesteps; that is every hour) results 147

Table of Tables

Table 1 – Discharge start and end times used in the GoldSim model..... 24
Table 2 – Local compartment parameters for the ‘Hunterston’ compartment in PC-CREAM 08..... 27
Table 3 – Updated recommendations for default PC-CREAM 08 parameter values [25]..... 28
Table 4 – List of compartments used in the GoldSim model..... 32
Table 5 – Summary of advective water flows in GoldSim model (terms defined following the table)..... 37

Table 6 – Channel compartment geometries 43
Table 7 – Bank compartment geometries 43
Table 8 – Tidal flows between channel compartments derived from references [10] and [28] 45
Table 9 – Tidal flows into bank compartments, derived from reference [] 46
Table 10 – Annual discharges used in the model (taken from references [3], [4] and [30]) 47
Table 11 – Radionuclide decay data (decay chains, half-lives and branching ratios based on an updated version [27] of ICRP publication 107 [31]) 49
Table 12 – Distribution coefficients [33] 50
Table 13 – Other data used in the model 50
Table 14 – Concentration of each radionuclide in unfiltered seawater after five years in each compartment for the baseline scenario (discharge cycle moving averages) (Bq l^{-1} per GBq y^{-1}) 66
Table 15 – Concentration of each radionuclide in dry upper sediment (all activity) after five years in each compartment for the baseline scenario (discharge-cycle moving averages) (Bq kg^{-1} per GBq y^{-1}) 67
Table 16 – Concentration of each radionuclide in unfiltered seawater after five years in each compartment for alternative discharge scenario to the bank (discharge cycle moving averages) (Bq l^{-1} per GBq y^{-1}) 74
Table 17 – Concentration of each radionuclide in dry upper sediment after five years in each compartment for alternative discharge scenario to the bank (discharge-cycle moving averages) (Bq kg^{-1} per GBq y^{-1}) 75
Table 18 – Concentration of each radionuclide in unfiltered seawater after five years in each compartment for both stations with alternative discharge scenario to the bank (discharging at permit limits) (discharge cycle moving averages) (Bq l^{-1}) 77
Table 19 – Concentration of each radionuclide in dry upper sediment after five years in each compartment for both stations with alternative discharge scenario to the bank (discharging at permit limits) (discharge cycle moving averages) (Bq kg^{-1}) 79
Table 20 – Concentration of each radionuclide in unfiltered seawater after five years in each compartment for Hunterston A with alternative discharge scenario to the bank (discharging at permit limits) (discharge cycle moving averages) (Bq l^{-1}) 81
Table 21 – Concentration of each radionuclide in dry upper sediment after five years in each compartment for Hunterston A with alternative discharge scenario to the bank (discharging at permit limits) (discharge cycle moving averages) (Bq kg^{-1}) 82
Table 22 – Concentration of each radionuclide in unfiltered seawater after five years in each compartment for Hunterston B with alternative discharge scenario to the bank (discharging at permit limits) (discharge cycle moving averages) (Bq l^{-1}) 83
Table 23 – Concentration of each radionuclide in dry upper sediment after five years in each compartment for Hunterston B with alternative discharge scenario to the bank (discharging at permit limits) (discharge cycle moving averages) (Bq kg^{-1}) 84
Table 24 – Concentration of each radionuclide in unfiltered seawater after five years in each compartment for discharges to the bank during flood tides (discharge cycle moving averages) (Bq l^{-1} per GBq y^{-1}) 92
Table 25 – Concentration of each radionuclide in dry upper sediment after five years in each compartment for discharges to the bank during flood tides (discharge cycle moving averages) (Bq kg^{-1} per GBq y^{-1}) 93
Table 26 – Concentration of each radionuclide in unfiltered seawater after five years in each compartment for discharges to the channel (discharge cycle moving averages) (Bq l^{-1} per GBq y^{-1}) 101

Table 27 – Concentration of each radionuclide in dry upper sediment after five years in each compartment discharges to the channel (discharge cycle moving averages) (Bq kg^{-1} per GBq y^{-1}) 102
Table 28 – PC-CREAM 08 results for the default Hunterston local compartment 107
Table 29 – Measured H-3 concentration at 39" outfall after discharges 116
Table 30 – Comparison of GoldSim results with H-3 concentrations measured at the 39" outfall 117
Table 31 – Measured and modelled radionuclide concentrations around the Firth of Clyde (all in Bq kg^{-1} (dry weight)) 119
Table 32 – Properties of the discharge pipe for each scenario 134
Table 33 – Exemplar pipe configurations 134
Table 34 – Admiralty tidal stream data, from references [10] and [28] 138
Table 35 – Properties of tidal reference points, from references [10] and [28] 138

1 Introduction

There are two power stations at Hunterston, Hunterston A and Hunterston B. Hunterston A is a former Magnox power station that is being decommissioned and is operated by Magnox Ltd [1]. Hunterston B is an advanced gas-cooled reactor (AGR) power station that stopped generating electricity in 2022 and will now be defueled and then decommissioned. It is operated by EDF Energy Nuclear Generation Ltd (EDF) [2].

Both power stations discharge aqueous effluent into the Firth of Clyde through the Hunterston B cooling water outlet, although the discharges from the two stations are governed by separate environmental permits [3,4]. Both permits allow discharges only when the cooling water flow is at least 7 $m^3 s^{-1}$; this is to ensure adequate dilution and dispersion of the radionuclides in the discharges.

Now that electricity generation at Hunterston B has ended, the reactors no longer need a constant, high flow of coolant. It will be expensive to operate and maintain the existing cooling water pumps, and they will eventually need to be decommissioned and removed as the station is decommissioned. Therefore, EDF are considering alternative discharge arrangements that will not need the cooling water flow [5]. Any new discharge arrangements could also be different to the current arrangements in other ways; for example, the discharge outlet may be at a different location or the discharges may be done at different times.

Any new discharge arrangements must be optimised and will require variations to the environmental permits for both Hunterston A and Hunterston B. The current environmental permits restrict [3,4]:

- The amount of activity that may be discharged (which must be less than the annual limits specified for each station)
- The location of the discharges (which must be through the current outfall)
- The flow of water through the outfall while discharging
- The time of the discharges (which must be between 1 hour after high tide and 1 hour before low tide)

EDF have asked us (Eden Nuclear and Environment Ltd) to model the dilution and dispersion in the Firth of Clyde of discharges from Hunterston A and B. This will allow them to understand the environmental performance of the existing discharge arrangements and how varying parameters such as discharge time, volumetric flow rate and discharge location affect this performance. They will use this understanding to help them assess the engineering options for the discharge system [5] to ensure that their new arrangements are optimised. They will also use it as the basis for a dose assessment to support their application to vary their environmental permit.

The model includes discharges from both A and B stations as the discharge system must be optimised for both sets of discharges. The discharges from each station can also be considered separately, as they will need to be assessed separately for each environmental permit variation. The dispersion model and this report have been prepared for EDF. EDF are responsible for designing and optimising the discharge arrangements (as the discharge system is part of the Hunterston B infrastructure) and for applying for the permit variation for Hunterston B. Magnox Ltd will be responsible for applying for the permit variation for Hunterston A; specific consideration of Hunterston A is outside the scope of this report.

1.1 Site context

The Hunterston power stations are located on the Firth of Clyde estuary on the west coast of Scotland, as shown in Figure 1. Details of their immediate vicinity, including seabed topography and outfall location, are shown in Figure 2. The power stations and outfall are opposite the island of Little Cumbrae, which is separated from the mainland by a channel that is around 50 m deep. The outfall is around 300 m from the shore in water between 0.3 m and 3.3 m deep. The outfall location reflected best practice at the time of construction. More details about the environmental setting of the site, including marine habitats and protected areas, are given in references [6], [7] and [8].

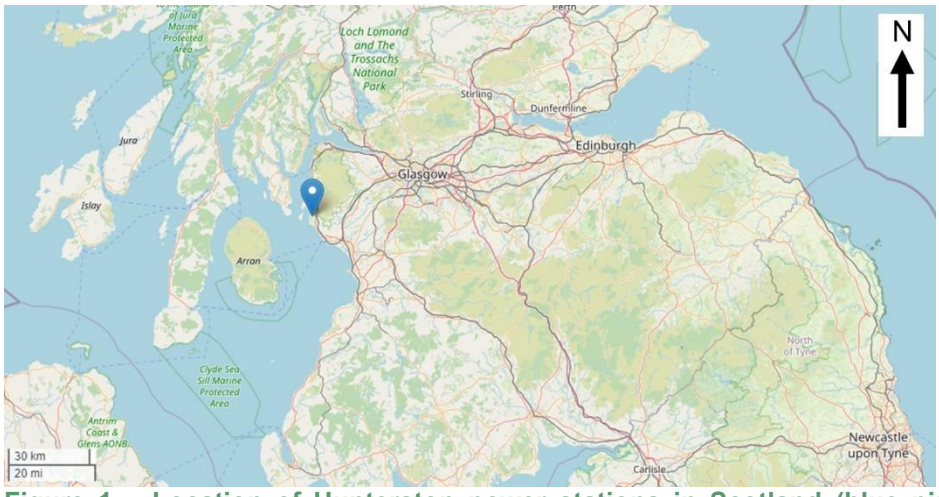

Figure 1 – Location of Hunterston power stations in Scotland (blue pin). Reproduced from reference [9].

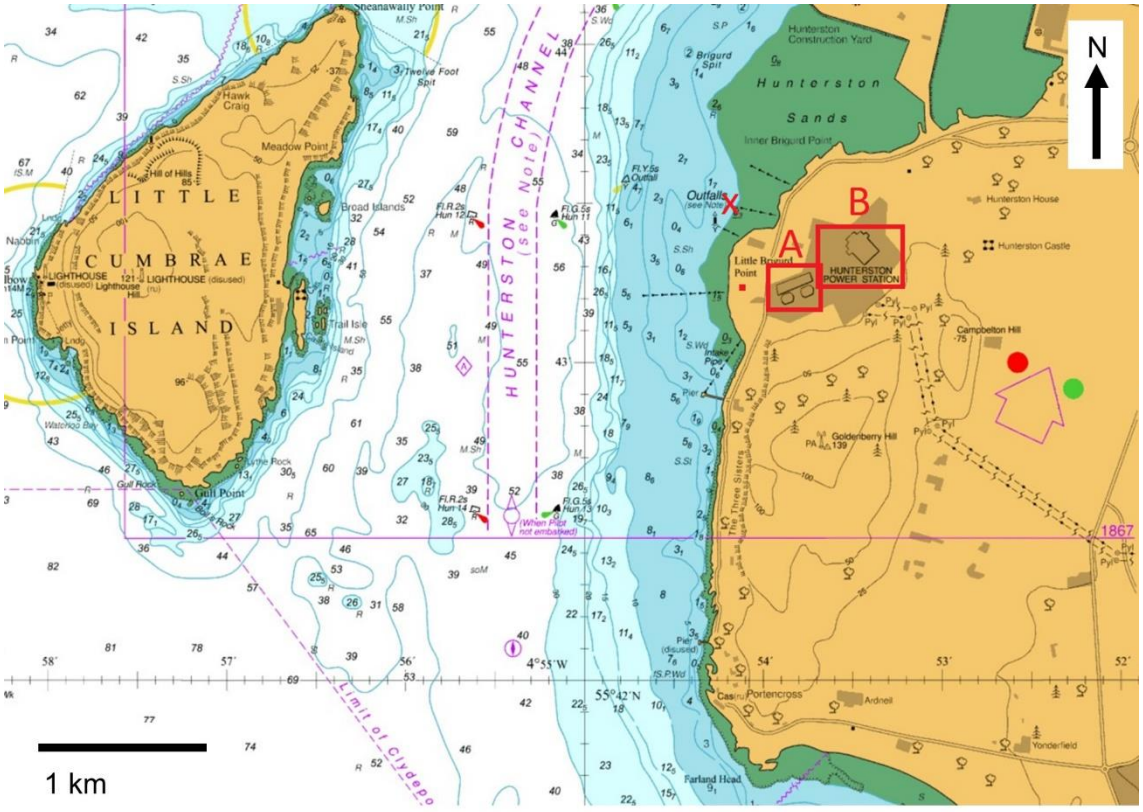

Figure 2 – Hunterston power stations (A and B stations labelled in red) in their immediate surroundings. The cooling water outfall (the current discharge location) is labelled with a red x. Seabed depths are in m at low tide. Adapted from reference [10].

Details of human habits around the sites can be found in references [11], [12] and [13].

1.2 Modelling approaches

The aim of this work was to model the dilution and dispersion of radionuclides in the Firth of Clyde, given different discharge parameters (location, time and volumetric flow rate). To do this, we used two models:

1. A large-scale, time-averaged compartment model, implemented using the commercial software package PC-CREAM 08 [14]

2. A bespoke compartment model of the Firth of Clyde, with greater temporal and spatial resolution (capable of modelling individual tidal cycles), implemented using GoldSim [15]

PC-CREAM 08 is developed by the UK Health Security Agency and is the standard software used to assess the dispersion and consequences of routine radionuclide releases to the environment. Its use is widely accepted by regulators. PC-CREAM 08 modelling is widely used to support environmental permit applications and optimisation assessments. Examples of use of PC-CREAM 08 for similar assessments include assessing aqueous discharges from new-build nuclear power stations [16,17] and during site decommissioning [18,19].

The river and marine models used by PC-CREAM 08 are compartment models. The marine model (the dispersion of radionuclides in seas – DORIS – model) comprises a local compartment (5×10^9 m^3 for Hunterston) that exchanges with a regional marine model. It uses annually averaged releases and exchange rates. This temporal and spatial averaging may not be appropriate for a highly dynamic estuarine environment and would not allow modelling of the discharge time window in the permit. Therefore, we developed a bespoke model to allow us to:

- Investigate the effect of discharging at different times in the tidal cycle

- Investigate the effect of discharging in the deep channel or shallower banks

- Investigate the effect of the volumetric flow rate (the cooling water, for the current discharge scenario) on concentrations near the discharge point

- Model radionuclide build-up in different regions of the Firth of Clyde to validate the applicability to the Firth of the spatial averaging in PC-CREAM 08, identify any regions of concern and demonstrate that radionuclides do dilute in and disperse from the Firth

- Investigate the effect of tidal cycles on radionuclide build-up, to determine whether the PC-CREAM 08 time-averaged model gives the same results as a model that considers tidal cycles

We developed this model in GoldSim [15]. GoldSim is numerical simulation software widely used for modelling radionuclide and contaminant transport in the environment. The GoldSim model is a compartment model based on the same principles as PC-CREAM 08, but with much higher spatial and temporal resolutions and a much more site-specific conceptual model. The GoldSim model is intended to be run over relatively short timescales (less than a year to a few years), while PC-CREAM 08 is intended to be run for medium- to long-term timescales (a few years to many years).

A detailed description of the PC-CREAM 08 model is given in Section 3 and reference [14]. A detailed description of the GoldSim model is given in Section 4.

Both models used in this study are compartment models. There are other approaches for radionuclide transport modelling in marine environments, such as hydrodynamic modelling. We have used compartment models in this study because:

- They are routinely used for modelling radionuclide discharges in support of optimisation assessments and to justify discharge limits for radioactive substances authorisations and permits [16-19].

- Studies of radionuclide transport have found agreement between the results of compartment models, hydrodynamic models and measured data [20,21].

- Compartment models are proportionate to the understanding of and data about the Firth of Clyde available to us.

This work considered radionuclide dispersion. The results are, therefore, radionuclide concentrations in environmental media at different times and in different places (for example, $Bq\,l^{-1}$ in unfiltered seawater). We did not assess doses or do other assessments of the consequences of the discharges. Such assessments will be done separately, if required.

2 Scenarios

We agreed with EDF five different discharge scenarios to assess in the GoldSim model. These scenarios cover the range of parameters that EDF may vary when specifying the new discharge system. They are intended to allow EDF to understand how varying parameters such as the discharge window or discharge location may affect dispersion.

The scenarios do not directly correspond to the engineering options EDF are considering [5] or may develop. Instead, they are focussed on understanding how the relevant parameters of the discharge system influence dispersion. From this, the performance of the options being considered may be derived. This approach allows EDF to add to or change their options without further modelling.

The scenarios modelled are:

1. Baseline scenario: current system with discharges to the bank[1] during ebb tides with a continuous flow of cooling water (unit discharges)

2. Alternative discharge to the bank: discharges to the bank during ebb tides with a low flow rate of water through the pipe while discharging (and no flow of water through the pipe when not discharging) (unit discharges)

3. Scenario 2 with site limits for A station and B station: as Scenario 2, (discharges from both power stations at the annual limits set in their permits [3,4])

4. Scenario 2 with discharges during the flood tide: as Scenario 2, but with discharges during the flood tide, rather than the ebb tide (unit discharges)

5. Discharge to the channel: discharges further from shore (to deeper water)[1] during ebb tides with a low flow rate of water through the pipe while discharging (and no flow of water through the pipe when not discharging) (unit discharges)

The model can be easily configured to run other scenarios or change the parameters of these scenarios if needed (see Subsection 4.8).

We modelled one discharge every three tides (that is, 243 or 244 per year). This was based on the frequency of recent discharges [22]. The annual discharges modelled (whether permitted or unit) were split evenly between these discharges (see Subsection 4.5 and 4.6.3).

The discharge start and finish times used in GoldSim for each scenario are given in Table 1. These are the times that radionuclides start and stop entering the Firth of Clyde from the outfall. These are different to the times that discharges are initiated and ended at the station because the effluent will take time to travel through the discharge pipe and because some residual effluent may be discharged from the system after discharges formally cease. Their derivation is explained in Appendix B.1.

[1] The banks are shallow water compartments overlying a single layer of sediment. They exchange only with their adjacent channel compartments. They represent sheltered areas of the shoreline, including the current discharge point. See Figure 5.

Table 1 – Discharge start and end times used in the GoldSim model

Scenario	Description	Start of release into Firth (h after HT)	End of release into Firth (h after HT)
1. Current operational system	Discharge of unit activity to bank during ebb tide; continuous flow of water through pipe at 7 $m^3 s^{-1}$*	1.3	4.5
2. Alternative discharge line into the bank	Discharge of unit activity to bank during ebb tide; water flow through pipe of 0.0086 $m^3 s^{-1}$** while discharging and 0 $m^3 s^{-1}$ the rest of the time	1.4	4.6
3. Scenario 2 with site limits for A station and B station	Discharge at permitted limits to bank during ebb tide; water flow through pipe of 0.0086 $m^3 s^{-1}$** while discharging and 0 $m^3 s^{-1}$ the rest of the time	1.4	4.6
4. Scenario 2 with discharges in the flood tide	Discharge of unit activity to bank during flood tide; water flow through pipe of 0.0086 $m^3 s^{-1}$** while discharging and 0 $m^3 s^{-1}$ the rest of the time	7.4	10.6
5. Alternative discharge line into the channel	Discharge of unit activity to channel during ebb tide; water flow through pipe of 0.0086 $m^3 s^{-1}$** while discharging and 0 $m^3 s^{-1}$ the rest of the time	1.8	5.0

*7 $m^3 s^{-1}$ is specified as the minimum flow rate in the existing permit.

**0.0086 $m^3 s^{-1}$ is the rate at which the final delay tanks can be emptied.

In all scenarios, the following assumptions are made:

- Activity is discharged at a constant rate within the GoldSim discharge window and no activity is discharged otherwise.
- Water flow through the pipe is at a constant rate while flowing and no water flows from the pipe otherwise.[2]
- The outfall is always submerged.
- Temperature differences between the effluent and sea will not significantly affect contaminant dispersion on the scales of interest.

Prevailing weather conditions (particularly wind conditions) are accounted for in the tidal flows used (see Subsection 4.6.2), and transient weather conditions are not modelled.

2.2 New discharge pipeline

Scenarios 2 to 5 assume that a new discharge pipeline has been installed. For Scenarios 2 to 4, we assume that the discharge point and pipeline length are the same as for the existing pipeline. This represents a new pipeline that follows the route of the existing pipeline. For Scenario 5, the discharge point is in the deeper channel, and the pipeline must extend beyond the existing route.

[2] In particular, we assume that the water flow rate though the pipe is not affected by changes in head at the discharge point as the tide changes.

We have calculated representative flow rates and travel times for Scenarios 2 to 4 and for Scenario 5 based on discharge systems with plausible specifications (such as pipe size and water velocity – see Appendix B). The actual parameters of the new discharge system will be a matter for the engineering design of the new system. The only requirements from a dilution and dispersion perspective are that:

- It must be able to discharge the full volume of effluent and purge water[3] within the discharge window.
- The flow velocity must be high enough to prevent sedimentation (perhaps between 0.75 and 1.8 m s^{-1} [23]).
- It must be compatible with operational and safety requirements.

The derivation of the representative flow rate and travel time for the new discharge pipeline is given in Appendix B.1. Other plausible system configurations are given in Appendix B.2.

[3] Discharges may be considered complete once the purge water reaches the outfall. However, the system will have had to discharge the equivalent volume of standing water before effluents reached the outfall. Thus, the minimum flow rate is *(purge volume+effluent volume)/duration of tidal window*.

This page has been intentionally left blank.

3 PC-CREAM 08 model

3.1 Model and parameters for Hunterston site

PC-CREAM 08 uses the DORIS model to represent dispersion of radionuclides in a marine environment. The conceptual and mathematical models used by PC-CREAM 08 are described in Subsection 4.4 of reference [14]. We set up a model using the Hunterston local compartment and the Scottish Waters W. regional compartment. We used the DORIS model in its default configuration (as in the database supplied with the software). This is the configuration used in other PC-CREAM 08 assessments by EDF of Hunterston B [24]. Table 2 summarises the PC-CREAM 08 local compartment parameters used.

Table 2 – Local compartment parameters for the 'Hunterston' compartment in PC-CREAM 08

Parameter	Default PC-CREAM 08 Hunterston compartment [14]
Volume /m^3	5.00×10^{9}
Depth /m	2.00×10^{1}
Coastline length /m	3.00×10^{4}
Volumetric exchange rate /m^3 y^{-1}	1.00×10^{11}
Suspended sediment load /t m^{-3}	1.00×10^{-5}
Sedimentation rate /t m^{-2} y^{-1}	1.00×10^{-4}
Sediment density /t m^{-3}	2.60
Diffusion rate /m^2 y^{-1}	3.15×10^{-2}

The relevant radionuclides (H-3, S-35, Co-60, Sr-90, Cs-134 (surrogate for other beta/gamma radionuclides), Cs-137, Pu-239 (surrogate for alpha radionuclides) and Pu-241) were considered at a unit discharge rate of 1 GBq y^{-1}. Pu-239 was considered in conjunction with its daughters U-235, Pa-231 and Ac-227; Pu-241 was considered in conjunction with its daughters Am-241, Np-237, U-233 and Th-229. Some short-lived daughters that we model explicitly in GoldSim are not included in the PC-CREAM 08 model. This is because PC-CREAM 08 does not allow us to customise the decay chains modelled. Instead, these daughters are assumed to be in secular equilibrium with their parents. They are Th-231, U-237 and Pa-233. The decay chains used in PC-CREAM 08 are shown in Figure 3.

Activity concentrations in unfiltered seawater and seabed sediment were reported for the output times 1 year, 2 years, 5 years, 10 years, and 50 years. Output times up to 5 years were used to compare the results with the results produced with the GoldSim model. PC-CREAM 08 reports activity concentrations in dry seabed sediment, including the activity associated with porewater.

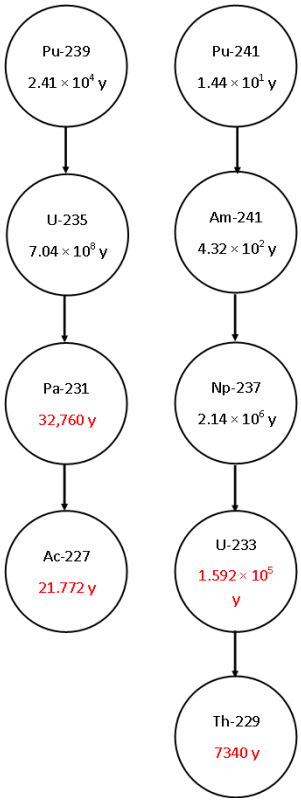

Figure 3 – Decay chains used in PC-CREAM 08 (half-lives in black from PC-CREAM 08 manual [14]; half-lives in red not given in the manual and assumed to be the same as those from reference [31])

3.2 Updated PC-CREAM 08 default parameters

In 2019, Public Health England published recommendations for updated default parameter values for the local marine compartments in PC-CREAM 08 [25]. These recommendations were based on Environment Agency measurements of hydrographic parameters at sites around England and Wales [26]. To maintain consistency with previous PC-CREAM 08 assessments of Hunterston B, we did not use the parameters. However, we briefly discuss them and what affect they would have had on the model.

The recommendations for the Hunterston local compartment are given in Table 3. They treat Hunterston as a sheltered coastal site, rather than an estuarine site.

Table 3 – Updated recommendations for default PC-CREAM 08 parameter values [25]

Parameter	Old value [14]	New value [25]
Volume /m^3	5.00×10^9	1.00×10^9
Exchange rate /$m^3\ y^{-1}$	1.00×10^{11}	2.00×10^{10}
Coastline length /m	3.00×10^4	1.00×10^4
Suspended sediment load /$t\ m^{-3}$	1.00×10^{-5}	1.00×10^{-5}
Sedimentation rate /$t\ m^{-2}\ y^{-1}$	1.00×10^{-4}	2.00×10^{-4}

The compartment volume and volumetric exchange rate have been reduced. As a result, the dilution factor (the approximate steady-state concentration per unit continuous release) has increased from 3.7×10^{-9} Bq m^{-3} per Bq d^{-1} to 1.8×10^{-8} Bq m^{-3} per Bq d^{-1} [25]. The new exchange rate assumes that 90% of the exchanged water returns to its compartment of origin

and only 10% of the exchanged water is truly from or lost to the other compartment. Only this 10% contributes to the net exchange of contaminants.[4] The suspended sediment loading has remained the same, but the sedimentation rate has been doubled.

The increased dilution factor would lead to higher radionuclide concentrations in water, particularly for less sorbing radionuclides. The increased sedimentation rate would lead to more removal of radionuclides to the lower sediment layers. Water concentrations and top sediment concentrations would, therefore, be expected to reduce, and this effect would be most pronounced for sorbing radionuclides.

There is no immediate need to remodel with the new PC-CREAM data. The new default exchange rate is a factor 5 lower, so using a rule of thumb we can predict that the activity concentrations calculated by PC-CREAM with the new values would be a factor 5 higher. The PC-CREAM model, covering all bank and channel compartments would still provide results between the GoldSim EoC_B and EoC results. It is not certain that the proposed values will be used in the new version of PC-CREAM.

3.3 Customised PC-CREAM 08 local compartment

We attempted to run PC-CREAM 08 with local compartment properties based on the GoldSim East of Little Cumbrae compartment. We hoped to:

- Compare the results of PC-CREAM 08 and GoldSim models with the same volumetric exchange rate (relative to the size of the local compartment – in PC-CREAM 08 – or the nearby channel compartment - GoldSim) to understand how much of the difference between the results of the two models was due to the site-specific input data and how much was due to the more detailed model

- Compare the results of PC-CREAM 08 and GoldSim models with similar amount of spatial averaging near the outfall

Running PC-CREAM 08 with a small local compartment and (relatively) high volumetric exchange did not produce sensible results. In Figure 58, both the GoldSim and default PC-CREAM 08 results share a consistent pattern of behaviour in the concentrations of different radionuclides (the same pattern is also present in the results in Figure 57, which includes the results for the bank compartment, but is less obvious because of the log scale of the plot). However, running PC-CREAM 08 with a small, high-exchange compartment gave seawater activity concentrations that were almost the same for all radionuclides. This suggests that the PC-CREAM 08 model does not function correctly for these input parameters.

There are two relevant conceptual differences between the PC-CREAM 08 and GoldSim models:

- The GoldSim model discretises the Firth of Clyde into several compartments. Although these compartments are well mixed, the whole Firth of Clyde need not be. The PC-CREAM 08 model with the small local compartment uses a single, well-mixed regional compartment to represent the Firth of Clyde. Exchange between local and regional compartments on this scale may require the increased discretisation of the GoldSim model to be represented correctly.

[4] As we model transfer between much smaller compartments, such recycling is implicit in our GoldSim model.

- The large regional compartment in the PC-CREAM 08 model means that the exchange of radionuclides into the local compartment from the regional compartment will be very low (as the concentrations in the regional compartment will be very low due to its large volume). In the GoldSim model, the greater discretisation means the neighbouring compartments are smaller and will have greater radionuclide concentrations. This means there will be appreciable exchange of radionuclides into the East of Little Cumbrae compartment from its neighbours. This also means that exchange between local and regional compartments on this scale may require the increased discretisation of the GoldSim model to be represented correctly.

It is, however, unlikely that a need for greater discretisation alone explains the differences observed. We would expect this to affect all radionuclides similarly and, therefore, maintain the general pattern in the results. The absence of this pattern suggests a more fundamental incompatibility between these parameters and the PC-CREAM 08 DORIS model.

4 GoldSim model

Most equations in this section are given in terms of activity (Bq). GoldSim is a mass transport model, and the equations in Subsection 4.1 are given in terms of mass. To convert between activity units and mass units, use the species specific activity, defined in Equation (38).

The GoldSim model is a compartment model. We divided the Firth of Clyde into a series of compartments, as shown in Figures 4 and 5 and Table 4. There are channel compartments, which represent the main estuary, and bank compartments, which represent the shore near Hunterston. The channel compartments have flow along the estuary, while the bank compartments do not. Some aspects of the model, such as the water-sediment interactions are based on the PC-CREAM 08 model.

Water containing dissolved radionuclides and suspended sediment (with sorbed radionuclides) is transferred between the channel compartments, as indicated by the arrows in, and between channel compartments and their adjacent bank compartments. Radionuclides in each compartment are partitioned between the solution phase, suspended sediment and bed sediments. Discharges are modelled by adding radionuclides and water to either the East of Little Cumbrae compartment (compartment 6 in Figure 5) or the East of Little Cumbrae Bank compartment (compartment 6B in Figure 5 (depending on the scenario being modelled).

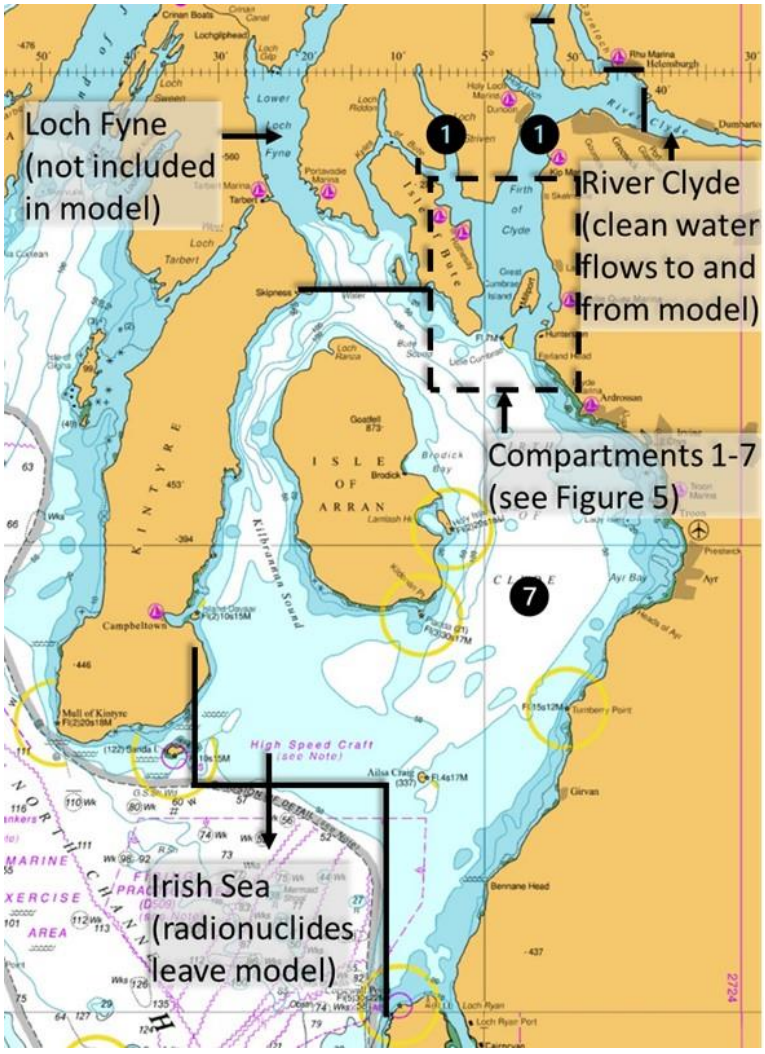

Figure 4 – Model in the context of the Firth of Clyde and North Channel (base map reproduced from reference [10])

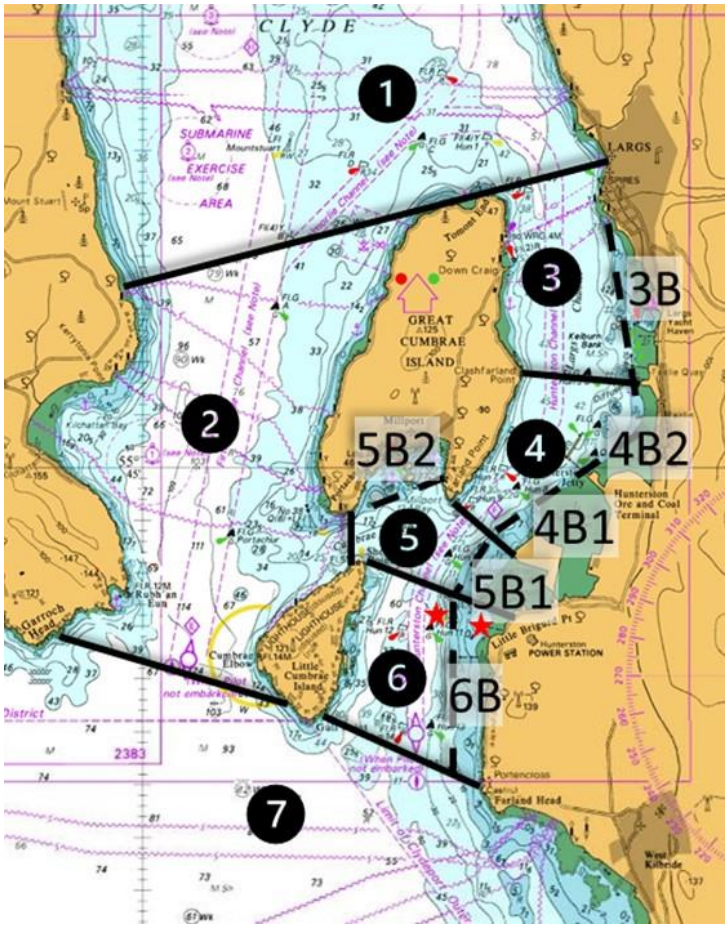

Figure 5 – Detail of compartments used in the GoldSim model. The boundaries of compartments 1 and 7 extend beyond this map, as shown in Figure 4. Discharges are made to either compartment 6 or 6B (each marked with a red star). (Base map reproduced from reference [10].)

Table 4 – List of compartments used in the GoldSim model

Compartment number (Figure 5)	Compartment name	Compartment abbreviation
1	North of Largs	NoL
2	West of Cumbrae	WoC
3	Northeast of Great Cumbrae	NEoC
3B	Northeast of Great Cumbrae Bank	NEoC_B
4	Southeast of Great Cumbrae	SEoC
4B1	Southeast of Great Cumbrae Bank 1	SEoC_B1
4B2	Southeast of Great Cumbrae Bank 2	SEoC_B2
5	Hunterston to Millport	HtM
5B1	Hunterston to Millport Bank 1	HtM_B1
5B2	Hunterston to Millport Bank 2	HtM_B2
6	East of Little Cumbrae	EoC
6B	East of Little Cumbrae Bank	EoC_B
7	Outer Firth	OF

4.1 Radionuclide transport (including decay and ingrowth)

GoldSim uses a radionuclide mass-balance model. The change in radionuclide mass in each cell is calculated over a discrete timestep. This change accounts for the flows in and out of the cells (Subsection 4.2), radioactive decay and ingrowth and the direct input of radionuclides (which, in this model, represents the discharges).

The GoldSim mass transport equations are given in the GoldSim contaminant transport module user's manual and are summarised here. The equations given here have been simplified to remove terms not used by our model.

Equation (1) gives the mass of a species in a GoldSim cell at time *t*.

$$m_{\mathrm{is},t} = m_{\mathrm{is,prev}} + m'_{\mathrm{is}} \cdot \Delta t \qquad (1)$$

Here:

$m_{\mathrm{is},t}$ is mass of species s in cell i at time *t* (kg);

$m_{\mathrm{is,prev}}$ is mass of species s in cell i at the previous timestep (initial value 0 kg);

m'_{is} is the rate of increase of mass of species s in cell i (kg h^{-1});

Δt is the length of the timestep (h). .

Equation (2) is the overall mass balance equation for a GoldSim cell [27].

$$m'_{\mathrm{is}} = -m_{is}\lambda_s + \sum_{p=1}^{\mathrm{NP_s}} (m_{\mathrm{ip}}\lambda_p f_{ps} A_{\mathrm{s}}/A_P) + \sum_{c=1}^{\mathrm{NF_i}} f_{cs} + S_{\mathrm{is}} \qquad (2)$$

Here:

m_{is} and m_{ip} are the masses of species s and parent p in cell i (kg) (see Equation (1));

λ_{s} and λ_p are the decay constants for species s and parent *p* (h^{-1}) (see Table 11);

NP_s is the number of direct parents for species s (dimensionless) (see decay chains in Figure 8);[5]

f_{ps} is the branching ratio for ingrowth of species s from parent *p* (dimensionless) (see Table 11);

A_{s} and A_p are the atomic masses of species s and parent *p* (kg mol^{-1}) (10^{-3} × the mass number of the isotopes);

NF_i is the number of mass flux links to or from cell i (dimensionless) (see Subsections 4.2, 4.3 and 4.4);

f_{cs} is the influx rate of species s (into cell i) through mass flux link *c* (kg h^{-1}) (see Equations (3) and (4));

[5] To allow the results to be used for dose assessments in terms of the discharged radionuclides, we define different species for all daughter radionuclides with different discharged ultimate parents. Therefore, the only situation where a species has more than one direct parent (NP > 1) is where a chain branches and then reconverges. This applies to Np-237, which is a daughter of Am-241 and U-237, which are both daughters of Pu-241.

S_{is} is direct input of species s to cell i (the discharges, see Equation (34)) (kg h^{-1}).

Exchange between water cells is modelled as advective flow. Equation (3) is the mass transport equation for advective flow [27].

$$f_{s,i\rightarrow j} = c_{iws} \cdot q + c_{is} \cdot \alpha_i \cdot q \quad (3)$$

Here:

$f_{s,i\rightarrow j}$ is the advective mass flux of species s from cell i to cell j (kg h^{-1});

c_{iws} is total dissolved, sorbed or precipitated concentration of species s in medium m in cell i (kg m^3) (see Equation (5));

q is the advective flow rate of the medium from cell i to cell j (m^3 h^{-1}) (see Table 5);

c_{is} is the sorbed concentration of species s on suspended sediment in cell i (kg kg^{-1}) (see Equation (7));

α_i is the suspended sediment loading in cell i (0.01 kg m^{-3}) (see Table 13);

For cell pathways (the type of GoldSim element used in our model), a negative advective flow is treated as a flow in the opposite direction to that specified. For other types of GoldSim element, a negative advective flow would result in an error.

Exchange between water and sediment cells and between sediment cells and other sediment cells is modelled as direct transfer (that is, transfer of radionuclides without flow of a host material such as water or sediment). Equation (4) is the mass transport equation for direct transfer [27].

$$f_{s,i\rightarrow j} = T_{ij,s} \cdot m_{is} \quad (4)$$

Here:

$f_{s,i\rightarrow j}$ is the direct transfer mass flux of species s from cell i to cell j (kg h^{-1});

$T_{ij,s}$ is the fractional transfer of mass of species s from cell i to cell j (h^{-1}) (see Equations (25) to (31)).

Equation (5) gives the concentration of radionuclides dissolved in water in cell i [27].

$$c_{iws} = m_{is}/(V_{iw} + k_{ds} \cdot M_{is}) \quad (5)$$

Here:

c_{iws} is the concentration of species s dissolved in water in cell i (kg m^{-3});

V_{iw} is the volume of water in cell i (m^3) (see Table 6 and Equation (54));

k_{ds} is the water-sediment distribution coefficient for species s (m^3 kg^{-1}) (see Table 12);

M_{is} is the total mass of sediment in cell i (kg) (see Equations (35) and (36)).

Equation (6) gives the concentration of radionuclides in sediment (whether suspended or not) in a cell [27].

$$c_{is} = m_{is} \cdot k_{ds}/(V_{iw} + k_{ds} \cdot M_{is}) \quad (6)$$

Here:

c_{is} is the concentration of species s in sediment in cell i (kg kg^{-1}).

Equation (7) gives the total concentration of radionuclides in water in a cell with water and suspended sediment (but no other sediment) [27].

$$c_{\mathrm{tot,iws}} = c_{\mathrm{iws}} + c_{\mathrm{is}} \cdot M_{\mathrm{is}}/V_{\mathrm{iw}} \quad (7)$$

Here:

$c_{tot,iws}$ is the concentration of species s in water (both dissolved and sorbed to suspended sediment) in cell i (kg m^{-3});

4.2 Flows

Advective water flows between the compartments carry dissolved radionuclides and suspended sediment with sorbed radionuclides between adjacent compartments. There are:

- Flows between adjacent channel compartments
- Flows between channel compartments and adjacent banks
- Water flows in and out of the model boundaries:
    - Clean water flows in and out upstream (in and out of the North of Largs compartment)
    - Clean water flows into the model downstream (into the Outer Firth compartment)
    - Contaminated water flows out of the model downstream (out of the Outer Firth compartment) to maintain water balance and represent the interaction of the Firth of Clyde with the Irish Sea
- Additional water flows to represent the outflow from the pipe (included because the water flow rate in the baseline scenario – 7 m^3 s^{-1} – has a significant cumulative effect on long-term water balance, although it is small compared to the tidal flows and, thus, has limited influence on dilution and dispersion)

These flows are described in more detail in the remainder of this subsection.

The flows between adjacent channel compartments are based on hourly tidal flow data; their derivation is explained in Subsection 4.6.2.1. The tidal flows are net flows. That is, they account for any river current in the estuary. These flows maintain water balance (that is, the net effect of the flows does not change the total volume of water) in all channel compartments except the North of Largs and Outer Firth compartments. These compartments represent boundaries of the model, and water flows in and out of the model are added to maintain the water balance.

The North of Largs compartment is at the upstream end of the model. Water would flow between this compartment and the upstream Clyde. Contaminants would leave the modelled area as the tide comes in, and some would return as the tide goes back out. As we do not model the upstream Clyde, we have no way of calculating the return flux of contaminants in the ebb current. Hence, we do not model the flow of contaminants in or out of the upstream

Clyde. Instead, the model approximates this by adding[6] and removing clean water to and from the boundary compartments to maintain water balance. This is preferable to removing an advective flow of contaminated water as the tide comes in, since doing so would remove it from the system.

The Outer Firth compartment is at the downstream end of the model. Water would flow between this compartment and the Irish Sea and Atlantic Ocean, via the North Channel (see Figure 1 and Figure 4). Given the relatively small magnitude of flows into the Firth from the North Channel (compared to flows through the North Channel) (see Appendix A.1), only a very small proportion of activity transferred from the Firth to the North Channel would be returned to the Firth when the tide changes. Therefore, this return can be ignored, and we model either a flow of contaminated water from the Outer Firth to the North Channel or a flow of clean water from the North Channel to the Outer Firth, as required to maintain the water balance in the Outer Firth.

The flows between the bank and channel compartments are based on the tide heights; their derivation is explained in Subsection 4.6.2.2. The flows are cyclic, with the flood and ebb currents cancelling each other out over a cycle. Therefore, the bank flows do not result in cumulative volume changes over time. The cyclic fluctuations are significant compared to the volumes of the bank compartments. Therefore, the volume of water in the bank compartments is varied with time to maintain water balance in the bank compartments. The cyclic fluctuations are small relative to the volumes of the channel compartments (see Appendix A.2). Therefore, the volume of water in the channel compartments is not varied to account for flows to the banks; that is, water balance is not maintained in the channel compartments.[6]

The current minimum cooling water flow is a continuous 7 $m^3 s^{-1}$ (25,200 $m^3 h^{-1}$) [3,4]. This is significant for cumulative water balance, although it is small compared to the tidal flows (and so has limited influence on dilution and dispersion). We account for it by adding the water flow through the pipe to the following flows:

- From the East of Little Cumbrae Bank compartment to the East of Little Cumbrae compartment
- From the East of Little Cumbrae compartment to the Outer Firth compartment
- From the Outer Firth compartment to the Irish Sea (that is, the water balance flow out of the model)

The cooling water for Hunterston B is abstracted from the East of Little Cumbrae compartment. This is not represented in the model.

Table 5 summarises the advective flows between the compartments.

[6] GoldSim automatically adds clean water to and removes clean water from cells when the inflows and outflows mean the volume of the compartment deviates from that specified (whether a constant or a function) [27].

Table 5 – Summary of advective water flows in GoldSim model (terms defined following the table)

Compartments	Flow /$m^3\ h^{-1}$	
North of Largs to upstream (out of model) (clean water only)*	$-F_{T,NoL\_WoC} - F_{T,NoL\_NEoC}$	(8)
North of Largs to West of Cumbrae	F_{T,NoL_WoC}	(9)
West of Cumbrae to Outer Firth	F_{T,WoC_OF}	(10)
North of Largs to Northeast of Great Cumbrae	F_{T,NoL_NEoC}	(11)
Northeast of Great Cumbrae to bank	$F_{B,\ NEoC}$	(12)
Northeast of Great Cumbrae to Southeast of Great Cumbrae	$F_{T,NEoC\_SEoC}$	(13)
Southeast of Great Cumbrae to bank 1	$F_{B,\ SEoC1}$	(14)
Southeast of Great Cumbrae to bank 2	$F_{B,\ SEoC2}$	(15)
Southeast of Great Cumbrae to Hunterston to Millport	$F_{T,SEoC\_HtM}$	(16)
Hunterston to Millport to bank 1	$F_{B,\ HtM1}$	(17)
Hunterston to Millport to bank 2	$F_{B,\ HtM2}$	(18)
Hunterston to Millport to West of Cumbrae	F_{T,HtM_WoC}	(19)
Hunterston to Millport to East of Little Cumbrae	F_{T,HtM_EoC}	(20)
East of Little Cumbrae to bank	$F_{B,\ EoC} - F_{P,B}$	(21)
East of Little Cumbrae to Outer Firth	$F_{T,EoC\_OF} + F_{P,B} + F_{P,C}$	(22)
Outer Firth to Irish Sea (contaminated water, ebb current only)**	$F_{T,WoC\_OF} + F_{T,EoC\_OF} + F_{P,B} + F_{P,C}$ if >0, else 0	(23)
Irish Sea to Outer Firth (clean water, flood current only)**	$-F_{T,WoC\_OF} - F_{T,EoC\_OF} - F_{P,B} - F_{P,C}$ if >0, else 0	(24)

Positive flows are in the direction stated in the term (or in the compartments column, for a net flow); negative flows are in the opposite direction [27].

*The clean water flood current is added automatically by GoldSim to maintain the compartment volume.

**These flows are cautious as they do not account for the component of the flow between the Outer Firth and Irish Sea that does not enter the compartments upstream of the Outer Firth. This reduces exchange between the model and the Irish Sea.

Here:

$F_{T,compartment1\_compartment2}$ is the tidal flow from compartment one to compartment two ($m^3\ h^{-1}$) (function of time; see Table 8);

$F_{B,compartmentx}$ is the flow from the stated channel compartment to its associated bank compartment x ($m^3\ h^{-1}$) (function of time; see Table 9);

$F_{P,B}$ is the water flow discharged from a pipe in the East of Little Cumbrae Bank compartment ($m^3\ h^{-1}$) (varies with time; see Subsection 4.6.2.4) (if $F_{P,C} > 0$, $F_{P,B} = 0$);

$F_{P,C}$ is the water flow discharged from a pipe in the East of Little Cumbrae compartment ($m^3\ h^{-1}$) (varies with time; see Subsection 4.6.2.4) (if $F_{P,B} > 0$, $F_{P,C} = 0$).

4.3 Channel compartments

The structure of the channel compartments is based on the PC-CREAM 08 marine compartment model [14]. They comprise a single, well-mixed water compartment and three sediment compartments, representing upper, middle and deep sediment. The water column compartment contains water and suspended sediment, and the sediment compartments contain sediment and porewater.

Radionuclide transfer between the water and sediment compartments is modelled, representing:

- Particle scavenging
- Molecular diffusion
- Porewater mixing
- Particle mixing
- Sedimentation

The deep sediment compartment is a sink. Activity in this compartment is assumed to not re-enter the system and not be accessible from the natural environment. Therefore, activity is only transferred into (not out of) this compartment, and no activity concentrations can be determined for it.

The channel compartment properties (size and material content) are described in Subsection 4.6.1.1.

A diagram of this model is given in Figure 6. The transfer of activity between the water and sediment layers (λ_1 to λ_5 in Figure 6) is identical to that in PC-CREAM 08. Equations for the fractional transfer of activity between compartments follow.

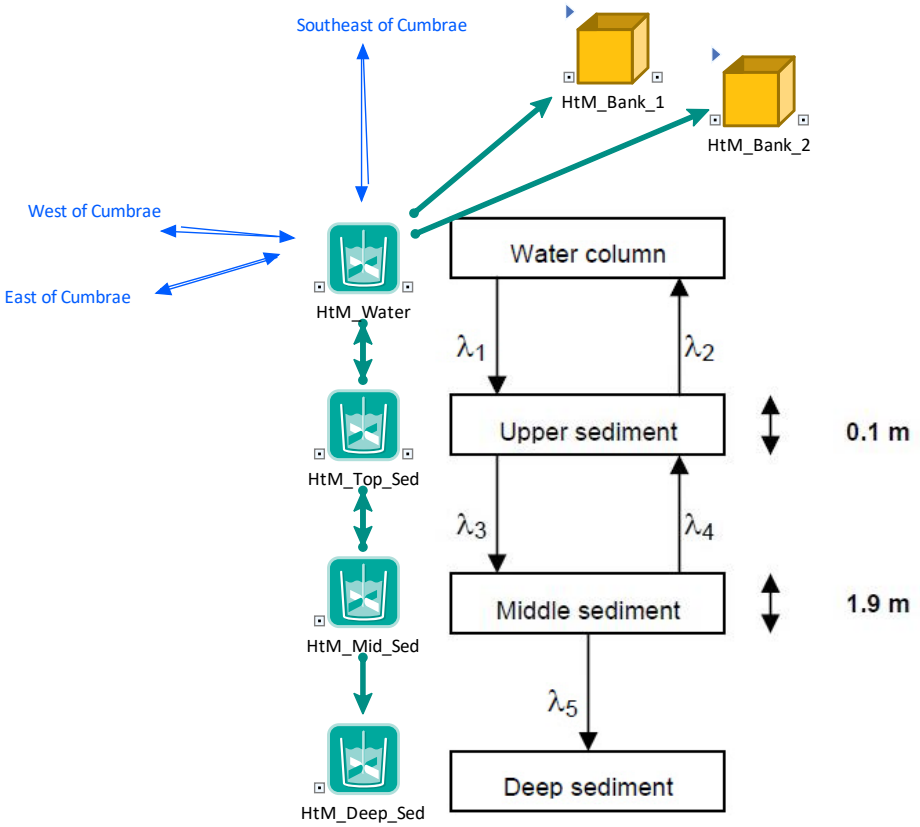

Figure 6 – Example of a channel compartment in GoldSim (Hunterston to Millport). The turquoise cells each represent either the water column or a sediment layer. The turquoise arrows between the cells represent radionclude transfer between the water and sediment layers, governed by the terms λ_1 to λ_5 (see equations (25) to (31)). The blue arrows represent advective transport of water and suspended sediment to adjacent compartments (see Subsection 4.2). The yellow containers each represent an adjacent bank compartment, and the turquoise arrows to these containers represent advective transport of water and suspended sediment (see Subsection 4.2).[7] Conceptual model reproduced from reference [14].

Fractional transfer of activity from water to upper sediment (λ_1) is given by:

$$\lambda_1 = (\mathrm{SR} \cdot k_\mathrm{d} + (D/L_\mathrm{t}) + R_\mathrm{T} \cdot \varepsilon \cdot L_\mathrm{t} + R_\mathrm{w} \cdot \rho_\mathrm{b} \cdot k_\mathrm{d})/(\mathrm{WD} \cdot (1 + k_\mathrm{d}\alpha)) \qquad (25)$$

Here:

λ_1 is the transfer of activity from water to upper sediment, as a fraction of total activity in the water (y^{-1});

SR is the sedimentation rate (0.0001 te m^{-2} y^{-1}) (see Table 13);

k_d is the sediment distribution coefficient for each radionuclide (m^3 t^{-1}) (see Table 12);

D is the sediment diffusion coefficient (0.0315 m^2 y^{-1}) (see Table 13);

L_t is the thickness of the upper sediment layer (0.1 m) (see Table 13);

R_T is the porewater turnover rate for shallow seas (up to 200 m deep) (1 y^{-1}) (see Table 13);

[7] This is bidirectional, despite the arrows being single-headed.

ε is the sediment porosity (0.75, dimensionless) (see Table 13);

R_w is the sediment reworking rate for shallow seas (up to 200 m deep) (5×10^{-3} m y^{-1}) (see Table 13);

ρ_b is the bulk density of the sediment (0.65 te m^{-3}) (see equation (26));

WD is the depth of the water layer (m) (see Subsection 4.6.1);

α is the suspended sediment load (1×10^{-5} te m^{-3}) (see Table 13).

This equation considers particle scavenging, molecular diffusion, porewater mixing and particle mixing.

The sediment bulk density, ρ_b (t m^{-3}), is given by:

$$\rho_b = \rho \cdot (1 - \varepsilon) \quad (26)$$

Here:

ρ is the sediment mineral (or grain) density (2.6 te m^{-3}) (see Table 13).

Fractional transfer of activity from upper sediment to water (λ_2) is given by:

$$\lambda_2 = D \cdot F_S/(L_t^2 \cdot \varepsilon) + R_T \cdot F_S + R_w \cdot (1 - F_S)/L_t \quad (27)$$

Here:

λ_2 is the transfer of activity from upper sediment to water, as a fraction of total activity in the top sediment (y^{-1});

F_S is the inverse of the reciprocal of the retardation coefficient (dimensionless) (see equation (28)).

This equation considers molecular diffusion, porewater mixing and particle mixing.

The inverse of the reciprocal of the retardation coefficient, F_S (dimensionless), is given by:

$$F_S = 1/(1 + k_d \cdot \rho_b/\epsilon) \quad (28)$$

Fractional transfer of activity from upper sediment to middle sediment (λ_3) is given by:

$$\lambda_3 = (1 - F_S) \cdot SR/(\rho_b \cdot L_t) + D \cdot F_S/L_t^2 \quad (29)$$

This equation considers sedimentation and diffusion.

Fractional transfer of activity from middle sediment to upper sediment (λ_4) is given by:

$$\lambda_4 = D \cdot F_S/(L_m \cdot L_t) \quad (30)$$

Here:

L_m is the thickness of the middle sediment (1.9 m) (see Table 13).

This equation considers diffusion.

Fractional transfer of activity from middle sediment to deep sediment (λ_5) is given by:

$$\lambda_5 = (1 - F_S) \cdot \mathrm{SR}/(\rho_b \cdot L_m) \quad (31)$$

This equation considers sedimentation.

The advective flow of radionuclides in the water column to adjacent compartments and banks is described in Subsection 4.2.

4.4 Bank compartments

The bank compartments are based on a simplified version of the PC-CREAM 08 marine compartment model [14]. They comprise a single, well-mixed water compartment and a single top sediment compartment. Radionuclide transfer between the water and sediment compartments is modelled. A diagram of this model is given in Figure 7.

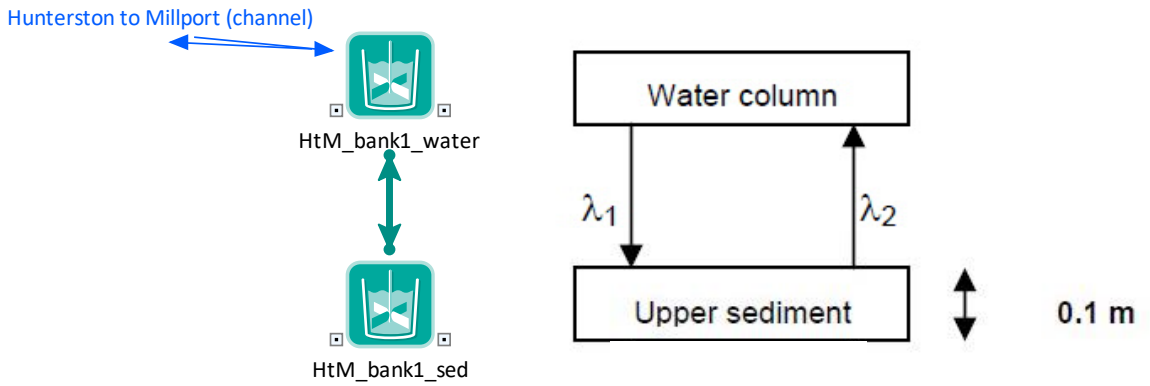

Figure 7 – Example of a bank compartment in GoldSim (Hunterston to Millport bank 1). The turquoise cells each represent the water column and the sediment. The turquoise arrows between the cells represent radionclude transfer between the water and sediment layers, governed by the terms λ_1 and λ_2 (see equations (25) and (27)). The blue arrow represents advective transport of water and suspended sediment to the adjacent channel compartment (see Subsection 4.2). Conceptual model adapted from reference [14].

The transfer of activity between the water and upper sediment (λ_1 and λ_2) is the same as it is for the channel compartments (equations (25) and (27)). No transfer from the upper sediment to the middle or deep sediments is modelled.

The bank compartments have a dynamic volume, to simulate the effect of high and low tide (see Equation (54)).[8] The bank compartment properties (initial water volume and material content) are described in Subsection 4.6.1.2.

4.5 Discharges

Discharges are modelled by direct addition of radionuclides to the receiving compartment (East of Little Cumbrae or East of Little Cumbrae Bank, depending on the scenario being modelled) while the model time is inside the discharge window specified. During this window, radionuclides are added at a constant rate (kg h^{-1}). This rate is determined by splitting the

[8] This is not simulated for the channel compartments. They have a much greater volume than the bank compartments, and the tidal changes are much less as a proportion of the total volume. See Subsection 4.2 and Appendix A.2.

annual discharge for each station (see Table 8) evenly between the total number of discharges per year from that station. The discharges are spaced regularly throughout the year. This is done according to Equations (29) to (31).

The frequency of discharges (for each station), $f_{d,}$ (discharge once in every f_d tidal cycles) is:

$$f_{\mathrm{d}} = 730/N_{\mathrm{d,u}} \quad (32)$$

Here (for each station):

730 is the number of tidal cycles per year (two per day);

$N_{d,u}$ is the number of discharges per year, (243 per year – see Section 2).

The actual number of discharges modelled per year, $N_{d,a}$, is:[9]

$$N_{\mathrm{d,a}} = 730/f_{\mathrm{d,int}} \quad (33)$$

Here (for each station):

$f_{d,int}$ is f_d (see Equation (53)) rounded to the nearest integer.

The activity release rate while discharging (GBq h^{-1}), A_{rr}, is;

$$A_{\mathrm{rr}} = A_{\mathrm{a}}/(N_{\mathrm{d,a}} \cdot D_{\mathrm{d}}) \quad (34)$$

Here (for each radionuclide from each station):

A_a is the total annual discharge (GBq) (see Table 10);

$N_{d,a}$ is the actual number of discharges per year modelled (see Equation (33)) with an option in the model to round this down (explained in Appendix C.5);

D_d is the discharge duration (h).

To calculate the contaminant release rate (A_{rr}), the model provides two options:

1. Use non-integer $N_{d,a}$
2. Conservatively round $N_{d,a}$ down to the nearest integer

The reason for providing this choice and the differences between these two options are discussed in Appendix C.5. Option 1 models regular discharges at a rate that, averaged over time, matches the annual discharges (A_a) in Table 10. Usually, this will be the most appropriate option to use. Option 2 is a highly conservative option that prevents the discharges modelled in any given year ever falling below the annual discharges in Table 10, with the consequence that the average annual discharge modelled will exceed the annual discharges in Table 10.

[9] For computational reasons, the model is constrained to discharge at regular intervals which must be an integer number of tidal cycles. This means only certain numbers of discharges per year can be modelled (every tidal cycle = 730 discharges per year, every other cycle = 365 discharges per year, every third cycle = 243 or 244 discharges per year *etc*).

4.6 Input data

4.6.1 Compartment properties

4.6.1.1 Channel water compartments

Table 6 summarises the channel compartment geometries. Their derivation is described in Appendix C.3.

Table 6 – Channel compartment geometries

Compartment	Depth /m	Area /m^2	Volume /m^3
North of Largs	38.2	1.79×10^8	6.83×10^9
West of Cumbrae	52.0	3.00×10^7	1.56×10^9
Northeast of Great Cumbrae	34.0	6.00×10^6	2.04×10^8
Southeast of Great Cumbrae	32.2	5.00×10^6	1.61×10^8
Hunterston to Millport	21.6	5.00×10^6	1.08×10^8
East of Little Cumbrae	40.7	6.00×10^6	2.44×10^8
Outer Firth	49.2	2.42×10^9	1.19×10^{11}

The mass of suspended sediment in each water compartment is calculated as follows:

$$M_{SS} = \alpha \cdot V \quad (35)$$

Here:

M_{SS} is the mass of suspended sediment in the compartment (kg);

α is the suspended sediment load (0.01 kg m^{-3}) (see Table 13).

4.6.1.2 Bank water compartments

Table 7 summaries the bank compartment geometries. Their derivation is described in Appendix C.4.

Table 7 – Bank compartment geometries

Compartment	Depth (at high tide) /m	Area /m^2	Volume (at high tide) /m^3
Northeast of Great Cumbrae Bank	7.38	6.07×10^5	4.49×10^6
Southeast of Great Cumbrae Bank 1	7.38	1.85×10^6	1.37×10^7
Southeast of Great Cumbrae Bank 2	7.38	9.78×10^5	7.22×10^6
Hunterston to Millport Bank 1	7.38	1.32×10^6	9.72×10^6
Hunterston to Millport Bank 2	7.38	8.34×10^5	6.16×10^6
East of Little Cumbrae Bank	7.38	1.89×10^6	1.40×10^7

The mass of suspended sediment in each water compartment is given by Equation (35).

4.6.1.3 Sediment compartments

The upper and (for channel compartments) middle sediment compartments have the same area as the corresponding water compartment (see Tables 6 and 7). Top sediment compartments are 0.1 m deep and middle sediment compartments are 1.9 m deep, which are generic sediment depths used in PC-CREAM 08 [14].

The mass of sediment in each upper and middle sediment compartment is calculated as follows:

$$M_S = A \cdot L \cdot \rho_B \quad (36)$$

Here:

M_S is the mass of sediment in the compartment (kg);

A is the area of the compartment (m^2) (see Tables 6 and 7);

L is the thickness of the compartment (0.1 m for top sediment and 1.9 m for middle sediment) (see Table 13);

ρ_b is the sediment bulk density (650 kg m^{-3}) (see Equation (26)).

The volume of sediment porewater in each upper and middle sediment compartment is calculated as follows:

$$V_{PW} = A \cdot L \cdot \varepsilon \quad (37)$$

Here:

V_{PW} is the volume of sediment porewater (m^3);

ε is the sediment porosity (0.75; dimensionless) (see Table 13).

The deep sediment compartment is a sink. We assume that radionuclides do not migrate from the deep sediment to the upper layers and that it is inaccessible to the environment. It contains an arbitrary mass of sediment and volume of porewater.

4.6.2 Flows

4.6.2.1 Flows between channel compartments

Advective flow between the channel compartment was based on tidal flow data taken from Admiralty charts [10] and an Admiralty tidal stream atlas [28]. Their derivation is described in Appendix C.1.

Table 8 summarises the tidal flows between the channel compartments. There are other contributions to some of the flows modelled in GoldSim. The total flows between each of the model compartments are given in Table 5.

Table 8 – Tidal flows between channel compartments derived from references [10] and [28]

h after high water	Flow (see Subsection 4.2) ($m^3\ h^{-1}$)							
	F_{T,NoL_WoC}	F_{T,WoC_OF}	F_{T,NoL_NEoC}	$F_{T,NEoC\_SEoC}$	$F_{T,SEoC\_HtM}$	F_{T,HtM_WoC}	F_{T,HtM_EoC}	F_{T,EoC_OF}
0	-7.72×10^7	-4.30×10^7	-3.62×10^6	-3.62×10^6	-3.62×10^6	3.42×10^7	-3.78×10^7	-3.78×10^7
1	3.44×10^7	5.32×10^7	1.88×10^7	1.88×10^7	1.88×10^7	1.88×10^7	0	0
2	1.62×10^8	1.63×10^8	3.90×10^7	3.90×10^7	3.90×10^7	1.28×10^6	3.77×10^7	3.77×10^7
3	1.98×10^8	2.04×10^8	4.35×10^7	4.35×10^7	4.35×10^7	6.04×10^6	3.74×10^7	3.74×10^7
4	2.02×10^8	1.82×10^8	3.98×10^7	3.98×10^7	3.98×10^7	-2.08×10^7	6.05×10^7	6.05×10^7
5	1.17×10^8	5.76×10^7	2.46×10^7	2.46×10^7	2.46×10^7	-5.89×10^7	8.35×10^7	8.35×10^7
6	6.68×10^5	-3.08×10^7	-1.48×10^7	-1.48×10^7	-1.48×10^7	-3.14×10^7	1.66×10^7	1.66×10^7
7	-1.13×10^8	-1.27×10^8	-3.41×10^7	-3.41×10^7	-3.41×10^7	-1.35×10^7	-2.06×10^7	-2.06×10^7
8	-1.47×10^8	-1.56×10^8	-3.04×10^7	-3.04×10^7	-3.04×10^7	-8.35×10^6	-2.21×10^7	-2.21×10^7
9	-1.47×10^8	-1.29×10^8	-2.60×10^7	-2.60×10^7	-2.60×10^7	1.81×10^7	-4.42×10^7	-4.42×10^7
10	-1.20×10^8	-9.35×10^7	-2.44×10^7	-2.44×10^7	-2.44×10^7	2.67×10^7	-5.11×10^7	-5.11×10^7
11	-9.72×10^7	-7.02×10^7	-1.88×10^7	-1.88×10^7	-1.88×10^7	2.70×10^7	-4.58×10^7	-4.58×10^7

The tidal flows in Table 8 are specified at hourly intervals. These are interpreted as the flow from the time specified until the next hourly interval. Thus flow at 3 h after high water is interpreted as flow between 3 h after high water and 4 h after high water. The model does not interpolate flows between the values specified in Table 8.

4.6.2.2 Flows between channel and bank compartments

Bank compartments are assumed to be dominated by flow into and out of the channel arising from the ebb and flood currents, rather than by flow along the shore. Therefore, the only tidal flows modelled for the bank compartments are flows into and out of the adjacent channel compartment. Their derivation is described in Appendix C.2.

Table 9 summarises the tidal flows into and out of the bank compartments. There are other contributions to some of the flows modelled in GoldSim. The total flows between each of the model compartments are given in Table 5.

The tidal flows in Table 9 are specified at hourly intervals. These are interpreted as the flow from the time specified until the next hourly interval. Thus flow at 3 h after high water is interpreted as flow between 3 h after high water and 4 h after high water. The model does not interpolate flows between the values specified in Table 9.

4.6.2.3 Flows between sediment compartments

We do not explicitly model exchange between adjacent sediment compartments. Instead, this is accounted for by the exchange between sediment compartments and the overlying water column and advective flow between the water columns of different compartments.

4.6.2.4 Flows from discharge pipe

The water flows from the discharge pipe are defined in Table 1 and Appendix B.1.

Table 9 – Tidal flows into bank compartments, derived from reference [29]

h after high water	Flow (see Subsection 4.2) ($m^3\ h^{-1}$)					
	$F_{B,\ NEoC}$	$F_{B,\ SEoC1}$	$F_{B,\ SEoC2}$	$F_{B,\ HtM1}$	$F_{B,\ HtM2}$	$F_{B,\ EoC}$
0	0	0	0	0	0	0
1	-2.90×10^5	-8.82×10^5	-4.66×10^5	-6.28×10^5	-3.98×10^5	-9.01×10^5
2	-2.90×10^5	-8.82×10^5	-4.66×10^5	-6.28×10^5	-3.98×10^5	-9.01×10^5
3	-2.90×10^5	-8.82×10^5	-4.66×10^5	-6.28×10^5	-3.98×10^5	-9.01×10^5
4	-2.90×10^5	-8.82×10^5	-4.66×10^5	-6.28×10^5	-3.98×10^5	-9.01×10^5
5	-2.90×10^5	-8.82×10^5	-4.66×10^5	-6.28×10^5	-3.98×10^5	-9.01×10^5
6	0	0	0	0	0	0
7	2.90×10^5	8.82×10^5	4.66×10^5	6.28×10^5	3.98×10^5	9.01×10^5
8	2.90×10^5	8.82×10^5	4.66×10^5	6.28×10^5	3.98×10^5	9.01×10^5
9	2.90×10^5	8.82×10^5	4.66×10^5	6.28×10^5	3.98×10^5	9.01×10^5
10	2.90×10^5	8.82×10^5	4.66×10^5	6.28×10^5	3.98×10^5	9.01×10^5
11	2.90×10^5	8.82×10^5	4.66×10^5	6.28×10^5	3.98×10^5	9.01×10^5

4.6.3 Source term

The model offers three options for the annual discharge activity modelled:

- unit activity (1 GBq y^{-1}) (both stations)
- annual discharge limits from the station permits (both stations) [3,4]
- forecast annual discharges during defueling (Hunterston B only) [30]

The radionuclides considered for each station are those listed in the permit. Additionally, we model Cs-134 as a surrogate for the other beta-gamma emitters (*"any non-alpha emitting radionuclides taken together excluding those listed individually in this table"* [3,4]) category in the permits and Pu-239 as a surrogate for the other alpha emitters category. We chose these surrogates for consistency with the approach used by EDF in other radiological assessments [24]. We also included discharges of Sr-90 from Hunterston A and Cs-137 from Hunterston B in the unit activity discharges. This was based on experience that these radionuclides can be significant for Magnox and AGR discharges, respectively, and (for Cs-137) previous radiological assessments by EDF [24].

The model results for unit annual discharges can be linearly scaled in proportion with activity to consider other annual discharge amounts.

To allow the results to be used for dose assessments in terms of the discharged radionuclides, we define different species for all daughter radionuclides with different discharged ultimate parents. In the model and in Section 5 we use the notation *daughter_parent* to indicate this (parent being the ultimate discharged parent, not the direct parent). For example Ac-227_Pu-239 denotes Ac-227 ingrown from Pu-239.

Table 10 – Annual discharges used in the model (taken from references [3], [4] and [30])

Radionuclide	Unit activity (GBq y^{-1})		Permit limits (GBq y^{-1}) [3,4]		Defueling forecast (GBq y^{-1}) [30]
	Hunterston A	Hunterston B	Hunterston A	Hunterston B	Hunterston B
H-3[a]	1	1	30	700,000	4512
S-35		1		6000	11.2
Co-60		1		10	1.1
Sr-90	1				
Cs-134[b]	1	1	60	150	25.4
Cs-137	1	1	160		
Pu-239[c]	1	1	2	1	0.2
Pu-241	1		2		

[a]Assumed to be in the form of tritiated water

[b]Surrogate for other beta-gamma emitters

[c]Surrogate for other alpha emitters

To allow discharges from the two stations to be assessed separately, we add a letter to the end of this notation to indicate the station the parent was discharged from. Thus, S-35_B denotes S-35 discharged from Hunterston B, and Ac-227_Pu-239_A denotes Ac-227 ingrown from Pu-239 discharged from Hunterston A.

4.6.4 Radionuclide properties and decay chains

Table 10 lists the radionuclides considered. Figure 8 shows the decay chains modelled. All other radionuclides are assumed to decay directly to stable progeny or be in secular equilibrium with their daughters (in which case, the daughters are not modelled explicitly).

These decay chains are based on the GoldSim database, with the addition of explicit consideration of Th-231, U-237 and Pa-233. We have added these radionuclides with relatively short half-lives as this model considers shorter timescales than many assessments. The half-lives and branching ratios are the GoldSim default values [27]. These are based on an updated version of International Commission on Radiological Protection (ICRP) publication 107 [31].

Table 11 summarises the decay data used.

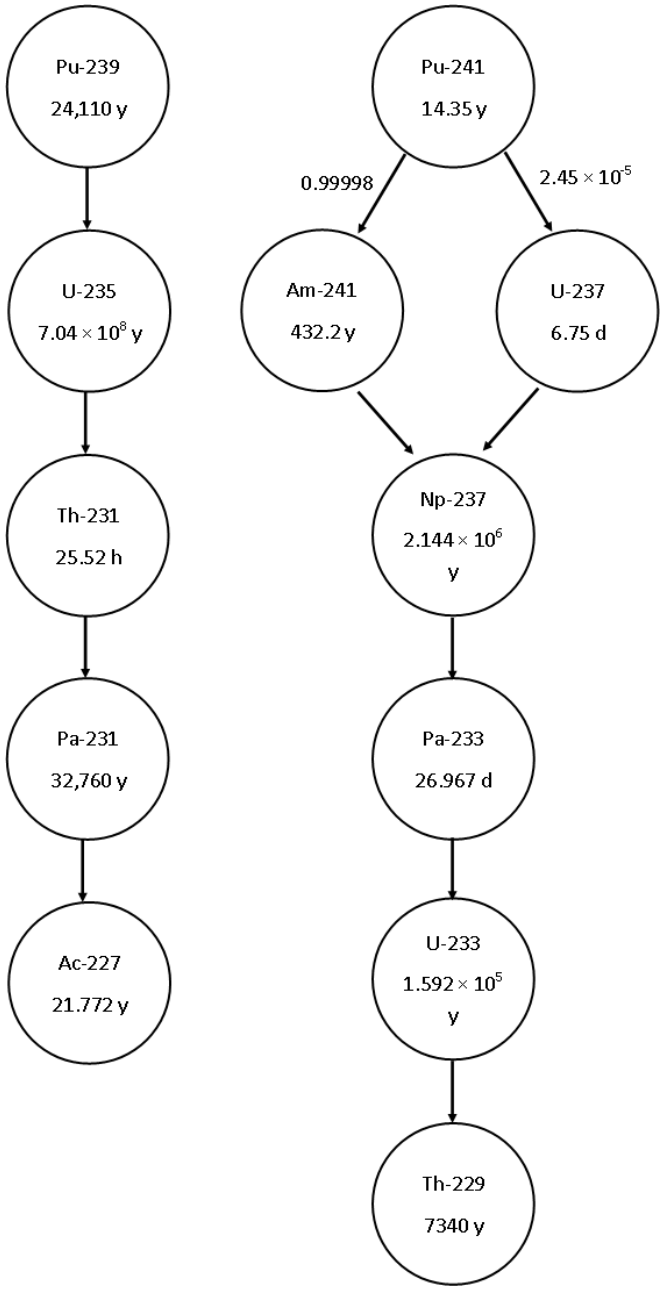

Figure 8 - Decay chains modelled (all branching ratios 1 unless otherwise stated) (decay chains, half-lives and branching ratios updated [27] from reference [31])

Table 11 – Radionuclide decay data (decay chains, half-lives and branching ratios based on an updated version [27] of ICRP publication 107 [31])

Nuclide	Half-life /y	Decay constant /y^{-1}	Daughter 1	Branching ratio	Daughter 2	Branching ratio
H-3	12.32	5.63×10^{-2}				
S-35	0.239589	2.89				
Co-60	5.2713	1.31×10^{-1}				
Sr-90	28.79	2.41×10^{-2}				
Cs-134	2.0648	3.36×10^{-1}				
Cs-137	30.167	2.30×10^{-2}				
Ac-227	21.772	3.18×10^{-2}				
Th-229	7340	9.44×10^{-5}				
Th-231	2.911×10^{-3}	2.38×10^{2}	Pa-231	1		
Pa-231	32760	2.12×10^{-5}	Ac-227	1		
Pa-233	7.3832×10^{-2}	9.39	U-233	1		
U-233	1.592×10^{5}	4.35×10^{4}	Th-229	1		
U-235	7.04×10^{8}	9.85×10^{6}	Th-231	1		
U-237	1.848×10^{-2}	3.75×10^{1}	Np-237	1		
Np-237	2.144×10^{6}	3.23×10^{5}	Pa-233	1		
Pu-239	24,110	2.87×10^{-5}	U-235	1		
Pu-241	14.35	4.83×10^{-2}	Am-241	0.99998	U-237	2.45×10^{-5}
Am-241	432.2	1.60×10^{-3}	Np-237	1		

The species specific activity (SA_S, Bq g^{-1}) is given by Equation (38). This is used to convert model input and output data in activity units into mass units for GoldSim's internal mass balance equations (Subsection 4.1).

$$SA_S = A_s/m_s = \lambda_s N_A/M_s \quad (38)$$

Here:

A_s is the activity of species s (Bq);

m_s is the mass of species s (g);

λ_s is the decay constant for species s (s^{-1}) (see Table 11);

N_A is Avogadro's number (6.02×10^{23} mol^{-1}) [32];

M_S is the molar mass of species s (g mol^{-1}) (the mass number of the isotope).

The distribution coefficients describe the partition of radionuclides between seawater and sediment (assuming reversible equilibrium behaviour). They were taken from International Atomic Energy Agency report TRS 422 [33]. They are the distribution coefficients for ocean margin sediment from Table II of that report. We used these values as TRS 422 is intended to

replace TRS 247 [34], which was the source for the default distribution factors used in PC-CREAM 08 [14] (and those used in previous EDF assessments [24]). Table 12 lists these distribution coefficients.

Table 12 – Distribution coefficients [33]

Element	Distribution coefficient /m^3 kg^{-1}
H	0.001
S	0.0005
Co	300
Sr	0.008
Cs	4
Ac	2000
Th	3000
Pa	5000
U	1
Np	1
Pu	100
Am	2000

4.6.5 Other model data

Table 13 summarises the other data used in the model.

Table 13 – Other data used in the model

Parameter	Value	Basis
Tidal period	12 h	Simplifying approximation of exactly two tidal cycles per day
Sediment loading	1×10^{-5} te m^{-3}	Default value from PC-CREAM 08 for the Hunterston local compartment [14]
Sedimentation rate	1×10^{-4} te m^{-2} y^{-1}	Default value from PC-CREAM 08 for the Hunterston local compartment [14]
Diffusion coefficient	3.15×10^{-2} m^{-2} y^{-1}	Default value from PC-CREAM 08 used for the Scottish waters west regional compartment [14]
Porewater turnover rate	1 y^{-1}	Default value from PC-CREAM 08 for shallow seas (<200 m deep) [14]
Sediment re-working rate	5×10^{-3} m y^{-1}	Default value from PC-CREAM 08 for shallow seas (<200 m deep) [14]
Sediment mineral density (i.e., density of sediment if porosity were 0)	2.6 te m^{-3}	Default value from PC-CREAM 08 [14], as no site-specific data.
Sediment porosity	0.75	Default value from PC-CREAM 08 [14], as no site-specific data.

Parameter	Value	Basis
Upper sediment thickness	0.1 m	Default value from PC-CREAM 08 [14], as no site-specific data.
Middle sediment thickness	1.9 m	Default value from PC-CREAM 08 [14], as no site-specific data.
Water density	1000 kg m^{-3}	By definition (unit conversion) [32]

GoldSim includes parameters for several processes not included in this model. These were set such that they had no effect on the model. They are:

- Diffusive flux (diffusivity, diffusion reduction, tortuosity, relative particulate diffusivity) – no diffusive fluxes are explicitly modelled,[10] so these values have no effect on the model results
- Solubility limits – set to −1 mol dm^{-3}, which disables solubility limitation [27]
- Available porosity – set to 1 so that available porosity and porosity are the same
- Advective velocity multiplier – set to 1 so that the advective velocities of suspended sediment and water are the same

4.6.6 Simulation parameters

The model was run with a basic timestep of 0.1 h. For shorter runs (100 days or less) results were saved for every timestep. For longer runs (more than 100 days), time data were only saved once every hour of model time (that is, once every ten timesteps). This was done to prevent result files reaching an unmanageable file size. The tidal flow data are specified in hourly timesteps, and saving results less frequently means the tidal cycles would not be visible in the results. If results are saved less (or more) frequently than the simulation timestep, there is a risk of introducing sampling bias. We compare discharge-cycle moving averages of the two sampling resolutions in C.6 to check that there is so sampling bias.

The simulation duration was set to allow equilibria and trends in results to manifest themselves and comparison with PC-CREAM 08. Each model was run for 100 d with results recorded every 6 minutes to record the early behaviour of the system in full detail. A model run of 5 y duration was performed, with results only recorded every hour so as to evaluate long-term behaviour but produce manageable output files. The simulation timestep was the same in both case (6 minutes).

The model begins at high tide (0 h after high tide) and the first discharge occurs in the first tidal cycle.

4.7 Outputs

The model calculates activity concentrations in environmental media for all the radionuclides and daughters considered. The following concentrations are discussed:

- Activity concentration in unfiltered seawater

[10] Radionuclide transfer between the water compartments and the sediment compartments does account for diffusion, but this is included in the direct transfer fluxes given in Subsection 4.3 and is not modelled as a diffusive flux in GoldSim. Diffusion is not modelled between water compartments we assume that advection dominates.

- Activity concentration in wet upper sediment
- Activity concentration in dry upper sediment (all activity)

The activity concentration in unfiltered seawater is the total activity per unit volume of seawater, including the activity sorbed to suspended sediment. It is given by Equation (39). This result corresponds to a sample of seawater as collected.

$$A_{\mathrm{UFW,s}} = c_{\mathrm{tot,iws}} \cdot \mathrm{SA_s} \quad (39)$$

Here:

$A_{\mathrm{UFW,s}}$ is the activity concentration of species s in unfiltered seawater (Bq m^{-3});

$c_{\mathrm{tot,iws}}$ is the total concentration of species s in water and suspended sediment (kg m^{-3}) (Equation (7));

$\mathrm{SA_s}$ is the specific activity of species s (Bq kg^{-1}) (Equation (38)).

The activity concentration in wet upper sediment is the total activity per unit mass of wet sediment. It includes the activity of the radionuclides sorbed to the sediment and dissolved to the porewater and it includes the mass of both the sediment and the porewater. It is given by Equation (40). This result corresponds to a sample of sediment as collected.

$$A_{\mathrm{WST,s}} = m_{\mathrm{is}} \cdot \mathrm{SA_s}/(M_{\mathrm{s}} + V_{\mathrm{PW}} \cdot \rho_{\mathrm{PW}}) \quad (40)$$

Here:

$A_{\mathrm{WST,s}}$ is the total activity concentration of species s in wet upper sediment (Bq kg^{-1});

m_{is} is the mass of species s in cell i (kg) (Equation (1));

M_{s} is the mass of sediment in the cell (kg) (Equation (36));

V_{PW} is the volume of porewater in the cell (m^3) (Equation (37));

ρ_{PW} is the density of water (1000 kg m^{-3}) (Table 13).

The activity concentration in dry upper sediment (all activity) is the total activity in a sediment sample per unit mass of dry sediment. It is given by Equation (41). For most radionuclides, this result corresponds to a sample of sediment that has been dried by evaporation.[11]

$$A_{\mathrm{DST,s}} = m_{\mathrm{is}} \cdot \mathrm{SA_s}/M_{\mathrm{s}} = A_{\mathrm{WST},s} \cdot (\rho_{\mathrm{b}} + \rho_{\mathrm{water}} \cdot \theta)/\rho_{\mathrm{b}} \quad (41)$$

Here:

$A_{\mathrm{DST,s}}$ is the activity concentration of species s in upper sediment per unit mass of dry sediment (Bq kg^{-1});

ρ_{b} is the dry sediment bulk density (kg m^{-3}) (Table 13);

[11] Some radionuclides, such as H-3 when incorporated into tritiated water, would be removed from a sample by evaporation. For these radionuclides, the activity concentration in dry sediment (sorbed activity only) (Equation (56)) would be more representative of drying by evaporation. However, Equation (41) should still be used where mathematically required.

ρ_{water} is the density of water (kg m^{-3}) (Table 13);

θ is the sediment porosity (dimensionless) (Table 13).

Results are recorded as a time series, final value and maximum value. The short-term discharge and tidal cycles modelled mean many of the results fluctuate rapidly. Comparing peak or final activity concentration can be misleading.

The moving average of the environmental media concentrations over the discharge cycle can be taken to smooth these fluctuations. This will give the time-averaged activity concentration in the environmental media of interest. This is the effective medium- and long-term concentration and is the concentration that chronic receptors would be exposed to (for example, uptake through the food chain). If acute exposure were considered (for example, a person exposed for a few hours or less during a recreational activity), the receptor may be exposed only to the peak concentration, and it may be more appropriate to use the peak concentration at the time of interest.

The GoldSim model also calculates and records the following environmental media concentrations, but they are not discussed in this report. Their derivations are given in Appendix C.6.

- Activity concentration in filtered seawater
- Activity concentration in upper sediment porewater
- Activity concentration in dry upper sediment (sorbed activity only)

4.8 Using the model

The model has been prepared so that it can be run and controlled using the free GoldSim Player application [35]. The model was prepared and run in GoldSim 14.0 R1 and should be run in that version of the player. To run the model, the accompanying spreadsheets that provide some input data and record the output data and run parameters must be saved in the same directory as the model (be aware they will be overwritten when the model runs).

The player dashboard provides the following controls:

- Discharge location (bank or channel)
- Discharge flow rate (controls the extra water added to the East of Little Cumbrae or East of Little Cumbrae Bank compartment, as described in Subsection 4.6.2.4)
- Whether water flow through the discharge pipe is continuous or only on while radionuclides are being discharged
- Whether the recommended or conservative approaches to discharge scheduling are used (see Subsection 4.5)
- Which source term is modelled (unit activity, permit limits or, for Hunterston B only, forecast discharges)
- Which of the stations are discharging, what the discharge window is (time of contaminant entry into the Firth – see Section 2) and how many discharges there are per year

- How long the simulation is run for

The dashboard also provides links that allow the user to view the simulation results, browse (but not edit) all elements of the model and view QA details about the model.

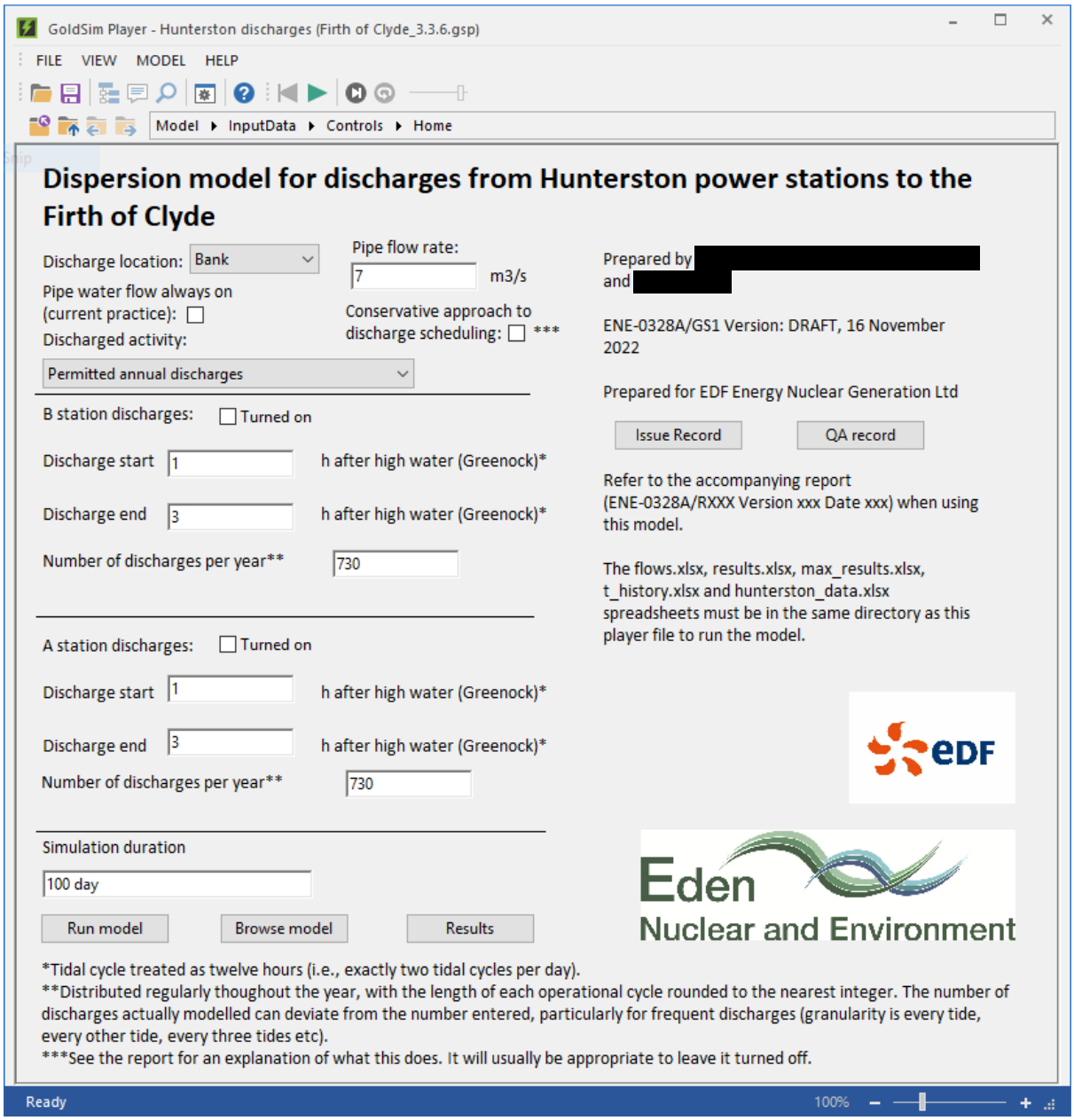

Figure 9 – Screenshot of the model interface, or dashboard, in GoldSim Player

5 Results

In this section, we give the results for each scenario. Because the total number of possible combinations of radionuclide, compartment, media (sediment or water, wet or dry, filtered or unfiltered) and reporting time is large, there are many possible results that we could discuss. Therefore, we present only a representative subset. We have chosen a consistent set of example radionuclides and media concentrations that allow us to describe and explain the model behaviour. We also give tables of those results that would be required to assess doses to people and wildlife.

The full set of possible result combinations can be accessed by running each scenario in the GoldSim Player model (see Subsection 4.8). Many of the results can then be viewed from the GoldSim Player dashboard. Activity concentrations for all combinations of radionuclide, compartment and media for all times are saved by the model in the time history Excel file.

In this section we present and discuss time history results for unfiltered seawater and wet sediment for three exemplar radionuclides over the long and short terms. We chose radionuclides that have different types of behaviour in the environment:

- H-3 is a mobile radionuclide with low sorption to sediment (k_d = 0.001 $m^3\,kg^{-1}$). It has a half-life of around 12 y. S-35 ($t_{½}$ = 87 d; k_d = 0.0005 $m^3\,kg^{-1}$) and Sr-90 ($t_{½}$ = 28 y; k_d = 0.008 $m^3\,kg^{-1}$) will show similar behaviour. These radionuclides are expected to show the least physicochemical build-up. Their relatively short half-lives will also reduce build up.

- Co-60 is a less mobile radionuclide with relatively high sorption to sediment (k_d = 300 $m^3\,kg^{-1}$). It has a half-life of around 5 y. Isotopes of Pu (k_d = 100 $m^3\,kg^{-1}$) will show similar physicochemical behaviour. These radionuclides are expected to show more physicochemical build-up. The amount of build-up of a given radionuclide will also be influenced by its half-life.

    - Isotopes of Cs (k_d = 4 $m^3\,kg^{-1}$), U (k_d = 1 $m^3\,kg^{-1}$) and Np (k_d = 1 $m^3\,kg^{-1}$) will have physicochemical behaviour intermediate between H-3 and Co-60. They will experience more physicochemical build-up than H-3, but less than Co-60. The half-life and ingrowth rate of the radionuclide in question will also influence the amount of build-up seen.

    - Some heavy elements are significantly more sorbing than Co (Ac, k_d = 2000 $m^3\,kg^{-1}$; Th, k_d = 3000 $m^3\,kg^{-1}$; Pa, k_d = 5000 $m^3\,kg^{-1}$; and Am, k_d = 2000 $m^3\,kg^{-1}$). They will experience more physicochemical build-up than Co. However, none of these elements are included in the discharges in the model; they are only included as ingrown daughters. Their build-up will be heavily influenced by their ingrowth and decay rates.

- U-235 is a daughter of Pu-239. Pu-239 has high sorption (k_d = 100 $m^3\,kg^{-1}$), while U-235 has moderate sorption (k_d = 1 $m^3\,kg^{-1}$). U-235 is significantly longer living than Pu-239 ($t_{½} \approx 7 \times 10^8$ y compared to 24,000 y). These properties make U-235 a good example of the behaviour of an ingrowing radionuclide.

We give tables with average activity concentration for all modelled radionuclides (discharge and ingrown) in dry sediment and unfiltered seawater. These are the results that will be required if a dose assessment is performed.

5.1 Scenario 1: baseline

The baseline scenario considers discharges to the East of Little Cumbrae Bank compartment during an ebb tide with a continuous water flow of 7 $m^3 s^{-1}$. Radionuclide discharges are every three tides. Unit annual discharges (1 GBq y^{-1}) were modelled. This represents the current discharge arrangements.

5.1.1 Exemplar mobile radionuclide – H-3

Figure 10 shows the activity concentration of H-3 (a mobile – less sorbing – radionuclide) in unfiltered seawater in all compartments (per unit annual discharge). It shows the behaviour over the first ten days after the first discharge, allowing the effects of tidal and discharge cycles to be visualised.

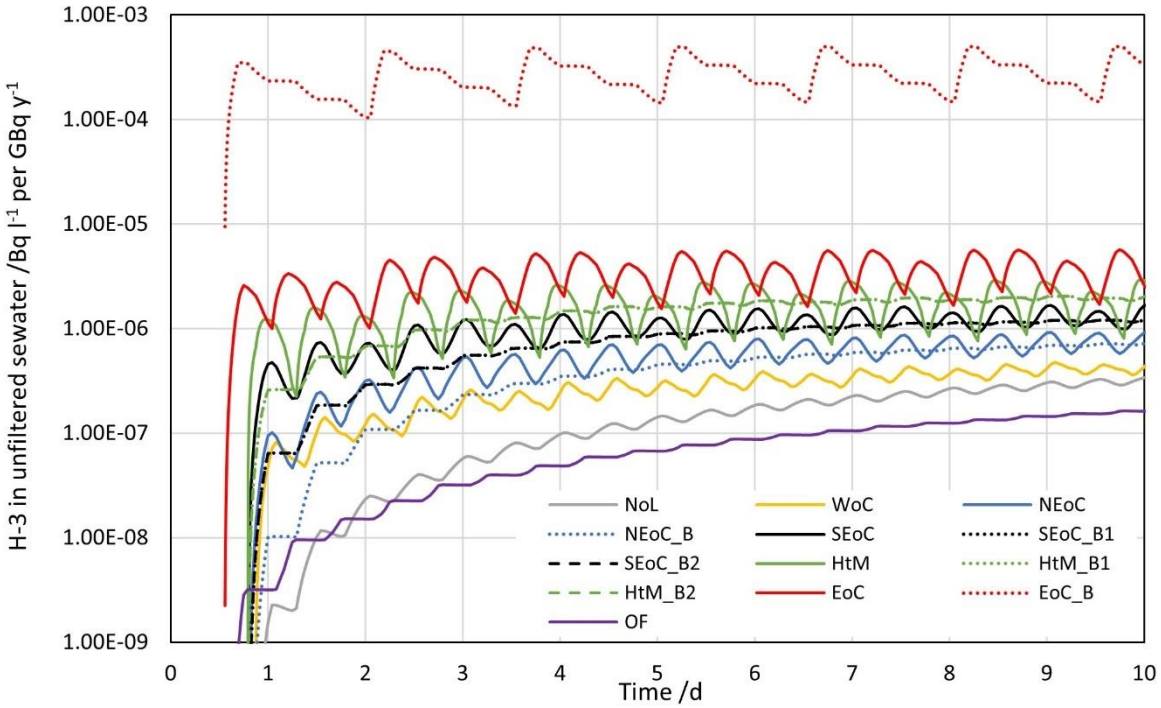

Figure 10 – Activity concentration of H-3 in unfiltered seawater for baseline scenario (per unit annual discharge) (semi-log plot)

Activity concentrations in the East of Little Cumbrae Bank compartment (EoC_B) are several orders of magnitude higher than in any other compartment. They display a clear dependency on discharges timing and tide. There is a peak in activity every 1.5 days (every three tides), when a discharge is modelled. There is then a short plateau in concentration for the remainder of the ebb tide. The concentration then drops off quickly in the flood tide and plateaus in the following ebb tide. It repeats this pattern twice, before the next discharge raises the concentration and the process repeats. The range in activity concentrations is constant after about 3 days of discharge.

The reason the activity concentration in the East of Little Cumbrae Bank compartment plateaus, rather than falls, during an ebb tide is that contaminated water is leaving the compartment (that is both H-3 and water are leaving). Therefore, although the compartment volume is reducing and H-3 is being removed, there is no effect on the H-3 concentration in the water that remains. During the flood tide, water with a much lower H-3 concentration enters the compartment, increasing the volume of the compartment and diluting the H-3. Therefore, the H-3 concentration falls during flood tides, even though the total activity in the compartment

will increase slightly. This phenomenon applies to all radionuclides discharged into the East of Little Cumbrae Bank compartment.

Fluctuations in the activity concentrations in the other compartments are governed mostly by the tides.

During the ebb tides, H-3 is transferred to the East of Little Cumbrae channel compartment, and its H-3 concentration increases. As discharges in this scenario are frequent (every three tidal cycles), the East of Little Cumbrae Bank compartment has a consistently high H-3 concentration compared to the channel compartment, and the rate of H-3 input to the channel compartment during ebb tides is similar regardless of whether or not there is a discharge in that tide. Therefore, the channel compartment returns to a similar H-3 concentration after every ebb tide. The activity concentration range in the channel compartment is constant after about 3 days of discharge.

Compartments upstream of the East of Little Cumbrae channel compartment (these are Hunterston to Millport, North- and South-east of Great Cumbrae and North of Largs) show increases in concentration during the flood tide, as H-3 is transferred upstream from the East of Little Cumbrae compartment. Fluctuations in H-3 concentrations in these compartments are, therefore, out-of-phase with those in the East of Little Cumbrae compartment.

The downstream compartment (Outer Firth) shows increased concentration during the ebb tide, as contaminants are transferred downstream from the East of Little Cumbrae compartment. The fluctuations are much smaller than in the other channel compartments and the concentration gradually increases over the 10 days modelled. The peaks in the West of Cumbrae compartment slightly lag behind the peaks in the Hunterston to Millport compartment, suggesting that contaminants mainly enter via flow from that compartment during flood tides.

The channel compartments do not show the plateauing and diluting behaviour that the bank compartments do. This is because the channel compartments have a constant volume and flows out of them are matched by a commensurate flow in. Therefore, a net loss or gain of H-3 always results in reduced and increased concentration, respectively.

The channel compartments do not show such a significant peak as the East of Little Cumbrae Bank compartment does following the discharge. In some of the compartments, the only discernible fluctuations in H-3 concentration are the tidal changes. This is because the bank compartment acts as a buffer, smoothing release to the other compartments. The entire discharge is added to the bank compartment over the discharge window, while (once equilibrium has been reached) it is released from the bank compartments to the channel gradually, over three ebb tides.

H-3 concentrations in unfiltered seawater rapidly converge around an equilibrium, where the rate of loss from the model is equal to the rate of input. If discharges were less frequent, equilibrium may not be reached. Instead, H-3 concentrations may reduce more, potentially to zero, between discharges. When discharges cease, the H-3 concentration will gradually decline, as it will no longer be replenished.

Figure 11 shows the H-3 concentration in the east of Cumbrae and east of Cumbrae bank compartments as a function of time in detail for the first ten days of the simulation. It also shows the discharge-cycle moving averages, demonstrating how these remove short term fluctuations due to the tidal and discharge cycles. The concentration can be said to have reached equilibrium once the gradient of the moving average is zero.

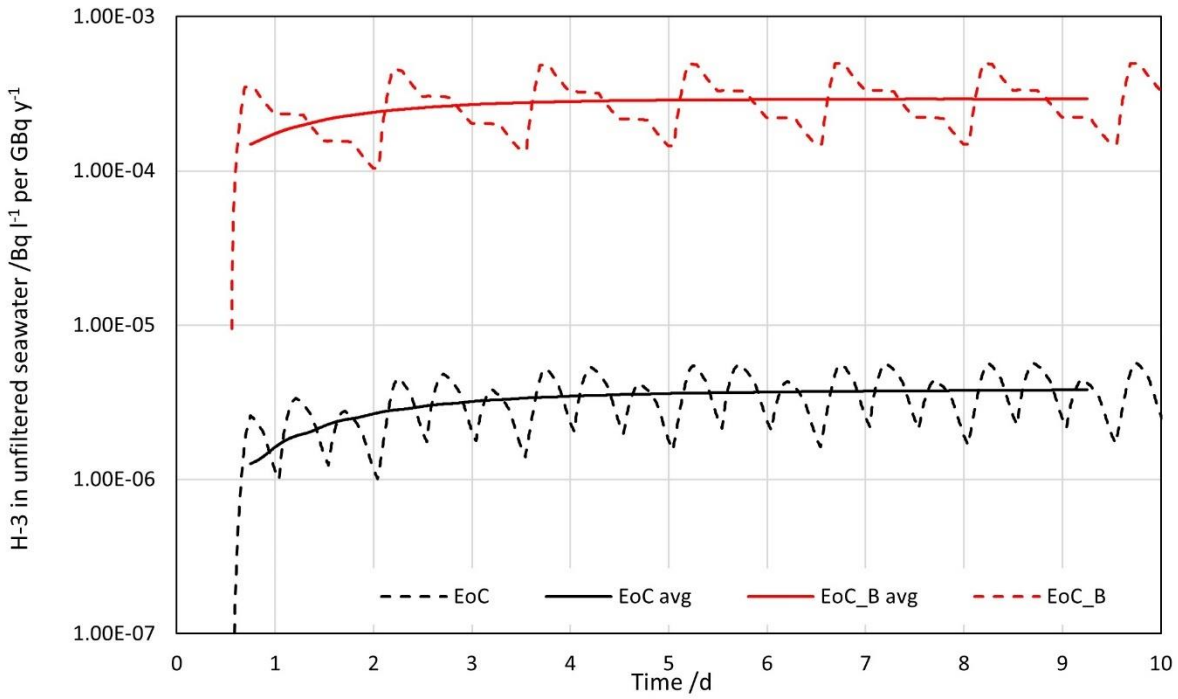

Figure 11 – H-3 concentration in unfiltered seawater for East of Little Cumbrae and East of Little Cumbrae Bank compartments and tidal-cycle moving average of H-3 concentrations (semi-log plot)

Figure 12 shows the discharge-cycle moving averages of the H-3 concentrations in all the model compartments over the longer term (five years). The H-3 concentrations in all compartments reach equilibrium within 400 days. Except for the East of Little Cumbrae compartment (where the discharges occur), the bank compartments all have similar H-3 concentrations to their adjacent channel compartments. This is expected. Once the channel compartment concentration has equilibrated, the flow from this compartment to the bank will always have the same concentration and, therefore, the concentration in the bank will tend toward the concentration in the channel.

Figure 13 shows H-3 concentration in wet upper sediment as a function of time for five years. There is no visible effect of tidal cycles, and the initial build-up phase is slower than for the unfiltered seawater concentration. These observations are expected as exchange between the water column and the sediment would not be instantaneous. The sediment concentrations are close to equilibrium after around 400 d, but continue growing slowly beyond this time.

Unlike the water concentrations, sediment concentrations in the bank compartments are slightly higher than their adjacent channel compartments (except for the East of Little Cumbrae Bank compartment, where the discharges occur, which has much greater activity concentration than the East of Little Cumbrae channel compartment). This is because we do not model transfer to the middle and deep sediment for these compartments. Therefore, more activity is retained in the upper sediment.

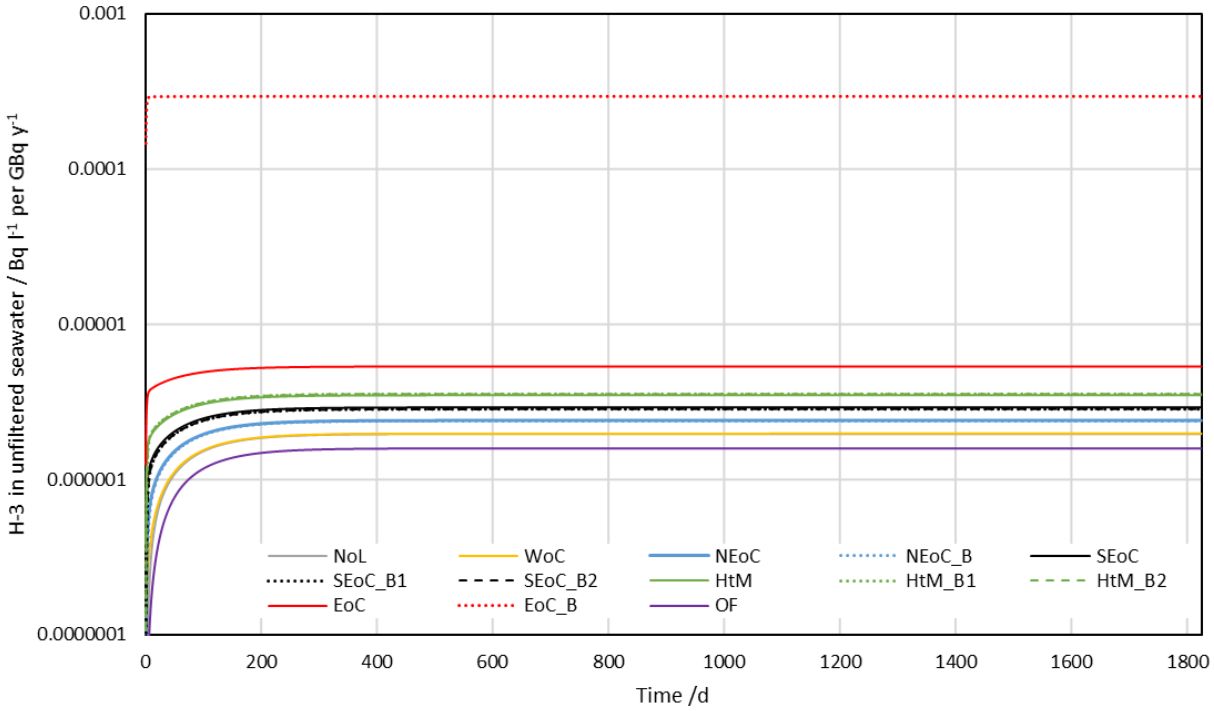

Figure 12 – Tidal-cycle moving average of H-3 concentration in unfiltered seawater for five years (semi-log plot)

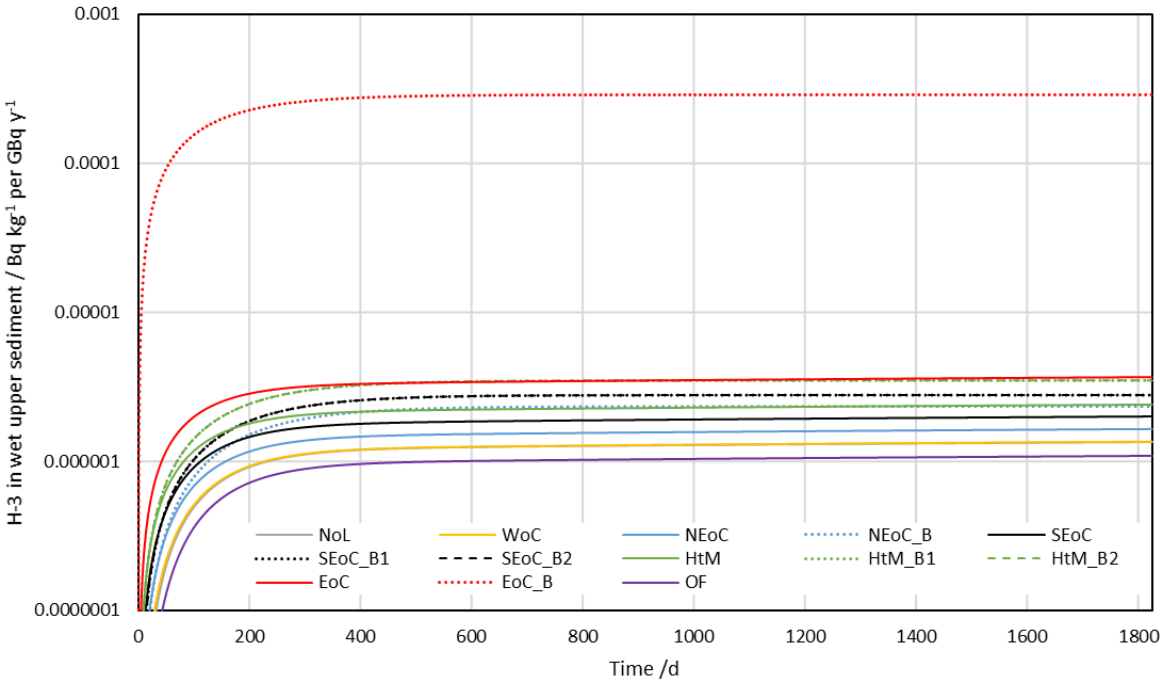

Figure 13 – H-3 concentration in wet top sediment for five years (semi-log plot)

5.1.2 Exemplar less-mobile radionuclide – Co-60

Figure 14 shows the activity concentration of Co-60 (a less mobile – more sorbing – radionuclide) in unfiltered seawater in all compartments (per unit discharge). It shows the behaviour over the first ten days after the first discharge, allowing the effects of tidal and

discharge cycles to be visualised. The behaviour of Co-60 is similar to that of H-3 (discussed in Subsection 5.1.1).

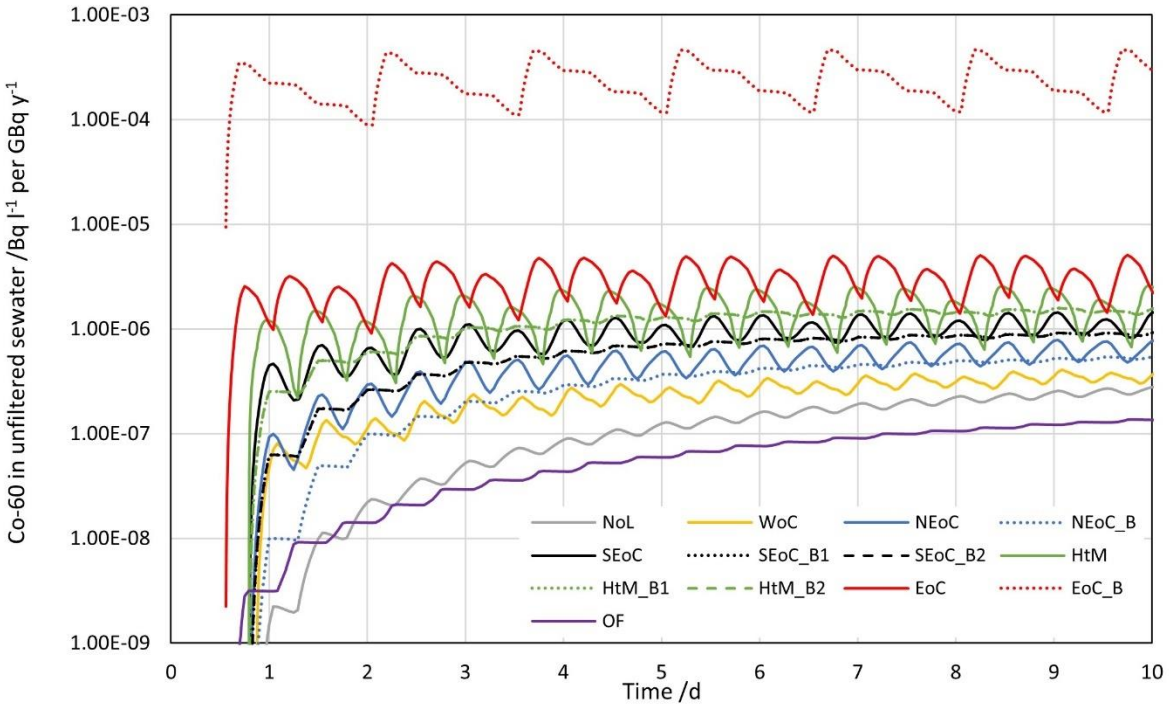

Figure 14 – Activity concentration of Co-60 in unfiltered seawater for baseline scenario (unit annual discharge) (semi-log plot)

Figure 15 shows the activity concentration of Co-60 in unfiltered seawater over the longer term (five years). The long-term behaviour of Co-60 in unfiltered seawater is also similar to H-3. There are two differences. The channel compartments have slightly higher Co-60 concentrations than their adjacent bank compartments (except for the East of Little Cumbrae compartment where the discharges occur). The activity concentration of Co-60 is slightly (around a factor of two) lower than the activity concentration of H-3; this is because Co-60 is more strongly sorbing than H-3 and, therefore, more Co-60 is partitioned to the sediment.

Figure 16 and Figure 17 show the build-up of Co-60 in sediment over five years. Unlike H-3, Co-60 does not reach equilibrium over five years; instead, the sediment concentration continues to increase (this is most obvious in Figure 17, which is plotted on linear axes). This is expected; it takes much longer for the strongly sorbed cobalt to equilibrate between the solution and sediment phases than for the much less strongly sorbed hydrogen.

Another difference between the behaviours of H-3 and Co-60 is that the bank compartments have lower Co-60 concentrations in wet sediment than their adjacent channel compartment, but slightly higher H-3 concentrations (with the exception of the East of Little Cumbrae Bank compartment where the discharges occur, which has much higher concentrations of both Co-60 and H-3).This is likely to be because the concentration of Co-60 in unfiltered seawater in the bank compartments is slightly lower than in the channel compartments, whereas the concentration of H-3 is similar in both.

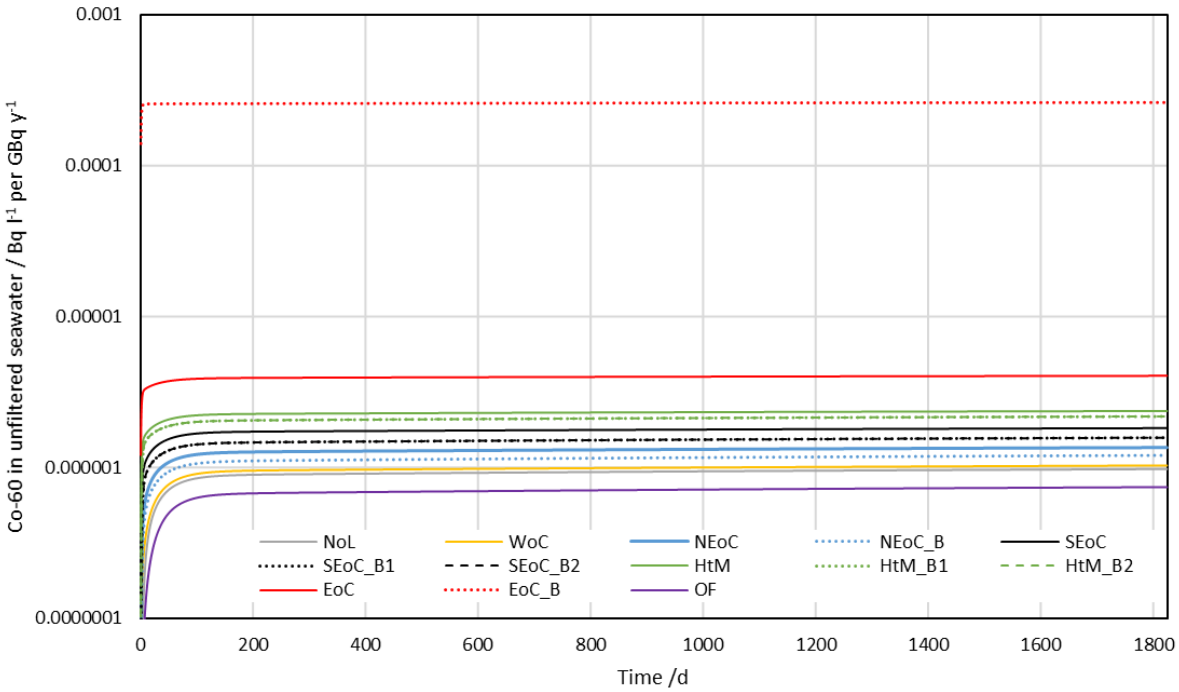

Figure 15 – Discharge-cycle moving average of Co-60 concentration in unfiltered seawater for five years (semi-log plot)

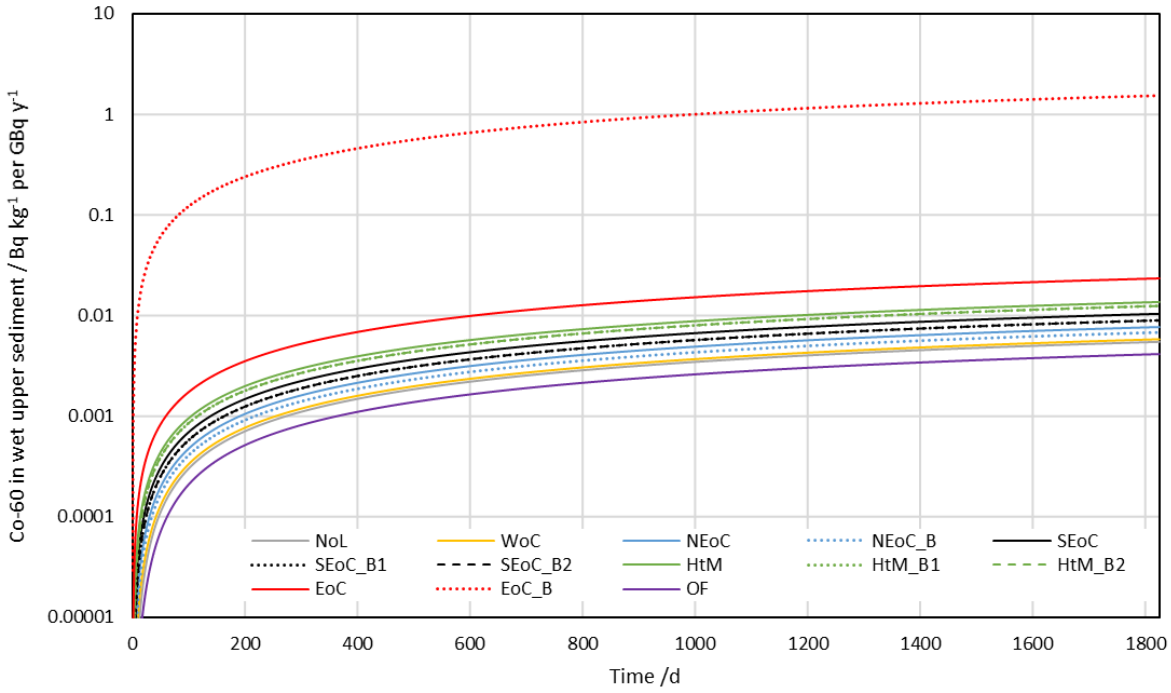

Figure 16 – Co-60 concentration in wet top sediment for five years (semi-log plot)

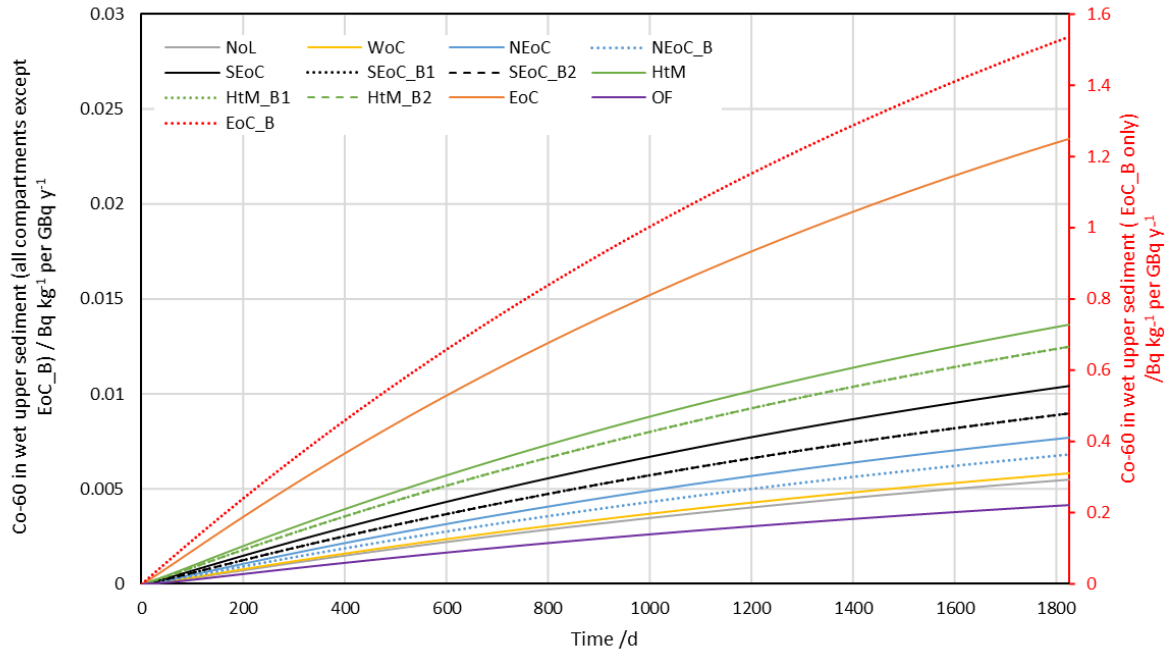

Figure 17 – Co-60 concentration in wet top sediment for five years (linear scale, EoC_B compartment has a different y-axis scale to the other compartments)

5.1.3 Exemplar daughter radionuclide – U-235

Figure 18 shows the activity concentration of U-235 (a daughter of Pu-239) in unfiltered seawater in all compartments (per unit discharge of Pu-239). It shows the behaviour over the first ten days after the first discharge, allowing the effects of tidal and discharge cycles to be identified. The pattern of behaviour of U-235 over this period is similar to that of H-3 and Co-60 (discussed in Subsections 5.1.1 and 5.1.2).

Early in the simulation, the concentration of U-235 is many orders of magnitude below those of H-3 and Co-60. This is because U-235 is only present because of ingrowth from Pu-239; the concentration of U-235 is, thus, limited by the amount of decay of Pu-239 ($t_{½}$ = 24,110 y). Over the time shown, the decay rate of Pu-239 is low compared to the rate of discharge of Pu-239, and the U-235 concentration reflects the discharge (and transfer through the system) of Pu-239. The low ingrowth does smooth the tidal- and discharge-cycle fluctuations, particularly in the East of Little Cumbrae Bank compartment.

Figure 19 and Figure 20 show the discharge-cycle moving averages of the U-235 concentrations in unfiltered seawater in all the model compartments over the longer term (five years). After the initial increase in and then plateau of U-235 concentration (Figure 18), U-235 enters a period of super-linear growth in concentration. This is not simple ingrowth from Pu-239 in the water compartments: the average Pu-239 concentration in the water compartments remains at or close to equilibrium (constant) throughout this period, which would lead to sublinear growth in U-235 concentration.

The super-linear increase in U-235 concentration is caused by build-up of the strongly sorbing U-235 parent Pu-239 in the sediment compartments (Figure 21) and the fact that U-235 is less sorbing than Pu-239. As Pu-239 decays to the more weakly sorbing U-235, some of the U-235 is released back to the water compartments. This adds to the U-235 ingrown from Pu-239 in the water compartments, leading to the super-linear growth seen in Figure 19 and Figure 20.

In Figure 18 and Figure 19, the concentrations of U-235 in unfiltered seawater in the bank compartments grow to slightly exceed the concentrations in the adjacent channel

compartments. This is because the main source of the U-235 is ingrowth from Pu-239 in the sediment compartments. The ingrown U-235 is then cleared more rapidly from the channel compartments, which have greater water turnover.

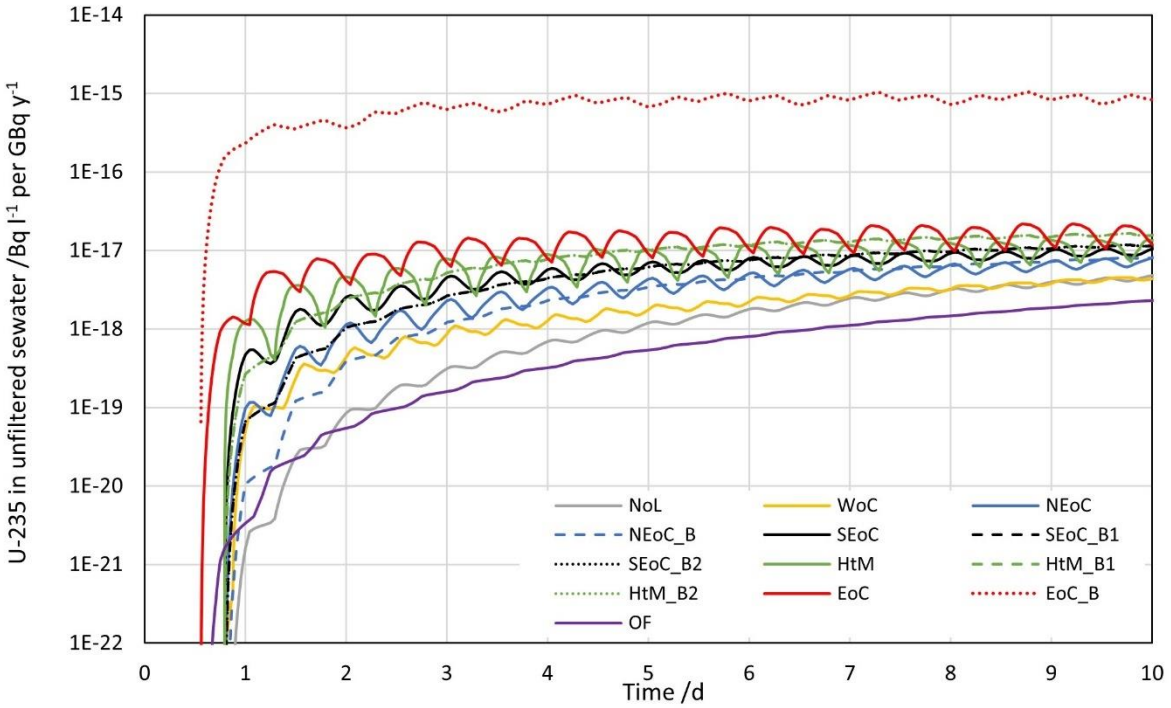

Figure 18 – Activity concentration of U-235 in unfiltered seawater for baseline scenario (unit annual discharge Pu-239) (semi-log plot)

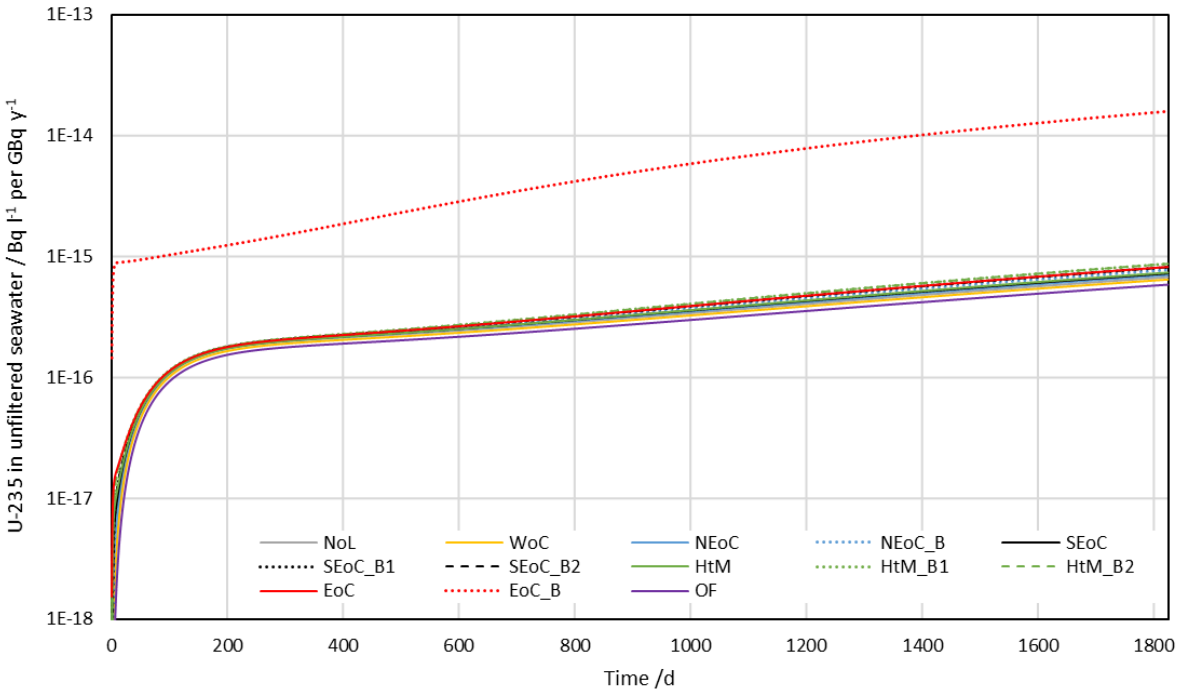

Figure 19 – Discharge-cycle moving average of U-235 concentration in unfiltered seawater for five years (semi-log plot)

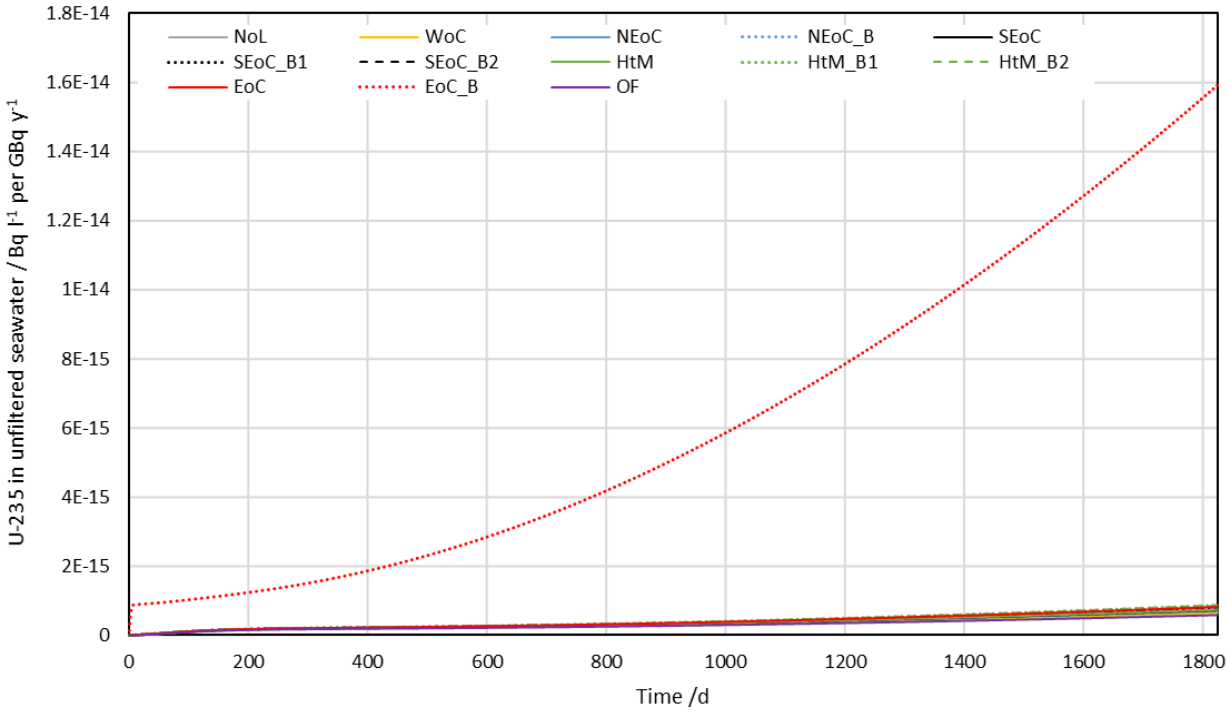

Figure 20 – Discharge-cycle moving average of U-235 concentration in unfiltered seawater for five years (linear plot)

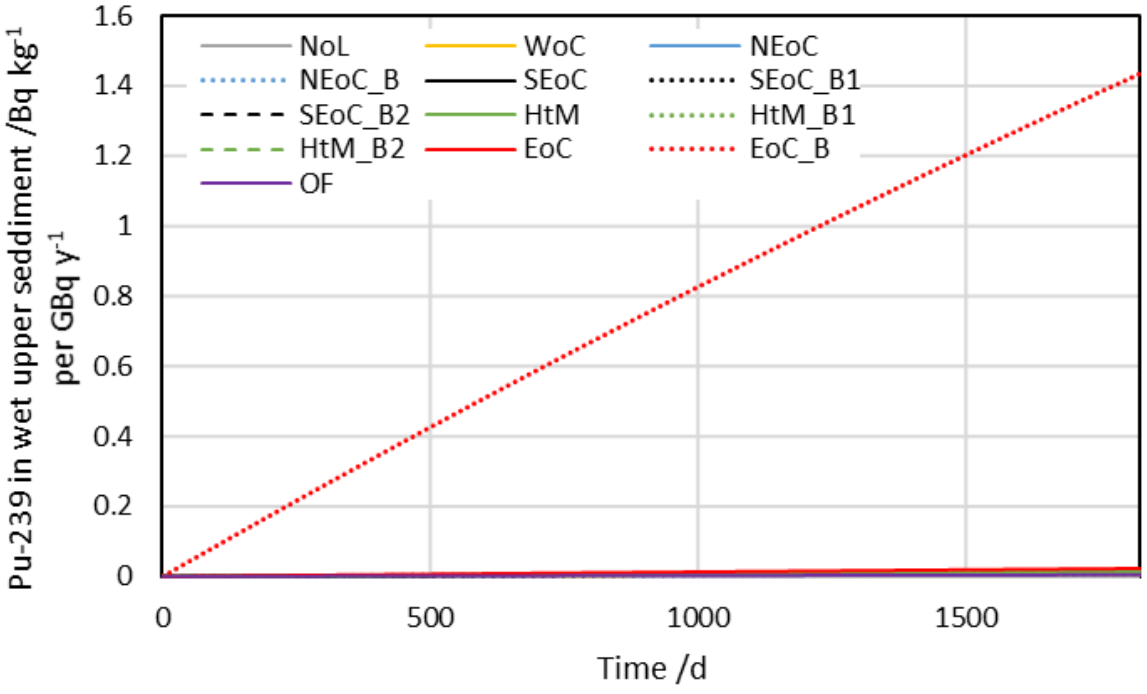

Figure 21 – Build-up of Pu-239 in sediment (the build-up happens in all compartments, but only the East of Little Cumbrae Bank compartment is visible on the scale of this figure)

Figure 22 and Figure 23 show U-235 build-up in wet top sediment for five years. Unlike both H-3 and Co-60 build up (but like U-235 build-up in unfiltered seawater), U-235 build-up is super-linear. As with U-235 in unfiltered seawater, this is because U-235 ingrows from Pu-239 in the sediment and the Pu-239 concentration in sediment is constantly increasing because of physicochemical build-up. As well as radioactive decay, some U-235 is lost to the water

compartment by desorption and other physicochemical processes. The relative U-235 and Pu-239 concentrations are not, therefore, governed solely by radiological processes (decay, ingrowth and equilibria).

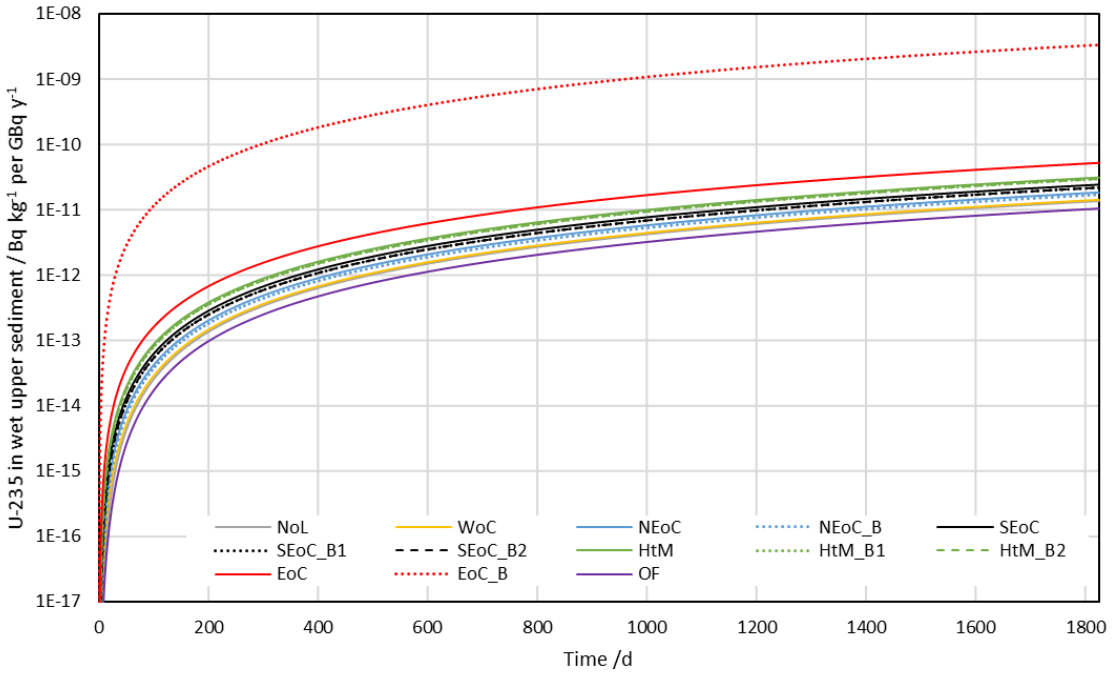

Figure 22 – U-235 concentration in wet top sediment for five years (semi-log plot)

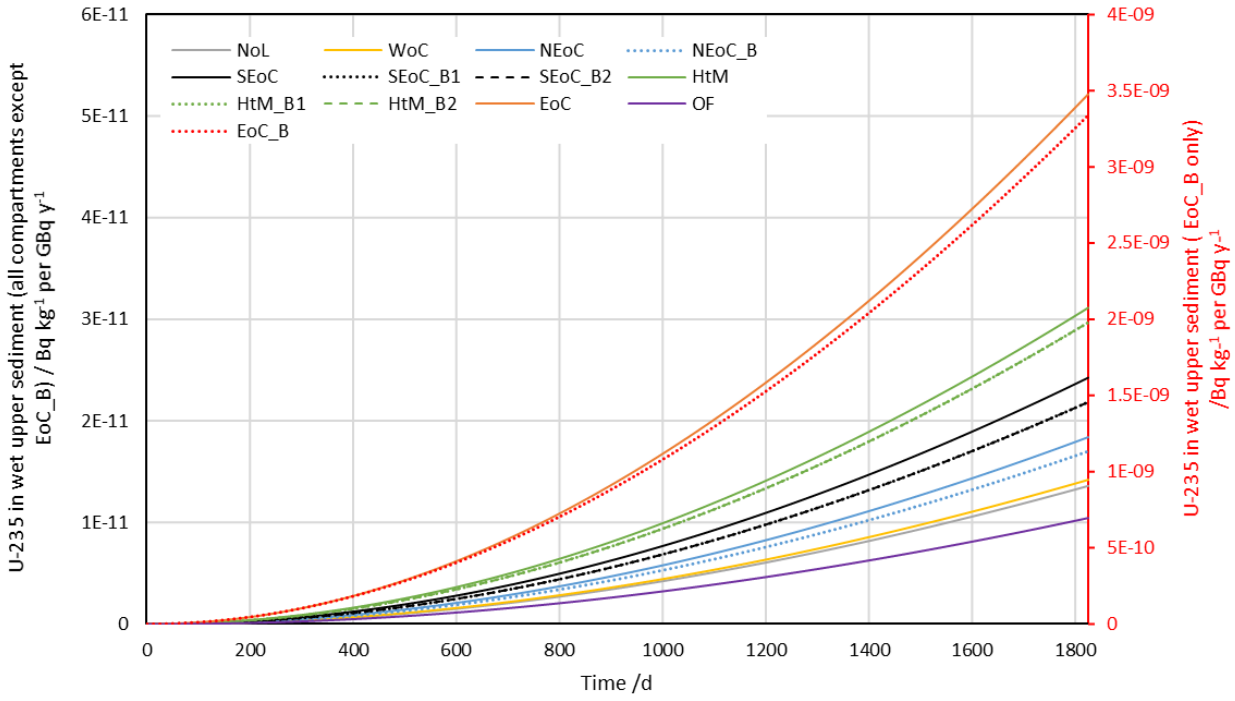

Figure 23 – U-235 concentration in wet top sediment for five years (linear scale, EoC_B compartment has a different y-axis scale to the other compartments)

5.1.4 Radionuclide concentrations after five years

Table 14 gives the concentration of each radionuclide that has built up in unfiltered seawater in each compartment after five years of continuous discharge. Table 15 gives the concentration of each radionuclide that has built up in wet upper sediment in each compartment after five years of continuous discharge

Table 14 – Concentration of each radionuclide in unfiltered seawater after five years in each compartment for the baseline scenario (discharge cycle moving averages) (Bq l^{-1} per GBq y^{-1})

Nuclide	NoL	WoC	NEoC	NEoC_B	SEoC	SEoC_B1	SEoC_B2	HtM	HtM_B1	HtM_B2	EoC	EoC_B	OF
H-3	1.97×10^{-6}	1.98×10^{-6}	2.40×10^{-6}	2.39×10^{-6}	2.92×10^{-6}	2.84×10^{-6}	2.84×10^{-6}	3.49×10^{-6}	3.56×10^{-6}	3.56×10^{-6}	5.35×10^{-6}	2.94×10^{-4}	1.59×10^{-6}
S-35	1.31×10^{-6}	1.35×10^{-6}	1.74×10^{-6}	1.71×10^{-6}	2.25×10^{-6}	2.16×10^{-6}	2.16×10^{-6}	2.84×10^{-6}	2.89×10^{-6}	2.89×10^{-6}	4.68×10^{-6}	2.91×10^{-4}	9.97×10^{-7}
Co-60	9.76×10^{-7}	1.03×10^{-6}	1.36×10^{-6}	1.20×10^{-6}	1.82×10^{-6}	1.58×10^{-6}	1.58×10^{-6}	2.37×10^{-6}	2.18×10^{-6}	2.18×10^{-6}	4.05×10^{-6}	2.62×10^{-4}	7.41×10^{-7}
Cs-134	1.78×10^{-6}	1.80×10^{-6}	2.21×10^{-6}	2.18×10^{-6}	2.73×10^{-6}	2.63×10^{-6}	2.63×10^{-6}	3.30×10^{-6}	3.35×10^{-6}	3.35×10^{-6}	5.15×10^{-6}	2.92×10^{-4}	1.43×10^{-6}
Cs-137	1.89×10^{-6}	1.90×10^{-6}	2.32×10^{-6}	2.29×10^{-6}	2.83×10^{-6}	2.75×10^{-6}	2.75×10^{-6}	3.41×10^{-6}	3.46×10^{-6}	3.46×10^{-6}	5.26×10^{-6}	2.92×10^{-4}	1.52×10^{-6}
Pu-239	1.23×10^{-6}	1.27×10^{-6}	1.63×10^{-6}	1.50×10^{-6}	2.11×10^{-6}	1.91×10^{-6}	1.91×10^{-6}	2.67×10^{-6}	2.55×10^{-6}	2.55×10^{-6}	4.42×10^{-6}	2.73×10^{-4}	9.52×10^{-7}
U-235_ Pu-239	6.75×10^{-16}	6.46×10^{-16}	7.04×10^{-16}	7.76×10^{-16}	7.25×10^{-16}	8.17×10^{-16}	8.17×10^{-16}	7.38×10^{-16}	8.71×10^{-16}	8.71×10^{-16}	8.21×10^{-16}	1.59×10^{-14}	5.86×10^{-16}
Th-231_ Pu-239	6.47×10^{-16}	6.20×10^{-16}	6.70×10^{-16}	6.83×10^{-16}	6.87×10^{-16}	7.16×10^{-16}	7.16×10^{-16}	6.96×10^{-16}	7.60×10^{-16}	7.60×10^{-16}	7.66×10^{-16}	1.32×10^{-14}	5.66×10^{-16}
Pa-231_ Pu-239	7.41×10^{-21}	7.13×10^{-21}	8.07×10^{-21}	8.79×10^{-21}	8.71×10^{-21}	9.82×10^{-21}	9.82×10^{-21}	9.27×10^{-21}	1.13×10^{-20}	1.13×10^{-20}	1.15×10^{-20}	3.85×10^{-19}	6.23×10^{-21}
Ac-227_ Pu-239	2.61×10^{-22}	2.50×10^{-22}	2.86×10^{-22}	3.18×10^{-22}	3.11×10^{-22}	3.58×10^{-22}	3.58×10^{-22}	3.32×10^{-22}	4.17×10^{-22}	4.16×10^{-22}	4.18×10^{-22}	1.48×10^{-20}	2.16×10^{-22}

Table 15 – Concentration of each radionuclide in dry upper sediment (all activity) after five years in each compartment for the baseline scenario (discharge-cycle moving averages) (Bq kg^{-1} per GBq y^{-1})

Nuclide	NoL	WoC	NEoC	NEoC_B	SEoC	SEoC_B1	SEoC_B2	HtM	HtM_B1	HtM_B2	EoC	EoC_B	OF
H-3	2.91×10^{-6}	2.93×10^{-6}	3.55×10^{-6}	5.04×10^{-6}	4.32×10^{-6}	6.00×10^{-6}	6.00×10^{-6}	5.19×10^{-6}	7.53×10^{-6}	7.53×10^{-6}	7.93×10^{-6}	6.21×10^{-4}	2.35×10^{-6}
S-35	9.12×10^{-7}	9.38×10^{-7}	1.21×10^{-6}	1.58×10^{-6}	1.57×10^{-6}	2.00×10^{-6}	2.00×10^{-6}	1.98×10^{-6}	2.66×10^{-6}	2.66×10^{-6}	3.26×10^{-6}	2.68×10^{-4}	6.95×10^{-7}
Co-60	1.18×10^{-2}	1.25×10^{-2}	1.66×10^{-2}	1.47×10^{-2}	2.24×10^{-2}	1.93×10^{-2}	1.93×10^{-2}	2.94×10^{-2}	2.69×10^{-2}	2.69×10^{-2}	5.04×10^{-2}	3.31×10^{0}	8.92×10^{-3}
Cs-134	7.90×10^{-4}	7.99×10^{-4}	9.83×10^{-4}	9.74×10^{-4}	1.21×10^{-3}	1.18×10^{-3}	1.18×10^{-3}	1.48×10^{-3}	1.50×10^{-3}	1.50×10^{-3}	2.30×10^{-3}	1.31×10^{-1}	6.31×10^{-4}
Cs-137	1.55×10^{-3}	1.56×10^{-3}	1.91×10^{-3}	1.90×10^{-3}	2.34×10^{-3}	2.28×10^{-3}	2.28×10^{-3}	2.84×10^{-3}	2.89×10^{-3}	2.89×10^{-3}	4.39×10^{-3}	2.49×10^{-1}	1.24×10^{-3}
Pu-239	1.31×10^{-2}	1.36×10^{-2}	1.75×10^{-2}	1.61×10^{-2}	2.30×10^{-2}	2.07×10^{-2}	2.06×10^{-2}	2.94×10^{-2}	2.79×10^{-2}	2.79×10^{-2}	4.90×10^{-2}	3.09×10^{0}	1.01×10^{-2}
U-235_ Pu-239	2.92×10^{-11}	3.05×10^{-11}	3.96×10^{-11}	3.66×10^{-11}	5.22×10^{-11}	4.70×10^{-11}	4.70×10^{-11}	6.70×10^{-11}	6.39×10^{-11}	6.39×10^{-11}	1.12×10^{-10}	7.19×10^{-9}	2.24×10^{-11}
Th-231_ Pu-239	2.92×10^{-11}	3.05×10^{-11}	3.95×10^{-11}	3.65×10^{-11}	5.21×10^{-11}	4.70×10^{-11}	4.70×10^{-11}	6.69×10^{-11}	6.38×10^{-11}	6.38×10^{-11}	1.12×10^{-10}	7.17×10^{-9}	2.24×10^{-11}
Pa-231_ Pu-239	1.03×10^{-15}	1.08×10^{-15}	1.39×10^{-15}	1.29×10^{-15}	1.83×10^{-15}	1.65×10^{-15}	1.65×10^{-15}	2.34×10^{-15}	2.24×10^{-15}	2.24×10^{-15}	3.91×10^{-15}	2.50×10^{-13}	7.93×10^{-16}
Ac-227_ Pu-239	3.95×10^{-17}	4.11×10^{-17}	5.32×10^{-17}	4.94×10^{-17}	7.00×10^{-17}	6.34×10^{-17}	6.34×10^{-17}	8.96×10^{-17}	8.60×10^{-17}	8.60×10^{-17}	1.50×10^{-16}	9.54×10^{-15}	3.03×10^{-17}

5.2 Scenario 2: alternative discharge scenario to the bank – as baseline, but with low water flow rate through pipe

Scenario 2 considers discharges to the bank during an ebb tide with a water flow of 0.0086 m^3 s^{-1} (with the water flow only operating while effluent is discharged). Discharges are every three tides. Unit annual discharges (1 GBq y^{-1}) were modelled. This represents alternative discharge arrangements that are equivalent to the existing arrangements, but without the continuous cooling water flow.

5.2.1 Exemplar mobile radionuclide – H-3

Figure 24 shows the activity concentration of H-3 (a mobile radionuclide) in unfiltered seawater in all compartments (per unit annual discharge) over the first ten days after the first discharge. Figure 25 shows the discharge-cycle moving average of H-3 concentration in unfiltered seawater in all compartments (per unit discharge) over five years of continuous discharges. The behaviour of H-3 in this scenario is almost identical to its behaviour in the baseline scenario (Subsection 5.1.1).

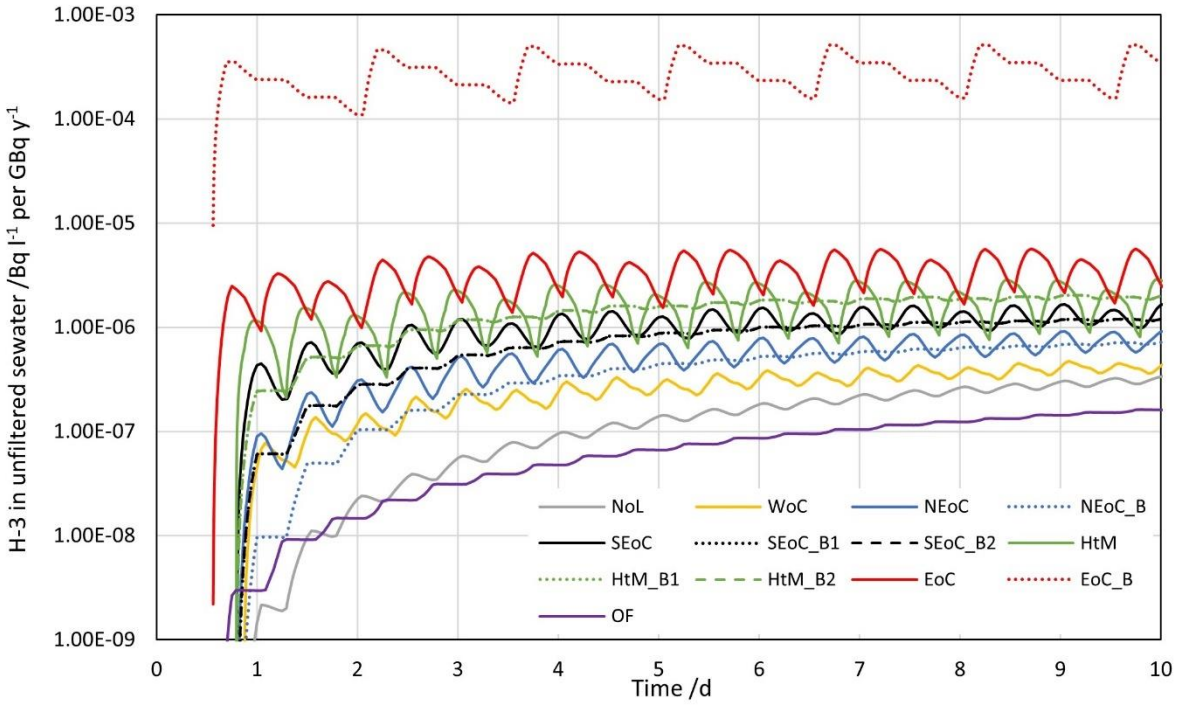

Figure 24 – Activity concentration of H-3 in unfiltered seawater for alternative discharge scenario to the bank (per unit annual discharge) (semi-log plot)

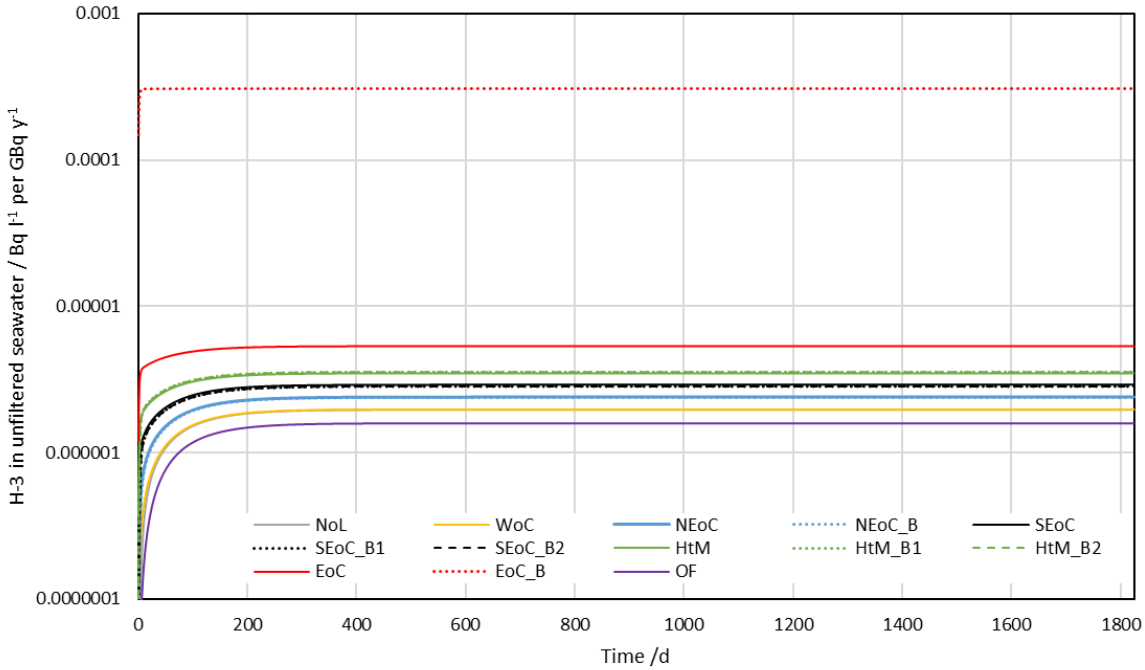

Figure 25 – Tidal-cycle moving average of H-3 concentration in unfiltered seawater for five years for alternative discharge scenario to the bank (per unit annual discharge) (semi-log plot)

Figure 26 shows the activity concentration of H-3 (a mobile radionuclide) in wet upper sediment in all compartments (per unit discharge) over five years of continuous discharges. The behaviour of H-3 in this scenario is almost identical to its behaviour in the baseline scenario (Subsection 5.1.1).

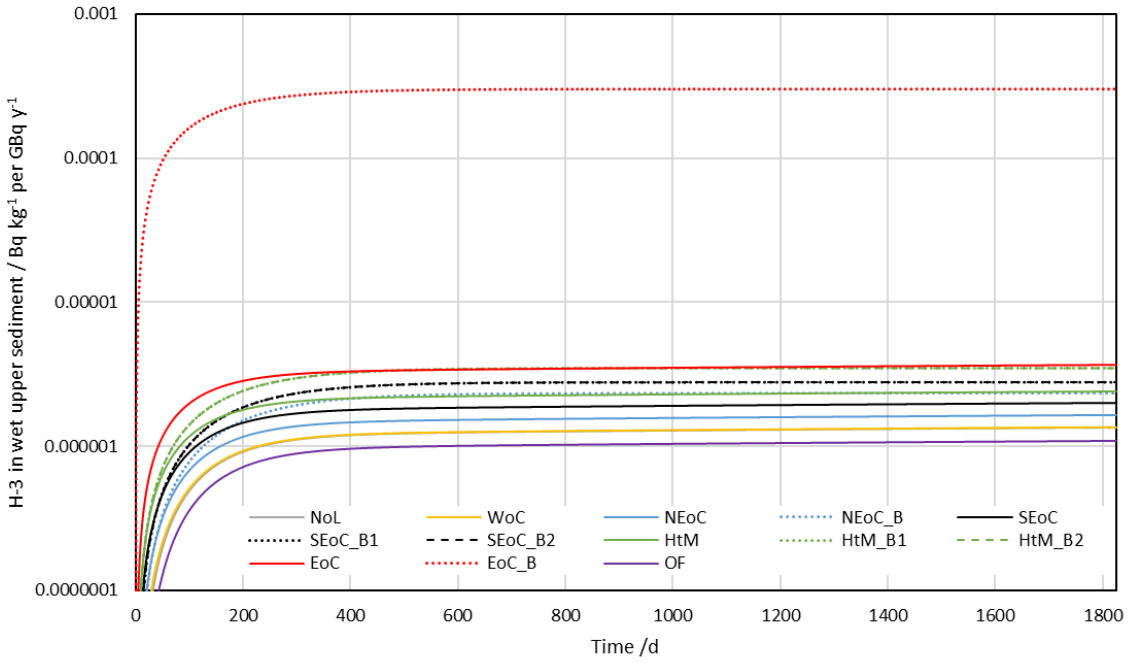

Figure 26 – H-3 concentration in wet top sediment for five years for alternative discharge scenario to the bank (per unit annual discharge) (semi-log plot)

The reason the concentrations in most compartments are not affected by the change in water flow is that the difference in water flow from the pipe (2.52×10^4 $m^3 h^{-1}$ in Scenario 1; *ca.* 30 $m^3 h^{-1}$ in Scenario 2) is very small compared to the flow rate between channel

compartments (of the order of 10^7 m^3 h^{-1}) (although it must still be included in the model, because the cumulative effect on water balance, over a five year run, would be significant).

The flow into and out of the East of Little Cumbrae Bank compartment is around an order of magnitude lower (of the order of 10^6 m^3 h^{-1}). The pipe flow in Scenario 2 is a few percent of this, and concentrations in the East of Little Cumbrae bank compartment are correspondingly lower in Scenario 1 (see Table 16). However, this difference in activity is of the order of 10^{-5} Bq l^{-1} per GBq y^{-1}, and is more than an order of magnitude less than the total activity concentrations. This difference is small and, given the model uncertainty, not meaningful.

5.2.2 Exemplar less-mobile radionuclide – Co-60

Figure 27 shows the activity concentration of Co-60 (a less-mobile radionuclide) in unfiltered seawater in all compartments (per unit annual discharge) over the first ten days after the first discharge. Figure 28 shows the discharge-cycle moving average of Co-60 concentration in unfiltered seawater in all compartments (per unit discharge) over five years of continuous discharges. The behaviour of Co-60 in this scenario is almost identical to its behaviour in the baseline scenario (Subsection 5.1.2).

Figure 29 shows the activity concentration of Co-60 (a less-mobile radionuclide) in wet upper sediment in all compartments (per unit discharge) over five years of continuous discharges. The behaviour of Co-60 in this scenario is almost identical to its behaviour in the baseline scenario (Subsection 5.1.2).

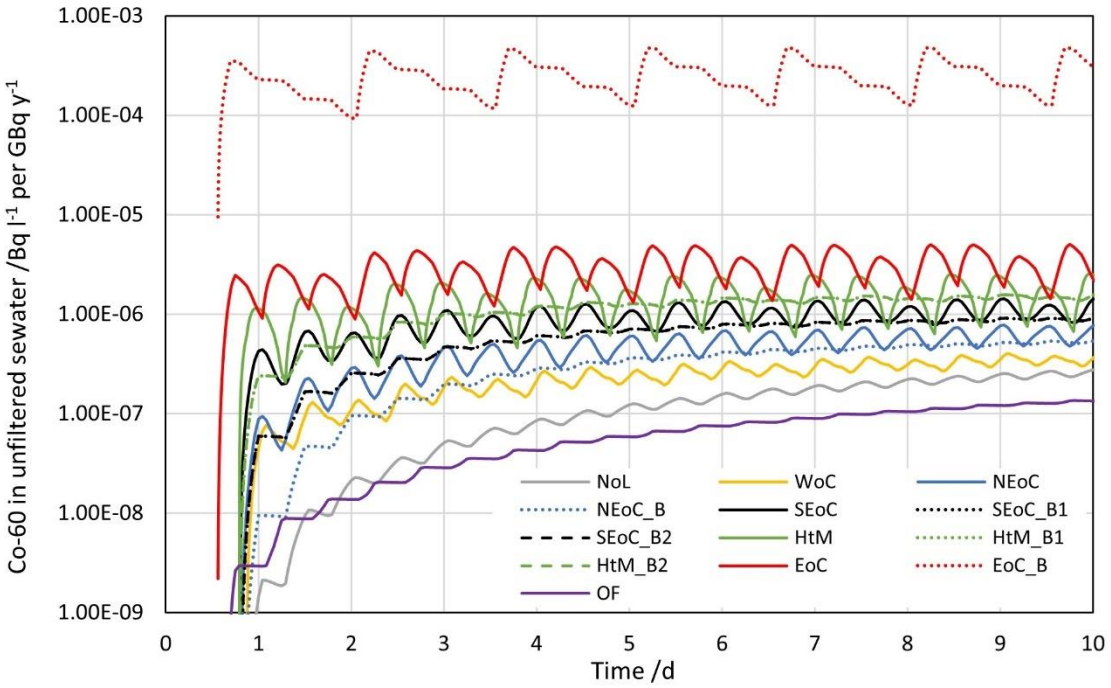

Figure 27 – Activity concentration of Co-60 in unfiltered seawater for alternative discharge scenario to the bank (per unit annual discharge) (semi-log plot)

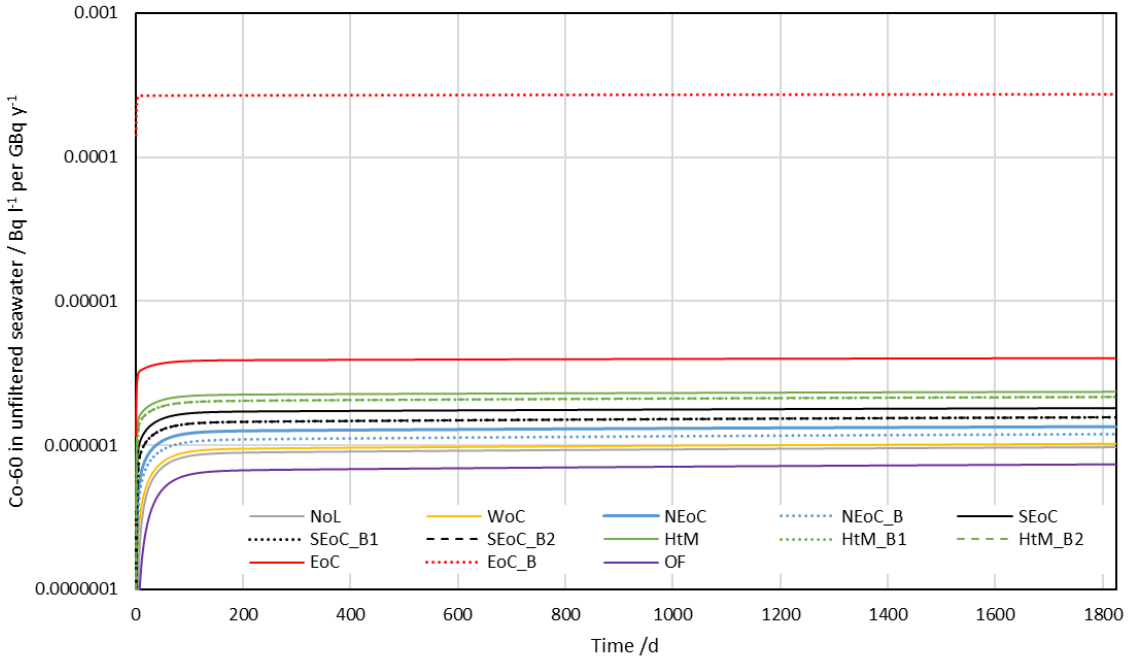

Figure 28 – Discharge-cycle moving average of Co 60 concentration in unfiltered seawater for alternative discharge scenario to the bank for five years (semi-log plot)

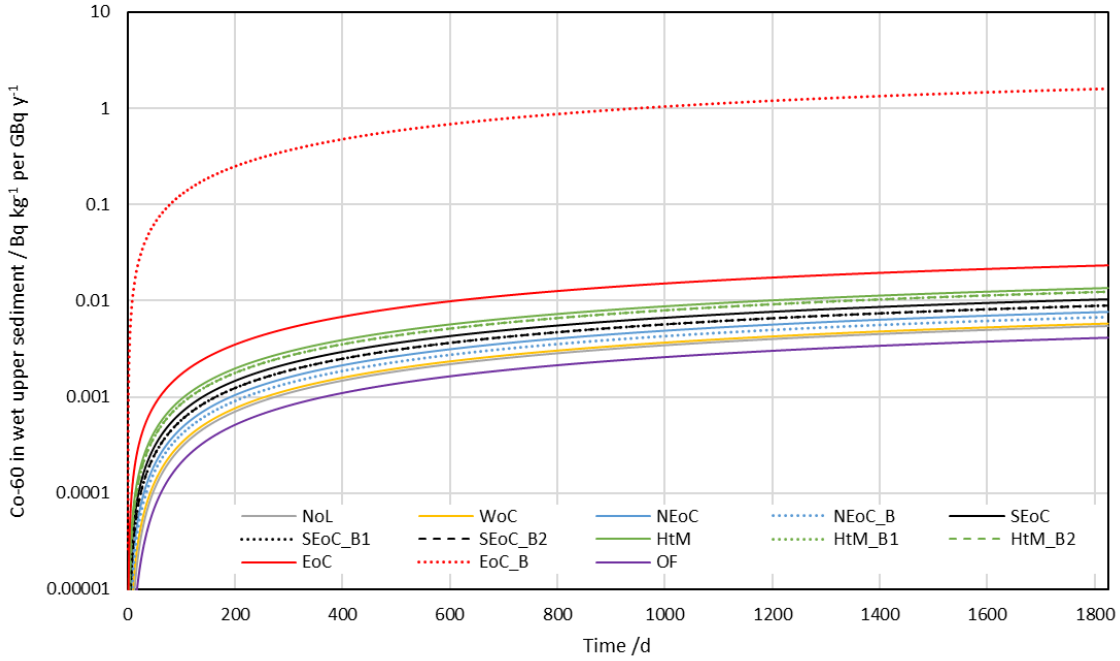

Figure 29 – Co-60 concentration in wet top sediment for five years for alternative discharge scenario to the bank (per unit annual discharge) (semi-log plot)

5.2.3 Exemplar daughter radionuclide – U-235

Figure 30 shows the activity concentration of U-235 (daughter of Pu-239) in unfiltered seawater in all compartments (per unit annual discharge of Pu-239) over the first ten days after the first discharge. Figure 31 shows the discharge-cycle moving average of U-235 concentration in unfiltered seawater in all compartments (per unit discharge) over five years of continuous discharges. The behaviour of U-235 in this scenario is almost identical to its behaviour in the baseline scenario (Subsection 5.1.3).

Figure 32 shows the activity concentration of U-235 in wet upper sediment in all compartments (per unit discharge) over five years of continuous discharges. The behaviour of U-235 in this scenario is almost identical to its behaviour in the baseline scenario (Subsection 5.1.3).

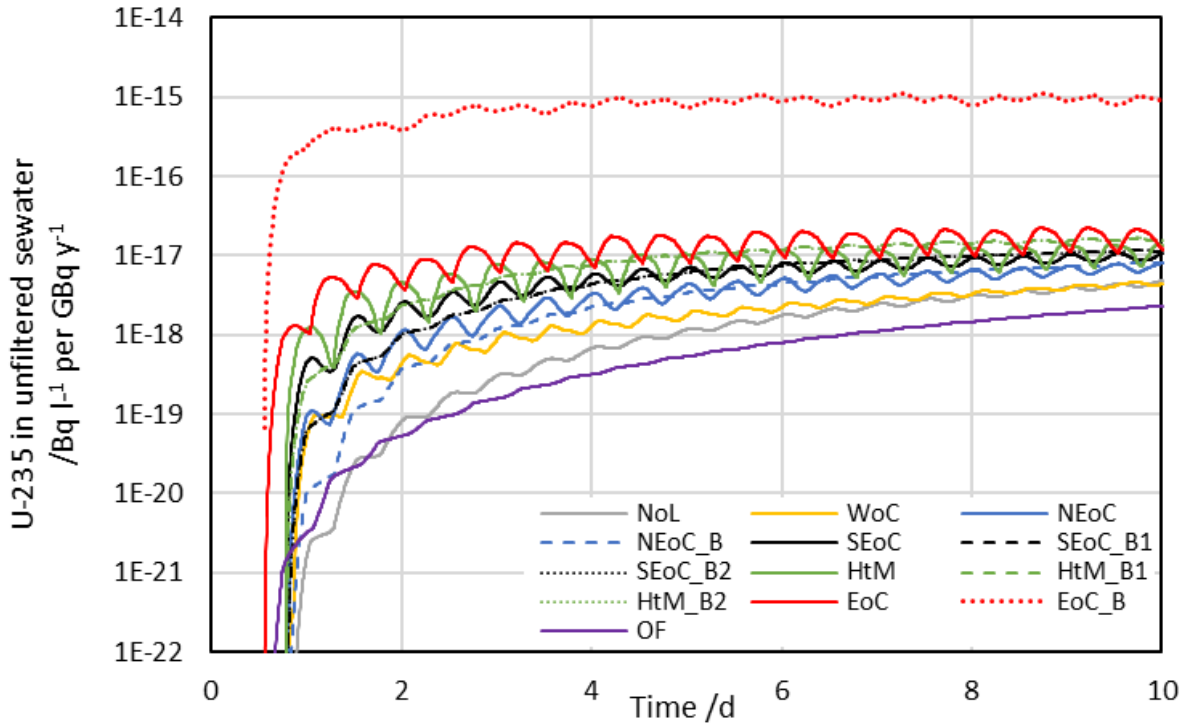

Figure 30 – Activity concentration of U-235 in unfiltered seawater for alternative discharge scenario to the bank (per unit annual discharge Pu-239) (semi-log plot)

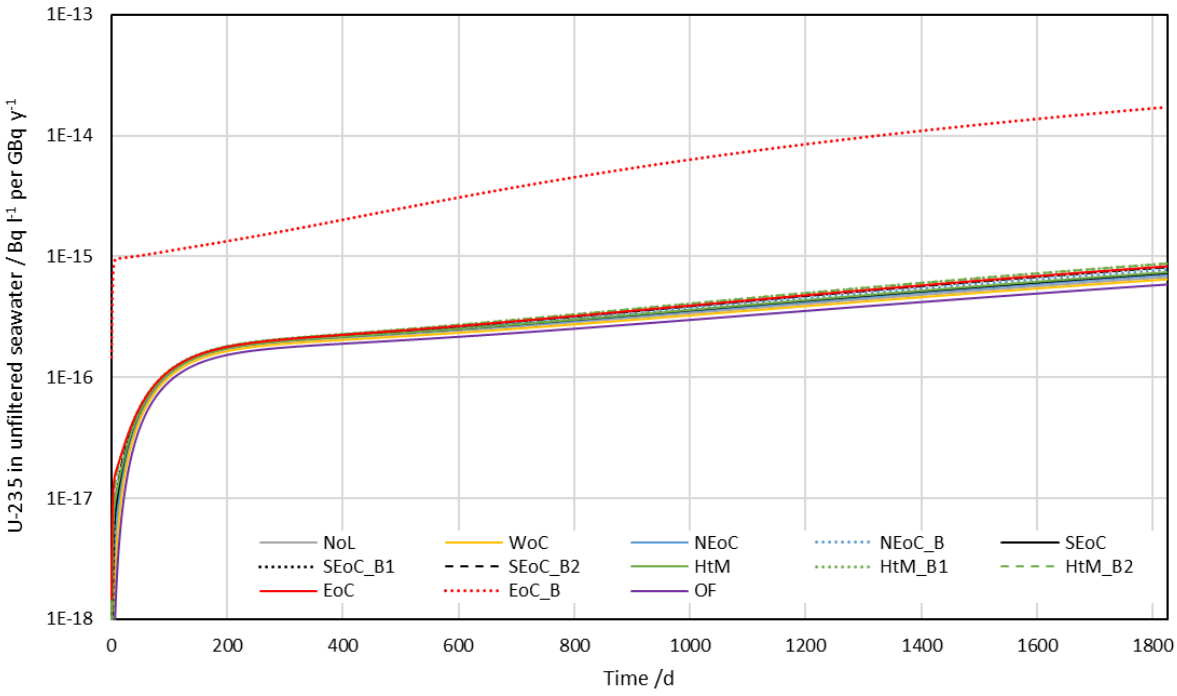

Figure 31 – Discharge-cycle moving average of U-235 concentration in unfiltered seawater for alternative discharge scenario to the bank for five years (semi-log plot)

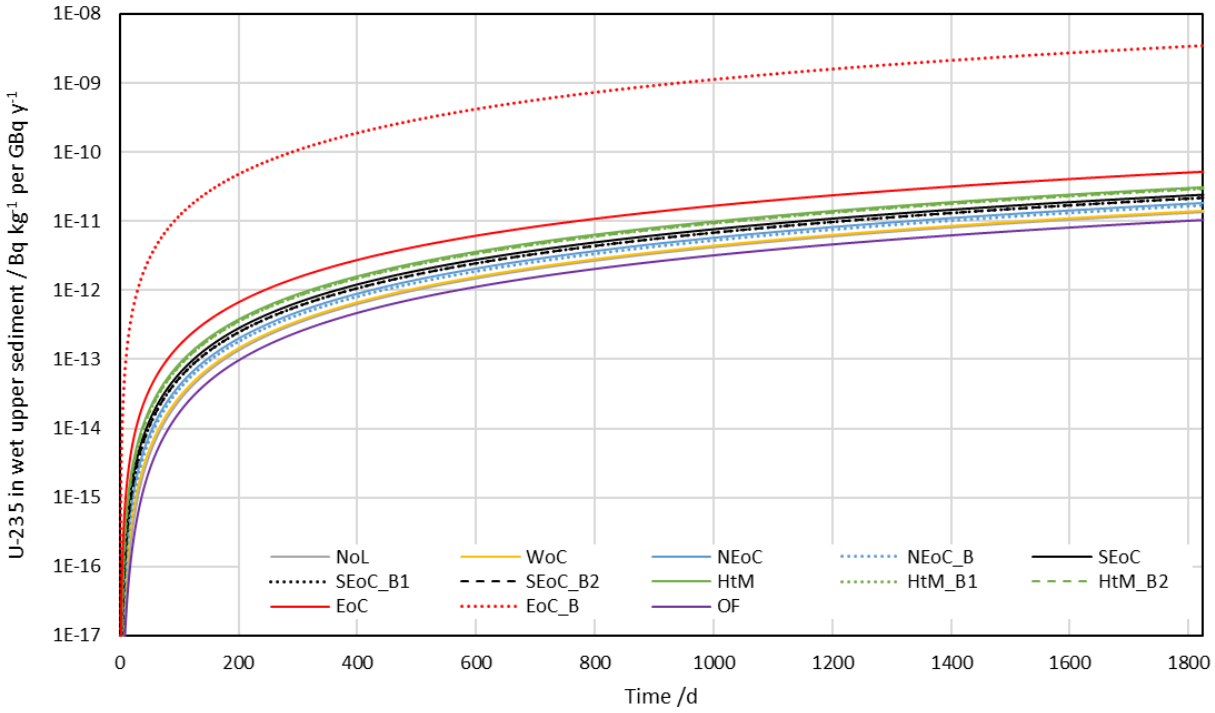

Figure 32 – U-235 concentration in wet top sediment for five years for alternative discharge scenario to the bank (per unit annual discharge) (semi-log plot)

5.2.4 Radionuclide concentrations after five years

Table 16 gives the concentration of each radionuclide that has built up in unfiltered seawater in each compartment after five years of continuous discharge. Table 17 gives the concentration of each radionuclide that has built up in wet upper sediment in each compartment after five years of continuous discharge.

Table 16 – Concentration of each radionuclide in unfiltered seawater after five years in each compartment for alternative discharge scenario to the bank (discharge cycle moving averages) (Bq l^{-1} per GBq y^{-1})

Nuclide	NoL	WoC	NEoC	NEoC_B	SEoC	SEoC_B1	SEoC_B2	HtM	HtM_B1	HtM_B2	EoC	EoC_B	OF
H-3	1.97×10^{-6}	1.98×10^{-6}	2.40×10^{-6}	2.39×10^{-6}	2.91×10^{-6}	2.84×10^{-6}	2.84×10^{-6}	3.49×10^{-6}	3.56×10^{-6}	3.56×10^{-6}	5.35×10^{-6}	3.08×10^{-4}	1.59×10^{-6}
S-35	1.31×10^{-6}	1.34×10^{-6}	1.73×10^{-6}	1.71×10^{-6}	2.25×10^{-6}	2.16×10^{-6}	2.16×10^{-6}	2.83×10^{-6}	2.88×10^{-6}	2.88×10^{-6}	4.68×10^{-6}	3.04×10^{-4}	9.97×10^{-7}
Co-60	9.70×10^{-7}	1.03×10^{-6}	1.35×10^{-6}	1.20×10^{-6}	1.81×10^{-6}	1.57×10^{-6}	1.57×10^{-6}	2.35×10^{-6}	2.17×10^{-6}	2.17×10^{-6}	4.03×10^{-6}	2.73×10^{-4}	7.38×10^{-7}
Cs-134	1.78×10^{-6}	1.80×10^{-6}	2.21×10^{-6}	2.18×10^{-6}	2.72×10^{-6}	2.63×10^{-6}	2.63×10^{-6}	3.30×10^{-6}	3.34×10^{-6}	3.34×10^{-6}	5.14×10^{-6}	3.05×10^{-4}	1.43×10^{-6}
Cs-137	1.89×10^{-6}	1.90×10^{-6}	2.32×10^{-6}	2.29×10^{-6}	2.83×10^{-6}	2.74×10^{-6}	2.74×10^{-6}	3.41×10^{-6}	3.46×10^{-6}	3.46×10^{-6}	5.25×10^{-6}	3.06×10^{-4}	1.52×10^{-6}
Pu-239	1.22×10^{-6}	1.27×10^{-6}	1.62×10^{-6}	1.50×10^{-6}	2.10×10^{-6}	1.90×10^{-6}	1.90×10^{-6}	2.66×10^{-6}	2.54×10^{-6}	2.54×10^{-6}	4.40×10^{-6}	2.85×10^{-4}	9.50×10^{-7}
U-235_ Pu-239	6.77×10^{-16}	6.48×10^{-16}	7.06×10^{-16}	7.79×10^{-16}	7.29×10^{-16}	8.20×10^{-16}	8.20×10^{-16}	7.43×10^{-16}	8.76×10^{-16}	8.76×10^{-16}	8.30×10^{-16}	1.72×10^{-14}	5.87×10^{-16}
Th-231_ Pu-239	6.49×10^{-16}	6.23×10^{-16}	6.73×10^{-16}	6.85×10^{-16}	6.90×10^{-16}	7.19×10^{-16}	7.19×10^{-16}	7.01×10^{-16}	7.64×10^{-16}	7.64×10^{-16}	7.74×10^{-16}	1.43×10^{-14}	5.67×10^{-16}
Pa-231_ Pu-239	7.43×10^{-21}	7.16×10^{-21}	8.11×10^{-21}	8.81×10^{-21}	8.77×10^{-21}	9.86×10^{-21}	9.86×10^{-21}	9.35×10^{-21}	1.14×10^{-20}	1.14×10^{-20}	1.17×10^{-20}	4.15×10^{-19}	6.25×10^{-21}
Ac-227_ Pu-239	2.62×10^{-22}	2.51×10^{-22}	2.88×10^{-22}	3.19×10^{-22}	3.13×10^{-22}	3.59×10^{-22}	3.59×10^{-22}	3.36×10^{-22}	4.19×10^{-22}	4.19×10^{-22}	4.25×10^{-22}	1.59×10^{-20}	2.17×10^{-22}

Table 17 – Concentration of each radionuclide in dry upper sediment after five years in each compartment for alternative discharge scenario to the bank (discharge-cycle moving averages) (Bq kg^{-1} per GBq y^{-1})

Nuclide	NoL	WoC	NEoC	NEoC_B	SEoC	SEoC_B1	SEoC_B2	HtM	HtM_B1	HtM_B2	EoC	EoC_B	OF
H-3	2.91×10^{-6}	2.93×10^{-6}	3.55×10^{-6}	5.04×10^{-6}	4.31×10^{-6}	6.00×10^{-6}	6.00×10^{-6}	5.18×10^{-6}	7.52×10^{-6}	7.52×10^{-6}	7.92×10^{-6}	6.50×10^{-4}	2.35×10^{-6}
S-35	9.11×10^{-7}	9.37×10^{-7}	1.21×10^{-6}	1.58×10^{-6}	1.57×10^{-6}	1.99×10^{-6}	1.99×10^{-6}	1.98×10^{-6}	2.66×10^{-6}	2.66×10^{-6}	3.26×10^{-6}	2.80×10^{-4}	6.95×10^{-7}
Co-60	1.17×10^{-2}	1.25×10^{-2}	1.65×10^{-2}	1.46×10^{-2}	2.23×10^{-2}	1.92×10^{-2}	1.92×10^{-2}	2.92×10^{-2}	2.67×10^{-2}	2.67×10^{-2}	5.02×10^{-2}	3.44×10^{0}	8.88×10^{-3}
Cs-134	7.90×10^{-4}	7.98×10^{-4}	9.82×10^{-4}	9.73×10^{-4}	1.21×10^{-3}	1.18×10^{-3}	1.18×10^{-3}	1.47×10^{-3}	1.50×10^{-3}	1.50×10^{-3}	2.30×10^{-3}	1.37×10^{-1}	6.31×10^{-4}
Cs-137	1.54×10^{-3}	1.56×10^{-3}	1.91×10^{-3}	1.89×10^{-3}	2.34×10^{-3}	2.28×10^{-3}	2.28×10^{-3}	2.83×10^{-3}	2.88×10^{-3}	2.88×10^{-3}	4.39×10^{-3}	2.60×10^{-1}	1.24×10^{-3}
Pu-239	1.30×10^{-2}	1.35×10^{-2}	1.75×10^{-2}	1.61×10^{-2}	2.29×10^{-2}	2.06×10^{-2}	2.06×10^{-2}	2.92×10^{-2}	2.78×10^{-2}	2.78×10^{-2}	4.88×10^{-2}	3.22×10^{0}	1.00×10^{-2}
U-235_ Pu-239	2.91×10^{-11}	3.04×10^{-11}	3.94×10^{-11}	3.64×10^{-11}	5.19×10^{-11}	4.68×10^{-11}	4.68×10^{-11}	6.66×10^{-11}	6.36×10^{-11}	6.36×10^{-11}	1.12×10^{-10}	7.49×10^{-9}	2.24×10^{-11}
Th-231_ Pu-239	2.91×10^{-11}	3.04×10^{-11}	3.93×10^{-11}	3.64×10^{-11}	5.19×10^{-11}	4.67×10^{-11}	4.67×10^{-11}	6.65×10^{-11}	6.35×10^{-11}	6.35×10^{-11}	1.12×10^{-10}	7.47×10^{-9}	2.23×10^{-11}
Pa-231_ Pu-239	1.03×10^{-15}	1.07×10^{-15}	1.38×10^{-15}	1.28×10^{-15}	1.82×10^{-15}	1.65×10^{-15}	1.65×10^{-15}	2.33×10^{-15}	2.23×10^{-15}	2.23×10^{-15}	3.90×10^{-15}	2.60×10^{-13}	7.90×10^{-16}
Ac-227_ Pu-239	3.93×10^{-17}	4.10×10^{-17}	5.30×10^{-17}	4.92×10^{-17}	6.97×10^{-17}	6.32×10^{-17}	6.32×10^{-17}	8.92×10^{-17}	8.56×10^{-17}	8.56×10^{-17}	1.49×10^{-16}	9.94×10^{-15}	3.02×10^{-17}

5.3 Scenario 3: alternative discharge scenario to the bank, with discharges at permit limits

Scenario 3 considers discharges to the bank during an ebb tide with a water flow of 0.0086 m^3 s^{-1} (with the water flow only operating while effluent is discharged). Discharges are every three tides, and the discharges from the permits of both stations were modelled. This represents alternative discharge arrangements that are equivalent to the existing arrangements, but without the continuous cooling water flow.

For this scenario, all parameters apart from the source term are identical to those used for Scenario 2 (alternative discharge scenario to the bank) (Subsection 5.2). Therefore, the radionuclide concentrations are linearly scaled to the permit limits from those in Scenario 2, and their changes over time are identical to those described for Scenario 2 (apart from the scaling). Consequently, the discussion in Subsection 5.2 is applicable to this scenario, and it is not repeated here.

5.3.1 Both Hunterston A and Hunterston B discharging at permit limits

Table 18 gives the concentration of each radionuclide that has built up in unfiltered seawater in each compartment after five years of continuous discharge. Table 19 gives the concentration of each radionuclide that has built up in wet upper sediment in each compartment after five years of continuous discharge. Both tables include activity discharged from both Hunterston A and Hunterston B. The largest activity concentrations in unfiltered water or wet upper sediment are for H-3 for all compartments. This is because the H-3 discharge is the largest. The contributions from each power station are given in Subsections 5.3.2 and 5.3.3.

5.3.2 Hunterston A discharging at permit limits

Table 20 gives the concentration of each radionuclide that has built up in unfiltered seawater in each compartment after five years of continuous discharge. Table 21 gives the concentration of each radionuclide that has built up in wet upper sediment in each compartment after five years of continuous discharge. Both tables include only activity discharged from Hunterston A. The highest concentration in unfiltered seawater and wet upper sediment is for Cs-137.

5.3.3 Hunterston B discharging at permit limits

Table 22 gives the concentration of each radionuclide that has built up in unfiltered seawater in each compartment after five years of continuous discharge. Table 23 gives the concentration of each radionuclide that has built up in wet upper sediment in each compartment after five years of continuous discharge. Both tables include only activity discharged from Hunterston B. The Hunterston B discharges give higher activity concentrations than the Hunterston A discharges, owing to the greater permitted limits for Hunterston B.

Table 18 – Concentration of each radionuclide in unfiltered seawater after five years in each compartment for both stations with alternative discharge scenario to the bank (discharging at permit limits) (discharge cycle moving averages) (Bq l^{-1})

Nuclide	NoL	WoC	NEoC	NEoC_B	SEoC	SEoC_B1	SEoC_B2	HtM	HtM_B1	HtM_B2	EoC	EoC_B	OF
H-3	1.38×10^{0}	1.38×10^{0}	1.68×10^{0}	1.67×10^{0}	2.04×10^{0}	1.99×10^{0}	1.99×10^{0}	2.44×10^{0}	2.49×10^{0}	2.49×10^{0}	3.74×10^{0}	2.15×10^{2}	1.11×10^{0}
S-35	7.85×10^{-3}	8.07×10^{-3}	1.04×10^{-2}	1.02×10^{-2}	1.35×10^{-2}	1.30×10^{-2}	1.30×10^{-2}	1.70×10^{-2}	1.73×10^{-2}	1.73×10^{-2}	2.81×10^{-2}	1.82×10^{0}	5.98×10^{-3}
Co-60	9.70×10^{-6}	1.03×10^{-5}	1.35×10^{-5}	1.20×10^{-5}	1.81×10^{-5}	1.57×10^{-5}	1.57×10^{-5}	2.35×10^{-5}	2.17×10^{-5}	2.17×10^{-5}	4.03×10^{-5}	2.73×10^{-3}	7.38×10^{-6}
Sr-90	0	0	0	0	0	0	0	0	0	0	0	0	0
Cs-134	3.74×10^{-4}	3.78×10^{-4}	4.65×10^{-4}	4.58×10^{-4}	5.72×10^{-4}	5.53×10^{-4}	5.53×10^{-4}	6.93×10^{-4}	7.02×10^{-4}	7.02×10^{-4}	1.08×10^{-3}	6.40×10^{-2}	3.00×10^{-4}
Cs-137	3.02×10^{-4}	3.05×10^{-4}	3.71×10^{-4}	3.67×10^{-4}	4.53×10^{-4}	4.39×10^{-4}	4.39×10^{-4}	5.45×10^{-4}	5.53×10^{-4}	5.53×10^{-4}	8.40×10^{-4}	4.89×10^{-2}	2.44×10^{-4}
Pu-239	3.67×10^{-6}	3.80×10^{-6}	4.86×10^{-6}	4.49×10^{-6}	6.31×10^{-6}	5.69×10^{-6}	5.69×10^{-6}	7.97×10^{-6}	7.62×10^{-6}	7.62×10^{-6}	1.32×10^{-5}	8.55×10^{-4}	2.85×10^{-6}
U-235_ Pu-239	2.03×10^{-15}	1.94×10^{-15}	2.12×10^{-15}	2.34×10^{-15}	2.19×10^{-15}	2.46×10^{-15}	2.46×10^{-15}	2.23×10^{-15}	2.63×10^{-15}	2.63×10^{-15}	2.49×10^{-15}	5.17×10^{-14}	1.76×10^{-15}
Th-231_ Pu-239	1.95×10^{-15}	1.87×10^{-15}	2.02×10^{-15}	2.06×10^{-15}	2.07×10^{-15}	2.16×10^{-15}	2.16×10^{-15}	2.10×10^{-15}	2.29×10^{-15}	2.29×10^{-15}	2.32×10^{-15}	4.30×10^{-14}	1.70×10^{-15}
Pa-231_ Pu-239	2.23×10^{-20}	2.15×10^{-20}	2.43×10^{-20}	2.64×10^{-20}	2.63×10^{-20}	2.96×10^{-20}	2.96×10^{-20}	2.81×10^{-20}	3.42×10^{-20}	3.42×10^{-20}	3.51×10^{-20}	1.25×10^{-18}	1.88×10^{-20}
Ac-227_ Pu-239	7.85×10^{-22}	7.54×10^{-22}	8.63×10^{-22}	9.57×10^{-22}	9.40×10^{-22}	1.08×10^{-21}	1.08×10^{-21}	1.01×10^{-21}	1.26×10^{-21}	1.26×10^{-21}	1.28×10^{-21}	4.77×10^{-20}	6.51×10^{-22}
Pu-241	2.41×10^{-6}	2.50×10^{-6}	3.20×10^{-6}	2.95×10^{-6}	4.16×10^{-6}	3.75×10^{-6}	3.75×10^{-6}	5.27×10^{-6}	5.03×10^{-6}	5.03×10^{-6}	8.75×10^{-6}	5.69×10^{-4}	1.87×10^{-6}
Am-241_ Pu-241	9.26×10^{-10}	8.92×10^{-10}	9.93×10^{-10}	1.04×10^{-9}	1.06×10^{-9}	1.14×10^{-9}	1.14×10^{-9}	1.11×10^{-9}	1.28×10^{-9}	1.28×10^{-9}	1.33×10^{-9}	3.99×10^{-8}	7.92×10^{-10}
U-237_ Pu-241	5.26×10^{-11}	5.00×10^{-11}	5.72×10^{-11}	5.97×10^{-11}	6.09×10^{-11}	6.51×10^{-11}	6.51×10^{-11}	6.32×10^{-11}	7.18×10^{-11}	7.18×10^{-11}	7.41×10^{-11}	1.92×10^{-9}	4.28×10^{-11}
Np-237_ Pu-241	8.52×10^{-16}	8.13×10^{-16}	8.96×10^{-16}	1.02×10^{-15}	9.33×10^{-16}	1.09×10^{-15}	1.09×10^{-15}	9.58×10^{-16}	1.18×10^{-15}	1.18×10^{-15}	1.10×10^{-15}	2.66×10^{-14}	7.30×10^{-16}
Pa-233_ Pu-241	5.26×10^{-16}	5.08×10^{-16}	5.56×10^{-16}	5.70×10^{-16}	5.83×10^{-16}	6.16×10^{-16}	6.16×10^{-16}	6.07×10^{-16}	6.82×10^{-16}	6.82×10^{-16}	7.10×10^{-16}	1.89×10^{-14}	4.59×10^{-16}
U-233_ Pu-241	4.20×10^{-21}	4.00×10^{-21}	4.42×10^{-21}	5.02×10^{-21}	4.60×10^{-21}	5.35×10^{-21}	5.35×10^{-21}	4.72×10^{-21}	5.81×10^{-21}	5.81×10^{-21}	5.41×10^{-21}	1.33×10^{-19}	3.59×10^{-21}

Nuclide	NoL	WoC	NEoC	NEoC_B	SEoC	SEoC_B1	SEoC_B2	HtM	HtM_B1	HtM_B2	EoC	EoC_B	OF
Th-229_ Pu-241	1.77×10^{-25}	1.71×10^{-25}	1.92×10^{-25}	2.09×10^{-25}	2.07×10^{-25}	2.32×10^{-25}	2.32×10^{-25}	2.20×10^{-25}	2.66×10^{-25}	2.66×10^{-25}	2.71×10^{-25}	9.21×10^{-24}	1.50×10^{-25}

Table 19 – Concentration of each radionuclide in dry upper sediment after five years in each compartment for both stations with alternative discharge scenario to the bank (discharging at permit limits) (discharge cycle moving averages) (Bq kg^{-1})

Nuclide	NoL	WoC	NEoC	NEoC_B	SEoC	SEoC_B1	SEoC_B2	HtM	HtM_B1	HtM_B2	EoC	EoC_B	OF
H-3	2.04×10^{0}	2.05×10^{0}	2.49×10^{0}	3.53×10^{0}	3.02×10^{0}	4.20×10^{0}	4.20×10^{0}	3.63×10^{0}	5.26×10^{0}	5.26×10^{0}	5.54×10^{0}	4.55×10^{2}	1.64×10^{0}
S-35	5.47×10^{-3}	5.62×10^{-3}	7.25×10^{-3}	9.45×10^{-3}	9.39×10^{-3}	1.20×10^{-2}	1.20×10^{-2}	1.19×10^{-2}	1.59×10^{-2}	1.59×10^{-2}	1.95×10^{-2}	1.68×10^{0}	4.17×10^{-3}
Co-60	1.17×10^{-1}	1.25×10^{-1}	1.65×10^{-1}	1.46×10^{-1}	2.23×10^{-1}	1.92×10^{-1}	1.92×10^{-1}	2.92×10^{-1}	2.67×10^{-1}	2.67×10^{-1}	5.02×10^{-1}	3.44×10^{1}	8.88×10^{-2}
Sr-90	0	0	0	0	0	0	0	0	0	0	0	0	0
Cs-134	1.66×10^{-1}	1.68×10^{-1}	2.06×10^{-1}	2.04×10^{-1}	2.54×10^{-1}	2.47×10^{-1}	2.47×10^{-1}	3.09×10^{-1}	3.14×10^{-1}	3.14×10^{-1}	4.82×10^{-1}	2.89×10^{1}	1.32×10^{-1}
Cs-137	2.47×10^{-1}	2.49×10^{-1}	3.05×10^{-1}	3.03×10^{-1}	3.74×10^{-1}	3.64×10^{-1}	3.64×10^{-1}	4.53×10^{-1}	4.61×10^{-1}	4.61×10^{-1}	7.02×10^{-1}	4.16×10^{1}	1.98×10^{-1}
Pu-239	3.90×10^{-2}	4.06×10^{-2}	5.24×10^{-2}	4.82×10^{-2}	6.87×10^{-2}	6.17×10^{-2}	6.17×10^{-2}	8.77×10^{-2}	8.33×10^{-2}	8.34×10^{-2}	1.46×10^{-1}	9.66×10^{0}	3.01×10^{-2}
U-235_ Pu-239	8.74×10^{-11}	9.13×10^{-11}	1.18×10^{-10}	1.09×10^{-10}	1.56×10^{-10}	1.40×10^{-10}	1.40×10^{-10}	2.00×10^{-10}	1.91×10^{-10}	1.91×10^{-10}	3.35×10^{-10}	2.25×10^{-8}	6.71×10^{-11}
Th-231_ Pu-239	8.73×10^{-11}	9.11×10^{-11}	1.18×10^{-10}	1.09×10^{-10}	1.56×10^{-10}	1.40×10^{-10}	1.40×10^{-10}	2.00×10^{-10}	1.90×10^{-10}	1.90×10^{-10}	3.35×10^{-10}	2.24×10^{-8}	6.70×10^{-11}
Pa-231_ Pu-239	3.08×10^{-15}	3.21×10^{-15}	4.15×10^{-15}	3.85×10^{-15}	5.46×10^{-15}	4.94×10^{-15}	4.94×10^{-15}	6.99×10^{-15}	6.70×10^{-15}	6.70×10^{-15}	1.17×10^{-14}	7.80×10^{-13}	2.37×10^{-15}
Ac-227_ Pu-239	1.18×10^{-16}	1.23×10^{-16}	1.59×10^{-16}	1.48×10^{-16}	2.09×10^{-16}	1.89×10^{-16}	1.89×10^{-16}	2.68×10^{-16}	2.57×10^{-16}	2.57×10^{-16}	4.47×10^{-16}	2.98×10^{-14}	9.07×10^{-17}
Pu-241	2.31×10^{-2}	2.41×10^{-2}	3.11×10^{-2}	2.86×10^{-2}	4.08×10^{-2}	3.66×10^{-2}	3.66×10^{-2}	5.21×10^{-2}	4.95×10^{-2}	4.95×10^{-2}	8.70×10^{-2}	5.75×10^{0}	1.78×10^{-2}
Am-241_ Pu-241	9.92×10^{-5}	1.03×10^{-4}	1.31×10^{-4}	1.21×10^{-4}	1.70×10^{-4}	1.54×10^{-4}	1.54×10^{-4}	2.15×10^{-4}	2.06×10^{-4}	2.06×10^{-4}	3.55×10^{-4}	2.31×10^{-2}	7.72×10^{-5}
U-237_ Pu-241	5.63×10^{-7}	5.87×10^{-7}	7.57×10^{-7}	6.96×10^{-7}	9.93×10^{-7}	8.91×10^{-7}	8.91×10^{-7}	1.27×10^{-6}	1.21×10^{-6}	1.21×10^{-6}	2.12×10^{-6}	1.40×10^{-4}	4.34×10^{-7}
Np-237_ Pu-241	5.22×10^{-11}	5.42×10^{-11}	6.92×10^{-11}	6.41×10^{-11}	8.99×10^{-11}	8.14×10^{-11}	8.14×10^{-11}	1.14×10^{-10}	1.09×10^{-10}	1.09×10^{-10}	1.89×10^{-10}	1.24×10^{-8}	4.06×10^{-11}
Pa-233_ Pu-241	4.92×10^{-11}	5.11×10^{-11}	6.52×10^{-11}	6.04×10^{-11}	8.47×10^{-11}	7.67×10^{-11}	7.67×10^{-11}	1.07×10^{-10}	1.03×10^{-10}	1.03×10^{-10}	1.77×10^{-10}	1.16×10^{-8}	3.83×10^{-11}
U-233_ Pu-241	2.59×10^{-16}	2.69×10^{-16}	3.43×10^{-16}	3.18×10^{-16}	4.46×10^{-16}	4.04×10^{-16}	4.04×10^{-16}	5.66×10^{-16}	5.43×10^{-16}	5.43×10^{-16}	9.37×10^{-16}	6.16×10^{-14}	2.01×10^{-16}

Nuclide	NoL	WoC	NEoC	NEoC_B	SEoC	SEoC_B1	SEoC_B2	HtM	HtM_B1	HtM_B2	EoC	EoC_B	OF
Th-229_ Pu-241	2.46×10^{-20}	2.55×10^{-20}	3.25×10^{-20}	3.02×10^{-20}	4.21×10^{-20}	3.82×10^{-20}	3.82×10^{-20}	5.34×10^{-20}	5.12×10^{-20}	5.12×10^{-20}	8.80×10^{-20}	5.75×10^{-18}	1.92×10^{-20}

Table 20 – Concentration of each radionuclide in unfiltered seawater after five years in each compartment for Hunterston A with alternative discharge scenario to the bank (discharging at permit limits) (discharge cycle moving averages) (Bq l^{-1})

Nuclide	NoL	WoC	NEoC	NEoC_B	SEoC	SEoC_B1	SEoC_B2	HtM	HtM_B1	HtM_B2	EoC	EoC_B	OF
H-3	5.90×10^{-5}	5.93×10^{-5}	7.20×10^{-5}	7.16×10^{-5}	8.74×10^{-5}	8.52×10^{-5}	8.52×10^{-5}	1.05×10^{-4}	1.07×10^{-4}	1.07×10^{-4}	1.60×10^{-4}	9.23×10^{-3}	4.77×10^{-5}
Sr-90	0	0	0	0	0	0	0	0	0	0	0	0	0
Cs-134	1.07×10^{-4}	1.08×10^{-4}	1.33×10^{-4}	1.31×10^{-4}	1.63×10^{-4}	1.58×10^{-4}	1.58×10^{-4}	1.98×10^{-4}	2.01×10^{-4}	2.01×10^{-4}	3.09×10^{-4}	1.83×10^{-2}	8.56×10^{-5}
Cs-137	3.02×10^{-4}	3.05×10^{-4}	3.71×10^{-4}	3.67×10^{-4}	4.53×10^{-4}	4.39×10^{-4}	4.39×10^{-4}	5.45×10^{-4}	5.53×10^{-4}	5.53×10^{-4}	8.40×10^{-4}	4.89×10^{-2}	2.44×10^{-4}
Pu-239	2.44×10^{-6}	2.53×10^{-6}	3.24×10^{-6}	2.99×10^{-6}	4.20×10^{-6}	3.79×10^{-6}	3.79×10^{-6}	5.31×10^{-6}	5.08×10^{-6}	5.08×10^{-6}	8.80×10^{-6}	5.70×10^{-4}	1.90×10^{-6}
U-235_ Pu-239	1.35×10^{-15}	1.30×10^{-15}	1.41×10^{-15}	1.56×10^{-15}	1.46×10^{-15}	1.64×10^{-15}	1.64×10^{-15}	1.49×10^{-15}	1.75×10^{-15}	1.75×10^{-15}	1.66×10^{-15}	3.45×10^{-14}	1.17×10^{-15}
Th-231_ Pu-239	1.30×10^{-15}	1.25×10^{-15}	1.35×10^{-15}	1.37×10^{-15}	1.38×10^{-15}	1.44×10^{-15}	1.44×10^{-15}	1.40×10^{-15}	1.53×10^{-15}	1.53×10^{-15}	1.55×10^{-15}	2.87×10^{-14}	1.13×10^{-15}
Pa-231_ Pu-239	1.49×10^{-20}	1.43×10^{-20}	1.62×10^{-20}	1.76×10^{-20}	1.75×10^{-20}	1.97×10^{-20}	1.97×10^{-20}	1.87×10^{-20}	2.28×10^{-20}	2.28×10^{-20}	2.34×10^{-20}	8.30×10^{-19}	1.25×10^{-20}
Ac-227_ Pu-239	5.23×10^{-22}	5.03×10^{-22}	5.75×10^{-22}	6.38×10^{-22}	6.27×10^{-22}	7.19×10^{-22}	7.19×10^{-22}	6.71×10^{-22}	8.38×10^{-22}	8.37×10^{-22}	8.50×10^{-22}	3.18×10^{-20}	4.34×10^{-22}
Pu-241	2.41×10^{-6}	2.50×10^{-6}	3.20×10^{-6}	2.95×10^{-6}	4.16×10^{-6}	3.75×10^{-6}	3.75×10^{-6}	5.27×10^{-6}	5.03×10^{-6}	5.03×10^{-6}	8.75×10^{-6}	5.69×10^{-4}	1.87×10^{-6}
Am-241_ Pu-241	9.26×10^{-10}	8.92×10^{-10}	9.93×10^{-10}	1.04×10^{-9}	1.06×10^{-9}	1.14×10^{-9}	1.14×10^{-9}	1.11×10^{-9}	1.28×10^{-9}	1.28×10^{-9}	1.33×10^{-9}	3.99×10^{-8}	7.92×10^{-10}
U-237_ Pu-241	5.26×10^{-11}	5.00×10^{-11}	5.72×10^{-11}	5.97×10^{-11}	6.09×10^{-11}	6.51×10^{-11}	6.51×10^{-11}	6.32×10^{-11}	7.18×10^{-11}	7.18×10^{-11}	7.41×10^{-11}	1.92×10^{-9}	4.28×10^{-11}
Np-237_ Pu-241	8.52×10^{-16}	8.13×10^{-16}	8.96×10^{-16}	1.02×10^{-15}	9.33×10^{-16}	1.09×10^{-15}	1.09×10^{-15}	9.58×10^{-16}	1.18×10^{-15}	1.18×10^{-15}	1.10×10^{-15}	2.66×10^{-14}	7.30×10^{-16}
Pa-233_ Pu-241	5.26×10^{-16}	5.08×10^{-16}	5.56×10^{-16}	5.70×10^{-16}	5.83×10^{-16}	6.16×10^{-16}	6.16×10^{-16}	6.07×10^{-16}	6.82×10^{-16}	6.82×10^{-16}	7.10×10^{-16}	1.89×10^{-14}	4.59×10^{-16}
U-233_ Pu-241	4.20×10^{-21}	4.00×10^{-21}	4.42×10^{-21}	5.02×10^{-21}	4.60×10^{-21}	5.35×10^{-21}	5.35×10^{-21}	4.72×10^{-21}	5.81×10^{-21}	5.81×10^{-21}	5.41×10^{-21}	1.33×10^{-19}	3.59×10^{-21}
Th-229_ Pu-241	1.77×10^{-25}	1.71×10^{-25}	1.92×10^{-25}	2.09×10^{-25}	2.07×10^{-25}	2.32×10^{-25}	2.32×10^{-25}	2.20×10^{-25}	2.66×10^{-25}	2.66×10^{-25}	2.71×10^{-25}	9.21×10^{-24}	1.50×10^{-25}

Table 21 – Concentration of each radionuclide in dry upper sediment after five years in each compartment for Hunterston A with alternative discharge scenario to the bank (discharging at permit limits) (discharge cycle moving averages) (Bq kg^{-1})

Nuclide	NoL	WoC	NEoC	NEoC_B	SEoC	SEoC_B1	SEoC_B2	HtM	HtM_B1	HtM_B2	EoC	EoC_B	OF
H-3	8.73×10^{-5}	8.78×10^{-5}	1.07×10^{-4}	1.51×10^{-4}	1.29×10^{-4}	1.80×10^{-4}	1.80×10^{-4}	1.55×10^{-4}	2.26×10^{-4}	2.26×10^{-4}	2.38×10^{-4}	1.95×10^{-2}	7.05×10^{-5}
Sr-90	0	0	0	0	0	0	0	0	0	0	0	0	0
Cs-134	4.74×10^{-2}	4.79×10^{-2}	5.89×10^{-2}	5.84×10^{-2}	7.27×10^{-2}	7.05×10^{-2}	7.05×10^{-2}	8.84×10^{-2}	8.98×10^{-2}	8.98×10^{-2}	1.38×10^{-1}	8.24×10^{0}	3.78×10^{-2}
Cs-137	2.47×10^{-1}	2.49×10^{-1}	3.05×10^{-1}	3.03×10^{-1}	3.74×10^{-1}	3.64×10^{-1}	3.64×10^{-1}	4.53×10^{-1}	4.61×10^{-1}	4.61×10^{-1}	7.02×10^{-1}	4.16×10^{1}	1.98×10^{-1}
Pu-239	2.60×10^{-2}	2.71×10^{-2}	3.49×10^{-2}	3.22×10^{-2}	4.58×10^{-2}	4.11×10^{-2}	4.11×10^{-2}	5.85×10^{-2}	5.56×10^{-2}	5.56×10^{-2}	9.76×10^{-2}	6.44×10^{0}	2.01×10^{-2}
U-235_ Pu-239	5.83×10^{-11}	6.08×10^{-11}	7.88×10^{-11}	7.28×10^{-11}	1.04×10^{-10}	9.36×10^{-11}	9.36×10^{-11}	1.33×10^{-10}	1.27×10^{-10}	1.27×10^{-10}	2.24×10^{-10}	1.50×10^{-8}	4.48×10^{-11}
Th-231_ Pu-239	5.82×10^{-11}	6.08×10^{-11}	7.87×10^{-11}	7.27×10^{-11}	1.04×10^{-10}	9.35×10^{-11}	9.35×10^{-11}	1.33×10^{-10}	1.27×10^{-10}	1.27×10^{-10}	2.23×10^{-10}	1.49×10^{-8}	4.47×10^{-11}
Pa-231_ Pu-239	2.05×10^{-15}	2.14×10^{-15}	2.77×10^{-15}	2.57×10^{-15}	3.64×10^{-15}	3.29×10^{-15}	3.29×10^{-15}	4.66×10^{-15}	4.47×10^{-15}	4.47×10^{-15}	7.80×10^{-15}	5.20×10^{-13}	1.58×10^{-15}
Ac-227_ Pu-239	7.87×10^{-17}	8.20×10^{-17}	1.06×10^{-16}	9.85×10^{-17}	1.39×10^{-16}	1.26×10^{-16}	1.26×10^{-16}	1.78×10^{-16}	1.71×10^{-16}	1.71×10^{-16}	2.98×10^{-16}	1.99×10^{-14}	6.05×10^{-17}
Pu-241	2.31×10^{-2}	2.41×10^{-2}	3.11×10^{-2}	2.86×10^{-2}	4.08×10^{-2}	3.66×10^{-2}	3.66×10^{-2}	5.21×10^{-2}	4.95×10^{-2}	4.95×10^{-2}	8.70×10^{-2}	5.75×10^{0}	1.78×10^{-2}
Am-241_ Pu-241	9.92×10^{-5}	1.03×10^{-4}	1.31×10^{-4}	1.21×10^{-4}	1.70×10^{-4}	1.54×10^{-4}	1.54×10^{-4}	2.15×10^{-4}	2.06×10^{-4}	2.06×10^{-4}	3.55×10^{-4}	2.31×10^{-2}	7.72×10^{-5}
U-237_ Pu-241	5.63×10^{-7}	5.87×10^{-7}	7.57×10^{-7}	6.96×10^{-7}	9.93×10^{-7}	8.91×10^{-7}	8.91×10^{-7}	1.27×10^{-6}	1.21×10^{-6}	1.21×10^{-6}	2.12×10^{-6}	1.40×10^{-4}	4.34×10^{-7}
Np-237_ Pu-241	5.22×10^{-11}	5.42×10^{-11}	6.92×10^{-11}	6.41×10^{-11}	8.99×10^{-11}	8.14×10^{-11}	8.14×10^{-11}	1.14×10^{-10}	1.09×10^{-10}	1.09×10^{-10}	1.89×10^{-10}	1.24×10^{-8}	4.06×10^{-11}
Pa-233_ Pu-241	4.92×10^{-11}	5.11×10^{-11}	6.52×10^{-11}	6.04×10^{-11}	8.47×10^{-11}	7.67×10^{-11}	7.67×10^{-11}	1.07×10^{-10}	1.03×10^{-10}	1.03×10^{-10}	1.77×10^{-10}	1.16×10^{-8}	3.83×10^{-11}
U-233_ Pu-241	2.59×10^{-16}	2.69×10^{-16}	3.43×10^{-16}	3.18×10^{-16}	4.46×10^{-16}	4.04×10^{-16}	4.04×10^{-16}	5.66×10^{-16}	5.43×10^{-16}	5.43×10^{-16}	9.37×10^{-16}	6.16×10^{-14}	2.01×10^{-16}
Th-229_ Pu-241	2.46×10^{-20}	2.55×10^{-20}	3.25×10^{-20}	3.02×10^{-20}	4.21×10^{-20}	3.82×10^{-20}	3.82×10^{-20}	5.34×10^{-20}	5.12×10^{-20}	5.12×10^{-20}	8.80×10^{-20}	5.75×10^{-18}	1.92×10^{-20}

Table 22 – Concentration of each radionuclide in unfiltered seawater after five years in each compartment for Hunterston B with alternative discharge scenario to the bank (discharging at permit limits) (discharge cycle moving averages) (Bq l^{-1})

Nuclide	NoL	WoC	NEoC	NEoC_B	SEoC	SEoC_B1	SEoC_B2	HtM	HtM_B1	HtM_B2	EoC	EoC_B	OF
H-3	1.38×10^{0}	1.38×10^{0}	1.68×10^{0}	1.67×10^{0}	2.04×10^{0}	1.99×10^{0}	1.99×10^{0}	2.44×10^{0}	2.49×10^{0}	2.49×10^{0}	3.74×10^{0}	2.15×10^{2}	1.11×10^{0}
S-35	7.85×10^{-3}	8.07×10^{-3}	1.04×10^{-2}	1.02×10^{-2}	1.35×10^{-2}	1.30×10^{-2}	1.30×10^{-2}	1.70×10^{-2}	1.73×10^{-2}	1.73×10^{-2}	2.81×10^{-2}	1.82×10^{0}	5.98×10^{-3}
Co-60	9.70×10^{-6}	1.03×10^{-5}	1.35×10^{-5}	1.20×10^{-5}	1.81×10^{-5}	1.57×10^{-5}	1.57×10^{-5}	2.35×10^{-5}	2.17×10^{-5}	2.17×10^{-5}	4.03×10^{-5}	2.73×10^{-3}	7.38×10^{-6}
Cs-134	2.67×10^{-4}	2.70×10^{-4}	3.32×10^{-4}	3.27×10^{-4}	4.08×10^{-4}	3.95×10^{-4}	3.95×10^{-4}	4.95×10^{-4}	5.02×10^{-4}	5.02×10^{-4}	7.72×10^{-4}	4.57×10^{-2}	2.14×10^{-4}
Cs-137	0	0	0	0	0	0	0	0	0	0	0	0	0
Pu-239	1.22×10^{-6}	1.27×10^{-6}	1.62×10^{-6}	1.50×10^{-6}	2.10×10^{-6}	1.90×10^{-6}	1.90×10^{-6}	2.66×10^{-6}	2.54×10^{-6}	2.54×10^{-6}	4.40×10^{-6}	2.85×10^{-4}	9.50×10^{-7}
U-235_ Pu-239	6.77×10^{-16}	6.48×10^{-16}	7.06×10^{-16}	7.79×10^{-16}	7.29×10^{-16}	8.20×10^{-16}	8.20×10^{-16}	7.43×10^{-16}	8.76×10^{-16}	8.76×10^{-16}	8.30×10^{-16}	1.72×10^{-14}	5.87×10^{-16}
Th-231_ Pu-239	6.49×10^{-16}	6.23×10^{-16}	6.73×10^{-16}	6.85×10^{-16}	6.90×10^{-16}	7.19×10^{-16}	7.19×10^{-16}	7.01×10^{-16}	7.64×10^{-16}	7.64×10^{-16}	7.74×10^{-16}	1.43×10^{-14}	5.67×10^{-16}
Pa-231_ Pu-239	7.43×10^{-21}	7.16×10^{-21}	8.11×10^{-21}	8.81×10^{-21}	8.77×10^{-21}	9.86×10^{-21}	9.86×10^{-21}	9.35×10^{-21}	1.14×10^{-20}	1.14×10^{-20}	1.17×10^{-20}	4.15×10^{-19}	6.25×10^{-21}
Ac-227_ Pu-239	2.62×10^{-22}	2.51×10^{-22}	2.88×10^{-22}	3.19×10^{-22}	3.13×10^{-22}	3.59×10^{-22}	3.59×10^{-22}	3.36×10^{-22}	4.19×10^{-22}	4.19×10^{-22}	4.25×10^{-22}	1.59×10^{-20}	2.17×10^{-22}

Table 23 – Concentration of each radionuclide in dry upper sediment after five years in each compartment for Hunterston B with alternative discharge scenario to the bank (discharging at permit limits) (discharge cycle moving averages) (Bq kg^{-1})

Nuclide	NoL	WoC	NEoC	NEoC_B	SEoC	SEoC_B1	SEoC_B2	HtM	HtM_B1	HtM_B2	EoC	EoC_B	OF
H-3	2.04×10^{0}	2.05×10^{0}	2.49×10^{0}	3.53×10^{0}	3.02×10^{0}	4.20×10^{0}	4.20×10^{0}	3.63×10^{0}	5.26×10^{0}	5.26×10^{0}	5.54×10^{0}	4.55×10^{2}	1.64×10^{0}
S-35	5.47×10^{-3}	5.62×10^{-3}	7.25×10^{-3}	9.45×10^{-3}	9.39×10^{-3}	1.20×10^{-2}	1.20×10^{-2}	1.19×10^{-2}	1.59×10^{-2}	1.59×10^{-2}	1.95×10^{-2}	1.68×10^{0}	4.17×10^{-3}
Co-60	1.17×10^{-1}	1.25×10^{-1}	1.65×10^{-1}	1.46×10^{-1}	2.23×10^{-1}	1.92×10^{-1}	1.92×10^{-1}	2.92×10^{-1}	2.67×10^{-1}	2.67×10^{-1}	5.02×10^{-1}	3.44×10^{1}	8.88×10^{-2}
Cs-134	1.18×10^{-1}	1.20×10^{-1}	1.47×10^{-1}	1.46×10^{-1}	1.82×10^{-1}	1.76×10^{-1}	1.76×10^{-1}	2.21×10^{-1}	2.25×10^{-1}	2.25×10^{-1}	3.45×10^{-1}	2.06×10^{1}	9.46×10^{-2}
Cs-137	0	0	0	0	0	0	0	0	0	0	0	0	0
Pu-239	1.30×10^{-2}	1.35×10^{-2}	1.75×10^{-2}	1.61×10^{-2}	2.29×10^{-2}	2.06×10^{-2}	2.06×10^{-2}	2.92×10^{-2}	2.78×10^{-2}	2.78×10^{-2}	4.88×10^{-2}	3.22×10^{0}	1.00×10^{-2}
U-235_ Pu-239	2.91×10^{-11}	3.04×10^{-11}	3.94×10^{-11}	3.64×10^{-11}	5.19×10^{-11}	4.68×10^{-11}	4.68×10^{-11}	6.66×10^{-11}	6.36×10^{-11}	6.36×10^{-11}	1.12×10^{-10}	7.49×10^{-9}	2.24×10^{-11}
Th-231_ Pu-239	2.91×10^{-11}	3.04×10^{-11}	3.93×10^{-11}	3.64×10^{-11}	5.19×10^{-11}	4.67×10^{-11}	4.67×10^{-11}	6.65×10^{-11}	6.35×10^{-11}	6.35×10^{-11}	1.12×10^{-10}	7.47×10^{-9}	2.23×10^{-11}
Pa-231_ Pu-239	1.03×10^{-15}	1.07×10^{-15}	1.38×10^{-15}	1.28×10^{-15}	1.82×10^{-15}	1.65×10^{-15}	1.65×10^{-15}	2.33×10^{-15}	2.23×10^{-15}	2.23×10^{-15}	3.90×10^{-15}	2.60×10^{-13}	7.90×10^{-16}
Ac-227_ Pu-239	3.93×10^{-17}	4.10×10^{-17}	5.30×10^{-17}	4.92×10^{-17}	6.97×10^{-17}	6.32×10^{-17}	6.32×10^{-17}	8.92×10^{-17}	8.56×10^{-17}	8.56×10^{-17}	1.49×10^{-16}	9.94×10^{-15}	3.02×10^{-17}

5.4 Scenario 4: discharge to the bank during flood tides

Scenario 4 considers discharges to the bank during a flood tide with a water flow of 0.0086 $m^3 s^{-1}$ (with the water flow only operating while effluent is discharged). Discharges are every three tides. Unit annual discharges (1 GBq y^{-1}) were modelled. This represents alternative discharge arrangements with the opposite discharge window to that specified in the current permit.

5.4.1 Exemplar mobile radionuclide – H-3

Figure 33 shows the activity concentration of H-3 (a mobile radionuclide) in unfiltered seawater in all compartments (per unit annual discharge) for discharges during flood tides. It shows the behaviour over the first ten days after the first discharge, allowing the effects of tidal and discharge cycles to be identified. Figure 34 compares H-3 concentration in the East of Little Cumbrae channel compartment and its adjacent bank compartment for discharges during ebb and flood tides.

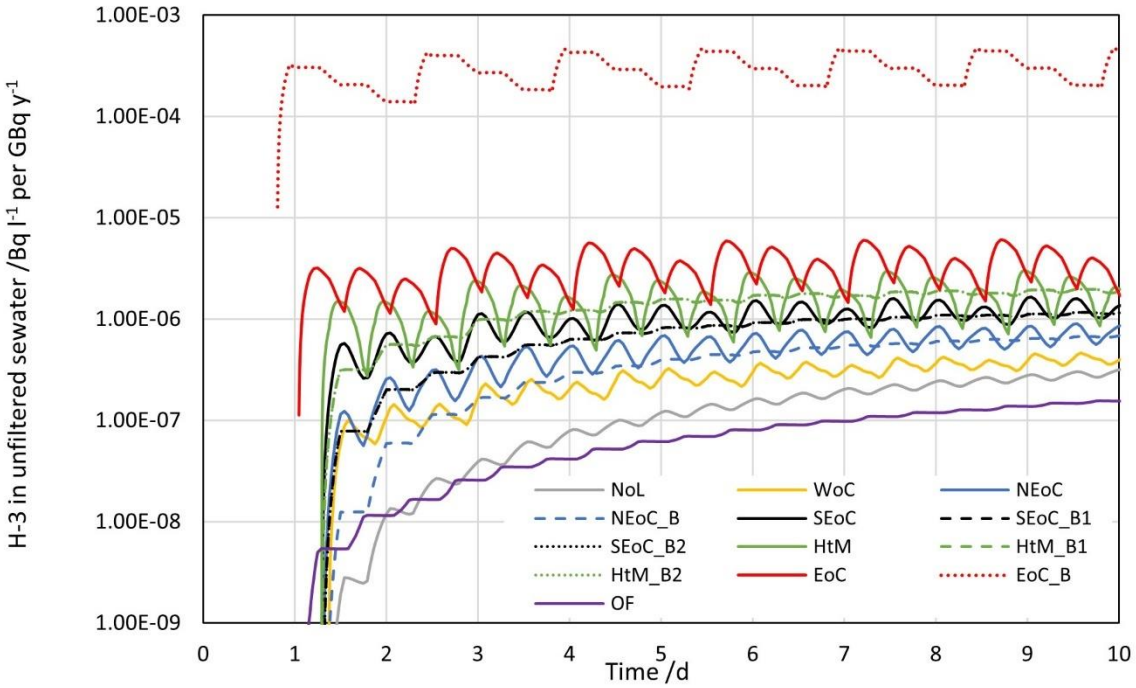

Figure 33 – Activity concentration of H-3 in unfiltered seawater for discharge to the bank during flood tides (per unit annual discharge) (semi-log plot)

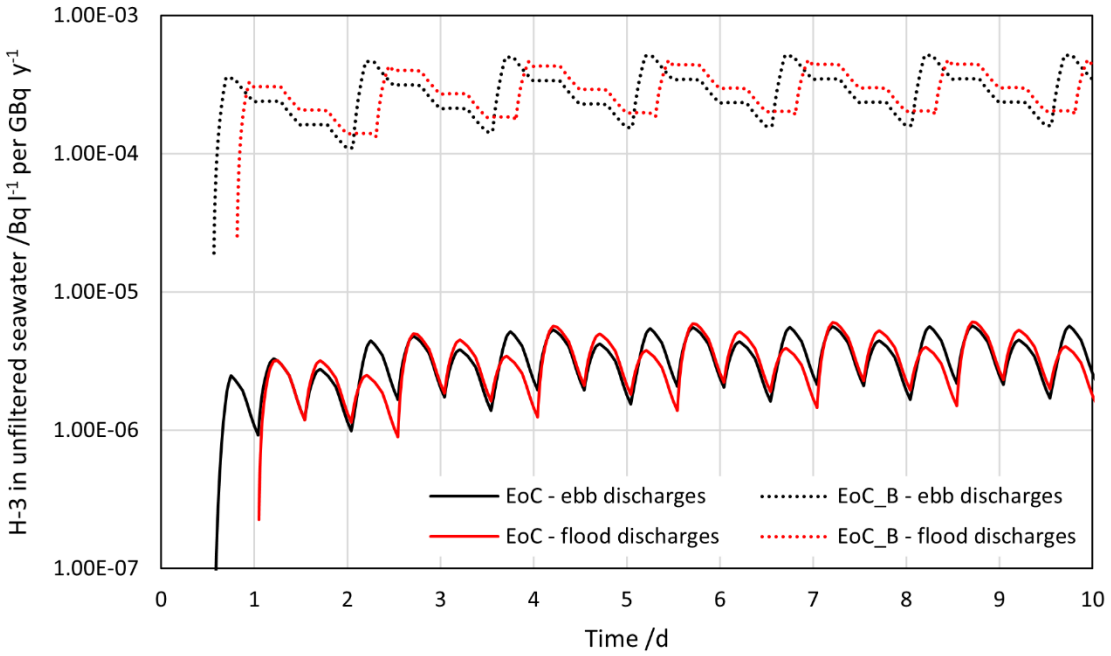

Figure 34 – Comparison of H-3 concentration in East of Little Cumbrae compartment (solid) and adjacent bank compartment (dotted) for discharge during ebb (black – see Subsection 5.2.1) and flood (red) tides

The H-3 concentrations in Figure 34 vary in a similar way regardless as to whether discharges are during the ebb or flood tides. Discharges to the bank compartment (top traces, dotted lines) during a flood tide result in a slightly lower peak concentration than discharges during an ebb tide. This is because the flood tide dilutes the H-3 in the compartment (so the activity concentration is slightly lower, even though there is slightly more total activity in the compartment).

Radionuclides from the East of Little Cumbrae Bank compartment enter the East of Little Cumbrae channel compartment during ebb tides, both when discharging during ebb tides and discharges during flood tides. Therefore, H-3 behaviour in the rest of the system is similar to H-3 behaviour regardless of discharge timing (relative to the tides) (described for discharge during ebb tides in Scenario 2, Subsection 5.2). This is, in turn, similar to H-3 behaviour in the baseline scenario.

Figure 35 shows the discharge-cycle moving average of H-3 concentration in unfiltered seawater in all compartments (per unit discharge) over five years of continuous discharges. The behaviour of the long-term moving average of H-3 concentrations is the same for discharges during flood tides as for discharges during ebb tides (see Figure 25).

Figure 36 shows the activity concentration of H-3 (a mobile radionuclide) in wet upper sediment in all compartments (per unit discharge) over five years of continuous discharges during flood tides. The behaviour of H-3 in this scenario is almost identical to its behaviour when discharged during ebb tides (see Subsection 5.2.1).

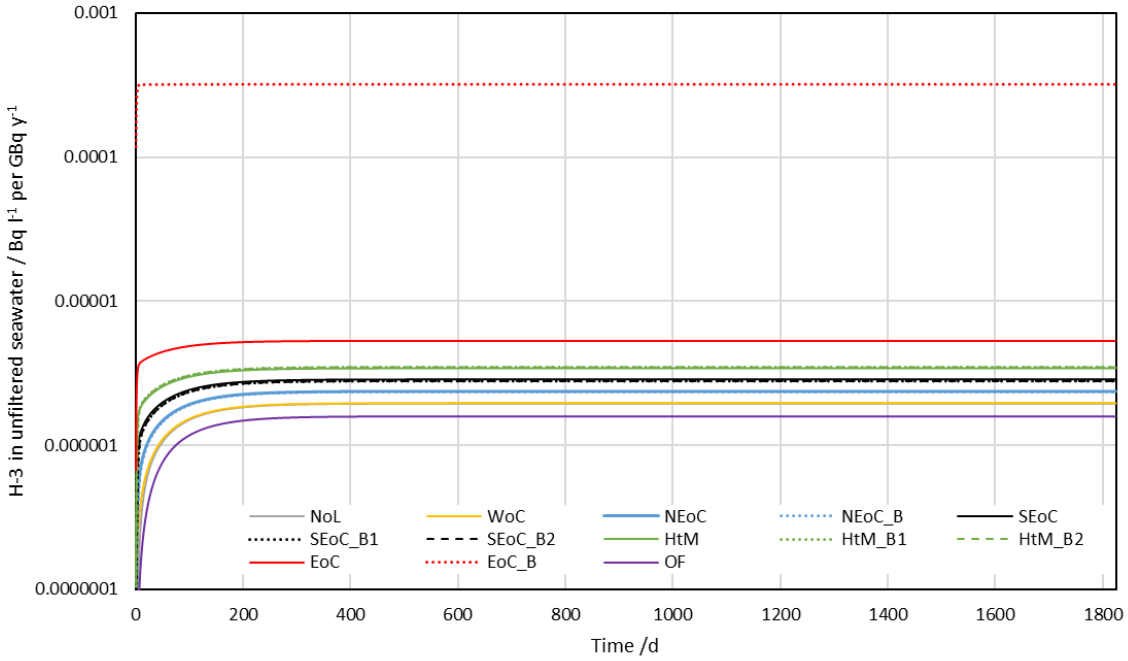

Figure 35 – Tidal-cycle moving average of H-3 concentration in unfiltered seawater for five years for discharge to the bank during flood tides (per unit annual discharge) (semi-log plot)

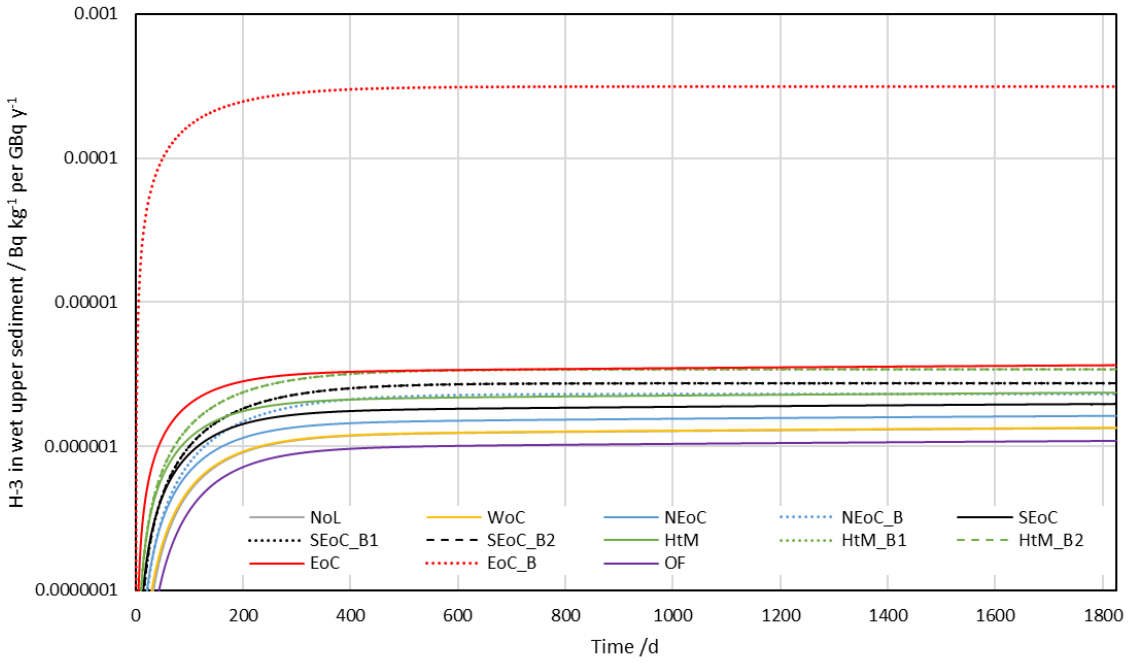

Figure 36 – H-3 concentration in wet top sediment for five years for discharge to the bank during flood tides (per unit annual discharge) (semi-log plot)

Although the differences are too small to be visible in the graphs, the concentrations in all compartments are slightly higher for discharges during a flood tide (this scenario) and discharges during an ebb tide (Scenario 2). These changes are of the order of 10^{-7} Bq l^{-1} per GBq y^{-1} in most compartments and 10^{-5} Bq l^{-1} per GBq y^{-1} in the East of Little Cumbrae Bank compartment. These differences are more than an order of magnitude less than the activity concentrations. They are small and, given the model uncertainty, not meaningful.

The reason that discharge time (relative to the tides) makes very little difference to the H-3 concentration profiles is that transfer from the bank to the channel happens during the ebb tide, regardless of when discharges are. Thus, contaminants always enter the channel (and, thence, the rest of the model) at roughly the same time.

This is a reasonable reflection of the behaviour we expect during an incoming tide, subject to the assumption that there is no flow between adjacent bank compartments. However, to understand what difference it would make if contaminants did enter the channel during a flood tide, we did a sensitivity analysis of the channel discharges scenario (Scenario 5) where we modelled discharges during a flood tide. We found that the assumption that contaminants only enter the channel during ebb tides has little effect on dilution and dispersion. This is described in Subsection 5.6.

5.4.2 Exemplar less-mobile radionuclide – Co-60

Figure 37 shows the activity concentration of Co-60 (a less-mobile radionuclide) in unfiltered seawater in all compartments (per unit annual discharge) for discharges during flood tides. It shows the behaviour over the first ten days after the first discharge, allowing the effects of tidal and discharge cycles to be identified. The behaviour of Co-60 in this scenario is similar to its behaviour for discharges during ebb tides (Subsection 5.2.2). The differences in Co-60 between discharges during flood tides and discharges during ebb tides are the same as the differences in H-3 behaviour between the two discharge windows. These differences are discussed in Subsection 5.4.1.

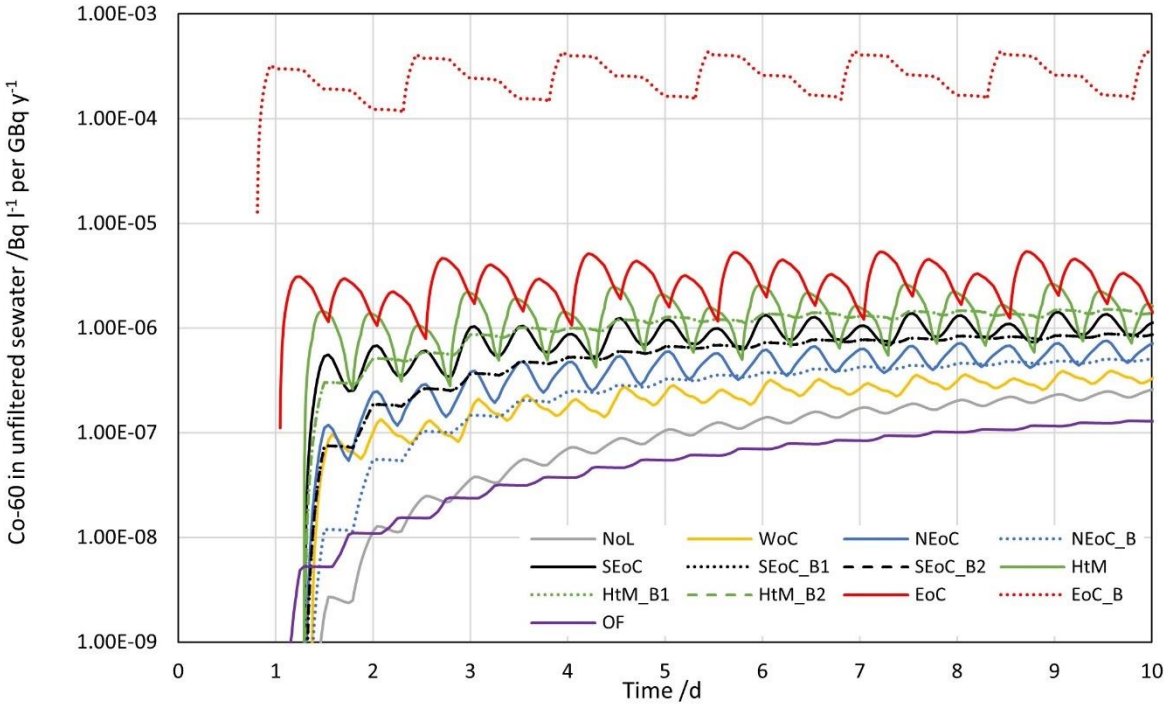

Figure 37 – Activity concentration of Co-60 in unfiltered seawater for discharge to the bank during flood tides (per unit annual discharge) (semi-log plot)

Figure 38 shows the discharge-cycle moving average of Co-60 concentration in unfiltered seawater in all compartments (per unit discharge) over five years of continuous discharges. The behaviour of the long-term moving average of Co-60 concentrations is the same for discharges during flood tides as for discharges during ebb tides (see Figure 28).

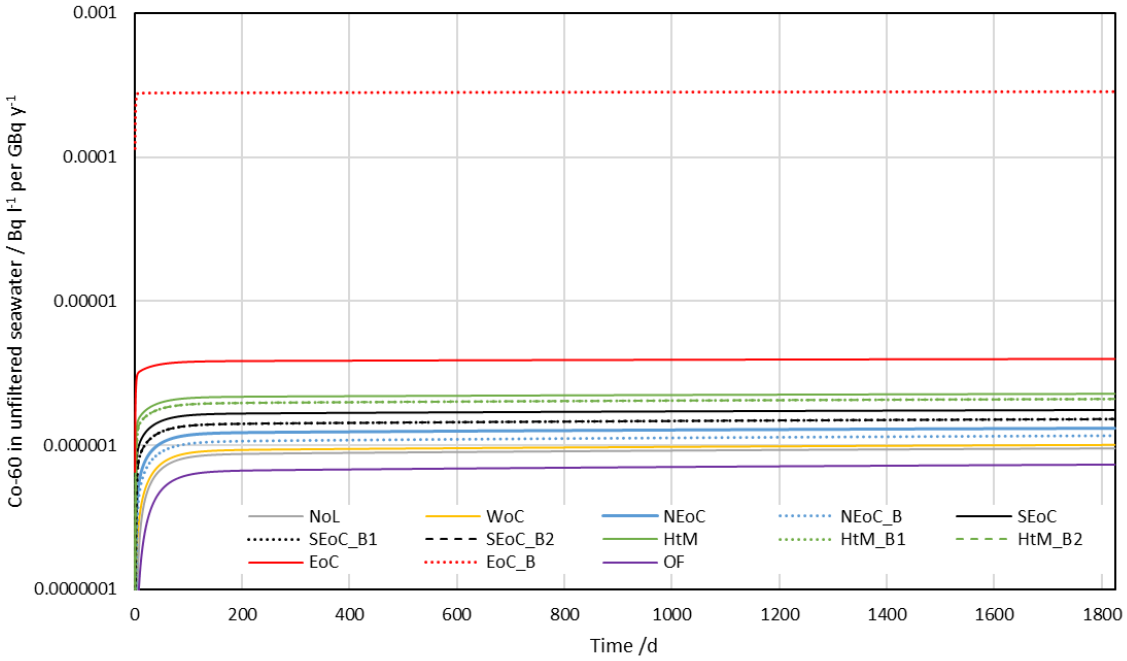

Figure 38 – Tidal-cycle moving average of Co-60 concentration in unfiltered seawater for five years for discharge to the bank during flood tides (per unit annual discharge) (semi-log plot)

Figure 39 shows the activity concentration of Co-60 (a less-mobile radionuclide) in wet upper sediment in all compartments (per unit discharge) over five years of continuous discharges during flood tides. The behaviour of Co-60 in this scenario is almost identical to its behaviour when discharged during ebb tides (see Subsection 5.2.2).

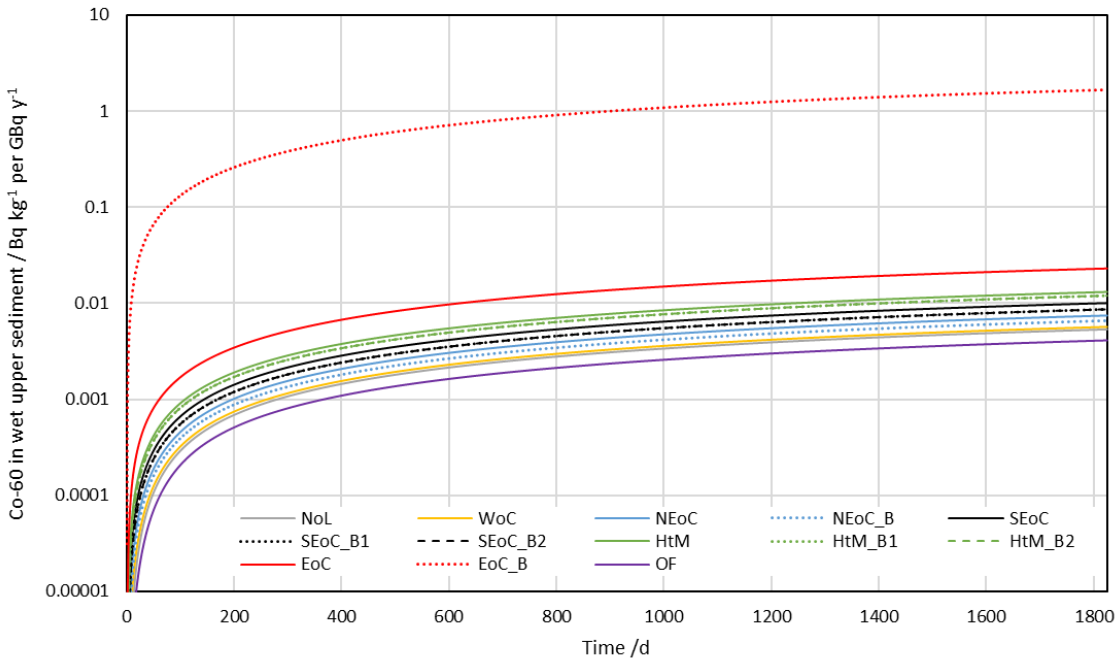

Figure 39 – Co-60 concentration in wet top sediment for five years for discharge to the bank during flood tides (per unit annual discharge) (semi-log plot)

5.4.3 Exemplar daughter radionuclide – U-235

Figure 40 and Figure 41 show the activity concentration of U-235 (a daughter of Pu-239) in unfiltered seawater in all compartments (per unit annual discharge) for discharges during flood tides. The behaviour of U-235 in this scenario is similar to its behaviour for discharges during ebb tides (Subsection 5.2.3).

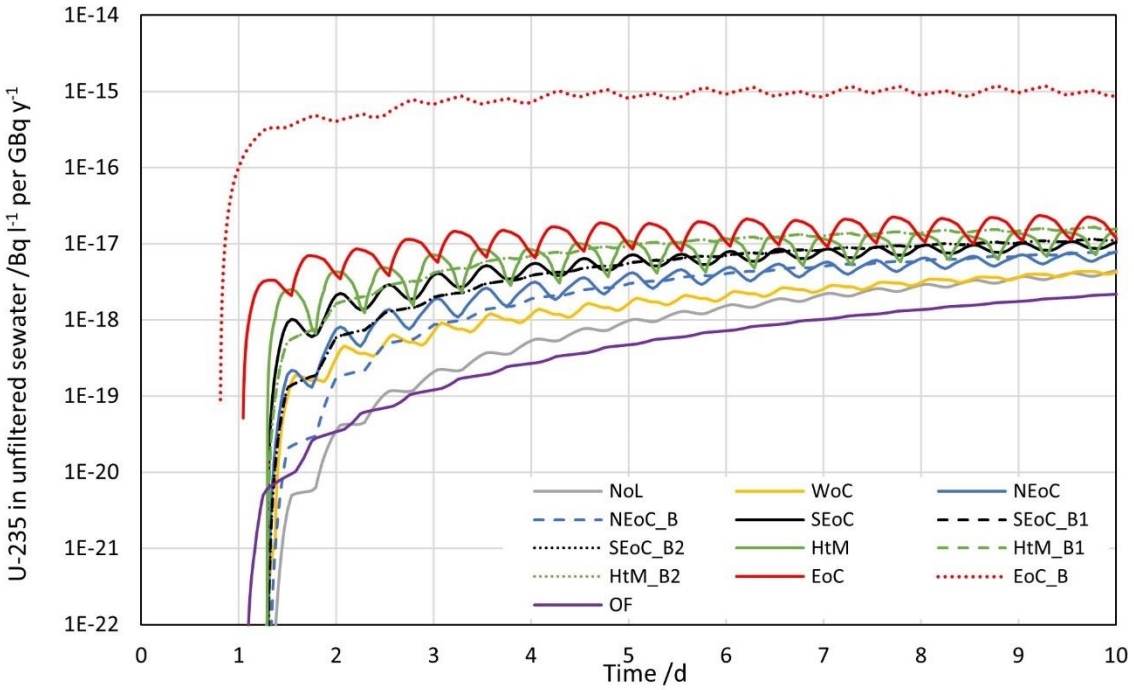

Figure 40 – Activity concentration of U-235 in unfiltered seawater for discharge to the bank during flood tides (per unit annual discharge Pu-239) (semi-log plot)

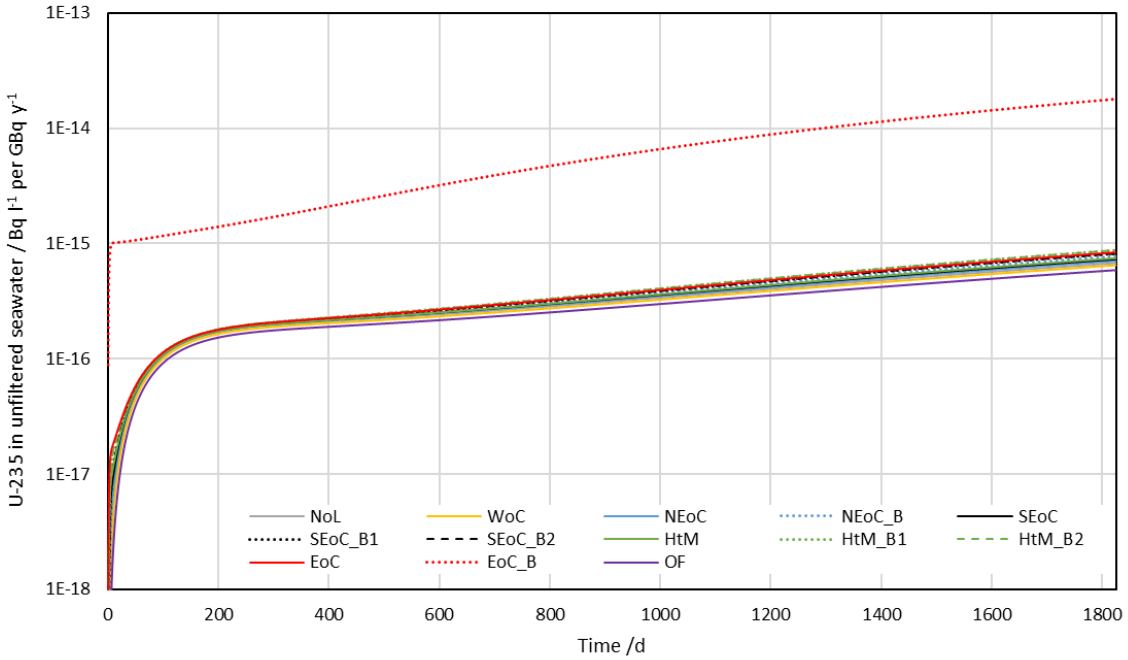

Figure 41 – Tidal-cycle moving average of U-235 concentration in unfiltered seawater for five years for discharge to the bank during flood tides (per unit annual discharge Pu-239) (semi-log plot)

Figure 42 shows the activity concentration of U-235 (a daughter of Pu-239) in wet upper sediment in all compartments (per unit discharge of Pu-239) over five years of continuous discharges during flood tides. The behaviour of U-235 in this scenario is almost identical to its behaviour when discharged during ebb tides (see Subsection 5.2.3).

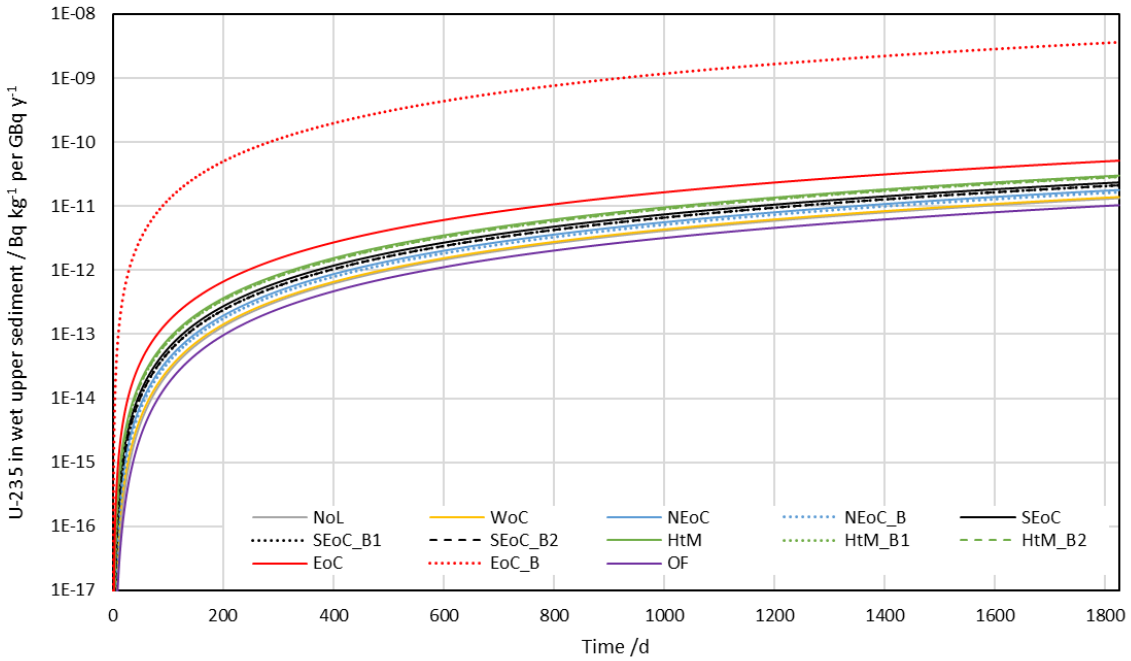

Figure 42 – U-235 concentration in wet top sediment for five years for discharge to the bank during flood tides (per unit annual discharge) (semi-log plot)

5.4.4 Radionuclide concentrations after five years

Table 24 gives the concentration of each radionuclide that has built up in unfiltered seawater in each compartment after five years of continuous discharge. Table 25 gives the concentration of each radionuclide that has built up in wet upper sediment in each compartment after five years of continuous discharge.

Table 24 – Concentration of each radionuclide in unfiltered seawater after five years in each compartment for discharges to the bank during flood tides (discharge cycle moving averages) (Bq l^{-1} per GBq y^{-1})

Nuclide	NoL	WoC	NEoC	NEoC_B	SEoC	SEoC_B1	SEoC_B2	HtM	HtM_B1	HtM_B2	EoC	EoC_B	OF
H-3	1.95×10^{-6}	1.96×10^{-6}	2.37×10^{-6}	2.36×10^{-6}	2.87×10^{-6}	2.79×10^{-6}	2.79×10^{-6}	3.42×10^{-6}	3.49×10^{-6}	3.49×10^{-6}	5.31×10^{-6}	3.20×10^{-4}	1.59×10^{-6}
S-35	1.29×10^{-6}	1.33×10^{-6}	1.70×10^{-6}	1.68×10^{-6}	2.20×10^{-6}	2.12×10^{-6}	2.12×10^{-6}	2.77×10^{-6}	2.81×10^{-6}	2.81×10^{-6}	4.64×10^{-6}	3.16×10^{-4}	9.97×10^{-7}
Co-60	9.52×10^{-7}	1.01×10^{-6}	1.31×10^{-6}	1.17×10^{-6}	1.76×10^{-6}	1.52×10^{-6}	1.52×10^{-6}	2.28×10^{-6}	2.10×10^{-6}	2.10×10^{-6}	3.98×10^{-6}	2.85×10^{-4}	7.35×10^{-7}
Cs-134	1.77×10^{-6}	1.79×10^{-6}	2.18×10^{-6}	2.15×10^{-6}	2.68×10^{-6}	2.59×10^{-6}	2.59×10^{-6}	3.23×10^{-6}	3.28×10^{-6}	3.28×10^{-6}	5.11×10^{-6}	3.18×10^{-4}	1.43×10^{-6}
Cs-137	1.87×10^{-6}	1.89×10^{-6}	2.29×10^{-6}	2.26×10^{-6}	2.78×10^{-6}	2.70×10^{-6}	2.70×10^{-6}	3.34×10^{-6}	3.39×10^{-6}	3.39×10^{-6}	5.22×10^{-6}	3.18×10^{-4}	1.52×10^{-6}
Pu-239	1.20×10^{-6}	1.25×10^{-6}	1.59×10^{-6}	1.47×10^{-6}	2.05×10^{-6}	1.85×10^{-6}	1.85×10^{-6}	2.59×10^{-6}	2.47×10^{-6}	2.47×10^{-6}	4.35×10^{-6}	2.97×10^{-4}	9.47×10^{-7}
U-235_ Pu-239	6.77×10^{-16}	6.49×10^{-16}	7.07×10^{-16}	7.78×10^{-16}	7.32×10^{-16}	8.20×10^{-16}	8.20×10^{-16}	7.47×10^{-16}	8.76×10^{-16}	8.76×10^{-16}	8.39×10^{-16}	1.79×10^{-14}	5.88×10^{-16}
Th-231_ Pu-239	6.49×10^{-16}	6.24×10^{-16}	6.74×10^{-16}	6.84×10^{-16}	6.92×10^{-16}	7.18×10^{-16}	7.18×10^{-16}	7.04×10^{-16}	7.64×10^{-16}	7.64×10^{-16}	7.82×10^{-16}	1.49×10^{-14}	5.68×10^{-16}
Pa-231_ Pu-239	7.43×10^{-21}	7.17×10^{-21}	8.13×10^{-21}	8.78×10^{-21}	8.82×10^{-21}	9.83×10^{-21}	9.83×10^{-21}	9.44×10^{-21}	1.14×10^{-20}	1.14×10^{-20}	1.19×10^{-20}	4.32×10^{-19}	6.27×10^{-21}
Ac-227_ Pu-239	2.61×10^{-22}	2.52×10^{-22}	2.88×10^{-22}	3.18×10^{-22}	3.15×10^{-22}	3.58×10^{-22}	3.58×10^{-22}	3.39×10^{-22}	4.18×10^{-22}	4.18×10^{-22}	4.33×10^{-22}	1.66×10^{-20}	2.17×10^{-22}

Table 25 – Concentration of each radionuclide in dry upper sediment after five years in each compartment for discharges to the bank during flood tides (discharge cycle moving averages) (Bq kg^{-1} per GBq y^{-1})

Nuclide	NoL	WoC	NEoC	NEoC_B	SEoC	SEoC_B1	SEoC_B2	HtM	HtM_B1	HtM_B2	EoC	EoC_B	OF
H-3	2.88×10^{-6}	2.90×10^{-6}	3.51×10^{-6}	4.98×10^{-6}	4.24×10^{-6}	5.90×10^{-6}	5.90×10^{-6}	5.08×10^{-6}	7.37×10^{-6}	7.37×10^{-6}	7.88×10^{-6}	6.76×10^{-4}	2.35×10^{-6}
S-35	9.00×10^{-7}	9.26×10^{-7}	1.19×10^{-6}	1.55×10^{-6}	1.53×10^{-6}	1.95×10^{-6}	1.95×10^{-6}	1.93×10^{-6}	2.59×10^{-6}	2.59×10^{-6}	3.23×10^{-6}	2.92×10^{-4}	6.94×10^{-7}
Co-60	1.15×10^{-2}	1.22×10^{-2}	1.60×10^{-2}	1.42×10^{-2}	2.16×10^{-2}	1.86×10^{-2}	1.86×10^{-2}	2.82×10^{-2}	2.58×10^{-2}	2.58×10^{-2}	4.95×10^{-2}	3.59×10^{0}	8.84×10^{-3}
Cs-134	7.82×10^{-4}	7.92×10^{-4}	9.69×10^{-4}	9.59×10^{-4}	1.19×10^{-3}	1.16×10^{-3}	1.16×10^{-3}	1.44×10^{-3}	1.47×10^{-3}	1.47×10^{-3}	2.28×10^{-3}	1.43×10^{-1}	6.31×10^{-4}
Cs-137	1.53×10^{-3}	1.55×10^{-3}	1.88×10^{-3}	1.87×10^{-3}	2.30×10^{-3}	2.24×10^{-3}	2.24×10^{-3}	2.78×10^{-3}	2.82×10^{-3}	2.82×10^{-3}	4.36×10^{-3}	2.70×10^{-1}	1.24×10^{-3}
Pu-239	1.28×10^{-2}	1.33×10^{-2}	1.71×10^{-2}	1.57×10^{-2}	2.23×10^{-2}	2.00×10^{-2}	2.00×10^{-2}	2.84×10^{-2}	2.70×10^{-2}	2.70×10^{-2}	4.83×10^{-2}	3.36×10^{0}	1.00×10^{-2}
U-235_ Pu-239	2.86×10^{-11}	2.99×10^{-11}	3.85×10^{-11}	3.56×10^{-11}	5.06×10^{-11}	4.56×10^{-11}	4.56×10^{-11}	6.47×10^{-11}	6.17×10^{-11}	6.17×10^{-11}	1.11×10^{-10}	7.80×10^{-9}	2.23×10^{-11}
Th-231_ Pu-239	2.86×10^{-11}	2.99×10^{-11}	3.85×10^{-11}	3.56×10^{-11}	5.05×10^{-11}	4.55×10^{-11}	4.55×10^{-11}	6.46×10^{-11}	6.16×10^{-11}	6.16×10^{-11}	1.10×10^{-10}	7.79×10^{-9}	2.23×10^{-11}
Pa-231_ Pu-239	1.01×10^{-15}	1.05×10^{-15}	1.35×10^{-15}	1.26×10^{-15}	1.77×10^{-15}	1.60×10^{-15}	1.60×10^{-15}	2.26×10^{-15}	2.17×10^{-15}	2.17×10^{-15}	3.86×10^{-15}	2.71×10^{-13}	7.88×10^{-16}
Ac-227_ Pu-239	3.87×10^{-17}	4.04×10^{-17}	5.18×10^{-17}	4.82×10^{-17}	6.79×10^{-17}	6.15×10^{-17}	6.15×10^{-17}	8.67×10^{-17}	8.31×10^{-17}	8.31×10^{-17}	1.48×10^{-16}	1.04×10^{-14}	3.01×10^{-17}

5.5 Scenario 5: discharge to the channel with low water flow rate through pipe

Scenario 5 considers discharges to the channel during an ebb tide with a water flow of 0.0086 $m^3 s^{-1}$ (with the water flow only operating while effluent is discharged). Discharges are every three tides. Unit annual discharges (1 GBq y^{-1}) were modelled. This represents alternative discharge arrangements with a discharge point in the channel.

5.5.1 Exemplar mobile radionuclide – H-3

Figure 43 shows the activity concentration of H-3 (a mobile radionuclide) in unfiltered seawater in all compartments (per unit annual discharge). It shows the behaviour over the first ten days after the first discharge, allowing the effects of tidal and discharge cycles to be identified. Figure 44 compares H-3 concentration in the East of Little Cumbrae channel compartment and its adjacent bank compartment for discharges to the bank and to the channel.

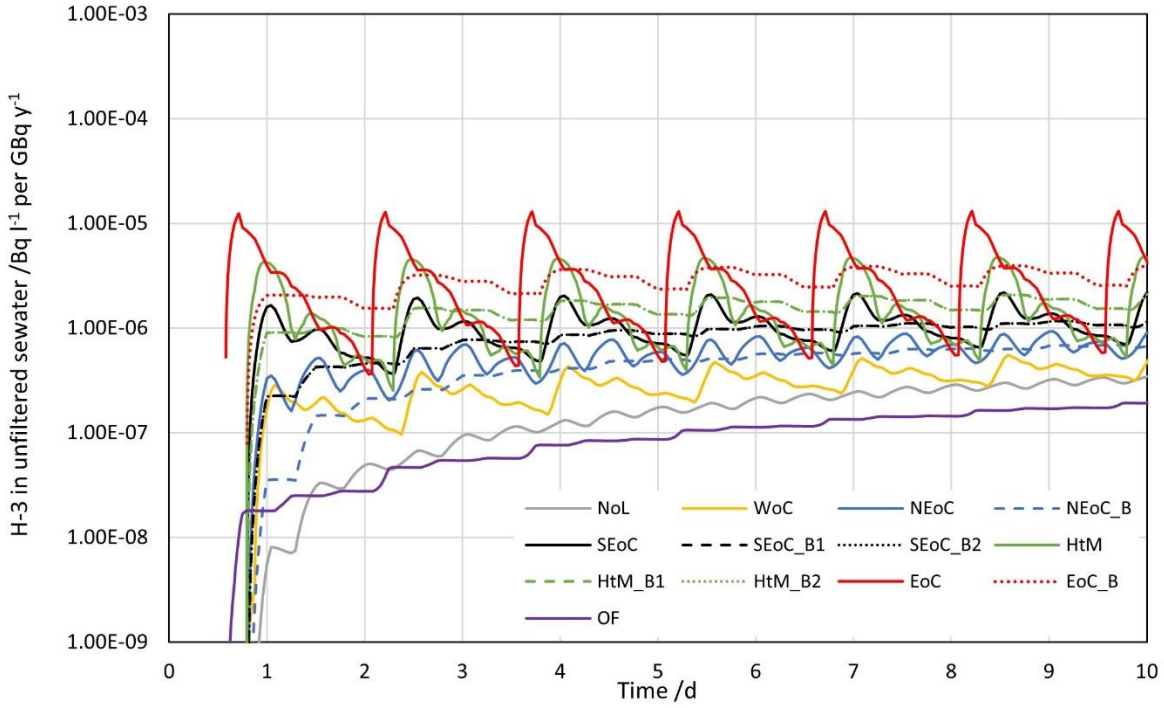

Figure 43 – Activity concentration of H-3 in unfiltered seawater for channel discharges scenario (per unit annual discharge) (semi-log plot)

Compared to the bank discharge scenarios (Subsections 5.1 and 5.2), discharging in the channel reduces H-3 concentration in the East of Little Cumbrae Bank compartment by several orders of magnitude (from *ca.* 10^{-4} Bq l^{-1} per GBq y^{-1} to *ca.* 10^{-6} Bq l^{-1} per GBq y^{-1}). This is because when discharges are to the channel, the only source of H-3 for the bank compartment is transfer from the channel compartment whereas, when discharges are to the bank, all the H-3 discharged enters the bank compartment.

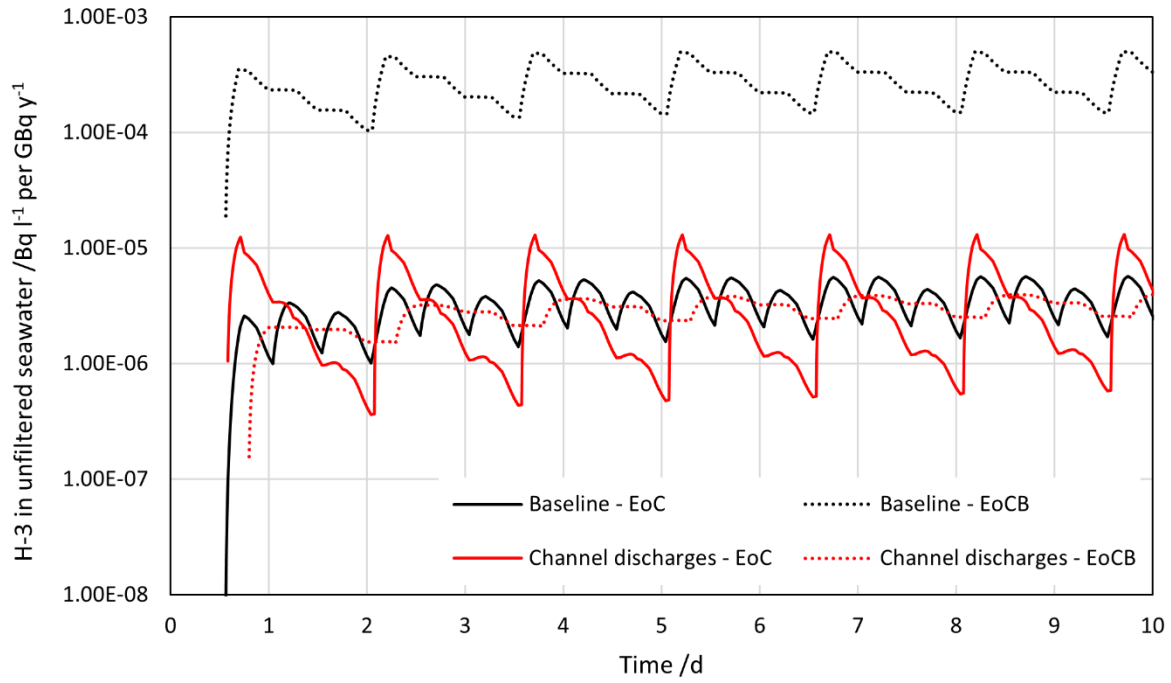

Figure 44 – Comparison of H-3 concentration in East of Little Cumbrae compartment (solid) and adjacent bank compartment (dotted) for bank (black) and channel (red) discharges

The H-3 concentration in the East of Little Cumbrae compartment is much more variable when discharges are made into that compartment than when discharges are made to the bank. This is expected. There is a concentration peak when the discharges are released (*ca.* 10^{-5} Bq l^{-1} per GBq y^{-1}). Once the discharge ceases, however, the contamination is quickly cleared by tidal flow. Unlike with bank discharges, contaminant concentrations in the East of Little Cumbrae compartment are not replenished (during ebb tides) by a roughly constant inflow for the bank compartment.

Among the other compartments, the main difference is that H-3 concentrations in the West of Cumbrae, Hunterston to Millport and Southeast of Great Cumbrae compartments are influenced by the discharge cycle for the channel discharges but not the bank discharges. This is because they are exposed (indirectly, in the case of the Southeast of Great Cumbrae compartment) to the discharge-dependent H-3 concentration in the East of Little Cumbrae compartment.

Figure 45 shows the discharge-cycle moving average of H-3 concentration in unfiltered seawater in all compartments (per unit discharge) over five years of continuous discharges.

In all compartments except the East of Little Cumbrae Bank compartment, the behaviour of H-3 in this scenario is almost identical to its behaviour in the baseline scenario (Subsection 5.1.1). H-3 concentration in the East of Little Cumbrae Bank compartment drops by around two orders of magnitude, from *ca.* 5×10^{-4} Bq l^{-1} per GBq y^{-1} to *ca.* 5×10^{-6} Bq l^{-1} per GBq y^{-1}. This is consistent with the discussion of the short-term concentration plot (Figure 43).

Average concentrations in all model compartments except East of Little Cumbrae bank are similar whether discharging to the bank (Scenario 2 – Subsection 5.2) or the channel. This is because once the bank compartment has reached equilibrium, the inflow rate of contaminants to the channel compartment is the same, whether discharges are to the channel or the bank.

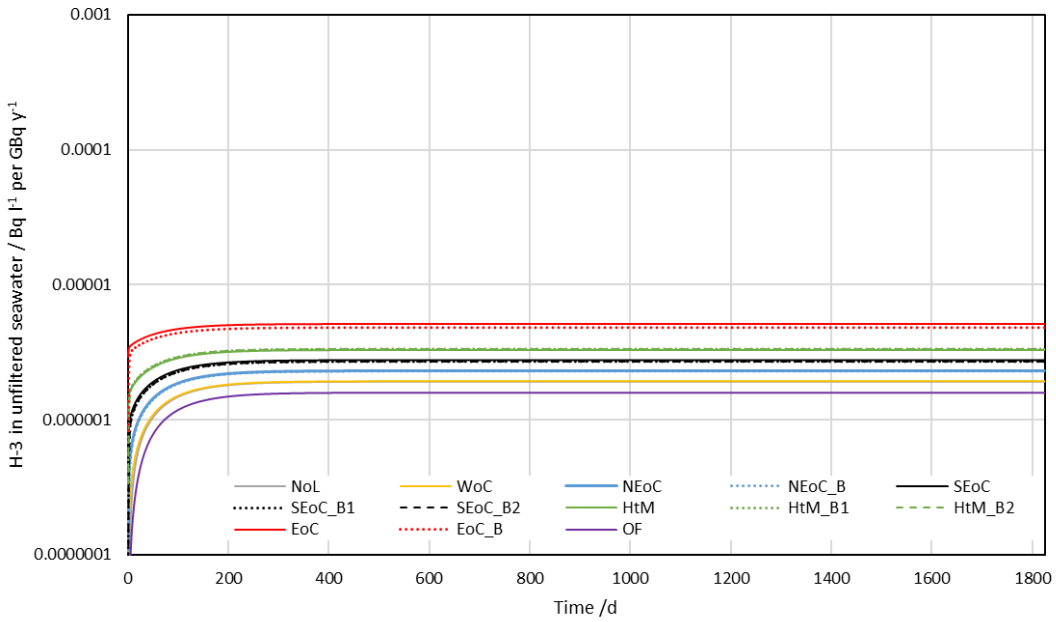

Figure 45 – Tidal-cycle moving average of H-3 concentration in unfiltered seawater for five years for discharge to the channel (per unit annual discharge) (semi-log plot)

Figure 46 shows the activity concentration of H-3 (a mobile radionuclide) in wet upper sediment in all compartments (per unit discharge) over five years of continuous discharges. The concentrations in the bank compartments are greater than the concentrations in the channel compartments. The behaviour of H-3 in this scenario is almost identical to its behaviour in the baseline scenario (Subsection 5.1.1), except in the East of Little Cumbrae Bank compartment. As for the concentration of H-3 in unfiltered seawater, the East of Little Cumbrae Bank compartment has H-3 concentrations that are around two orders of magnitude lower for channel discharges than for bank discharges.

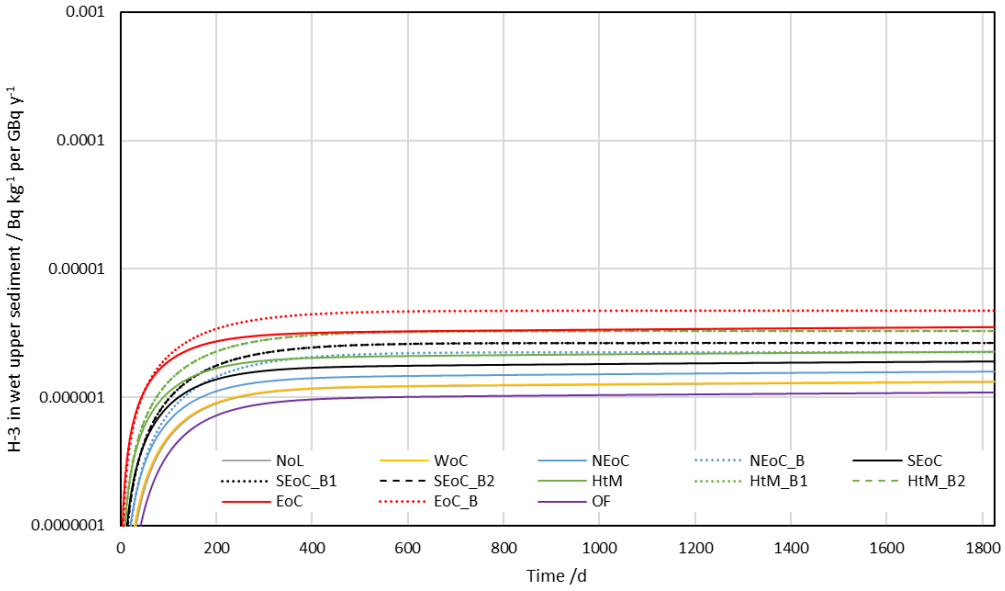

Figure 46 – H-3 concentration in wet top sediment for five years for discharge to the channel (per unit annual discharge) (semi-log plot)

The data in Figure 45 and Figure 46 show that discharging into the channel would not reduce build-up of H-3 in the Firth of Clyde overall. It would, however, reduce the H-3 concentration in the immediate vicinity of the outfall.

5.5.2 Exemplar less-mobile radionuclide – Co-60

Figure 47 shows the activity concentration of Co-60 (a less mobile radionuclide) in unfiltered seawater in all compartments (per unit discharge). It shows the behaviour over the first ten days after the first discharge, allowing the effects of tidal and discharge cycles to be identified. The behaviour of Co-60 is similar to that of H-3 (discussed in Subsection 5.5.1).

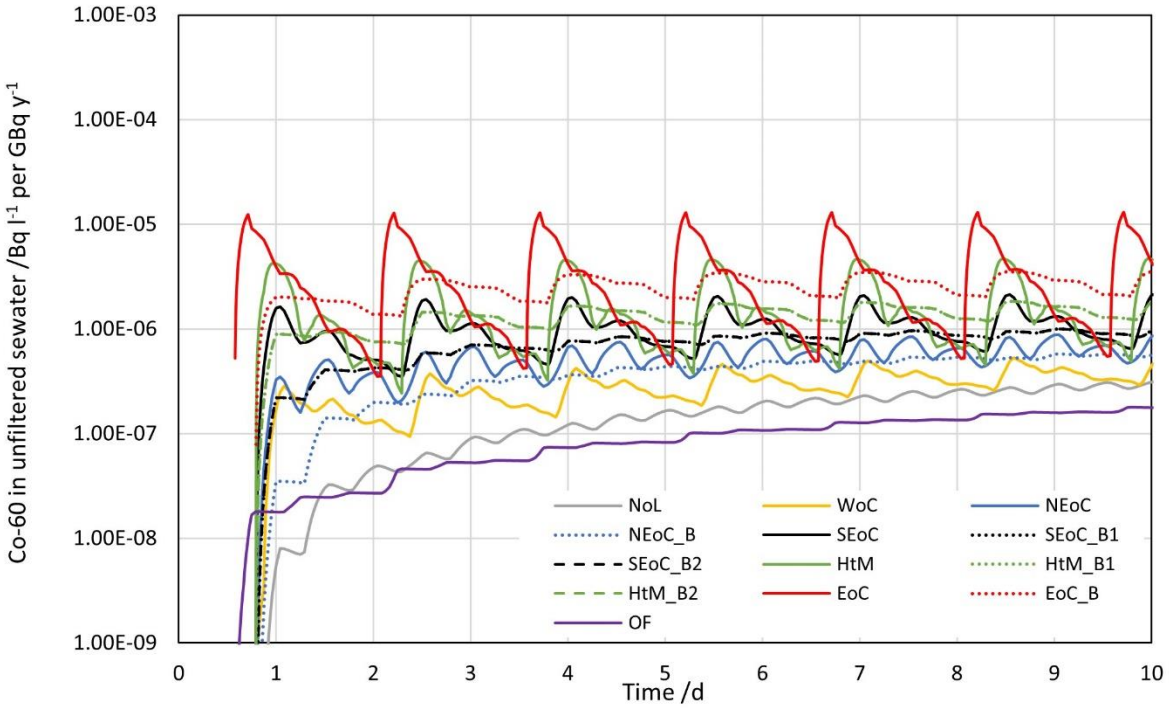

Figure 47 – Activity concentration of Co-60 in unfiltered seawater for channel discharges scenario (per unit annual discharge) (semi-log plot)

Figure 48 shows the activity concentration of Co-60 in unfiltered seawater over the longer term (five years). The channel compartments have slightly higher Co-60 concentrations than their adjacent bank compartments. The behaviour of Co-60 concentrations for channel discharges is almost identical to their behaviour for bank discharges (Subsection 5.1.2 and 5.2.2), except in the East of Little Cumbrae Bank compartment.

In the East of Little Cumbrae Bank compartment, Co-60 concentrations are around two orders of magnitude lower for channel discharges. This is because, when discharging to the channel, the only source of Co-60 in the bank is exchange with the channel whereas, when discharging to the bank, all Co-60 passes through the bank compartment.

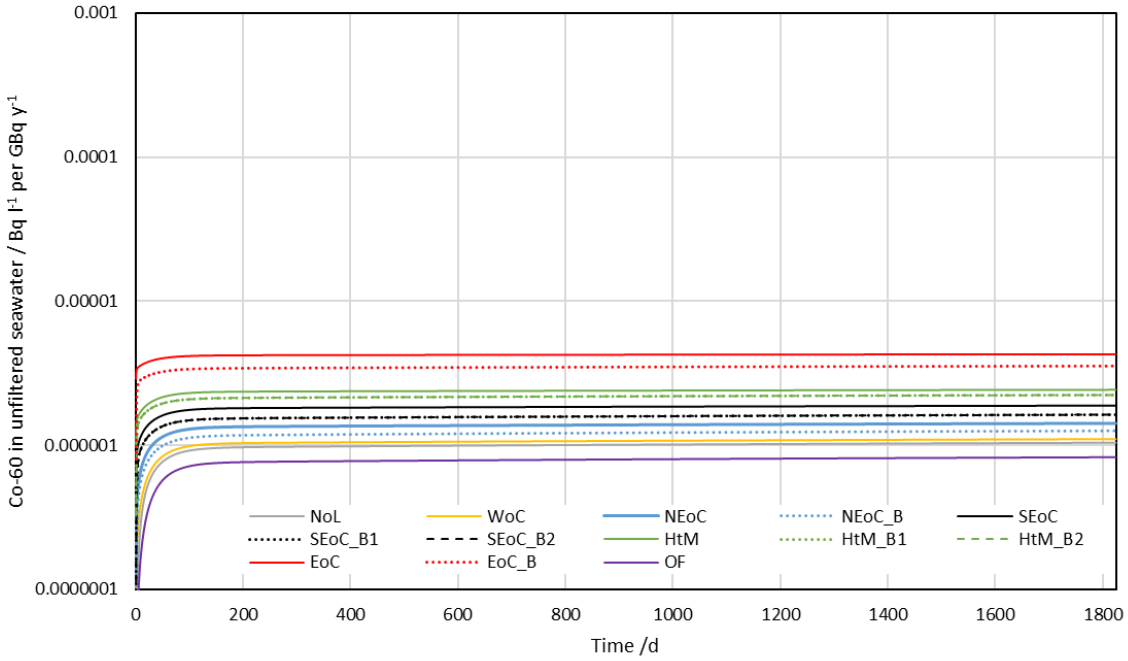

Figure 48 – Tidal-cycle moving average of Co-60 concentration in unfiltered seawater for five years for discharge to the channel (per unit annual discharge) (semi-log plot)

Figure 49 shows the activity concentration of Co-60 in wet upper sediment over the longer term (five years). The concentration of Co-60 in wet upper sediment is also almost identical for channel discharges and bank discharges (see Figure 11), except in the east of Little Cumbrae Bank compartment. There, it has reduced by around two orders of magnitude.

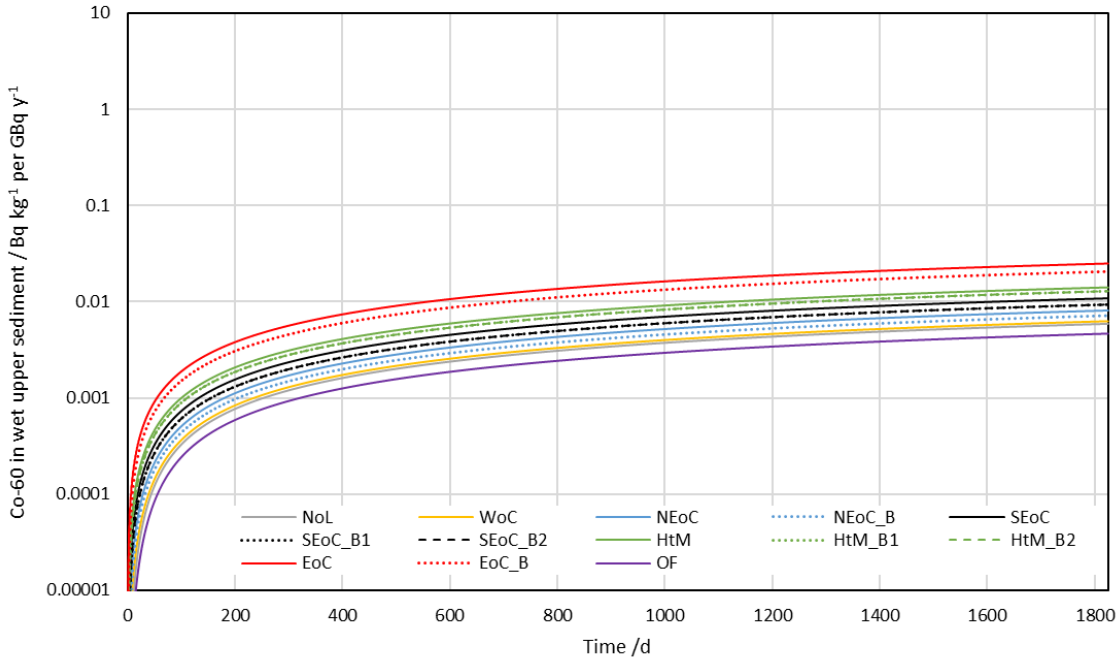

Figure 49 – Co-60 concentration in wet top sediment for five years for discharge to the channel (per unit annual discharge) (semi-log plot)

5.5.3 Exemplar daughter radionuclide – U-235

Figure 50 shows the activity concentration of U-235 (a daughter of Pu-239) in unfiltered seawater in all compartments (per unit discharge of Pu-239). It shows the behaviour over the first ten days after the first discharge, allowing the effects of tidal and discharge cycles to be identified. The pattern of behaviour of U-235 over this period is similar to that of H-3 and Co-60 (discussed in Subsections 5.5.1 and 5.5.2).

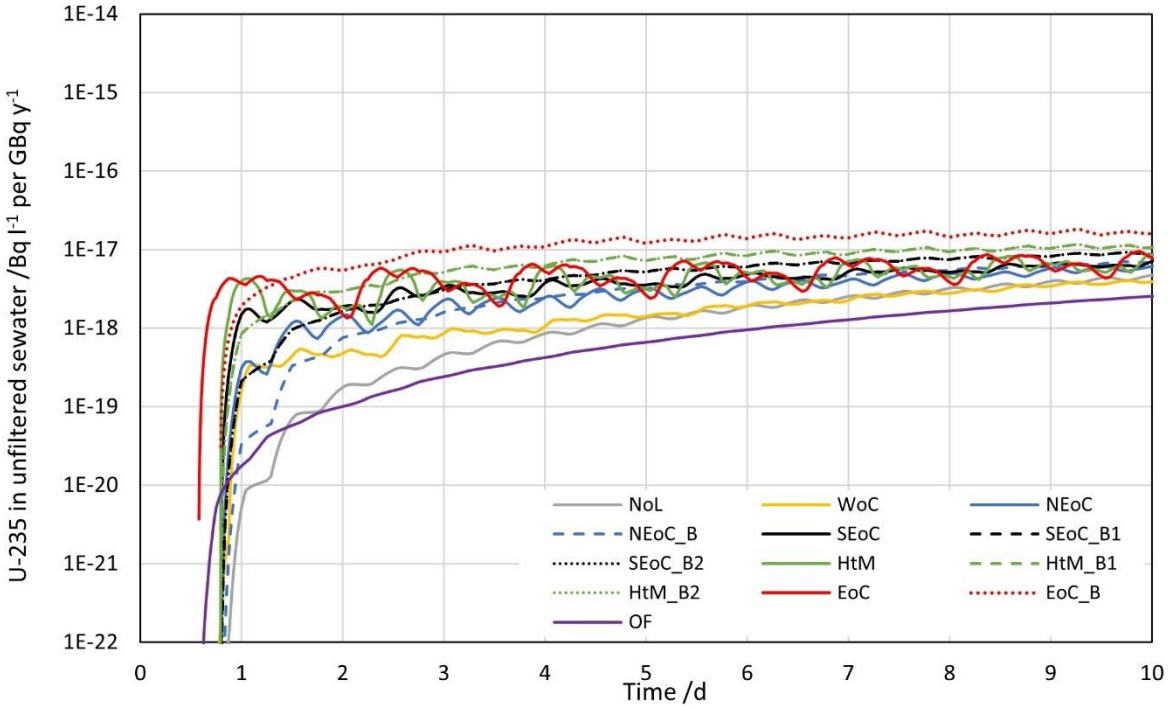

Figure 50 – Activity concentration of U-235 in unfiltered seawater for discharge to the channel (per unit annual discharge Pu-239) (semi-log plot)

The most significant difference between U-235 and H-3 and Co-60 is that U-235 is ingrown, rather than directly discharged. This smooths the concentration peaks during discharge compared to H-3 and Co-60. As for the baseline scenario, U-235 concentrations in the bank compartments slightly exceed those in the adjacent channel compartments after a short period of time. This is because ingrown U-235 is less effectively cleared from the bank compartments than the channel compartments, due to their lower water turnover.

Figure 51 shows the discharge-cycle moving average of U-235 concentration in unfiltered seawater in all compartments (per unit discharge) over five years of continuous discharges. In all compartments except the East of Little Cumbrae Bank compartment, the behaviour of U-235 in this scenario is almost identical to its behaviour in the baseline scenario (Subsection 5.1.3). The East of Little Cumbrae Bank compartment has U-235 concentrations around an order of magnitude lower than for the baseline scenario (*ca.* 10^{-15} Bq l^{-1} per GBq y^{-1} compared to *ca.* 10^{-14} Bq l^{-1} per GBq y^{-1}). The East of Little Cumbrae channel compartment has slightly lower U-235 concentrations than in the baseline scenario due to less transfer of activity from the bank compartment (due to their being less activity in the bank compartment).

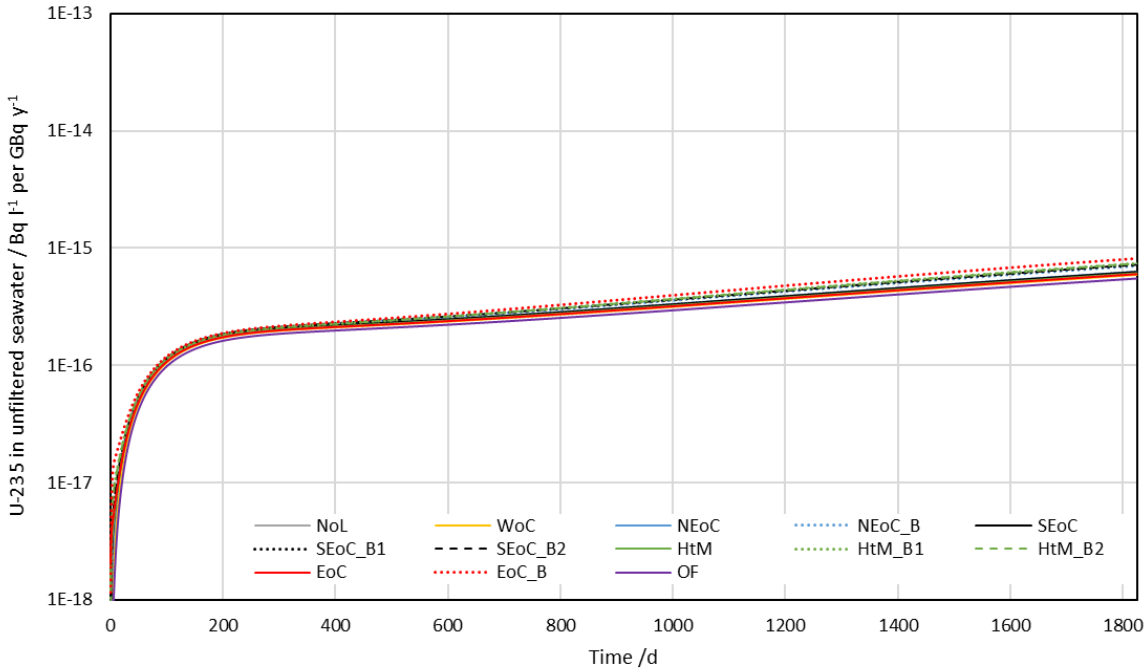

Figure 51 – Discharge-cycle moving average of U-235 concentration in unfiltered seawater for discharge to the channel for five years (semi-log plot)

Figure 52 shows the activity concentration of U-235 in wet upper sediment in all compartments (per unit discharge) over five years of continuous discharges. Except in the East of Little Cumbrae Bank compartment, the behaviour of U-235 in this scenario is almost identical to its behaviour in the baseline scenario (Subsection 5.1.3). U-235 concentrations in the east of Little Cumbrae Bank compartment are between one and two orders of magnitude below the baseline scenario.

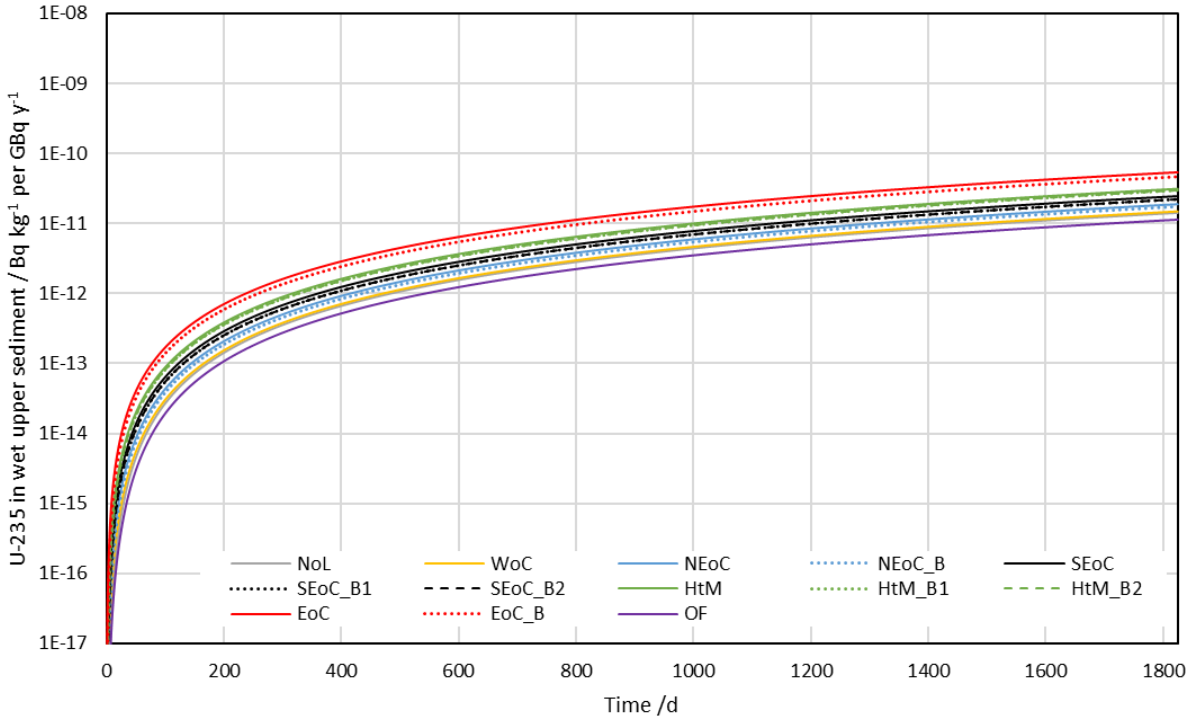

Figure 52 – U-235 concentration in wet top sediment for five years for discharge to the channel (per unit annual discharge Pu-239) (semi-log plot)

5.5.4 Radionuclide concentrations after five years

Table 26 gives the concentration of each radionuclide that has built up in unfiltered seawater in each compartment after five years of continuous discharge. Table 27 gives the concentration of each radionuclide that has built up in wet upper sediment in each compartment after five years of continuous discharge

Table 26 – Concentration of each radionuclide in unfiltered seawater after five years in each compartment for discharges to the channel (discharge cycle moving averages) (Bq l^{-1} per GBq y^{-1})

Nuclide	NoL	WoC	NEoC	NEoC_B	SEoC	SEoC_B1	SEoC_B2	HtM	HtM_B1	HtM_B2	EoC	EoC_B	OF
H-3	1.92×10^{-6}	1.93×10^{-6}	2.31×10^{-6}	2.29×10^{-6}	2.77×10^{-6}	2.70×10^{-6}	2.70×10^{-6}	3.29×10^{-6}	3.35×10^{-6}	3.35×10^{-6}	5.13×10^{-6}	4.82×10^{-6}	1.59×10^{-6}
S-35	1.28×10^{-6}	1.32×10^{-6}	1.66×10^{-6}	1.64×10^{-6}	2.13×10^{-6}	2.05×10^{-6}	2.05×10^{-6}	2.66×10^{-6}	2.70×10^{-6}	2.70×10^{-6}	4.51×10^{-6}	4.16×10^{-6}	1.01×10^{-6}
Co-60	1.04×10^{-6}	1.10×10^{-6}	1.42×10^{-6}	1.26×10^{-6}	1.89×10^{-6}	1.63×10^{-6}	1.63×10^{-6}	2.43×10^{-6}	2.23×10^{-6}	2.24×10^{-6}	4.29×10^{-6}	3.55×10^{-6}	8.27×10^{-7}
Cs-134	1.75×10^{-6}	1.77×10^{-6}	2.14×10^{-6}	2.11×10^{-6}	2.60×10^{-6}	2.52×10^{-6}	2.52×10^{-6}	3.12×10^{-6}	3.16×10^{-6}	3.16×10^{-6}	4.97×10^{-6}	4.62×10^{-6}	1.44×10^{-6}
Cs-137	1.85×10^{-6}	1.87×10^{-6}	2.24×10^{-6}	2.21×10^{-6}	2.70×10^{-6}	2.62×10^{-6}	2.62×10^{-6}	3.22×10^{-6}	3.27×10^{-6}	3.27×10^{-6}	5.07×10^{-6}	4.73×10^{-6}	1.53×10^{-6}
Pu-239	1.27×10^{-6}	1.32×10^{-6}	1.65×10^{-6}	1.53×10^{-6}	2.12×10^{-6}	1.91×10^{-6}	1.91×10^{-6}	2.65×10^{-6}	2.53×10^{-6}	2.53×10^{-6}	4.51×10^{-6}	3.91×10^{-6}	1.02×10^{-6}
U-235_ Pu-239	6.24×10^{-16}	5.93×10^{-16}	6.31×10^{-16}	7.06×10^{-16}	6.27×10^{-16}	7.23×10^{-16}	7.23×10^{-16}	6.11×10^{-16}	7.41×10^{-16}	7.41×10^{-16}	6.01×10^{-16}	8.18×10^{-16}	5.51×10^{-16}
Th-231_ Pu-239	5.97×10^{-16}	5.70×10^{-16}	6.01×10^{-16}	6.21×10^{-16}	5.96×10^{-16}	6.34×10^{-16}	6.34×10^{-16}	5.81×10^{-16}	6.48×10^{-16}	6.48×10^{-16}	5.72×10^{-16}	7.12×10^{-16}	5.32×10^{-16}
Pa-231_ Pu-239	6.61×10^{-21}	6.25×10^{-21}	6.77×10^{-21}	7.73×10^{-21}	6.78×10^{-21}	8.27×10^{-21}	8.27×10^{-21}	6.60×10^{-21}	8.98×10^{-21}	8.98×10^{-21}	6.49×10^{-21}	1.09×10^{-20}	5.72×10^{-21}
Ac-227_ Pu-239	2.30×10^{-22}	2.17×10^{-22}	2.36×10^{-22}	2.77×10^{-22}	2.37×10^{-22}	2.98×10^{-22}	2.98×10^{-22}	2.30×10^{-22}	3.26×10^{-22}	3.25×10^{-22}	2.26×10^{-22}	4.00×10^{-22}	1.97×10^{-22}

Table 27 – Concentration of each radionuclide in dry upper sediment after five years in each compartment discharges to the channel (discharge cycle moving averages) (Bq kg^{-1} per GBq y^{-1})

Nuclide	NoL	WoC	NEoC	NEoC_B	SEoC	SEoC_B1	SEoC_B2	HtM	HtM_B1	HtM_B2	EoC	EoC_B	OF
H-3	2.84×10^{-6}	2.86×10^{-6}	3.42×10^{-6}	4.84×10^{-6}	4.10×10^{-6}	5.71×10^{-6}	5.71×10^{-6}	4.88×10^{-6}	7.07×10^{-6}	7.07×10^{-6}	7.60×10^{-6}	1.02×10^{-5}	2.35×10^{-6}
S-35	8.89×10^{-7}	9.16×10^{-7}	1.16×10^{-6}	1.51×10^{-6}	1.48×10^{-6}	1.89×10^{-6}	1.89×10^{-6}	1.86×10^{-6}	2.49×10^{-6}	2.49×10^{-6}	3.14×10^{-6}	3.84×10^{-6}	7.03×10^{-7}
Co-60	1.27×10^{-2}	1.35×10^{-2}	1.75×10^{-2}	1.54×10^{-2}	2.33×10^{-2}	2.01×10^{-2}	2.01×10^{-2}	3.03×10^{-2}	2.77×10^{-2}	2.77×10^{-2}	5.37×10^{-2}	4.44×10^{-2}	1.00×10^{-2}
Cs-134	7.74×10^{-4}	7.85×10^{-4}	9.49×10^{-4}	9.40×10^{-4}	1.16×10^{-3}	1.12×10^{-3}	1.12×10^{-3}	1.39×10^{-3}	1.42×10^{-3}	1.42×10^{-3}	2.22×10^{-3}	2.08×10^{-3}	6.36×10^{-4}
Cs-137	1.51×10^{-3}	1.53×10^{-3}	1.84×10^{-3}	1.83×10^{-3}	2.23×10^{-3}	2.18×10^{-3}	2.18×10^{-3}	2.68×10^{-3}	2.73×10^{-3}	2.73×10^{-3}	4.23×10^{-3}	3.97×10^{-3}	1.25×10^{-3}
Pu-239	1.36×10^{-2}	1.42×10^{-2}	1.79×10^{-2}	1.65×10^{-2}	2.32×10^{-2}	2.09×10^{-2}	2.09×10^{-2}	2.94×10^{-2}	2.79×10^{-2}	2.79×10^{-2}	5.03×10^{-2}	4.34×10^{-2}	1.09×10^{-2}
U-235_ Pu-239	3.05×10^{-11}	3.19×10^{-11}	4.05×10^{-11}	3.74×10^{-11}	5.28×10^{-11}	4.76×10^{-11}	4.76×10^{-11}	6.72×10^{-11}	6.40×10^{-11}	6.40×10^{-11}	1.16×10^{-10}	1.00×10^{-10}	2.44×10^{-11}
Th-231_ Pu-239	3.05×10^{-11}	3.19×10^{-11}	4.05×10^{-11}	3.74×10^{-11}	5.27×10^{-11}	4.75×10^{-11}	4.75×10^{-11}	6.71×10^{-11}	6.39×10^{-11}	6.39×10^{-11}	1.15×10^{-10}	1.00×10^{-10}	2.43×10^{-11}
Pa-231_ Pu-239	1.07×10^{-15}	1.12×10^{-15}	1.42×10^{-15}	1.31×10^{-15}	1.84×10^{-15}	1.67×10^{-15}	1.67×10^{-15}	2.34×10^{-15}	2.23×10^{-15}	2.24×10^{-15}	4.01×10^{-15}	3.49×10^{-15}	8.55×10^{-16}
Ac-227_ Pu-239	4.08×10^{-17}	4.27×10^{-17}	5.41×10^{-17}	5.02×10^{-17}	7.01×10^{-17}	6.37×10^{-17}	6.37×10^{-17}	8.90×10^{-17}	8.54×10^{-17}	8.55×10^{-17}	1.53×10^{-16}	1.33×10^{-16}	3.26×10^{-17}

5.6 Sensitivity analysis – direct discharge to channel during flood tide

In Scenario 4, we found that, when discharging to the bank, the time of the discharge (relative to the tides) made very little difference to dilution and dispersion. This was because contaminants only enter the channel compartment during ebb tides, regardless of when the discharge happens. This was a consequence of the assumptions we made about flows between the compartments. To understand what difference it would make if contaminants did enter the channel during a flood tide (that is, if our assumptions do not hold), we did a sensitivity analysis of the channel discharges scenario (this scenario) where we modelled discharges during a flood tide.

Figures 53 and 54 show the behaviour of H-3 concentrations over time for discharge to the channel during flood tides. In order to understand the effect of the assumption made in the model, we compare Figures 53 and 54 with Figures 33 and 35 (discharges to the bank during flood tides) and Figures 43 and 45 (discharges to the channel during ebb tides).

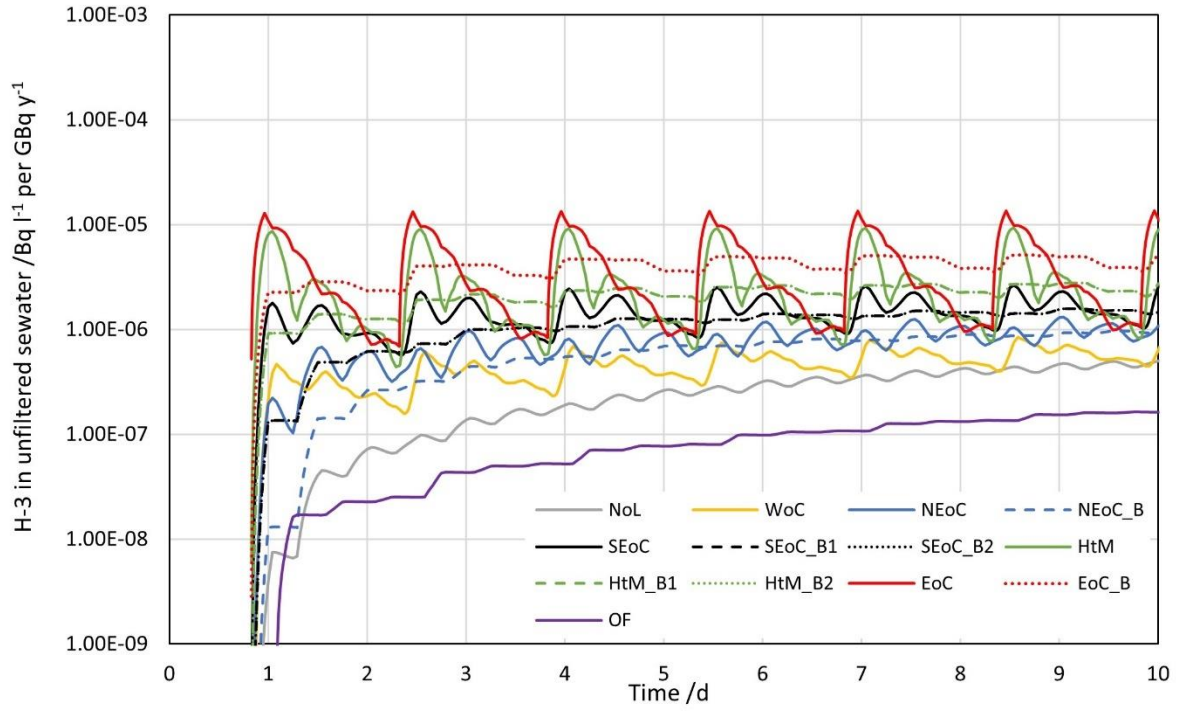

Figure 53 – Activity concentration of H-3 in unfiltered seawater for discharge to the channel during flood tides (per unit annual discharge) (semi-log plot)

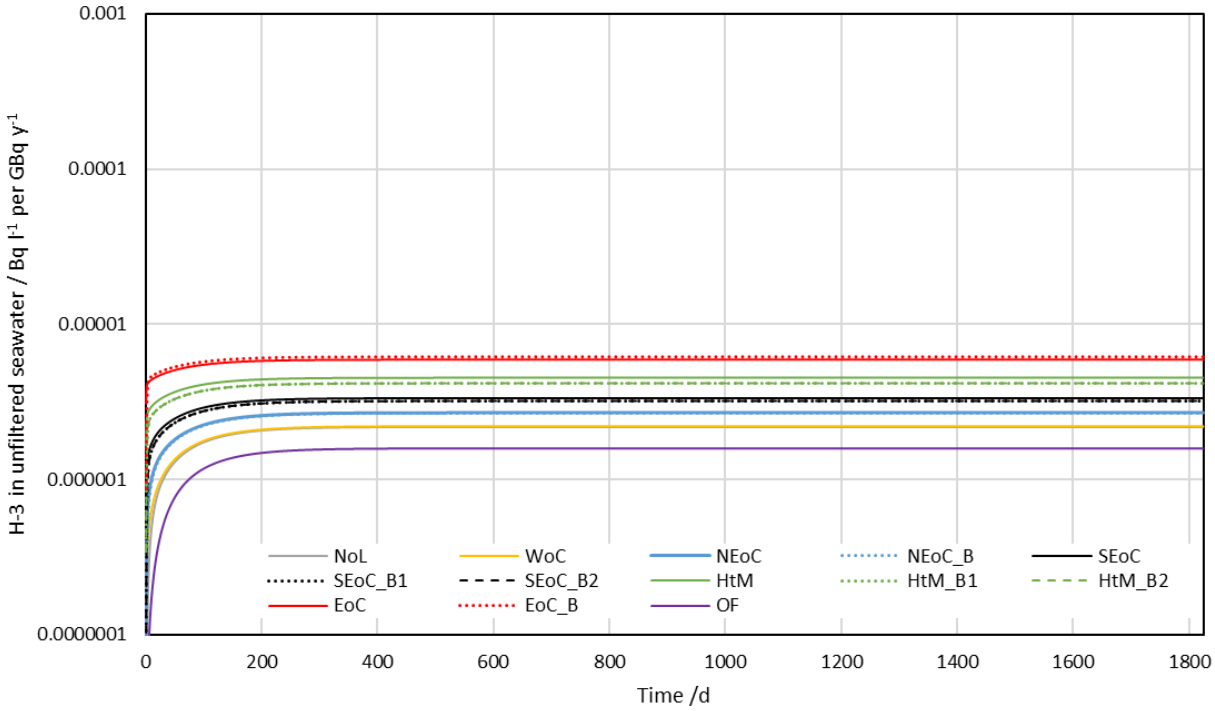

Figure 54 - Tidal-cycle moving average of H-3 concentration in unfiltered seawater for five years for discharge to the channel during flood tides (per unit annual discharge) (semi-log plot)

Figures 53 and 54 (discharges to the channel during flood tides) are very similar to Figures 43 and 45 (discharges to the channel during ebb tides). Therefore, upstream transport is similar in both cases, and the approximation made in the model for bank discharges is unlikely to be significant. The following paragraph summarises those differences that there are.

The main difference between discharge during the flood tide and discharge during the ebb tide is that the flow from the East of Little Cumbrae channel compartment is to the Outer Firth compartment during the ebb tide and to the Hunterston to Millport compartment during the flood tide. Therefore, when discharging during the flood tide the concentration peaks in the upstream compartments are aligned with the concentration peaks in the East of Little Cumbrae channel compartment (as the discharges enter the East of Little Cumbrae compartment and then a fraction of them is immediately transferred to the Hunterston to Millport compartment and through the rest of the model). When discharging during the ebb tide, the concentration peaks in the upstream compartments are offset from the East of Little Cumbrae compartment (as the discharges do not enter any of the upstream compartments until the next flood tide). The concentration peaks in the upstream compartments are also slightly lower when discharging during the ebb tide since some of the activity moves downstream (to the Outer Firth compartment and then out of the model) during the ebb.

These differences occur over individual tidal or discharge cycles, but do not significantly influence the average concentrations in a compartment over a whole discharge cycle. That is, Figures 54 (discharge to channel during flood tides) and 45 (discharge to channel during ebb tides) are very similar. The average concentrations of H-3 in the bank compartments, relative to their adjacent channel compartments, change slightly depending on whether channel compartment concentration peaks during the ebb tide (transfer to the bank compartment occurs when the channel concentration is not at its peak) or the flood tide (transfer to the bank compartment occurs when the channel concentration is at its peak).

Figures 35 (discharge to bank during flood tide) and 54 (discharge to channel during flood tide) are very similar, except for the East of Little Cumbrae Bank compartment. The means that even if the approximation that there is no transfer from the bank to the channel during flood tides were to break down, the model results would still be valid. The East of Little Cumbrae Bank compartment has much higher concentrations when discharges are to the bank during ebb tides than to the channel during flood tides, but this difference is due to the discharge location, not timing.

The medium- and long-term radionuclide build-ups in Scenarios 2 (Figure 25), 4 (Figure 35) and 5 (Figure 45) and this sensitivity analysis (Figure 46) are very similar (except in the East of Little Cumbrae Bank compartment). This is probably because the medium- and long-term behaviour is governed by temporally and spatially averaged exchange, rather than the short-term dynamics.

In conclusion, therefore, the assumption that there is no transfer of radionuclides from bank compartments to channel compartments during flood tides does not have a significant effect on the conclusions of the model. We, therefore, have confidence in the results of Scenario 4, which considers discharges to the bank during a flood tide.

5.7 PC-CREAM 08 model results

We ran a PC-CREAM 08 assessment for unit discharge for 50 y using the default configuration for the Hunterston compartment. The calculation results were reported for 1 year, 2 years, 5 years, 10 years and 50 years.

Figure 55 presents the activity concentrations in unfiltered seawater in the local compartment for the default Hunterston local compartment.

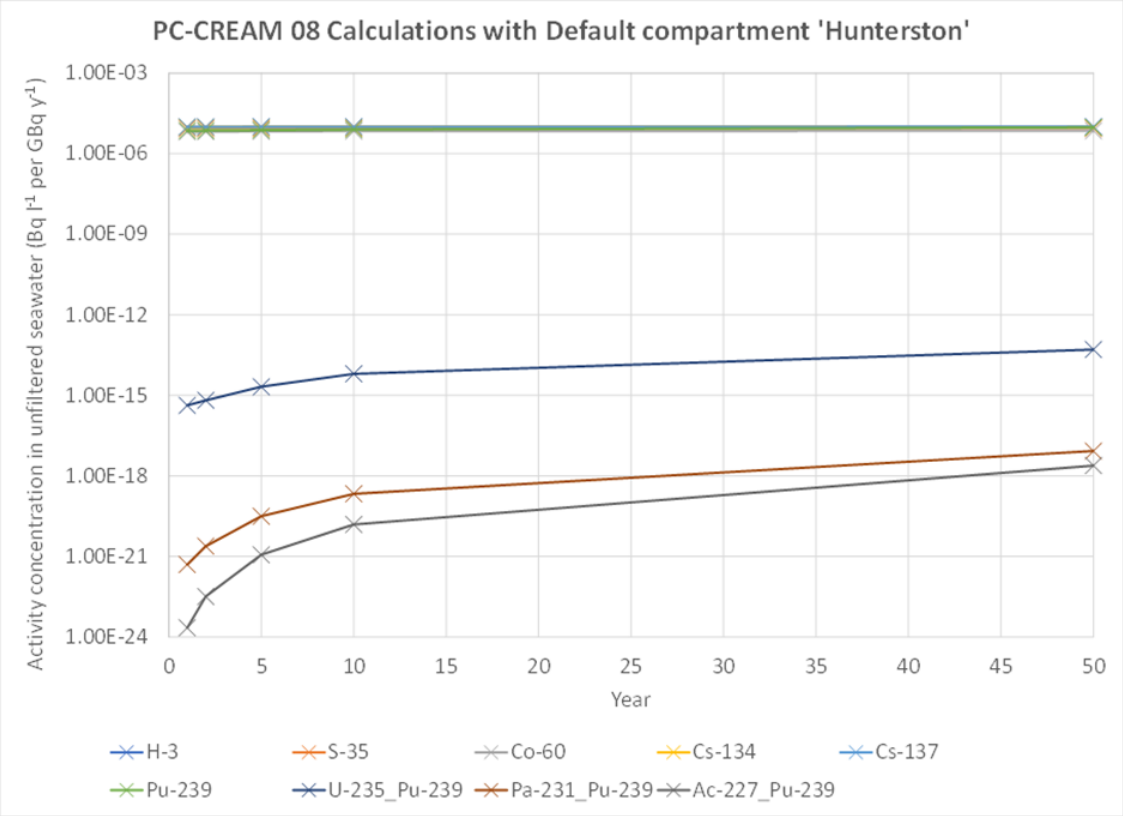

Figure 55 – Activity concentrations in unfiltered seawater per unit annual discharge (1 GBq y^{-1}) calculated by PC-CREAM 08 for the default Hunterston local compartment (semi-log plot).

Apart from very early in the simulation, the discharged radionuclides have constant concentrations in unfiltered seawater. The concentrations (per unit activity) of the discharged radionuclides are within a factor of two of each other (they appear much closer in Figure 55 because of the scale, but see Figure 58). The differences in concentration between the discharged radionuclides are due to the different rates of removal by partition to sediment and radioactive decay.

The activity concentrations of U-235, Pa-231 and Ac-227 increase because the activity in sediment increases over time (owing to ingrowth from Pu-239), and some of this ingrown activity is released to the seawater. Over 50 years, the activity concentrations of these daughters remain orders of magnitude below the activity concentrations of the directly discharged radionuclides.

Figure 56 presents the activity concentrations in dry sediment in the local compartment for the default Hunterston local compartment.

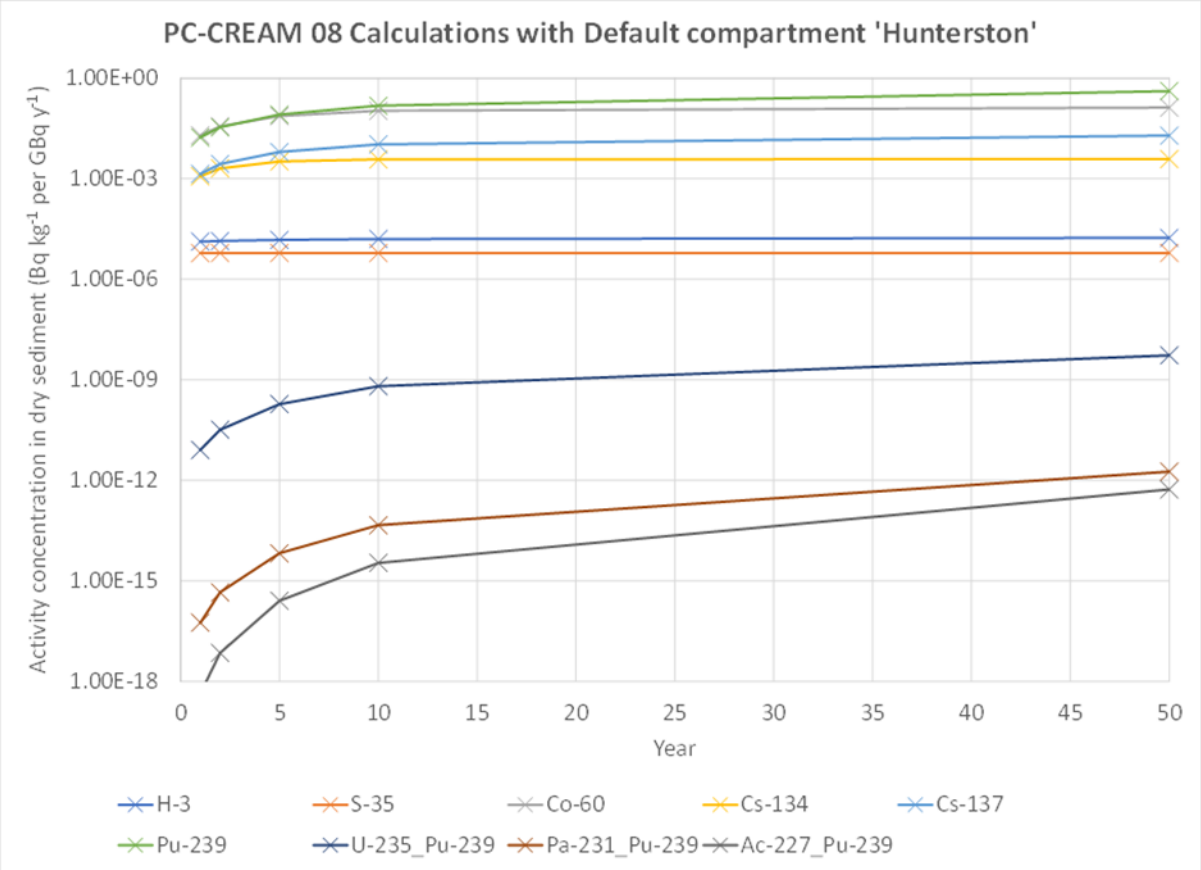

Figure 56 – Activity concentration in dry sediment per unit annual discharge (1 GBq y^{-1}) calculated by PC-CREAM 08 for the default Hunterston local compartment (semi-log plot).

Co-60 and Pu-239 predominate in sediment due to their low mobility (high k_d value). The activity concentration in dry sediment depends on mobility and decay characteristics. Mobile radionuclides (H-3 and S-35) have a constant activity concentration because they do not experience a significant build-up in sediment. Short-lived radionuclides with low to medium mobility (Co-60 and Cs-134) reach an equilibrium after about 10 years, when the new supply balances the decay. Long-lived radionuclides with low to medium mobility (Cs-137 and Pu-239) carry on slowly building up after 10 years. U-235, Pa-231 and Ac-227 activity concentrations continue increasing due to ingrowth from Pu-239 in the sediment.

Table 28 summarises the PC-CREAM 08 results for the default Hunterston local compartment.

Table 28 – PC-CREAM 08 results for the default Hunterston local compartment

Nuclide	Activity concentration in unfiltered seawater /Bq l^{-1}			Activity concentration in dry sediment /Bq kg^{-1}		
	1 year	5 years	50 years	1 year	5 years	50 years
H-3	1.00×10^{-5}	1.01×10^{-5}	1.01×10^{-5}	1.34×10^{-5}	1.49×10^{-5}	1.73×10^{-5}
S-35	8.75×10^{-6}	8.75×10^{-6}	8.75×10^{-6}	6.09×10^{-6}	6.10×10^{-6}	6.10×10^{-6}
Co-60	6.50×10^{-6}	6.78×10^{-6}	7.09×10^{-6}	1.97×10^{-2}	7.45×10^{-2}	1.33×10^{-1}
Cs-134	9.65×10^{-6}	9.68×10^{-6}	9.69×10^{-6}	1.19×10^{-3}	3.30×10^{-3}	3.86×10^{-3}
Cs-137	9.81×10^{-6}	9.87×10^{-6}	9.99×10^{-6}	1.40×10^{-3}	6.30×10^{-3}	1.96×10^{-2}
Pu-239	7.16×10^{-6}	7.53×10^{-6}	9.47×10^{-6}	1.72×10^{-2}	8.26×10^{-2}	4.17×10^{-1}
U-235_Pu-239	4.25×10^{-16}	2.08×10^{-15}	5.07×10^{-14}	8.11×10^{-12}	1.88×10^{-10}	5.40×10^{-9}
Pa-231_Pu-239	4.99×10^{-22}	3.14×10^{-20}	8.42×10^{-18}	5.63×10^{-17}	6.63×10^{-15}	1.82×10^{-12}
Ac-227_Pu-239	2.21×10^{-24}	1.15×10^{-21}	2.42×10^{-18}	4.38×10^{-19}	2.55×10^{-16}	5.35×10^{-13}

This page has been intentionally left blank.

6 Discussion

6.1 Interpreting radionuclide concentrations in compartment models

The radionuclide concentrations calculated by a compartment model can be influenced by two things:

- The understanding of the system being modelled, controlled by the input data and conceptual model
- The discretisation of the model, which does not inherently represent a difference in understanding of the model

A highly discretised model, or a model with a small compartment around the source will calculate significantly higher concentrations in this initial dilution compartment than a model with a larger compartment around the source. However, this does not mean that the results of the two models are inconsistent, making different predictions or reflect different understanding of the system. It is just that the less discretised model averages an inhomogeneous plume over a larger area than a more discretised model does. This is illustrated in Figure 65 in Appendix A.3. The more well-mixed the system, the less the difference between the levels of discretisation. The further from the source, the less the difference between the levels of discretisation.

The appropriate level of discretisation for the compartment where initial dilution occurs depends on the system being modelled and the objectives of the model. Local conditions must be considered. For example, a source in an enclosed bay that has restricted mixing with the main body of the sea may require a local compartment that considers only that bay. The receptor or event being assessed must also be considered. An immobile receptor (such as seaweed) or an event that is restricted to occurring near the source (such as a recreational beach user) may require more discretisation. A mobile receptor (such as a fish with a large range, or consumption of seafood harvested over a large area) may require more averaging and, thus, less discretisation.

In this report, we consider three different initial dilution compartments:

- Default PC-CREAM 08 local compartment (volume 5.00×10^9 m^3)
- East of Little Cumbrae compartment (channel; volume 2.44×10^8 m^3)
- East of Little Cumbrae Bank compartment (volume 1.40×10^7 m^3)

If the models showed the same rate of clearance of the initial dilution compartment (relative to its volume), we would expect the lowest concentrations in the PC-CREAM 08 local compartment, higher concentrations in the East of Little Cumbrae compartment,[12] and the highest concentrations in the East of Little Cumbrae Bank compartment. When comparing the GoldSim and PC-CREAM 08 model results, we will discuss whether the differences in

[12] Strictly, this statement is true when the outfall is modelled in this compartment. However, as discussed in Subsection 6.1, discharges into the bank result in the same contaminant introduction rates to the East of Little Cumbrae compartment from the bank compartment as from direct discharge once the bank compartment has reached equilibrium. Thus, this statement is in practice true for discharges to the bank too.

concentrations differences in the modelled system behaviour, or simply differences in the level of discretisation.

6.2 Summary of GoldSim results

The GoldSim results show that, outside the East of Little Cumbrae Bank compartment, all the discharge scenarios result in similar activity concentrations and dispersion (at the compartment scale). There can be some differences to the short-term behaviour in some compartments (for example if discharging directly to the channel), but these do not influence the long-term build up or equilibrium of radionuclides (determined from the discharge-cycle moving average over five years). Medium- and long-term build-up is influenced by the temporally and spatially averaged exchange.

Concentrations in the East of Little Cumbrae Bank compartment are around two orders of magnitude higher when discharging to the bank (Scenarios 1, 2 and 4) than when discharging to the channel (Scenario 5). This is partly because the initial dilution volume is lower in the bank compartment, and partly because exchange out of the compartment is lower (the bank compartment only has cyclic tidal exchange with its neighbouring channel compartment, while the channel compartment exchanges up and down the Firth too). Scenario 1 represents the current discharge arrangements (the baseline).

The behaviour of each of the exemplar radionuclides considered is summarised below.

After five years, H-3 concentrations in unfiltered seawater are consistently between 1×10^{-6} and 5×10^{-6} Bq l^{-1} per GBq y^{-1} in all compartments except the East of Little Cumbrae Bank compartment (when discharging to the bank). The H-3 concentration in the East of Little Cumbrae Bank compartment, when discharging to the bank, is around 3×10^{-4} Bq l^{-1} per GBq y^{-1}. The behaviour of H-3 in sediment is similar to its behaviour in seawater, with activity concentrations between 10^{-6} Bq kg^{-1} per GBq y^{-1} and 10^{-5} Bq kg^{-1} per GBq y^{-1} (for dry sediment) in all compartments (except East of Little Cumbrae Bank when discharging to the bank) and 6×10^{-4} Bq kg^{-1} per GBq y^{-1} in East of Little Cumbrae Bank when discharging to the bank. The discharge flow rate and discharging in flood or ebb tides do not change the activity concentrations (Scenarios 1, 2 and 4 give similar results).

Co-60 concentrations in unfiltered seawater are slightly lower than H-3 concentrations as more is partitioned to the bed sediments. They are consistently between 7×10^{-7} and 4×10^{-6} Bq l^{-1} per GBq y^{-1} in all compartments except the East of Little Cumbrae Bank compartment (when discharging to the bank). The Co-60 concentration in the East of Little Cumbrae Bank compartment, when discharging to the bank, is around 3×10^{-4} Bq l^{-1} per GBq y^{-1}. The discharge flow rate and discharging in flood or ebb tides do not change the activity concentrations (Scenarios 1, 2 and 4 give similar results).

Co-60 is more strongly sorbing than H-3. Therefore, Co-60 concentrations in sediment are greater than H-3 concentrations and do not reach equilibrium over five years. After five years, they are between around 9×10^{-3} and 5×10^{-2} Bq kg^{-1} per GBq y^{-1} (for dry sediment) in all compartments (except East of Little Cumbrae Bank when discharging to the bank) and 3 to 4 Bq kg^{-1} per GBq y^{-1} in East of Little Cumbrae Bank when discharging to the bank.

U-235 concentrations are much lower than those of H-3 and Co-60. This is because U-235 is present only as a daughter of Pu-239 ($t_{½}$ = 24,110 y). The U-235 concentrations in unfiltered seawater (in all compartments, except East of Little Cumbrae Bank when discharging to the bank) are around 10^{-15} Bq l^{-1} per GBq y^{-1} after five years and still increasing. In the East of Little Cumbrae Bank compartment when discharging to the bank, U-235 concentrations in unfiltered seawater are around 10^{-14} Bq l^{-1} per GBq y^{-1}.

To begin with, U-235 concentration in unfiltered seawater increases rapidly; this is due to the increase in Pu-239 concentration as it is discharged. Once the Pu-239 concentration in unfiltered seawater equilibrates, the U-235 concentration continues to increase, but more slowly (although the increase is still super-linear). This increase is due to physicochemical build-up of Pu-239 in sediment. Uranium is significantly less sorbing than plutonium and present in the seawater at much lower concentration. Therefore, as Pu-239 builds up in sediment, U-235 ingrows more rapidly, and a significant proportion of this ingrowth is returned to the seawater.

The behaviour of U-235 in sediment is similar to its behaviour in seawater, although slightly simpler. It displays a super-linear increase due to increasing ingrowth from Pu-239, as that physicochemically builds up in sediment. After five years, U-235 concentrations in dry top sediment are between around 10^{-11} and 10^{-12} Bq kg^{-1} per GBq y^{-1} in all compartments (except East of Little Cumbrae Bank when discharging to the bank) and around 10^{-8} Bq kg^{-1} per GBq y^{-1} in East of Little Cumbrae Bank when discharging to the bank. U-235 concentrations in sediment are significantly below H-3 and Co-60 concentrations. This is because there is less U-235 in the system, as it is not directly discharged. The discharge flow rate and discharging in flood or ebb tides do not change the activity concentrations (Scenarios 1, 2 and 4 give similar results).

Scenario 2 (alternative discharge scenario to the bank) gives very similar results to the baseline scenario. This is because the extra water flow required to meet the permit criterion (7 m^3 s^{-1}) is small compared to the tidal flows.

Scenario 5 (discharges to the channel) gives lower concentrations in the East of Little Cumbrae Bank compartment than the other scenarios. However, average concentrations in the East of Little Cumbrae channel compartment (and the other model compartments) are similar whether discharging to the bank or the channel. This is because once the bank compartment has reached equilibrium, the inflow rate of contaminants to the channel compartment is the same, whether discharges are to the channel or the bank.

Scenario 3 gives the results for Scenario 2 (alternative discharge scenario to the bank) for the permit discharge limits. H-3 from Hunterston B discharges is the greatest contributor to total activity in environmental media. This is because it is the greatest component of the permitted discharge limits (by activity).

6.3 Comparison of GoldSim model with PC-CREAM 08

6.3.1 Comparison

Figure 57 and Figure 58 compare the activity concentrations of discharged radionuclides in unfiltered seawater after 5 years, for the baseline scenario calculated in GoldSim (discharge to East of Little Cumbrae Bank compartment) and PC-CREAM 08. The GoldSim results for the East of Little Cumbrae channel and bank compartments are shown in Figure 57 and the results for only the channel compartment in Figure 58.

The activity concentrations calculated in GoldSim for the East of Little Cumbrae channel compartment are lower than the activity concentrations calculated in PC-CREAM 08 by a factor less than two. However, the activity concentrations in the East of Little Cumbrae Bank compartment are much higher than the activity concentrations calculated in PC-CREAM 08.

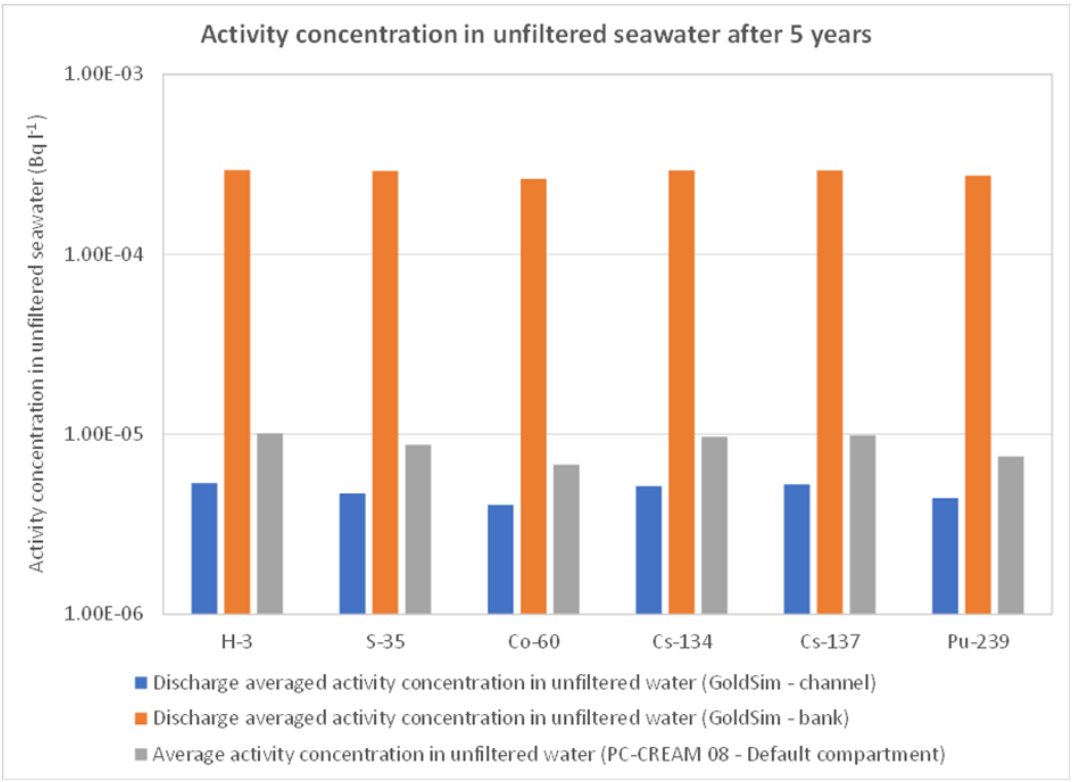

Figure 57 – Comparison of activity concentrations in unfiltered seawater after 5 years per unit discharge (1 GBq y^{-1}), calculated in GoldSim (East of Little Cumbrae and East of Little Cumbrae Bank compartments) and PC-CREAM 08 (log scale)

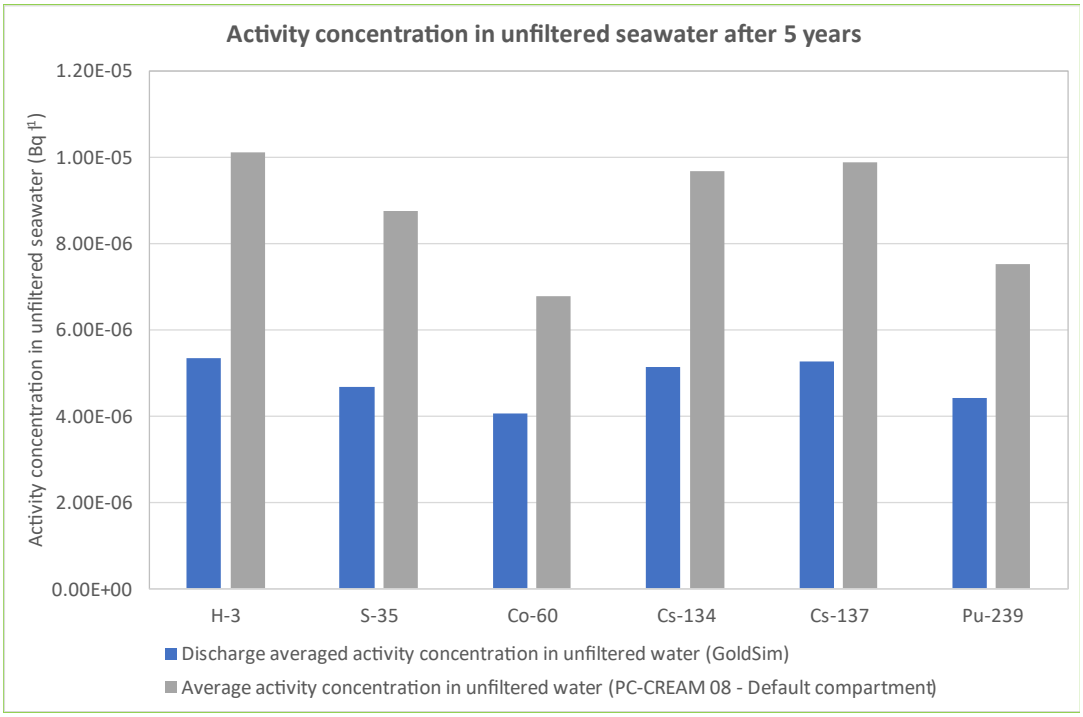

Figure 58 – Comparison of activity concentrations in unfiltered seawater after 5 years per unit discharge (1 GBq y^{-1}), calculated in GoldSim (East of Little Cumbrae compartment) and PC-CREAM 08 (linear scale)

These differences reflect:

- That the PC-CREAM 08 local compartment is larger than the GoldSim bank compartment, resulting in a greater initial dilution volume in PC-CREAM 08

- The use of “sheltered coastal” site parameters for the Hunterston local compartment in the PC-CREAM 08 model, resulting in smaller exchange with the regional compartment than the GoldSim model has with the Irish Sea (via the Outer Firth compartment)

- That the GoldSim East of Little Cumbrae channel compartment exchanges rapidly with its neighbouring compartments

Thus, the bank compartment has much greater concentrations than the PC-CREAM 08 local compartment because initial dilution occurs in a much smaller volume. However, the ratio of volumetric exchange rate to compartment volume is around ten times greater for the GoldSim bank compartment than for the default PC-CREAM 08 local compartment. This suggests that the greater concentration is wholly an artefact of the discretisation and that radionuclide build-up in the GoldSim East of Little Cumbrae Bank compartment is actually lower than in the PC-CREAM 08 local compartment

The channel compartment has lower concentrations than the PC-CREAM 08 local compartment (despite being smaller) because it exchanges more rapidly with its surroundings.

It is interesting to compare the PC-CREAM 08 results to the GoldSim results for discharge to the channel (Scenario 5, Subsection 5.5) (that is, with initial dilution to the channel). When discharging to the channel, radionuclide concentrations around the outfall are lower than the concentrations in the PC-CREAM 08 local compartment. This is despite the initial dilution volume in the GoldSim model still being lower than in PC-CREAM 08. As the channel compartment exchanges rapidly with adjacent compartments in the Firth, this is widespread mixing over a day. This mixing means that discharges to the channel are not well represented by the sheltered coastal site assumed by PC-CREAM 08.

Figure 59 compares the activity concentrations in dry sediment, for the baseline scenario calculated in GoldSim and PC-CREAM 08. It shows discharged radionuclides and the GoldSim results are for the East of Little Cumbrae channel compartment.

The activity concentrations calculated by GoldSim are lower than those calculated by PC-CREAM 08 by a factor less than two; however, the activity concentrations calculated by GoldSim for the East of Little Cumbrae Bank compartment are several orders of magnitude greater (not shown in Figure 59, see Table 15). This is a consequence of differences in the water concentrations calculated by the models, as discussed earlier in this subsection.

In summary, the activity concentrations calculated by GoldSim (for the East of Little Cumbrae channel compartment) are lower than but within a factor of two of the activity concentrations calculated by PC-CREAM 08. For bank discharges, the GoldSim East of Little Cumbrae Bank compartment has activity concentrations several orders of magnitude greater than those calculated by PC-CREAM 08. The concentrations calculated by the GoldSim model vary by radionuclide in the same manner as the concentrations calculated by PC-CREAM 08.

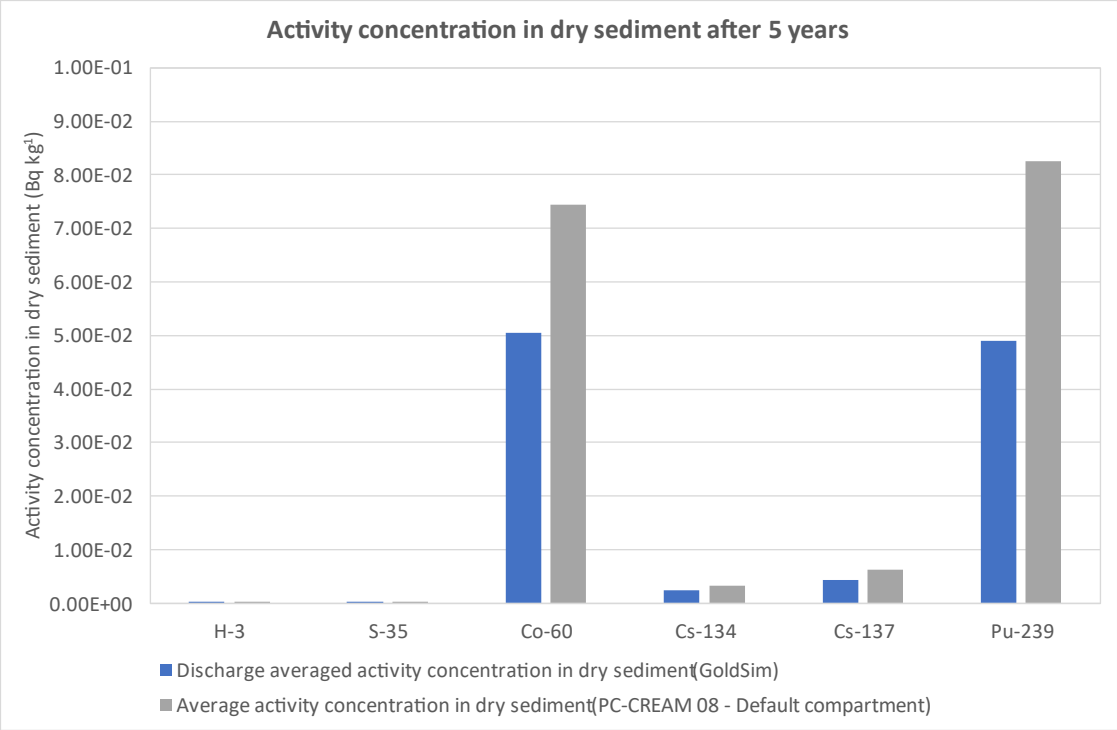

Figure 59 – Comparison of activity concentrations in dry sediment after 5 years, calculated in GoldSim (East of Little Cumbrae channel compartment) and PC-CREAM 08

6.4 Confidence building and validation

6.4.1 Empirical input data

The tidal flows used by the model are based on empirical hydrographic data [10,28,29]. Therefore, we have high confidence in these.

Much of the other input data are generic data based on measurements taken at similar sites. We have generally usually used the latest available data [25,26,33] and these data are widely used in similar radiological assessments. Therefore, we are confident that they are appropriate for this model.

Site specific data for Hunterston used for earlier modelling by CEFAS and the Food Standards Agency are also available [36]. The hydrographic data used by CEFAS were derived from Admiralty data using a similar approach to ours. The data derived by CEFAS were temporally and spatially averaged.

6.4.2 Confidence in underlying models

The UK Health Security Agency have published a literature review summarising various studies that have compared the PC-CREAM 08 DORIS model with experimental data and other models [21]. The DORIS model generally agrees well with other models and measured data once factors such as the inherent conservatism of different models and availability of site-specific data are taken into account. Periáñez *et al.* compared compartment and hydrodynamic models and measured data, finding generally good agreement [20].

6.4.3 Hunterston site monitoring data

6.4.3.1 39” outfall H-3 monitoring

The environmental monitoring programme at Hunterston has found transient elevated H-3 concentrations near the outfall for site’s main surface water drain (the 39” outfall) [37]. These have been attributed to discharges from the tritiated water storage tanks and final delay tanks through the radioactive discharge system (through the cooling water outfall, not through the 39” outfall). These H-3 measurements can be directly correlated to specific discharges, and the reduction in H-3 concentration with time after the discharge has been measured [37,38]. Therefore, they are a good comparator for our model.

Figure 61 shows how H-3 concentration varies with time along the beach either side of the 39” outfall. The vertical lines are radioactive effluent discharges. The seawater concentrations after each discharge are given in Table 29. These data are loosely analogous to the modelled H-3 concentrations in the East of Little Cumbrae Bank compartment shown in Figures 10 and 12 and Table 14 in Subsection 5.1.

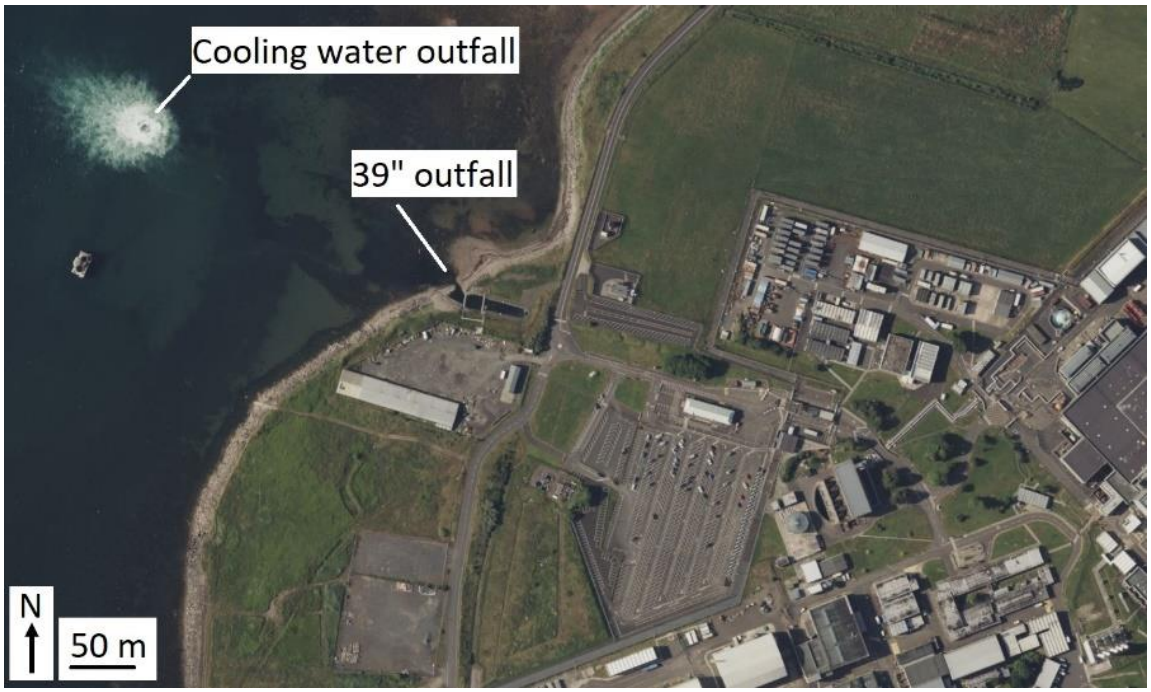

Figure 60 – Aerial photograph showing location of cooling water outfall and 39" outfall (base photograph from reference [39])

There is significant variability in H-3 concentration, both between locations on the beach and between different discharges. Not all discharges result in noticeable H-3 peaks. References [37] and [38] ascribe this variability to changes in wind speed and direction during discharge. There may also be some variability in the H-3 activity in each discharge. Although high H-3 concentration peaks (around 1200 Bq l^{-1}) occur, the H-3 is quickly dispersed and cleared from the area. Figure 61 shows no evidence of sustained high H-3 concentrations.

Figure 61 covers discharges in August, September and October 2017. Over these three months, 304 GBq H-3 was discharged from the final delay tanks [40]. This is equivalent to a discharge rate of around 1217 GBq y^{-1}. Tritiated effluent also arose from the tritiated water storage tanks at a rate of 1 m^3 per month [5] and with a concentration of 2.6 GBq l^{-1} [37]. This is equivalent to a discharge rate of around 31,200 GBq y^{-1}. The total discharge rate from the final delay tanks and tritiated water storage tanks, ignoring minor sources, would then have been around 32,400 GBq y^{-1}. This is around 5% of the permit limit (700,000 GBq).

Table 29 – Measured H-3 concentration at 39" outfall after discharges

Discharge date	Post-discharge H-3 concentration /Bq l^{-1}			
	Beach – north, far	Beach – north, near	Beach – south, near	Beach – south, far
29th August 2017	176	639	1183	170
7th September 2017	444	210	162	50
20th September 2017	8	6	12	7
6th October 2017	89	235	61	76
22nd October 2017	20	31	10	4
Average	147	224	286	61
	180			

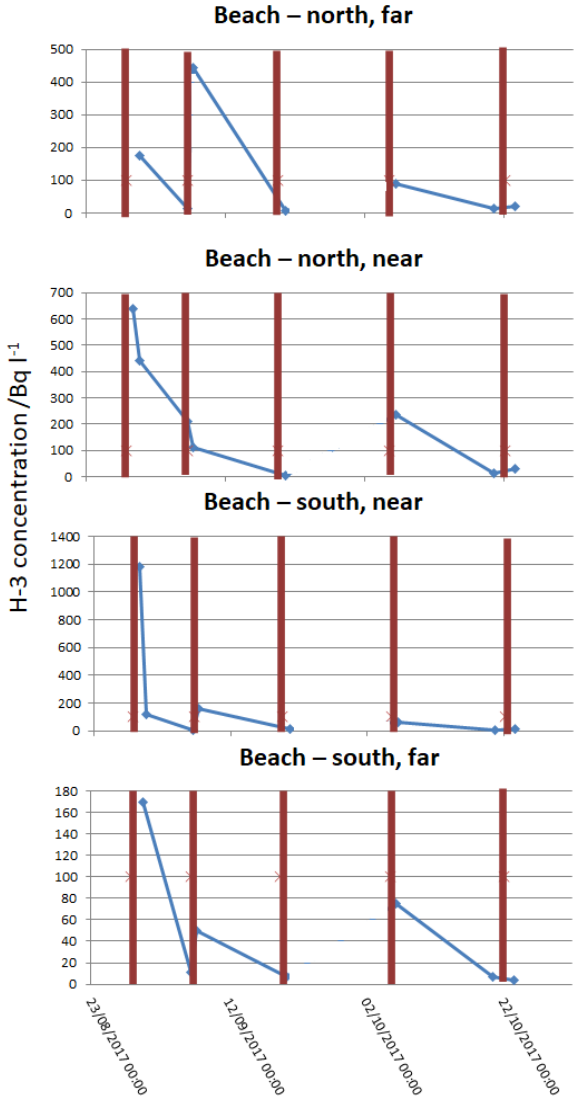

Figure 61 – Measured H-3 concentrations (blue points) on the beach to the north and south of the 39" outfall following discharges through the cooling water outfall (maroon bars). Interpolations have been removed where they misleadingly imply a gradual build-up to the discharge peak. Adapted from reference [38].

Table 14 gives the discharge-cycle moving average concentration of H-3 in the East of Little Cumbrae Bank compartment (after five years and once equilibrium has been reached) as 2.94×10^{-4} Bq l^{-1} per GBq y^{-1}. Permitted annual aqueous discharges of H-3 for Hunterston B are 700,000 GBq. Therefore, the average activity concentration of H-3 would be around 206 Bq l^{-1} if discharging at the permit limits. Based on Figure 10, the peak H-3 concentration is around 5×10^{-4} Bq l^{-1} per GBq y^{-1}, leading to 350 Bq l^{-1} peak. If only 5% of the permitted H-3 were discharged, the average concentration would be around 10 Bq l^{-1} and the peak concentration around 18 Bq l^{-1}. Table 30 compares the GoldSim results to the H-3 concentrations measured at the 39" outfall.

Table 30 – Comparison of GoldSim results with H-3 concentrations measured at the 39" outfall

	39" outfall monitoring	GoldSim baseline	GoldSim as baseline but discharge every 30 tides
Post-discharge concentration	Between 4 Bq l^{-1} and 1200 Bq l^{-1}; average 180 Bq l^{-1}	18 Bq l^{-1}	118 Bq l^{-1}
Typical or time-averaged concentration	Not directly calculable from data in Figure 61, but low (perhaps tens of Bq l^{-1} at most)	10 Bq l^{-1}	10 Bq l^{-1}

The GoldSim model results are within the range of measured concentrations. The peak concentration calculated by GoldSim is toward the lower end of the range and below the average post-discharge concentration by around an order of magnitude. The maximum measured contribution is slightly less than two orders of magnitude above the modelled peak. Concentrations in the measured data drop much further than in the model (to, or to close to, 0 Bq l^{-1}, rather than sustaining an equilibrium). Many discharges do not lead to such high concentrations, most likely because of the weather conditions.

The GoldSim model baseline scenario models much more frequent discharges than the measured data (one every three tides, compared to one every fortnight), but with less activity per discharge. Modelling less frequent, but larger discharges would be expected to lead to higher peak concentrations and lower equilibrium concentrations (or no equilibrium), as seen in the measured data. A GoldSim run as for the baseline scenario, but with discharges every 30 tides instead of every 3 tides, gave a peak H-3 concentration of 3.38×10^{-3} Bq l^{-1} per GBq y^{-1}. If discharging at the permit limits, this would give 2368 Bq l^{-1}; if discharging at 5% of the permit limits, it would give 118 Bq l^{-1} (see Table 30). This is relatively close to the average measured post-discharge concentration of 180 Bq l^{-1}.

Concentrations in the model are averaged over the entire East of Little Cumbrae Bank compartment (see Figure 5). The variability in Figure 61 suggests that the high peaks are localised. Spatially averaged peak concentrations are, therefore, likely to be lower than the peaks in Figure 61. Further, the highest peaks in Figure 61 are likely to be due to inopportune weather. Similarly, some discharges do not lead to noticeable concentration increases; this is likely to be in part due to wind acting away from the shore. The GoldSim model does not account for variable weather. The water flows are based on tidal data and are assumed to implicitly account for prevailing conditions, but do not account for short-term aberrant weather. The measured data would include any H-3 discharges from Hunterston A, but these model runs only consider discharges from Hunterston B.

All these considerations taken into account, the measured data are broadly consistent with the model results. The model may underestimate localised, short-term peak concentrations,

but these are not expected to dominate dose calculations or other radiological impacts. Dose calculations are likely to focus on chronic exposure, such as uptake through the food chain. For these receptors, it is the time-averaged and, potentially, spatially averaged activity concentrations that will govern dose and impacts.

6.4.3.2 District sampling – sediment

EDF operate a district sampling programme around Hunterston. They take regular samples of sediment and seaweed from the locations shown in Figure 62 and fish from the Firth and measure the activity concentrations of several radionuclides. These measurements report all activity arising from the measured radionuclides, regardless of its source. Therefore, the activity measured will include contributions from natural background and other manmade sources, as well as Hunterston power stations.

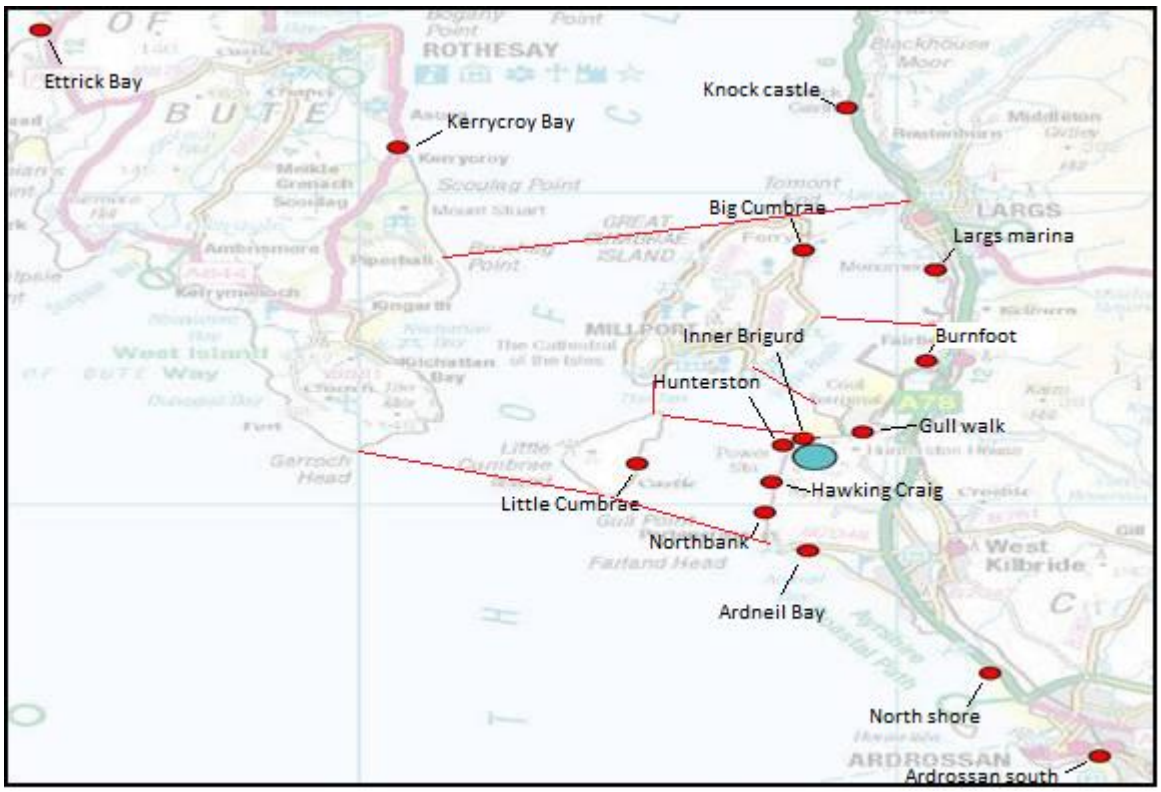

Figure 62 – Hunterston district sampling locations for sediment and seaweed (red circles), shown with GoldSim model compartments (red lines). Adapted from reference [41].

Average measured activity concentrations in sediment for each GoldSim compartment are given in Table 31. These were calculated by averaging all the district sampling measurements done between 2007 and 2022 for all locations within each compartment These are compared with GoldSim results for both stations discharging at 5% of their permit limits and at their permit limits. The sampling points are on or near the shore, so these concentrations should be compared to modelled concentrations in beach compartments where possible.

In almost all cases, the model results are lower than the measured concentrations. This is due to the inclusion of other sources of radionuclides. The modelled total alpha and beta activities in Table 31 only include those radionuclides explicitly modelled (see Table 10); they include neither radionuclides in secular equilibrium, but not explicitly modelled, nor K-40. K-40 is a major contributor to the total beta activity measurement. This is a natural radionuclide and is not included in the model.

Table 31 – Measured and modelled radionuclide concentrations around the Firth of Clyde (all in Bq kg^{-1} (dry weight))

	Alpha			Beta			K-40		Cs-137			Co-60		
	Measured	GoldSim		Measured	GoldSim		Measured	GoldSim	Measured	GoldSim		Measured	GoldSim	
Compartment		5% permit	permit		5% permit	permit				5% permit	permit		5% permit	permit
NoL	107	1.96×10^{-3}	0.0393	210	0.130	2.60	191	Natural radionuclide, not modelled	3.37	0.0124	0.247	0.48	5.90×10^{-3}	0.118
NEoC	122	2.64×10^{-3}	0.0528	254	0.160	3.20	233		6.25	0.0153	0.306	0.39	8.29×10^{-3}	0.165
NEoC_B		2.43×10^{-3}	0.0486		0.211	4.22				0.0152	0.303		7.33×10^{-3}	0.147
SEoC	198	3.46×10^{-3}	0.0692	313	0.196	3.93	259		9.61	0.0187	0.375	0.48	1.12×10^{-3}	0.224
SEoC_B1		3.11×10^{-3}	0.0621		0.253	5.06				0.0182	0.365		9.66×10^{-3}	0.193
SEoC_B2		3.11×10^{-3}	0.0621		0.253	5.06				0.0182	0.365		9.66×10^{-3}	0.193
EoC	148	7.37×10^{-3}	0.147	294	0.367	7.35	284		5.19	0.0351	0.703	0.48	2.52×10^{-3}	0.505
EoC_B		0.465	9.30		27.1	543				1.99	39.8		1.65	33.1
OF	101	1.51×10^{-3}	0.0303	277	0.104	2.09	257		2.94	9.92×10^{-3}	0.198	0.41	4.46×10^{-3}	0.089

Sellafield is also a major source of background radioactivity in the Firth of Clyde [42,43,44]; the latest *Radioactivity in food and the environment* (RIFE) report finds that *"the concentrations of artificial radionuclides in the marine environment* [near Hunterston] *are predominantly due to Sellafield discharges, the general values being consistent with those to be expected at this distance from Sellafield"* [42].In 2021, Sellafield discharged 1400 TBq of Cs-137 and 10 GBq of Co-60 [45]. This compares to limits of 160 GBq for Cs-137 (Hunterston A) and 10 GBq Co-60 (Hunterston B) at Hunterston. Sellafield discharges of both radionuclides were somewhat higher in preceding years [45].

The modelled values are closer to the measured values for Co-60 than Cs-137, suggesting that the contribution of the Hunterston power stations to local Co-60 concentrations may be greater than to local Cs-137 concentrations. This is consistent with the greater ratio of Hunterston permit limit to Sellafield discharges for Co-60 than for Cs-137 Modelled activity concentrations for the East of Little Cumbrae Bank compartment are comparable to the measured values, and in some cases greater (although the measured values include contributions from more distant areas of the shore). However, the measured values for this compartment are similar to those for other parts of the Firth of Clyde.

In summary, as the district sampling results are dominated by natural background and Sellafield discharges, they are not a good benchmark for comparison with the model.

6.4.3.3 *Radioactivity in food and the environment* reports

The environment agencies and food standard agencies publish annual RIFE reports. These contain details of environmental monitoring done around nuclear sites. The latest RIFE report is RIFE-27 [42] and covers 2021, the last full year of generation at Hunterston B. Rife-27 finds that *"the concentrations of artificial radionuclides in the marine environment* [near Hunterston] *are predominantly due to Sellafield discharges, the general values being consistent with those to be expected at this distance from Sellafield"* [42].

RIFE-27 reports radionuclide concentrations at a single seawater sampling location near the Hunterston cooling water outfall. The H-3 activity concentration was 210 Bq l^{-1}, and all other radionuclide concentrations were below the limit of detection. This H-3 concentration is consistent with those measured around the 39" outfall; therefore, the discussion in Subsection 6.4.3.1 applies. To summarise, this measurement is consistent with the model results for peak concentration, but higher than the model results for average concentration.

RIFE-27 also reports radionuclide concentrations in dry sediment samples from various locations in the Firth of Clyde. All radionuclides except Cs-137 and Am-241 were below the limit of detection.[13] The Cs-137 concentrations reported are similar to those that have been measured as part of EDF's district sampling programme; therefore, the discussion in Subsection 6.4.3.2 applies.

Several of the Am-241 activity concentrations reported in RIFE-27 are below the limit of detection. The remainder range from 0.25 Bq kg^{-1} to 0.92 Bq kg^{-1}. The model concentrations are typically of the order of 10^{-4} Bq kg^{-1} if Hunterston A[14] discharges at its permit limit and

[13] A single sediment sample also had a measurable concentration of Eu-155, but that radionuclide is not considered in our model.

[14] Am-241 is only included in the model as a daughter of Pu-241. This is not included in the permit for Hunterston B and, therefore, is only included in the model source term for Hunterston A. The permit also allows a total 3 GBq of other alpha-emitting radionuclides to be discharged from Hunterston A and B, but this is included in the model as Pu-239 and doesn't contribute to modelled Am-241 concentrations.

10^{-6} Bq kg^{-1} if it discharges at 5% of its permit limits. These are significantly below those concentrations in the RIFE report that are above the limit of detection. Given that several of the samples in the RIFE report were below the limit of detection, it is not clear how representative the reported Am-241 concentrations are.

Sellafield Pu-241 (Am-241 parent) discharges in 2021 were 830 GBq and direct Am-241 discharges were 10 GBq, and discharges in preceding years were higher [45]. The corresponding permit limit for Hunterston A is 2 GBq Pu-241.

In summary, as the RIFE monitoring results are dominated by Sellafield discharges, they are not a good benchmark for comparison with the model.

6.4.3.4 Thermal plume monitoring

Reference [46] summarises the results of aerial surveys of the thermal plume from the Hunterston power stations [47,48]. The behaviour of the contaminant and thermal plumes will be related. They will both be influenced by water flows in the receiving water body, and thermally driven water flows in the plume will carry contaminants with them. However, there will be some differences; in particular, the thermal plume will cool down with time and distance from the power stations, but there is no equivalent phenomenon for the contaminant plume.

During calm weather and slack tides, the thermal plume spreads perpendicular to the shoreline toward Little Cumbrae. There is a return flow to the east shore of the Firth of Clyde and then lateral spreading along the shore, leading to an accumulation along the Portencross coast (south of Hunterston). If the weather is not calm, this accumulation may be either alleviated or enhanced, depending on the wind direction.

The spread of the thermal plume normal to the shore during slack tides is presumably driven by the large volumes of water being pumped from the outfall. In our GoldSim model, transport during a slack tide would be from the bank compartment to the channel compartment at a rate governed by the water flow from the cooling water outfall. This corresponds to the observed spread normal to the shoreline. The model does not include a return flow to the discharge compartment during slack tides (noting that water balance would require any such return flow to be compensated for by a further outflow from the bank compartment to the channel compartment). From the channel compartment, there is a downstream flow at the net of cooling water flow plus or minus (depending on direction) the tidal flow. Localised southward spreading is represented by the well-mixed compartments.

During ebb tides, the thermal plume is spread southward by the receding tide. The thermal plume is attached to the shoreline and can affect the shore up to 2 km south of the cooling water intake. Reference [46] does not discuss the behaviour of the plume during flood tides. The greatest increases in temperature, due to the thermal plume, are predicted to occur along the Portencross coast. This is due to both the spread and accumulation of the plume, described above, and naturally variable temperatures around the discharge point lessening the thermal effect of the plume there.

Modelled transport during an ebb tide is similar to the plume spreading observed, with contaminants being driven southward by the tide. In the survey results, the near-shore plume spread is observed until around 2 km south of the power stations. This is within the same model compartment as the outfall and is represented by the well-mixed compartment approximation.

We would not expect channel discharges to be attached to the shoreline in the way that the current plume is. For bank discharges, the plume is discharged near the shore and immediately diverted south (instead of west) by the tide. If discharging to the channel, the tidal

flow would still be southward, and there would be no eastward flow to push the plume back toward the shore.

Thus, the model behaviour is consistent with the observed behaviour of the thermal plume in both slack and ebb tides. The near-shore plume spread during the ebb tide is well represented using a well-mixed bank compartment, justifying the modelling of a separate bank compartment.

7 Conclusions

We have created a compartment model of the Firth of Clyde and used this to model the dilution and dispersion of discharges from Hunterston nuclear power stations. This model calculates average radionuclide concentrations in seawater and sediment in several regions of the Firth of Clyde. We have compared the results of the model to real-world observations and to a model run in the standard PC-CREAM 08 software. We have used the model to investigate the effect of discharge location, timing and flow rate on dilution and dispersion.

We have considered five scenarios:

1. Baseline scenario: current system with discharges to the bank during ebb tides with a continuous flow of cooling water (unit discharges)

2. Alternative discharge to the bank: discharges to the bank during ebb tides with a low flow rate of water through the pipe while discharging (unit discharges)

3. Scenario 2 with site limits for A station and B station: as Scenario 2, (discharges from both power stations at the annual limits set in their permits [3,4])

4. Scenario 2 with discharges during the flood tide: as Scenario 2, but with discharges during the flood tide (unit discharges)

5. Discharge to the channel: discharges to deeper water during ebb tides with a low flow rate of water through the pipe while discharging (unit discharges)

The behaviour of radionuclides is very similar for all the scenarios considered in all compartments except the East of Little Cumbrae Bank compartment. There are some differences in the short-term behaviour (over a single tidal or discharge cycle), but these have no effect on the long-term build-up or average radionuclide concentrations. Discharge to the East of Little Cumbrae Bank compartment (Scenarios 1 to 4) results in localised higher activity concentrations in that compartment (by one to two orders of magnitude, depending on radionuclide). This is due to the smaller initial dilution volume and lower flow through the compartment, compared to discharges to the deeper channel. Concentrations elsewhere in the model are not affected.

The results show that neither reducing the water flow in the discharge nor changing the timing of the discharge (relative to the tide time) change the activity concentrations (Scenario 2 and Scenario 4 results are similar to the baseline results Scenario 1). Scenario 5 (discharge into the channel) gives lower concentrations in the bank compartment but the concentrations in the other compartments are similar to those in Scenario 1.

The significance of the higher concentrations in the bank compartment when discharging to the bank (Scenarios 1 to 4) compared to when discharging to the channel (Scenario 5) will depend on the amount of activity discharged and the dose that could result. These are not considered in this report. As the activity is quite localised, the difference in dose may not be significant. A human receptor and many animal receptors would be likely to move around the beach or sea and would not be solely exposed to the higher activity concentrations near the discharge line. Similarly, anyone harvesting foodstuffs is likely to do so from a larger area and would not eat food gathered solely from the immediate vicinity of the outfall.

These results, together with a dose assessment based on them, will be used by EDF to optimise their new discharge arrangements and apply for the required permit variation.

We compared the results of our compartment model to a model run in PC-CREAM. This used the default parameters provided in PC-CREAM 08 for the Hunterston site. Results from our compartment model were several orders of magnitude higher in the bank compartment but around a factor of two lower in the channel compartment than the results from the PC-CREAM 08 model. This is because the bank compartment we modelled is much smaller than the PC-CREAM 08 local compartment, leading to less initial dilution, but the ratio of exchange rate to compartment size in the channel compartment and out to the Irish Sea (based on Admiralty tidal data) was much greater than for PC-CREAM 08.

This reflects the fact that the channel is not well represented by the “sheltered coastal” parameters used in PC-CREAM 08. However, the rapid mixing and closely clustered concentrations in the Firth of Clyde support the use of the larger, well-mixed local compartment in PC-CREAM 08. Our model also shows a similar pattern of behaviour between different radionuclides as the PC-CREAM 08 model (allowing for the use of an updated distribution coefficient for cobalt).

The agreement between the PC-CREAM 08 model and our model builds confidence in the applicability of the annually and spatially averaged PC-CREAM 08 model to Hunterston (and, therefore, their use to assess the long-term build-up of discharges) and helps verify our model. It shows that the modelled short-term effects such as tidal-cycles and discharge scheduling do not influence the long-term build-up of radionuclides (except in the immediate vicinity of the outfall, the East of Little Cumbrae Bank compartment), but that the use of site-specific hydrography does.

Our model can reproduce the average results of environmental monitoring of H-3 concentrations following discharges through the current discharge arrangements. The average H-3 concentration measured on the beach near the power stations after discharges is 180 $Bq\,l^{-1}$. A model run simulating such discharges calculates unfiltered seawater H-3 concentrations of 118 $Bq\,l^{-1}$. This is within a factor of two, which is good agreement for this type of model.

The measured H-3 concentrations have a significant range, from 1183 $Bq\,l^{-1}$ to 4 $Bq\,l^{-1}$, depending on the location of the measurement and the discharge event in question. Much of this variation is likely to be due to the weather during the discharge. The model does not attempt to simulate varying weather, instead assuming average conditions, nor does it calculate results for areas as localised as the sampling campaign. Therefore we do not expect it to reproduce the extremes of the range, only the average.

We attempted to compare the model to activity concentrations in sediment collected by EDF as part of their district sampling campaign and activity concentrations in sediment and seawater reported in RIFE-27. However, these concentrations are dominated by activity from Sellafield discharges that has migrated northward. Therefore, they are not suitable for comparison with the model results, which consider only discharges from the Hunterston power stations.

8 References

1. Magnox Ltd, *Our sites – GOV.UK,* https://www.gov.uk/government/collections/our-sites, December 2019. Accessed 9th January 2023.
2. EDF, *Hunterston B power station | EDF,* https://www.edfenergy.com/energy/power-stations/hunterston-b. Accessed 9th January 2023.
3. Scottish Environment Protection Agency, *Permit EAS/P/1173609,* March 2019.
4. Scottish Environment Protection Agency, *Permit EAS/P/1173596,* March 2019.
5. [redacted] *Hunterston B (HNB) station: liquid effluent "stage A" (credible options) review,* EDF Energy Nuclear Generation Ltd Engineering Report ND/REP/TAD/0004/HNB/21 Revision 001, June 2022.
6. [redacted], *Decommissioning of Hunterston B nuclear power station: EIA scoping report,* Wood Group UK Ltd Doc Ref 808125-WOOD-XX-XX-RP-O-00001_S3_CO1, August 2022. https://www.edfenergy.com/file/9823060/, https://www.edfenergy.com/file/9823057/ and https://www.edfenergy.com/file/9823053/
7. [redacted], *Hunterston B seaweed removal: environmental appraisal,* [redacted] Document Ref R.2827 Version 2, June 2017. https://marine.gov.scot/sites/default/files/06954_-_environmental_appraisal_redacted.pdf
8. [redacted], PG Fernandes and [redacted], *Clyde ecosystem review,* Scottish Marine and Freshwater Science Report Volume 3 Number 3, The Scottish Government and Marine Scotland Science, ISBN 78-1-78045-877-9, 2012. https://www.gov.scot/publications/scottish-marine-freshwater-science-volume-3-number-3-clyde-ecosystem/.
9. Open Street Map Contributors, *OpenStreetMap,* https://www.openstreetmap.org/?mlat=55.724&mlon=-4.889#map=8/55.724/-4.889. Accessed 9th January 2023.
10. United Kingdom Hydrographic Office, *Scotland – West Coast – Firth of Clyde – Ardrossan to Largs,* Admiralty Chart 2491, October 2022. http://mobile.visitmyharbour.com/defaced/p/9475-B3D52B7DC4F4-249102d.html
11. [redacted] *Radiological habits survey: Hunterston, 2012,* CEFAS Environment Report RL 26/13, 2013. https://publications-api.cefas.co.uk/api/Attachments/download/354
12. [redacted] *Radiological habits survey: Hunterston 2017,* Scottish Environment Protection Agency Report Version 2.0, June 2022. https://www.sepa.org.uk/environment/radioactive-substances/environmental-monitoring-and-assessment/reports/
13. [redacted], *Radiological habits survey: covid-19 2020,* Scottish Environment Protection Agency Report, August 2022. https://www.sepa.org.uk/environment/radioactive-substances/environmental-monitoring-and-assessment/reports/
14. [redacted](eds), *The methodology for assessing the radiological consequences of routine releases of radionuclides to the environment used in PC-CREAM 08,* Health Protection Agency Report HPA-RPD-058 Version 1.1, June 2015. https://www.gov.uk/government/publications/pc-cream-08-radiological-consequences-of-routine-releases
15. GoldSim Technology Group, *User's guide: GoldSim,* Version 14.0, October 2021. https://www.goldsim.com/Web/Customers/Education/Documentation/
16. NNB Generation Company Ltd, *UK EPR – Hinkley Point C – radioactive substances regulation environmental permit application,* 2011. https://www.edfenergy.com/file/1723

17. NNB Generation Company (SZC) Ltd, *Sizewell C project – radioactive substances regulation (RSR) permit application – appendix D – support document D1 – human radiological impact assessment,* NNB GenCo Report 100197432 Version 1.0. https://www.edfenergy.com/file/9634642/

18. [redacted] *An assessment of the radiological impacts of proposed atmospheric and liquid radioactive waste disposals from Dounreay,* Dounreay Site Restoration Ltd Document Ref RSA AUTH(09)Dose Issue 1.1, September 2009. https://www.sepa.org.uk/media/116485/paper-10-an-assessment-of-the-radiological-impacts-of-proposed-atmospheric-and-liquid-radioactive-waste-disposals-from-dounreay.pdf

19. [redacted], *Oldbury site effluent dispersion model study,* Eden Nuclear and Environment Ltd Report ENE-092/03 Final Issue 1.0, December 2012.

20. [redacted], *A comparison of marine radionuclide dispersion models for the Baltic Sea in the frame of IAEA MODARIA program*, Journal of Environmental Radioactivity, 139, 66-77, 2015. https://doi.org/10.1016/j.jenvrad.2014.09.013

21. [redacted], *Verification and validation of models used in radiological assessment tools PACE and PC CREAM 08*, UK Health Security Agency Report UKHSA-RCE-004, November 2022. https://www.gov.uk/government/publications/verification-and-validation-of-models-in-pace-and-pc-cream-08

22. [redacted], *Discharges from B station and A station discharge line information,* Email to [redacted], 8th November 2022.

23. Water UK, *Design and construction for foul and surface water sewers offered for adoption under the code for adoption agreements for water and sewerage companies operating wholly or mainly in England ("the code"),* Sewerage Sector Guidance Document Appendix C, Approved Version 2.1, May 2021. https://www.water.org.uk/wp-content/uploads/2021/07/SSG-App-C-Des-Con-Guide.pdf

24. [redacted], *PC-CREAM input files,* Email to [redacted], 12th October 2022.

25. [redacted] *Review of local compartment parameter values for use with UK sites in the DORIS marine dispersion model,* Public Health England Report PHE-CRCE-051 Version 1.3, September 2019. https://www.gov.uk/government/publications/radiation-marine-dispersion-model-parameters-for-uk-sites

26. [redacted], *Parameter values used in coastal dispersion modelling for radiological assessments,* Environment Agency Evidence Report SC060080/R3, February 2011. https://www.gov.uk/government/publications/parameter-values-used-in-coastal-dispersion-modelling-for-radiological-assessments

27. GoldSim Technology Group, *User's guide: GoldSim contaminant transport module,* Version 14.0, October 2021. https://www.goldsim.com/Web/Customers/Education/Documentation/

28. United Kingdom Hydrographic Office, *Firth of Clyde and approaches,* Admiralty Tidal Stream Atlas NP222 1st Edition, 1992. https://www.visitmyharbour.com/articles/3168/hourly-tidal-streams-around-the-firth-of-clyde

29. WillyWeather, *Hunterston tide times, North Ayrshire – WillyWeather,* https://tides.willyweather.co.uk/st/north-ayrshire/hunterston.html. Accessed Autumn 2022.

30. EDF Energy Nuclear Generation Ltd, EDF Report ERO/EAN/0047/AGR.

31. International Commission on Radiological Protection, *Nuclear decay data for dosimetric calculations,* ICRP Publication 107, 2008. https://doi.org/10.1016/j.icrp.2008.10.002

32. [redacted] (ed), *Revised Nuffield advanced science book of data,* Longman Group Ltd, Harlow, ISBN 978-0-582-35448-7, 1984. https://www.stem.org.uk/rxvme

33. International Atomic Energy Agency, *Sediment distribution coefficients and concentration factors for biota in the marine environment,* IAEA Technical Reports Series No. 422, April 2004. https://www.iaea.org/publications/6855/sediment-distribution-coefficients-and-concentration-factors-for-biota-in-the-marine-environment

34. International Atomic Energy Agency, *Sediment K_ds and concentration factors for radionuclides in the marine environment,* IAEA Technical Reports Series No. 247, July 1985. https://inis.iaea.org/search/16080387

35. GoldSim Technology Group, *GoldSim Player – GoldSim,* https://www.goldsim.com/Web/Products/GoldSimPlayer/. Accessed 30th January 2023.

36. [redacted], *Nuclear site specific hydrographic parameters for use with the WAT/ADO models,* CEFAS Environment Report RL12/06 Update V1.3, August 2006. https://publications-api.cefas.co.uk/api/Attachments/download/279

37. EDF Energy Nuclear Generation Ltd, *39 inch outfall – elevated tritium,* Hunterston B Technical Communication.

38. [redacted] *A station discharge data,* Email to [redacted] 16th September 2022.

39. Microsoft, *Bing Maps – directions, trip planning, traffic cameras & more,* https://www.bing.com/maps?osid=38d62a49-12db-4fad-8e2a-65d2ae7ad622&cp=55.723382~-4.899261&lvl=17.081743&style=a&pi=0&v=2&sV=2&form=S00027. Accessed 31st January 2023.

40. [redacted], *Additional information as requested,* Email to [redacted], 16th September 2022.

41. [redacted], *RE: updated scenarios spreadsheet,* Email to [redacted] and [redacted] 10th January 2023.

42. Environment Agency, Food Standards Agency, Food Standards Scotland, Natural Resources Wales, Northern Ireland Environment Agency and Scottish Environment Protection Agency, *Radioactivity in food and the environment, 2021,* RIFE 27, November 2022. https://www.gov.uk/government/publications/radioactivity-in-food-and-the-environment-rife-reports

43. [redacted] *Windscale radiocaesium in the Clyde Sea area,* Marine Pollution Bulletin, 10(4), 116-120, 1979. https://doi.org/10.1016/0025-326X(79)90104-8

44. [redacted], *A radionuclide study of the Clyde Sea area,* PhD Thesis, University of Glasgow, 1977. http://theses.gla.ac.uk/id/eprint/78748

45. Sellafield Ltd, *Monitoring our environment – discharges and environmental monitoring: annual report 2021,* Sellafield Ltd Report, December 2022. https://www.gov.uk/government/publications/discharges-and-environmental-monitoring-annual-report-2021

46. [redacted], *A synopsis report of the marine biological work carried out in the vicinity of Hunterston power station and potential habitat sensitivities to thermal effluents within a 2-5 km radius,* University of London Marine Biological Station Millport Report, 2007.

47. [redacted] *Remote sensing observations and analyses of cooling water discharges from a coastal power station,* International Journal of Remote Sensing, 14(2), 253-273, 1993. https://doi.org/10.1080/01431169308904336

48. [redacted], *Foam lines generated by a spreading buoyant plume,* International Journal of Remote Sensing 14(14), 2647-2663, 1993. https://doi.org/10.1080/01431169308904299

49. EDF Energy, *Chapter 04: culvert system, main valves and outfall* in *Hunterston 'B' power station plant item operating instructions,* Volume 16.00.04.

This page has been intentionally left blank.

Appendix A – Additional figures

A.1 Tidal flow from the North Channel to the outer Firth of Clyde

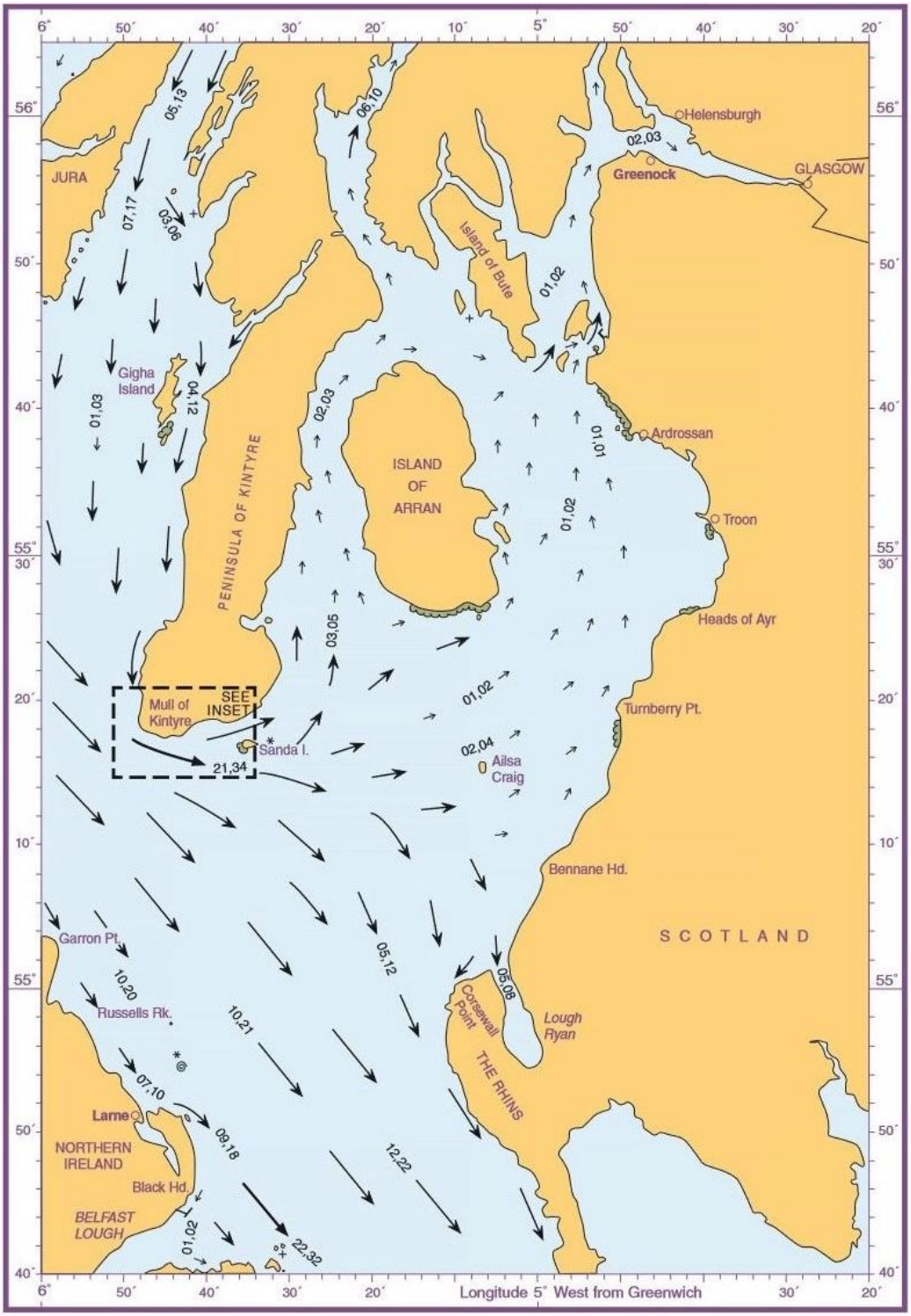

Figure 63 – Excerpt from tidal stream atlas showing tidal flow through the North Channel and from the North Channel into the outer Firth as the tide comes in (4 h 20 min before high water at Greenock). Flow speed is in units of 10^{-1} knots (1 knot = 0.5144 m s^{-1} [32]). Flow rates for spring and neap tides are separated by a comma (neap,spring). Reproduced from reference [28].

A.2 Water balance in channel compartments that have flows to bank compartments

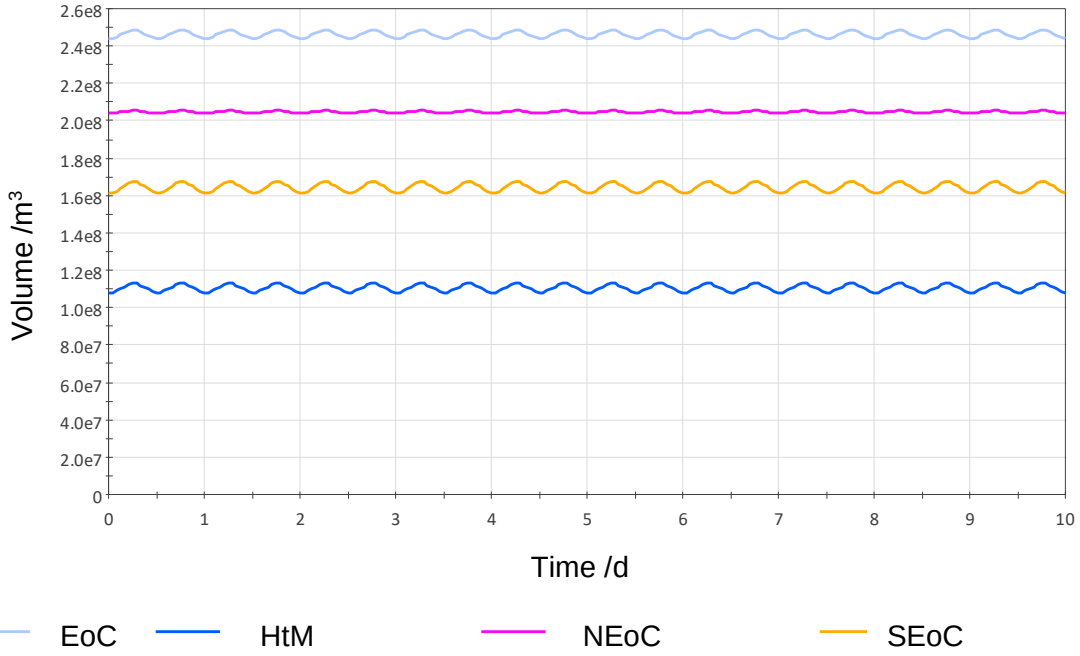

Figure 64 – Water balance calculations showing the variation in volume in channel compartments due to flow to bank compartments. (The GoldSim model treats all channel compartments as having a constant volume and does not use these results.)

Figure 64 shows the variation in volume of the channel compartments that would arise from the flows to the banks if water balance were maintained. The volume changes are small compared to the channel compartment volumes, and the constant volume approximation used in GoldSim is reasonable.

If it were necessary to account for these flows in the water balance, the water balance model in Figure 64 could not be used. As water flows from the channels to the banks at high tide, the channel compartment volumes drop. This is unrealistic. A more sophisticated water balance model would need to supplement the tidal flows into the channel compartments (and throughout the system) to make up for these flows, rather than alter the compartment volume.

A.3 Effect of discretisation on interpretation of results

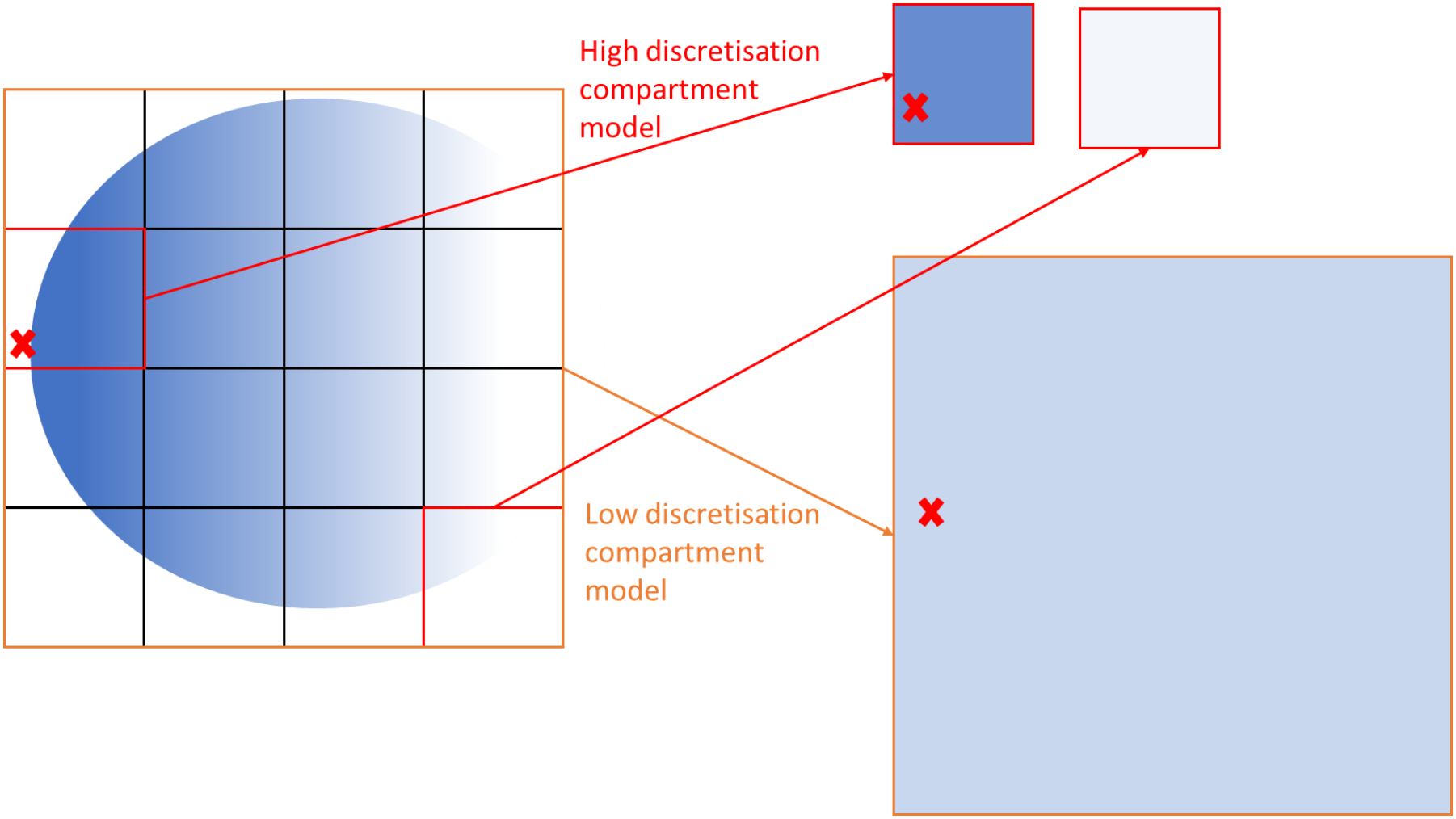

Figure 65 – Schematic of a hypothetical plume (blue) from a source (red x), showing how it would be represented in both low- and high-discretisation compartment models. Darker shading represents a higher concentration (not to scale).

This page has been intentionally left blank.

Appendix B – Discharge pipe properties

B.1 Calculation of discharge start and end times

This appendix explains how the discharge start and end times used in the GoldSim model (Table 1) were calculated.

The discharge start time in GoldSim is the time discharges are initiated at the stations plus the travel time for effluent in the pipe (Equation (42)). The discharge finish time is the time the final delay tank is emptied plus the effluent travel time (Equation (43)).

$$T_{\mathrm{d,p}} = T_{\mathrm{d,s}} + L \cdot A/F \quad (42)$$

Here:

$T_{\mathrm{d,p}}$ is the time of discharge from the pipe (h after high water);

$T_{\mathrm{d,s}}$ is the time discharges are initiated at the station (1 h after high water [3,4] for all scenarios except Scenario 4 and 1 h after low water – 7 h after high water – for Scenario 4);

L is the length of the discharge pipe (745 m for bank discharges [49] and 1400 m for channel discharges – see later);

A is the cross-sectional surface area of the pipe (8.8 m^2 for the baseline scenario [49] and 0.018 m^2 for all other scenarios – see later);

F is the flow rate through the pipe (7 $m^3 s^{-1}$ [3,4] for the baseline scenario and 0.0086 $m^3 s^{-1}$ for the other scenarios – see later).

$$T_{\mathrm{e,p}} = T_{\mathrm{d,s}} + 3.2 + L \cdot A/F \quad (43)$$

Here:

$T_{\mathrm{e,p}}$ is the time discharges from the pipe end (h after high water);

3.2 h is the time taken to empty the final delay tank, which stores the contaminated effluent until discharge [22].

The parameters for the baseline scenario are based on the minimum requirements in the current permits [3,4] and information about the current discharge system [49]. The length of the discharge pipe for channel discharges was derived by measuring from the power station site to the deeper water in reference (see Figure 5) [10]. The cross-sectional area for the new discharge pipe was based on a representative diameter of 15 cm and the flow rate was assumed to be the same as the rate at which the final delay tanks are drained. We chose these parameters to represent a smaller discharge system.

The velocity in the pipe is 0.5 m s^{-1}, slightly below the self-cleaning velocity limit of 0.75 m s^{-1} [23]; this is conservative because it reduces the flow modelled in GoldSim to the minimum possible flow (that of the delay tanks without any extra water).

The actual parameters of the new discharge system (such as pipe size and water velocity) will be a matter for the engineering design of the new system.

Table 32 – Properties of the discharge pipe for each scenario

Scenario	Outfall	Internal pipe diameter /m	Cross-sectional area /m^2	Length of the pipe /m	Flow /$m^3\ s^{-1}$
1. Current operational system	Bank	3.35	8.8	745	7
2. Alternative discharge line into the bank	Bank	0.15	0.018	745	0.0086
3. Scenario 2 with site limits for A station and B station	Bank	0.15	0.018	745	0.0086
4. Scenario 2 with discharges in the flood tide	Bank	0.15	0.018	745	0.0086
5. Alternative discharge line into the channel	Channel	0.15	0.018	1400	0.0086

The GoldSim discharge windows for Scenarios 2 to 5 allow for the discharge line to be purged after the tank has been emptied. This assumes that the tidal window specified in the permit applies to release of contaminants from the discharge point, not the delay tanks. An alternative engineering solution, such as a duck-bill valve, could be used to meet this requirement by sealing the seaward end of the discharge line outside the allowed tidal window instead.

B.2 Other exemplar pipe configurations

Table 33 shows other pipe configurations that would achieve adequate velocity [23] and turnover. It also shows what the effect on these configurations would be if extra water were required for effluent dilution and dispersion (although the results in this report show that it is not). These are not engineering design calculations. For example, they simplistically assume that there is no limit on the capacity of the pipe and that a pipe cannot be underfilled. They show the sorts of systems for which the results in this report would be valid but are not intended to be specifications for the new discharge system. There will also be configurations not included in this table that would provide the requisite performance.

Table 33 – Exemplar pipe configurations

Description	Outfall	Internal diameter /m	Length of pipe /m	Flow (including make-up water) /$m^3\ s^{-1}$	Velocity /$m\ s^{-1}$	Make-up water /$m^3\ s^{-1}$
Discharge into the bank with a smaller pipe	Bank	0.10	745	0.0086	1.1	No make-up water during discharge, then 0.0086 for purging flow after discharge.
Discharge into the bank with additional water flow	Bank	0.15	745	0.0186	1.1	0.010 during discharge, then 0.0186 for purging flow after discharge

Description	Outfall	Internal diameter /m	Length of pipe /m	Flow (including make-up water) /m^3 s^{-1}	Velocity /m s^{-1}	Make-up water /m^3 s^{-1}
Discharge into the bank with a larger pipe and additional water flow	Bank	0.30	745	0.0586	1.0 during discharge; 0.8 while purging	0.06
Discharge into the bank with additional water flow	Channel	0.15	745	0.0286	1.6	0.020 during discharge, then 0.0286 for purging flow after discharge

All the configurations in Table 33 assume that the final delay tanks may contain up to 99 m^3 and may be drained at 0.0086 m^3 s^{-1}.

Changing the pipe configurations would result in different flow rates and discharge times. The results in this report show that this would have no effect on dispersion and dilution.

This page has been intentionally left blank.

Appendix C – Further detail on model and derivation of input data

C.1 Channel compartment flows

Advective flow between the channel compartments was based on tidal stream data taken from Admiralty charts [10] and an Admiralty tidal stream atlas [28]. Tidal streams (velocity and direction) are given for several locations in the Firth of Clyde (blue diamonds in Figure 66).

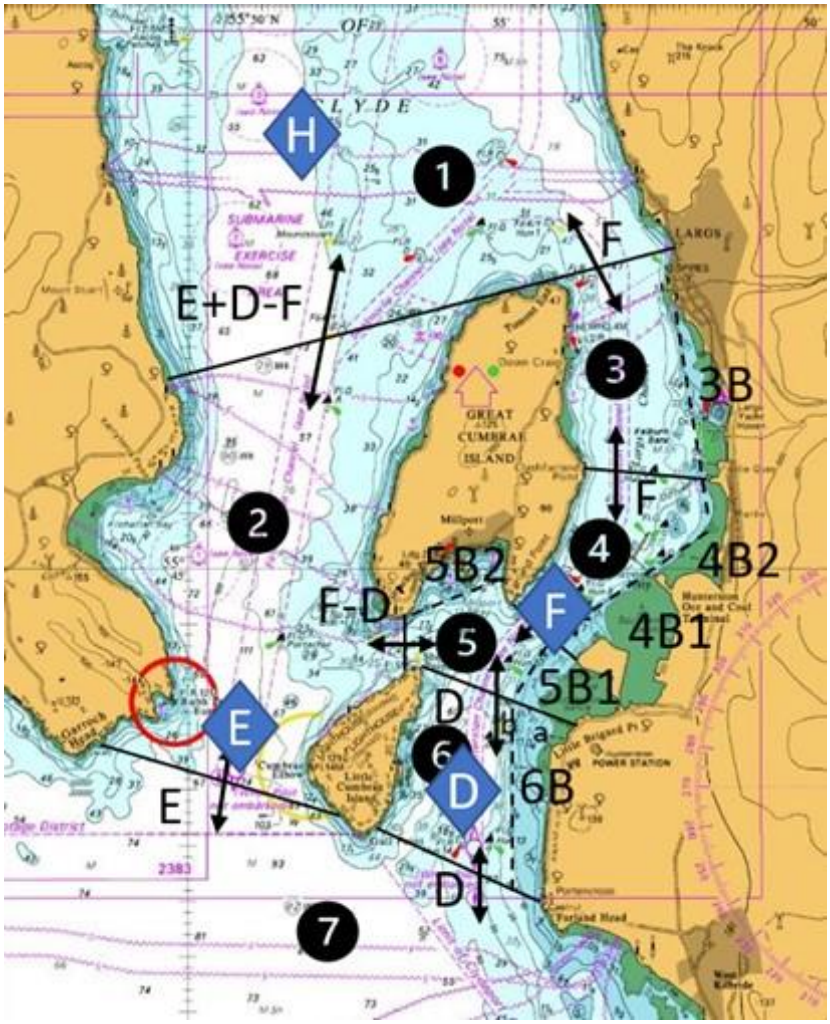

Figure 66 – Locations for which admiralty tidal stream data are available. Base map reproduced from reference [10].

The Admiralty tables (Table 34 and Table 35) give, for each location (D, E and F in Figure 66) and at times throughout the tidal cycle, the tidal velocity at spring and neap tides (kn) and the tidal direction (°).

Table 34 – Admiralty tidal stream data, from references [10] and [28]

h after high water	Tidal stream directions (θ /°), velocities at spring tides (V_s /kn) and velocities at neap tides (V_n /kn)								
	θ(D)	V_s(D)	V_n(D)	θ(E)	V_s(E)	V_n(E)	θ(F)	V_s(F)	V_n(F)
0	9	0.3	0.2	18	0.2	0.1	35	0.1	0.1
1	-	-	-	257	0.4	0.3	231	0.6	0.4
2	193	0.3	0.2	235	0.9	0.5	237	1.3	0.8
3	198	0.3	0.2	215	0.9	0.6	229	1.4	0.9
4	196	0.5	0.3	209	0.8	0.5	229	1.3	0.8
5	196	0.7	0.4	152	0.4	0.2	230	0.8	0.5
6*	218	0.15	0.1	78	0.25	0.15	145	0.7	0.45
7	343	0.2	0.1	46	0.6	0.4	48	1.1	0.7
8	27	0.2	0.1	26	0.7	0.4	44	1.0	0.6
9	27	0.4	0.2	44	0.6	0.4	52	0.8	0.6
10	23	0.4	0.3	37	0.4	0.3	53	0.8	0.5
11	17	0.4	0.2	16	0.3	0.2	50	0.6	0.4

* The low tide values (6h after high tide) are the average of 6 hours before high tide and 6 hours after high tide.

Table 35 – Properties of tidal reference points, from references [10] and [28]

Location	Direction perpendicular to the cross section (θ_0 /°)	Cross-sectional area (C /m^2)
D	150	8.00×10^4
E	225	2.00×10^4
F	200	1.49×10^5

We calculate the flow rate ($m^3\ s^{-1}$) at each location by:

1. Calculating the average of the spring and neap tide velocities
2. Converting the average velocity from kn to $m\ s^{-1}$
3. Calculating the component of the velocity that is travelling up or down the Firth (rather than toward or away from the shore)
4. Multiplying the up- or downstream velocity by the cross-sectional area at the location (derived from Figure 68)

This process is given by Equation (44).

$$F_{T,Loc} = 0.51\ \mathrm{m\ s^{-1}\ kn^{-1}} \cdot \frac{V_s(Loc) + V_n(Loc)}{2} \cdot \cos\big(\theta(Loc) - \theta_0(Loc)\big) \cdot \mathrm{C}(Loc) \quad (44)$$

Here:

0.51 $m\ s^{-1}\ kn^{-1}$ is the conversion from knots to $m\ s^{-1}$ [32];

$V_s(Loc)$ and $V_n(Loc)$ are the flow rates at each location for spring and neap tides, respectively ($m^3 s^{-1}$) (see Table 34);

$\theta(Loc)$ and $\theta_0(Loc)$ are the flow directions at each location at t and 0 hours after high tide, respectively (°, north = 0°) (see Table 34);

C(*Loc*) is the cross-sectional area at each location (m^2) (see Table 35).

We then calculate the tidal flows between compartments by water balance:

$$F_{\mathrm{T,NoL\_WoC}} = F_{\mathrm{T}}(E) + F_{\mathrm{T}}(D) - F_{\mathrm{T}}(F) \quad (45)$$

$$F_{\mathrm{T,NoL\_NEoC}} = F_{\mathrm{T,NEoC\_SEoC}} = F_{\mathrm{T,SEoC\_HtM}} = F_{\mathrm{T}}(F) \quad (46)$$

$$F_{\mathrm{T,HtM\_EoC}} = F_{\mathrm{T,EoC\_OF}} = F_{\mathrm{T}}(D) \quad (47)$$

$$F_{\mathrm{T,HtM\_WoC}} = F_{\mathrm{T}}(F) - F_{\mathrm{T}}(D) \quad (48)$$

$$F_{\mathrm{T,WoC\_OF}} = F_{\mathrm{T}}(E) \quad (49)$$

Here:

$F_{\mathrm{T,compA\_compB}}$ is the tidal flow from compartment A to compartment B at a given time ($m^3 h^{-1}$) (Table 8);

$F_T(Loc)$ is the admiralty tidal flow for the specified location ($m^3 h^{-1}$) (see Equation (44)).

The flows at the boundaries of the model and the total flows between compartments (including non-tidal components) are then calculated as given in Table 5.

This approach makes the following assumptions and simplifications:

- Admiralty tidal flow data are representative of the whole depth of the water column, not just the surface
- Tidal cycles take exactly 12 h
- That there is a single flow system, with flows in one direction at any time (and not, for example, stratification leading to surface and deep flows with different patterns)
- That tidal currents and riverine currents can be represented as a single net (empirically determined) flow
- That the (empirically determined) net tidal flow implicitly accounts for prevailing weather patterns (for example, dominant wind direction)
- That thermal effects, saline and freshwater mixing and highly localised seabed features (such as sills) do not influence flows on the model scale.

There is stratification in the Firth of Clyde, with flow in the deeper waters being blocked by sills on the seafloor. However, less than 20% of the Firth (by area) is more than 70 m deep and less than 6% is more than 100 m deep (probably even less in the region covered by our model, as it does not include Loch Fyne) [8]. Therefore, we consider a vertically well-mixed water

column with vertically uniform flows to be a proportionate approximation. This is consistent with the approach taken by PC-CREAM 08, which also considers local and regional compartments to be vertically well mixed [14].

C.2 Bank compartment flows

Bank compartments are assumed to be dominated by flow into and out of the channel arising from the ebb and flood currents, rather than by flow along the shore. Therefore, the only tidal flows modelled for the bank compartments are flows into and out of the adjacent bank compartment.

We have derived advective flow between the bank and channel compartments, $F_{\mathrm{T,Bank}}$ ($m^3\ h^{-1}$) by:

1. Looking up the tidal range at the bank locations [29]
2. Calculating the volume difference of the compartment between high and low tides (tidal range multiplied by compartment area
3. Assuming that this volume of water enters or leaves the compartment at a uniform rate during the duration of the flood or ebb tide (5 h) and that the tide is slack for 1 h each at high and low tide

This is described in Equations (50) to (52).

$$F_{T,Bank} = 0 \text{ at high or low water} \quad (50)$$

$$F_{\mathrm{T,Bank}} = -\frac{A(Bank) \cdot \mathrm{TD}}{5\ \mathrm{h}} \text{ during ebb tides (1 h to 5 h after high tide)} \quad (51)$$

$$F_{\mathrm{T,Bank}} = \frac{A(Bank) \cdot \mathrm{TD}}{5\ \mathrm{h}} \text{ during flood tides (7 h to 11 h after high tide)} \quad (52)$$

Here:

- *A(Bank)* is the area of the bank, measured on the admiralty charts [10] (m^2);
- TD is the tidal difference for the Firth of Clyde [29], assumed to be the same for all bank compartments (m);
- 5 h is the duration of an ebb or flood tide.

C.3 Channel compartment geometry

The volumes of the channel compartments were determined by overlaying the map of the Firth with a grid of 1 km × 1 km. The depth of the Firth in each grid square was determined from admiralty charts [10]. The volume of each compartment was taken to be the sum of the volumes of the grid squares within that compartment and the area (in km^2) to be the number of grid squares. This is shown in Figure 67 and Figure 68.

	F	G	H	I	J	K	L	M	N	O	P	Q	R	S
39														
40														
41			14	26	50	93	45	9	13					
42	116	158	100	71	66	72	67	69	46	20	40	10		
43	29	61	42	78	162	151	170	70	56	31	56	20	10	
44	50				29	67	70	100	65	50	65	50	20	
45	80					28	42	59	66	80	65	57	20	
46	100							44	100	73	64	65	37	
47	50	50							103	59	63	60	36	
48		33	85						45	70	54	56	46	
49		20	73	79	12			34	48	70	50	50	38	7
50			23	52	25	22	39	52	50	55	51	45	41	10
51			25	35	22	48	50	53	53	50	50	38	29	8
52			29	34	44	43	46	49	46	48	60	60	37	13
53					28	39	47	44	44	44	46	50	23	13
54					28	71	40	46	38	48	49	20	20	20
55					29	57	47	50	52	52	53	50	33	36
56					26	58	70	60	60	59	62	54	26	30
57						60	74	73	78	75	77	57	50	20
58						100	99	100	95	77	50	57	57	26
59							98	95	106	100	100	100	70	41
60								110	128	107	110	125	100	39

7 Outer Firth of Clyde

Irish Channel

PC-CREAM 08 local compartment (Based on approximate volume)

Scale: Each cell represents 4 km × 4 km

Figure 67 – Map showing grid used to define the Outer Firth compartment. The numbers in each grid square are depths in m, taken from reference [10].

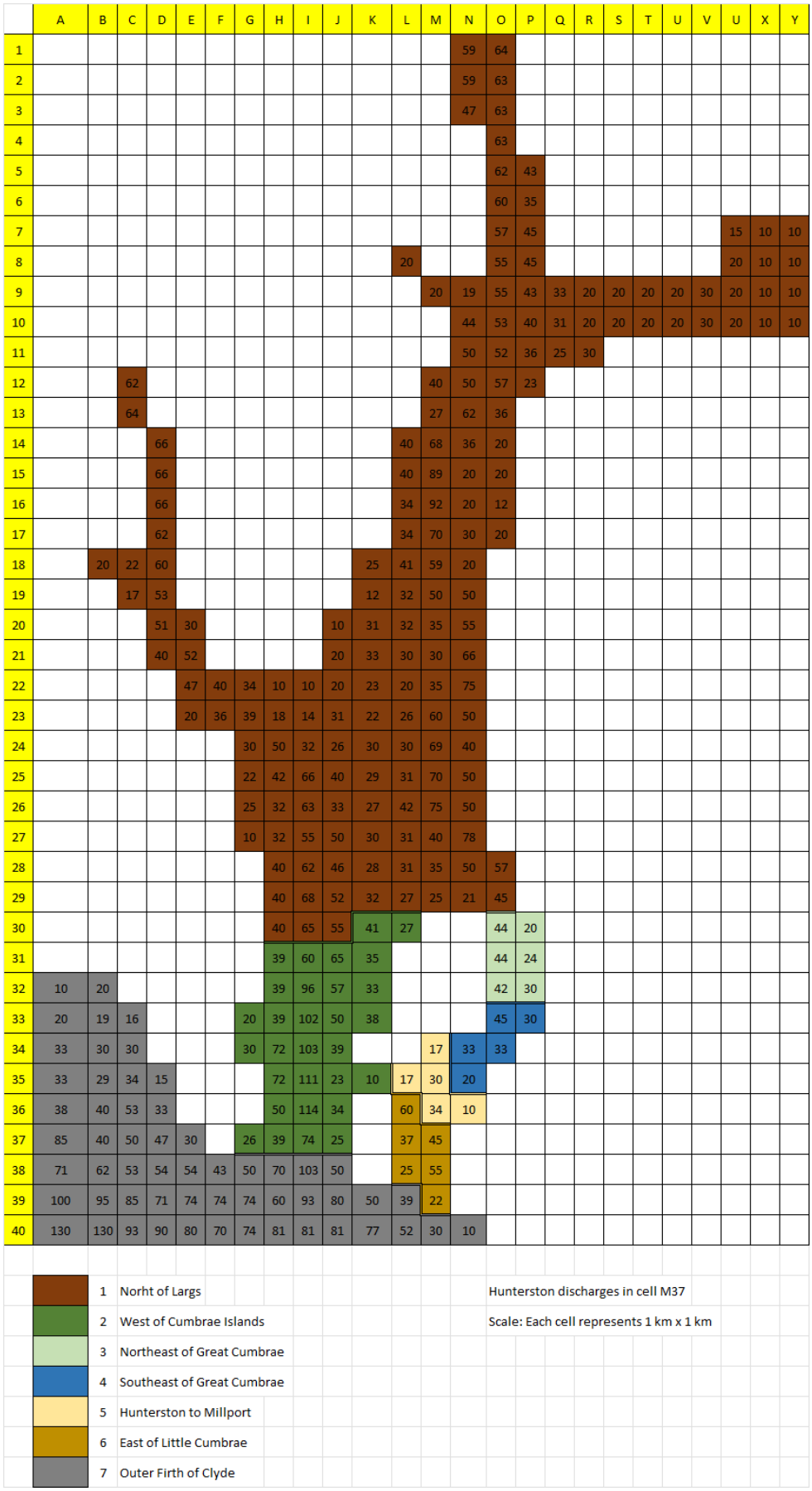

	A	B	C	D	E	F	G	H	I	J	K	L	M	N	O	P	Q	R	S	T	U	V	U	X	Y
1														59	64										
2														59	63										
3														47	63										
4															63										
5															62	43									
6															60	35									
7															57	45							15	10	10
8												20			55	45							20	10	10
9													20	19	55	43	33	20	20	20	20	30	20	10	10
10														44	53	40	31	20	20	20	20	30	20	10	10
11														50	52	36	25	30							
12			62										40	50	57	23									
13			64										27	62	36										
14				66								40	68	36	20										
15				66								40	89	20	20										
16				66								34	92	20	12										
17				62								34	70	30	20										
18		20	22	60							25	41	59	20											
19			17	53							12	32	50	50											
20				51	30					10	31	32	35	55											
21				40	52					20	33	30	30	66											
22					47	40	34	10	10	20	23	20	35	75											
23					20	36	39	18	14	31	22	26	60	50											
24							30	50	32	26	30	30	69	40											
25							22	42	66	40	29	31	70	50											
26							25	32	63	33	27	42	75	50											
27							10	32	55	50	30	31	40	78											
28								40	62	46	28	31	35	50	57										
29								40	68	52	32	27	25	21	45										
30								40	65	55	41	27			44	20									
31								39	60	65	35				44	24									
32	10	20						39	96	57	33				42	30									
33	20	19	16				20	39	102	50	38				45	30									
34	33	30	30				30	72	103	39			17	33	33										
35	33	29	34	15				72	111	23	10	17	30	20											
36	38	40	53	33				50	114	34		60	34	10											
37	85	40	50	47	30		26	39	74	25		37	45												
38	71	62	53	54	54	43	50	70	103	50		25	55												
39	100	95	85	71	74	74	74	60	93	80	50	39	22												
40	130	130	93	90	80	70	74	81	81	81	77	52	30	10											

1	Norht of Largs	Hunterston discharges in cell M37
2	West of Cumbrae Islands	Scale: Each cell represents 1 km x 1 km
3	Northeast of Great Cumbrae	
4	Southeast of Great Cumbrae	
5	Hunterston to Millport	
6	East of Little Cumbrae	
7	Outer Firth of Clyde	

Figure 68 – Maps showing grids used to define compartments in the Firth of Clyde. The numbers in each grid square are depths in m, taken from reference [10].

Average depths for the channel compartments are calculated as follows:

$$\mathrm{WD} = V/A \quad (53)$$

Here:

WD is the depth of the water (m) (see Tables 6 and 7);
V is the volume of water in the compartment (m^3) (see Tables 6 and 7);
A is the area of the compartment (m^2) (see Tables 6 and 7).

C.4 Bank compartment geometry

The areas of the bank compartments were measured on the admiralty charts. The volumes at low tide were determined by multiplying the areas by a nominal depth of 5 m. The volume at high tide was calculated by adding to the volume at low tide the area multiplied by the three-month average of the tidal difference [29].

The volume of water in each bank compartment at time t is calculated as follows:[15]

$$V_{\mathrm{B},t} = V_{\mathrm{B,prev}} + F_{\mathrm{B,compartment},t} \cdot \Delta t \quad (54)$$

Here:

$V_{\mathrm{B},t}$ is the volume of water in the bank compartment at time t (m^3);

$V_{\mathrm{B,prev}}$ is the volume of water in the bank compartment at the previous timestep (m^3) (initially the volume at high tide – see Table 7);

$F_{\mathrm{B,compartment},t}$ is the flow (due to the tide) into the bank compartment from the channel compartment at time t ($m^3\ h^{-1}$) (see Table 5);

Δt is the timestep length (h).

We simplistically treat the banks as having a constant area and a variable depth as the tide rises. The depth of the bank compartments at a given time is, therefore, given by Equation (53).

C.5 Discharge scheduling and conservatism

The number of discharges per calendar year will vary depending on the number of tides between discharges ($f_{\mathrm{d,int}}$). If the number of discharges ($N_{\mathrm{d,a}}$) is not an integer, the number of discharges can vary by one between years. For example, if $f_{\mathrm{d,int}} = 3$ then $N_{\mathrm{d,a}} = 243.3$. This means that in two out of every three years the model models 243 discharges and in one out of every three years it models 244 discharges. Similarly for monthly discharges (once every 61 tidal cycles), $N_{\mathrm{d,a}} = 11.97$ and hence there will be one year (every 30 years) when there are 11 discharges modelled rather than 12. The model always discharges in the first tidal cycle. Therefore, if $N_{\mathrm{d,a}}$ is not an integer, the model always begins in a year with more discharges.

This is illustrated in Figure 69. This shows twelve discharges per year with one discharge every 61 tidal cycles (an approximation for monthly discharges). The top timeline shows a typical year, with twelve discharges. The bottom timeline shows a rare occurrence (around once every thirty years) where the discharges at the start and end of the year fall in the

[15] This equation is used even for the East of Little Cumbrae Bank compartment when water flow from the pipe is being modelled in this compartment. The additional water from the pipe is passed straight through to the channel compartment. The additional inflow and additional outflow (or reduced flood current) cancel each other out and the pipe flow has no effect on the compartment volume.

preceding and following years by a single tidal cycle, leading to only eleven discharges in that calendar year.

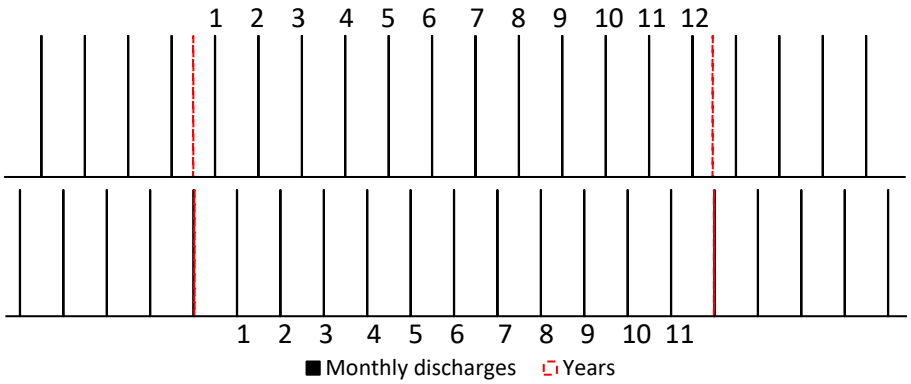

Figure 69 – Timelines showing how the number of discharges per calendar year can vary depending on the juxtaposition between the discharge schedule and the calendar year.

To calculate the contaminant release rate (A_{rr}), the model provides two options:

1. Use the non-integer $N_{d,a}$
2. Conservatively round $N_{d,a}$ down to the nearest integer

When using the first option:

- In years with fewer discharges, the annual discharges modelled will be less than those specified in Table 10.
- In years with more discharges, the annual discharges modelled will be greater than those specified in Table 10.
- The time-averaged annual discharges will converge around those specified in Table 10.

When using the second option:

- In years with fewer discharges, the annual discharges modelled will be those specified in Table 10
- In years with more discharges, the annual discharges modelled will be greater than those specified in Table 10
- The time-averaged annual discharges will be greater than those specified in Table 10

The magnitude of the difference between the options will vary depending on the discharge schedule being considered. To illustrate the difference, consider the example of monthly discharges. In this case $N_{d,a} = 11.97$. The activity per discharge is then $A_a/N_{d,a}$.

The first option results in annual discharges slightly above A_a in most years ($12A_a/11.97 = 1.003A_a$) and activities a little more below A_a approximately every 30th year ($11A_a/11.97 = 0.919A_a$). The average annual discharge over 30 years would, therefore, be approximately A_a. The second option results in annual discharges around 10% above A_a in most years ($12A_a/11 = 1.091A_a$) and activities of A_a approximately every 30th year

($11A_a/11 = A_a$). The average annual discharge over 30 years would, therefore, be slightly under $1.09A_a$.

Usually the first option will be most appropriate to use. It represents regular discharges with an average annual rate corresponding to those specified in Table 10. As the model always begins in a year with more discharges, a short-term run does not risk considering a year with low discharges.

The second option will usually be excessively conservative. There may be some situations, however, where this is required.

C.6 Calculation of alternative environmental media concentrations

The GoldSim model also calculates the following concentrations. They are not discussed in this report, but the results given in the GoldSim output files in case they are needed.

The activity concentration in filtered seawater is the total activity dissolved in a unit volume of seawater, not including activity sorbed to suspended sediment. It is given by Equation (55).This result corresponds to a sample of seawater after filtering it to remove the suspended sediment.

$$A_{\mathrm{FW,s}} = c_{\mathrm{iws}} \cdot \mathrm{SA_s} \qquad (55)$$

Here:

$A_{FW,s}$ is the activity concentration of species s in filtered seawater (Bq m^{-3});

c_{iws} is the concentration of species s in water (kg m^{-3}) (Equation (5)).

The activity concentration in upper sediment porewater is the total activity dissolved in a unit volume of the sediment porewater (not including the volume occupied by the sediment). It is given by Equation (55). This corresponds to a sample of the leachate drained or pressed from wet sediment.

The activity concentration in dry upper sediment (sorbed activity only) is the activity sorbed to sediment per unit mass of dry sediment. It is given by Equation (56). This result corresponds to a sample of sediment that has been dried by draining or pressing.

$$A_{\mathrm{DSS,s}} = c_{\mathrm{is}} \cdot \mathrm{SA_s} \qquad (56)$$

Here:

$A_{DSS,s}$ is the activity concentration of species s sorbed to upper sediment per unit mass of dry sediment (Bq kg^{-1});

c_{is} is the concentration of species s sorbed to sediment in cell i (kg kg^{-1}) (Equation (6)).

This page has been intentionally left blank.

Appendix D – Results sampling

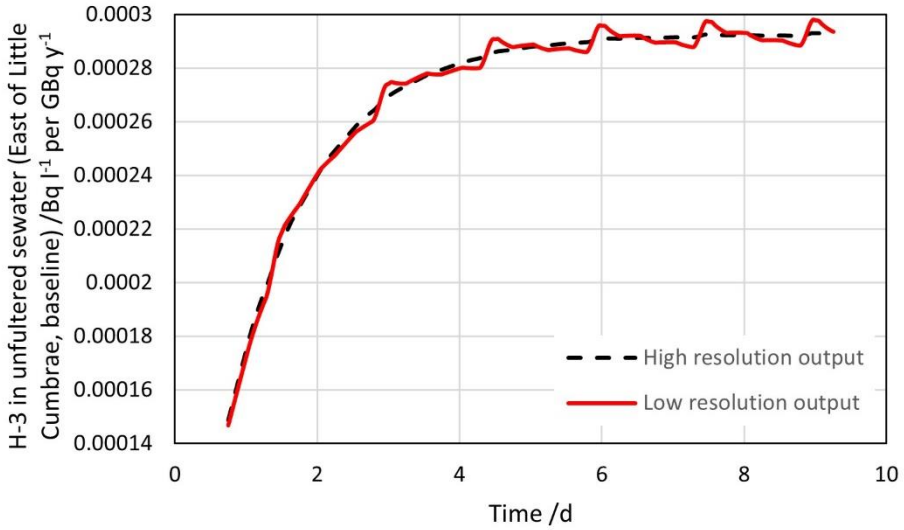

Figure 70 – Comparison of the moving average of H-3 concentration over a discharge cycle for the high-resolution (every timestep; that is, every 0.1 h) and low resolution (every ten timesteps; that is every hour) results

If results are reported less frequently than every timestep, sampling error could be introduced to the model. For example, if the sampling frequency chosen consistently misses a concentration peak, the average concentration reported will be too low. Figure 70 compares H-3 moving average concentrations for identical simulations with results sampled at both timesteps used in this report. Although there is more uncertainty in the low-resolution results, there is no systematic error. Use of the low-resolution results is, therefore, acceptable.

This page has been intentionally left blank.

Appendix E – List of Terms and Acronyms

AGR	Advanced gas-cooled reactor
CEFAS	Centre for Environment, Fisheries and Aquaculture Science
DORIS	Dispersion of Radionuclides in Seas (mathematical model)
EDF	EDF Energy Nuclear Generation Ltd
EoC	East of Little Cumbrae (model compartment)
EoC_B	East of Little Cumbrae Bank (model compartment)
HT	High tide
HtM	Hunterston to Millport (model compartment)
HtM_B1	Hunterston to Millport Bank 1 (model compartment)
HtM_B2	Hunterston to Millport Bank 2 (model compartment)
IAEA	International Atomic Energy Agency
ICRP	International Commission on Radiological Protection
LT	Low tide
NEoC	Northeast of Great Cumbrae (model compartment)
NEoC_B	Northeast of Great Cumbrae Bank (model compartment)
NoL	North of Largs (model compartment)
OF	Outer Firth (model compartment)
PC-CREAM	PC Consequences of Release to the Environment: Assessment Methodology (computer software)
RIFE	Radioactivity in Food and the Environment (report series)
SEoC	Southeast of Great Cumbrae (model compartment)
SEoC_B1	Southeast of Great Cumbrae Bank 1 (model compartment)
SEoC_B2	Southeast of Great Cumbrae Bank 2 (model compartment)
WoC	West of Cumbrae Islands (model compartment)

Eden Nuclear and Environment Ltd registered address:
Unit 1 Mereside,
Greenbank Road,
Eden Business Park,
Penrith,
Cumbria,
CA11 9FB

Eden
Nuclear and Environment

ISOQAR REGISTERED
UKAS MANAGEMENT SYSTEMS
0026
Certificate Number 12469
ISO 9001

Company No 6314579, registered in England and Wales